



University of HUDDERSFIELD

University of Huddersfield Repository

Towsyfyán, Hossein

Investigation of the Nonlinear Tribological Behaviour of Mechanical Seals for Online Condition Monitoring

Original Citation

Towsyfyán, Hossein (2017) Investigation of the Nonlinear Tribological Behaviour of Mechanical Seals for Online Condition Monitoring. Doctoral thesis, University of Huddersfield.

This version is available at <http://eprints.hud.ac.uk/id/eprint/34340/>

The University Repository is a digital collection of the research output of the University, available on Open Access. Copyright and Moral Rights for the items on this site are retained by the individual author and/or other copyright owners. Users may access full items free of charge; copies of full text items generally can be reproduced, displayed or performed and given to third parties in any format or medium for personal research or study, educational or not-for-profit purposes without prior permission or charge, provided:

- The authors, title and full bibliographic details is credited in any copy;
- A hyperlink and/or URL is included for the original metadata page; and
- The content is not changed in any way.

For more information, including our policy and submission procedure, please contact the Repository Team at: E.mailbox@hud.ac.uk.

<http://eprints.hud.ac.uk/>

**INVESTIGATION OF THE NONLINEAR TRIBOLOGICAL
BEHAVIOUR OF MECHANICAL SEALS FOR ONLINE
CONDITION MONITORING**

HOSSEIN TOWSYFYAN

A thesis submitted to the University of Huddersfield in partial fulfilment of the
requirements for the degree of Doctor of Philosophy

Department of Mechanical Engineering

School of Computing and Engineering

University of Huddersfield

March 2017

Copyright Statement

- I. The author of this thesis (including any appendices and/or schedules to this thesis) owns any copyright in it (the “Copyright”) and s/he has given The University of Huddersfield the right to use such copyright for any administrative, promotional, educational and/or teaching purposes.
- II. Copies of this thesis, either in full or in extracts, may be made only in accordance with the regulations of the University Library. Details of these regulations may be obtained from the Librarian. This page must form part of any such copies made.
- III. The ownership of any patents, designs, trademarks and any and all other intellectual property rights except for the Copyright (the “Intellectual Property Rights”) and any reproductions of copyright works, for example graphs and tables (“Reproductions”), which may be described in this thesis, may not be owned by the author and may be owned by third parties. Such Intellectual Property Rights and Reproductions cannot and must not be made available for use without the prior written permission of the owner(s) of the relevant Intellectual Property Rights and/or Reproductions.

ABSTRACT

Mechanical seals have increasingly been used for sealing rotating shafts in centrifugal pumps, propeller shafts in ships and submarines, compressors, liquid propellant rocket motors in aerospace industry, pumps, turbines, mixers and many other rotating machines during last two decades. Abnormal operating conditions in the mechanical seals will degrade machine performance, increase operating cost and may cause unexpected sudden failures which are dangerous in both engineering and safety terms. Hence it is necessary to investigate the tribological behaviour of mechanical seals operating based on nonlinear coupling between fluid and surface dynamics, in order to develop more advanced diagnostic technologies to improve the reliability of such machines operating with mechanical seals.

Different condition monitoring techniques have been studied to evaluate the lubrication state and severity of contact between the mating faces in mechanical seals. However, some of them are not cost effective others are not practical in industrial applications. Acoustic emission (AE) has been proved to be a sensitive indicator of lubrication conditions and changes in the lubricant properties, however the application of technique for identification of lubrication regimes in mechanical seals has not been reported yet. Moreover, previous studies give relatively little information to acoustic emission condition monitoring of mechanical seals, nor has comprehensive fault detection been implemented for a particular case. In addition, a review on previous works reveals the lack of comprehensive mathematical models to explain the relationship between AE energy and tribological characteristics of the mating faces under healthy and faulty conditions.

In this research, the tribological behaviour of mechanical seals is investigated using acoustic emission measurements to pave a way for fault detection at early stage. Three common seal failures i.e. dry running, spring fault, and defective seal are studied in this thesis. The main objective is to extract AE features that can explain the tribological behaviour of mechanical seals under both healthy and faulty conditions. To achieve this, a purpose-built test rig was employed for collecting AE signals from the mechanical seals. Then, the collected data was processed using time domain, frequency domain and time frequency domain analysis methods which are of the most common techniques used for monitoring in AE applications.

Based on results the main frequency band that can present the tribological behaviour of mechanical seals was detected. Also it has been proved that AE features in time domain and

frequency domain can be effectively applied to indicate the lubrication condition of mechanical seals as well as early fault detection.

Moreover, mathematical models were developed to establish a relationship between AE root mean square (RMS) value of AE signals and working parameters of seals (rotational speed, load and number of asperities in contact) under different lubrication regimes. A good agreement was achieved between measured and predicted signals that gives a good evidence of the effectiveness of proposed models. Especially in case of leakage that is one of the main situations indicating the seal failure, a significant difference was observed between the predicted signal for healthy case and the measured signal under faulty conditions.

Therefore, it can be deduced that the AE measurement system and signal processing developed in this work has a promising potential to be used to diagnose and monitor the mechanical seals online.

Finally, the conclusions and achievements are given based on the entirety of this research work, and online monitoring incorporating with AE features and mathematical models developed in this thesis are suggested as the main works for further research.

DECLARATION

No portion of this work referred to in this thesis has been submitted in support of an application for another degree or qualification of this or any other university or other institute of learning.

(HOSSEIN TOWSYFYAN)

DEDICATION

To Mahsa, my wife,

for her love, support and inspiration beyond measure.

To Khosrow, my dad,

for giving me strength to reach for the stars and chase my dreams.

ACKNOWLEDGMENT

First of all, I would like to express my sincere gratitude to my academic supervisors, **Prof Andrew Ball** and **Dr. Fengshou Gu** at the **University of Huddersfield** for the continuous support, motivation, guidance and making so many valuable experiences possible. They are also a source of inspiration throughout my research study and in my academic life. Most vital of all, they provided me immense knowledge and enthusiasm in various ways to achieve my target. It was a great pleasure and honour to work under their guidance; the fruits of which I will benefit from for the rest of my career.

Besides my supervisors, I am also particularly grateful to **Dr. Bob Robert Catley** for his encouragement, technical advice and insightful help. Not only he did give me advice relating to scientific matters, but he also gave me a great deal of confidence and motivation to carry out my work and studies. I owe him many favours.

My doctoral scholarship was sponsored by the **University of Huddersfield**, for which I am very appreciative.

At **John Crane**, I would like to thank **Mr Klaus-Dieter Meck** for his continued support, technical advice and for introducing me to so many useful contacts.

I would also like to express my gratitude to my colleagues at the **Centre for Efficiency and Performance Engineering**, past and present, for their technical support and friendship.

Deep appreciation to my families for their support and encouragement especially to my beloved mother Zahra and my aunt Fatima for their endless love and assistance.

Last, but by no means least, my special thanks, love and deep indebtedness to **Mahsa**, my wife. Firstly, for giving up her personal ambitions when the opportunity to study Ph.D. in Iran; and later for so wholeheartedly supporting me throughout my studies. I know there were times when it was not easy to be the wife of a PhD student, but she was a strong encouragement to my work as well as to our marriage. In her I find love beyond measure, companionship and inspiration that is impossible to express here. It is a true blessing to have her by my side. **Mahsa** deserves much of the credit for the completion of this thesis.

LIST OF PUBLICATIONS

1. Towsyfyan, Hossein, Gu, Fengshou and Ball, Andrew (2013), A review of mechanical seals tribology and condition monitoring. In: Proceedings of Computing and Engineering Annual Researchers' Conference 2013, CEARC'13. University of Huddersfield, Huddersfield, pp. 200-205. ISBN 9781862181212.
2. Towsyfyan, Hossein, Raharjo, Parno, Gu, Fengshou and Ball, Andrew (2013) Characterization of Acoustic Emissions from Journal Bearings for Fault Detection. In: NDT 2013, 10th-12th September 2013, Telford, UK.
3. Towsyfyan, Hossein, Ossama, Hassin, Gu, Fengshou and Ball, Andrew (2014) Characterization of Acoustic Emissions from Mechanical Seals for Fault Detection. In: NDT 2014, 10th-12th September 2014, Manchester, UK.
4. Towsyfyan, Hossein, Wei, Nasha, Gu, Fengshou and Ball, Andrew (2015), Identification of Lubrication Regimes in Mechanical Seals using Acoustic Emission for Condition Monitoring. The 54rd Annual Conference of the British Institute of Non-Destructive Testing BINDT 2015, 8th-10th September 2015, Telford, UK.
5. Osama A. Hassin, Nasha Wei , Hossein Towsyfyan, Fengshou Gu and Andrew D. Ball, Journal Bearing Lubrication Monitoring Based on Spectrum Cluster Analysis of Vibration Signals, 28th International Congress of Condition Monitoring and 10th regional Congress on Non Destructive and Structural Testing COMADEM 2015.

LIST OF CONTENT

ABSTRACT	ii
DECLARATION	iv
DEDICATION	v
ACKNOWLEDGMENT	vi
LIST OF PUBLICATIONS	vii
LIST OF FIGURES.....	xv
LIST OF TABLES.....	xx
LIST OF ABBREVIATIONS	xxi
LIST OF NOTATIONS	xxii
CHAPTER ONE;.....	1
1. INTRODUCTION.....	1
1.1 An Overview of Mechanical Seals	2
1.2 Failure Modes of Mechanical Seals.....	4
1.3 Research Background	6
1.3.1 Condition Monitoring of Mechanical Seals	8
1.3.2 Acoustic Emission Condition Monitoring of Mechanical Seals	9
1.4 Research Motivation	12
1.5 Aims and Objectives	13
1.6 Organization of Thesis.....	14
Chapter Two;	16
2. Tribological Behaviour of Mechanical Seals	16
2.1 The Principles of Mechanical Seals.....	17
2.1.1 Internal vs. External Pressurized Mechanical Seals	17
2.1.2 Balanced vs. Unbalanced Mechanical Seals	18
2.1.3 Closing Force vs. Opening Force	19
2.1.4 Pressure Drop Factor	21

2.1.5	Hydrostatic Vs Hydrodynamic Pressure Distribution	22
2.2	Tribology Concept	23
2.2.1	Mechanical Seal as a Tribosystem	23
2.2.2	Lubrication Regimes	24
2.3	Measurement of Surface Characteristics	28
2.3.1	Geometrical Features	28
2.3.2	Surface Roughness Considerations for Sealing Performance	31
2.4	Friction.....	32
2.4.1	Friction Laws and Origin of Friction.....	32
2.4.2	Friction Components	34
2.4.3	Mechanical Seal’s Friction	35
2.5	Wear.....	38
2.6	Wear Mechanisms.....	39
2.6.1	Adhesive Wear	39
2.6.2	Abrasive Wear	40
2.6.3	Fatigue Wear.....	40
2.7	Face Pressure-Velocity Product.....	41
2.8	Heat Transfer Consideration in Mechanical Seals.....	42
2.9	Seal Face Materials	45
2.10	Main Findings	47
Chapter Three;		48
3	Acoustic Emission Technology	48
3.1	History and Background of Acoustic Emission.....	49
3.2	Application of AE Condition Monitoring to Rotating Machines	50
3.2.1	Rolling Element Bearings.....	51
3.2.2	Journal Bearings	51
3.2.3	Gearboxes	52

3.3	Principals of AE Testing	52
3.3.1	Transient vs. Continuous AE Signal	54
3.3.2	AE Signal Measurement Parameters	55
3.4	AE Sensor Considerations	57
3.4.1	Sensor and System Response	58
3.4.2	Calibration	59
3.5	Propagation of Stress Waves	61
3.5.1	Waves in Infinite (Unbounded) Medium	61
3.5.2	Waves in Semi-Infinite Medium (One Bounding Surface).....	63
3.5.3	Waves in Infinite Medium Bounded by Two Surfaces	64
3.6	AE Waves in Real Measurements	66
3.6.1	Wave Attenuation.....	66
3.6.2	Wave Reflection and Refraction	68
3.7	Summary.....	69
	Chapter Four;	70
4.	Condition Monitoring of Mechanical Seals, a Literature Review	70
4.1	Mechanical seals Condition Monitoring and Diagnostic.....	71
4.1.1	Vibration Analysis.....	71
4.1.2	Eddy current testing.....	72
4.1.3	Ultrasonic Testing	73
4.2	Literature on the AE Condition Monitoring of Mechanical Seals.....	74
4.2.1	Traditional Acoustic Emission sources at Seal Faces	75
4.2.2	Application of Acoustic Emission to the Sliding Contact.....	76
4.3	Literature on AE Signals and Signal Processing Methods	78
4.3.1	Time domain analysis.....	80
4.3.2	Frequency Domain Analysis	82
4.3.3	Time-Frequency Analysis	84

4.4	Main Findings	85
Chapter Five;		86
5	Mathematical Modelling	86
5.1	Background of AE Source Modelling	87
5.1.1	Empirical AE Models Related to Friction	87
5.1.2	Mathematical AE Models.....	88
5.2	Quantifying of AE Energy Released in Frictional Process.....	90
5.3	Novel AE Source Mechanisms	92
5.3.1	Asperity Collision Induced Emissions	95
5.3.2	Flow Induced Emissions in Asperities	96
5.3.3	Friction Induced Emissions in Fluid Lubricant	98
5.4	Contact Mechanics of Randomly Rough Surfaces	100
5.5	Modelling Asperity Collision	102
5.6	Flow Induced Asperity Deformation Model.....	106
5.7	Viscous Friction Model	110
5.8	The Effect of Source Mechanisms on the AE Signal	116
5.9	Main Findings	117
Chapter Six;		118
6	Experimental Set up Facilities	118
6.1	Introduction.....	119
6.1.1	Limitations of the Primary Design	119
6.1.2	Design Objectives of the Test Rig.....	120
6.2	Development of the New Test Rig Facilities.....	121
6.2.1	Test Rig Construction and Components.....	122
6.2.2	New Design of the Auxiliary Circulating System.....	127
6.3	Signal Measurement	132
6.3.1	Data Acquisition System	133

6.3.2	Temperature Sensor	137
6.3.3	Pressure Sensor	138
6.3.4	Acoustic Emission Sensor	139
6.3.5	Shaft Encoder	140
6.4	Surface Roughness Measurement	141
6.5	Test Procedure and Fault Simulation	142
6.5.1	Seal Free Test	144
6.5.2	Static Test	145
6.5.3	Transient Speed Test	145
6.5.4	Tests under different operating conditions	146
6.5.5	Partial Dry Running Test	147
6.5.6	Spring Fault Test	147
6.5.7	Defective Seal Test	148
6.6	Main Findings	149
Chapter Seven;.....		150
7.	Experimental Study of AE from the Tribology of Mechanical Seals	150
7.1	Introduction to the Baseline Experimental Study	151
7.2	Identification of the Tribological AEs	151
7.2.1	Results of the Seal Free Test	152
7.2.2	Results of the Static Test	153
7.2.3	Results of the Transient Speed Test	154
7.3	The Observation of Mechanical Seal’s Tribological Behaviour.....	156
7.3.1	AE Signal Characteristics in the Time Domain.....	157
7.3.2	The Variation of AE RMS Value under Different Operating Conditions...	158
7.3.3	The Variation of AE Kurtosis Value under Different Operating Condition	161
7.3.4	Frequency Domain Analysis	164
7.4	Model Verification.....	167

7.4.1	The Influence of Sliding Speed on AE RMS	167
7.4.2	The Influence of Sealed Pressure on AE RMS.....	170
7.5	Main Findings	172
Chapter Eight;		174
8	Application of AE Measurements to the Fault Detection of Mechanical Seals..	174
8.1	Introduction.....	175
8.2	Partial Dry Running Test	175
8.2.1	Time Domain Analysis	176
8.2.2	The Variation of AE RMS Value under Partial Dry Running Test.....	178
8.2.3	The Variation of AE Kurtosis Value under Different Operating Conditions 179	
8.2.4	Frequency Domain Analysis	181
8.2.5	Model Response to Partial Dry Running Test.....	182
8.3	Spring Fault Test.....	183
8.3.1	Time Domain Analysis.....	184
8.3.2	The Variation of AE RMS Value under Different Operating Conditions...	185
8.3.3	The Variation of AE Kurtosis Value under Different Operating Conditions 187	
8.3.3	Frequency Domain Analysis	188
8.3.4	Model Response to Spring Fault Test	189
8.4	Defective Seal Test	192
8.4.1	Time Domain Analysis.....	193
8.4.2	The Variation of AE RMS Value under Different Operating Conditions...	194
8.4.3	The Variation of AE Kurtosis Value under Different Operating Conditions 195	
8.4.4	Frequency Domain Analysis	197
8.4.5	Model Response to Defective Seal Test.....	198
8.5	Main Findings	202

Chapter Nine;	203
9 Conclusions and Future Work	203
9.1 Review of the Thesis Objectives and Achievements.....	204
9.2 Conclusions of the Research.....	208
9.2.1 Conclusions on the AE Measurement and Signal Processing.....	208
9.2.2 Conclusions on Monitoring the Tribological Behaviour of Mechanical Seals using AE Measurements.....	209
9.2.3 Conclusions on Fault Detection in Mechanical Seals using AE Measurements 211	
9.3 Novel Feature Summary and Contribution to the Knowledge	212
9.4 Recommendations for future work	213
Bibliography	216
Appendix A	226
Appendix B	229
Appendix C	230
Appendix D	231
Appendix E	233
Appendix F	234

LIST OF FIGURES

Figure 1.1 Static and dynamic seals	2
Figure 1.2 Schematic illustration of face seals	3
Figure 1.3 Pusher type of mechanical seals.....	4
Figure 1.4 Effect of seal gap can produce leakage (left), or excessive contact (right).....	4
Figure 1.5 Examples of the common types of faults in mechanical seals[4]	5
Figure 1.6 Causes of mechanical seals failures [6]	6
Figure 1.7 The interactive nature of a mechanical seal system	8
Figure 2.1 Interval vs. external mechanical seals.....	17
Figure 2.2 The concept of balance ratio	19
Figure 2.3 Forces acting on sealing gap [39].....	19
Figure 2.4 Pressure drop factor configurations	21
Figure 2.5 Schematic illustration of mechanical seals as a tribosystem.....	23
Figure 2.6 Schematic illustration of asperity contact in the sealing interface.....	24
Figure 2.7 Asperity level illustration of Lubrication regimes	25
Figure 2.8 Stribeck curve.....	26
Figure 2.9 Stribeck curves obtained by different experiments [2]	28
Figure 2.10 Illustration of a surface profile element [55].....	30
Figure 2.11 The effect of waviness on hydrodynamic pressure generation	30
Figure 2.12 Total waviness height representation.....	31
Figure 2.13 A description of energy path during friction [67]	34
Figure 2.14 Schematic representation of the rig to measure frictional torque [78].....	36
Figure 2.15 The effect of seal working parameters on friction factor.....	37
Figure 2.16 Heat Generation in a Mechanical Seal [1]	43
Figure 2.17 Predicted contact pressure and temperature distribution[95].....	44
Figure 3.1 Principles of AE wave propagation.....	53
Figure 3.2 Different types of AE signal	54
Figure 3.3 Definitions of AE signal parameters	55
Figure 3.4 Schematic view of a piezoelectric sensor.....	57
Figure 3.5 AE detection system [131]	58
Figure 3.6 A linear system[131].	58
Figure 3.7 Calibration curves of commercial AE sensors [131].	60
Figure 3.8 AE "Pencil Lead Break" method [99].....	60

Figure 3.9 Plane wave propagating in three dimensions	62
Figure 3.10 AE wave types in infinite media	63
Figure 3.11 Surface wave or Rayleigh wave in the material [141]	63
Figure 3.12 Two classes of Lamb wave	65
Figure 3.13 Extensional vs. flexural wave	65
Figure 3.14 Schematic representation of mechanical seal test rig.....	67
Figure 3.15 Turbine unit investigated by Mba and Hall [149].....	68
Figure 4.1 Mechanical seal test rig for eddy current testing principle [159]	73
Figure 4.2 Illustration of film collapse detection using ultrasonic waves [160]	73
Figure 4.3 Basic concept of film collapse detection using ultrasonic waves [20].....	74
Figure 4.4 Illustration of acoustic emission sources in mechanical seals	75
Figure 4.5 Illustration of pin-on-block-type test rig [133]	76
Figure 4.6 Overview of fault diagnosis based on AE signals.....	79
Figure 5.1 Schematic illustration of direct asperity contact	88
Figure 5.2 The concept of sliding distance in asperity contact	89
Figure 5.3 The concept of strain energy released in sliding contact	89
Figure 5.4 Schematic illustration of AE generating mechanisms at sealing gap	93
Figure 5.5 AE signal generated due to fluid induced asperity deformation	93
Figure 5.6 AE signal generated due to shearing in the lubricant fluid	94
Figure 5.7 AE wave generated due to bending of asperities in direct contact	95
Figure 5.8 The changes in fluid passing area confined between asperities	97
Figure 5.9 The changes in the fluid forces exerted into asperities	98
Figure 5.10 Single degree of freedom friction drive oscillator	99
Figure 5.11 Shear induced vibration [203].....	99
Figure 5.12 Greenwood and Williamson for contact model	101
Figure 5.13 Schematic of the bending of an asperity during sliding contact	103
Figure 5.14 AE from mechanical seals running with different contact loads [187].....	106
Figure 5.15 Contact model adopted for fluid induced asperity deformation.....	107
Figure 5.16 Illustration of sliding distance in fluid induced deformation of asperities	109
Figure 5.17 Cartesian geometry for general lubrication theory [1].....	111
Figure 5.18 Stress components acting on a differential element of fluid	113
Figure 5.19 Differential elements in viscous friction model	114
Figure 5.20 Waviness amplitude	115
Figure 5.21 The concept of peak and massive asperity deformation	117

Figure 6.1 New design of the mechanical seal test rig	121
Figure 6.2 The main components of the test rig	122
Figure 6.3 Siemens Micro Master Controller system.....	124
Figure 6.4 Siemens Micro Master data acquisition system	125
Figure 6.5 Grounding cables on different components of the test rig	125
Figure 6.6 John Crane type 1648 MP cartridge seal	126
Figure 6.7 Different components of the auxiliary system	127
Figure 6.8 The system for supplying fresh water to the heat exchanger	128
Figure 6.9 Connections to the radiator	128
Figure 6.10 The temperature change in a test.....	129
Figure 6.11 Multistage regulator mounted on the nitrogen cylinder.....	130
Figure 6.12 Connections to the radiator	130
Figure 6.13 Connections from and into the chamber	131
Figure 6.14 The pump employed in circulating system	132
Figure 6.15 Sensor configuration and data acquisition	133
Figure 6.16 Sinocera YE6230B.....	134
Figure 6.17 Operational condition control system	135
Figure 6.18 PCI-2 AE System board.....	136
Figure 6.19 AE signal measurement and data streaming system configuration.....	137
Figure 6.20 The position of temperature sensors	137
Figure 6.21 The position of the pressure gage and pressure transducer.....	138
Figure 6.22 AE sensor mounted on the seal cartridge.....	140
Figure 6.23 Taylor Hobson Form Talysurf applied in this research	141
Figure 6.24 Schematic illustration of the seal free test configuration.....	145
Figure 6.25 Motor speed variations up to 1500 rpm under 4bar load	146
Figure 6.26 Operational conditions during the tests.....	146
Figure 6.27 Seal head assembly in spring fault simulation	148
Figure 6.28 Defective seal test (a) Damaged face (b) Scratches on stationary ring.....	148
Figure 6.29 Leakage during the defective seal test	149
Figure 7.1 The spectrogram of the AE signal measured in manual turning of shaft.....	152
Figure 7.2 The spectrogram of the AE signal measured in seal free test	153
Figure 7.3 The spectrogram of the AE signal measured in static test	154
Figure 7.4 The spectrogram of the AE signal from transient speed test at 0 bar load.....	155

Figure 7.5 The spectrogram of the AE signal from transient speed test at different loads (a) 4 bar (b) 8 bar 156

Figure 7.6 AE signal for different operating conditions..... 157

Figure 7.7 The AE RMS values under different speeds and pressures 159

Figure 7.8 The AE RMS values in terms of duty parameter 161

Figure 7.9 The distribution of AE signals against normal distribution 162

Figure 7.10 The AE kurtosis values under different speeds and pressures 163

Figure 7.11 AE spectra for different operating conditions..... 164

Figure 7.12 AE spectra for lower speeds and different sealed pressures 165

Figure 7.13 AE spectra for higher speeds and different sealed pressures 166

Figure 7.14 The relationship between AE RMS value and sliding speed 169

Figure 7.15 The relationship between AE RMS value and sealed pressure in ML region 171

Figure 7.16 The relationship between AE RMS value and sealed pressure for higher speeds 172

Figure 8.1 Sealed pressure values during the partial dry running test..... 176

Figure 8.2 AE signal for healthy seal and partial dry running test..... 177

Figure 8.3 The AE RMS values for healthy seal and dry running test under different operating conditions 178

Figure 8.4 The AE kurtosis values for healthy seal and dry running test under different operating conditions 180

Figure 8.5 AE spectra for healthy seal and dry running test under different operating conditions 181

Figure 8.6 The relationship between AE RMS value and sliding speed in dry running test 182

Figure 8.7 The concept of parallel springs 184

Figure 8.8 The concept of increase in the net hydraulic loaded area 184

Figure 8.9 AE signal for healthy seal and spring out test..... 185

Figure 8.10 The AE RMS values for healthy seal and spring out test under different operating conditions 186

Figure 8.11 The AE RMS values for healthy seal and spring out test under different operating conditions 187

Figure 8.12 AE spectra for healthy seal and spring out test under different operating conditions 188

Figure 8.13 The relationship between AE RMS value and sliding speed in spring out test under 2 bar	189
Figure 8.14 The relationship between AE RMS and sliding speed in spring fault test under 5 bar	190
Figure 8.15 The relationship between AE RMS and sliding speed in spring out test under 7	190
Figure 8.16 The relationship between AE RMS value and sealed pressure in defective seal test.....	191
Figure 8.17 Common seal face defects.....	192
Figure 8.18 AE signal for healthy seal and defective seal test.....	193
Figure 8.19 The AE RMS values for healthy seal and defective seal test under different operating conditions.	195
Figure 8.20 The AE kurtosis values for healthy and defective seal	196
Figure 8.21 AE spectra for baseline and defective seal test	198
Figure 8.22 The relationship between AE RMS value and sliding speed in defective seal test under 8 bar	199
Figure 8.23 The relationship between AE RMS value and sliding speed in defective seal test under 5 bar	200
Figure 8.24 The relationship between AE RMS value and sliding speed in defective seal test under 8 bar	200
Figure 8.25 The relationship between AE RMS value and sealed pressure in defective seal test.....	201

LIST OF TABLES

Table 1.1 Summary table for limitations of mechanical seals CM	9
Table 1.2 Summary table for AE condition monitoring of mechanical seals.....	11
Table 1.3 Summary table for major limitations in previous works	11
Table 2.1 Duty parameter in different lubrication regimes	27
Table 2.2 Coefficient of friction in different lubrication regimes [79]	36
Table 2.3 PV limits of material pairs [91]	42
Table 2.4 Thermal effects on sealing gap.....	45
Table 2.5 Typical Properties of seal face materials.....	46
Table 3.1 values of density and phase velocities for different materials and waves.....	64
Table 4.1 Summary of typical statistical parameters used for continuous signals [101, 141]	81
Table 6.1 Specifications of deep groove ball bearings.....	123
Table 6.2 General specifications of the electrical motor	123
Table 6.3 The specification of John Crane Type 1648 mechanical seal	126
Table 6.4 Main parts of the auxiliary circulating system	127
Table 6.5 The general specifications of pump.....	131
Table 6.6 The parameters measured in the experiments.....	132
Table 6.7 Technical specifications of the Sinocera	135
Table 6.8 Technical specifications of the PCI-2	136
Table 6.9 Thermocouple specifications.....	138
Table 6.10 Pressure sensor specifications	139
Table 6.11 AE sensor specifications.....	140
Table 6.12 Shaft encoder specifications	141
Table 6.13 Summary of experimental program.....	143

LIST OF ABBREVIATIONS

AA	Arithmetical average
ADC	Analogue to digital convertor
AE	Acoustic Emission
BL	Boundary lubrication
BS	British standard
CFD	Computational fluid dynamic
CLA	Centre line average
CM	Condition monitoring
DAS	Data acquisition system
FEM	Finite element model
FFT	Fast Fourier transform
FIV	Flow induced vibration
FT	Fourier transform
HL	Hydrodynamic lubrication
ISO	International organization for standardization
KT	kurtosis
ML	Mixed lubrication
MSPS	Million Samples per Second
PZT	porous lead zirconate titanate
RMS	Root mean square
SK	Skewness
STFT	Short-time Fourier transform
WT	Wavelet transform
WVD	Winger-Ville distribution

LIST OF NOTATIONS

A	Area of a vibrating system/ Asperity deformation area
A_f	Sealing interface area
A_h	Net hydraulic loaded face area
A_i	Amplitude of particle displacement
A_s	Actual area of a contact
A_{tot}	Total contact area
A_0	Fluid induced asperity deformation area
B	Balance ratio
C	Damping coefficient
D	Number of asperity summits per unit area
D_b	Balance diameter
D_i	Inside diameter of sealing interface
D_o	Outside diameter of sealing interface
E	Elastic modulus /Hertzian contact elastic modulus
F	Axial load on a vibrating system
F_b	Body force
F_c	Closing force
F_D	Drag force
F_f	Frictional force.
F_h	Hydraulic force
F_N	Normal load
F_o	Opening force
F_P	Fluid pressure force
F_R	Resultant force on asperities

F_s	Spring force
F_{si}	Installed spring load
G	Duty parameter
G_E	Electrical conductance
H	Hardness of the softer contact surface
I	Area moment of inertia
K_e	The portion of elastic strain energy that is converted to AE
K_g	The gain of the AE measurement system
K	Pressure drop factor
K_m	Constant determined by the material system
K_w	Dimensionless wear coefficient
K_s	Spring stiffness
$K_{1,2,\dots,V,P}$	Proportional constants
L	Length
N	Number of data points
N_f	Frictional power lost
N_{tot}	Total number of asperity deformation
P_a	Pressure to be protected
P_f	Absolute sealed fluid pressure
P_s	Normal pressure in a single asperity contact
Q	Flow rate in the sealing gap
Q_L	Leakage rate in face seals
R	Radius of the curvature in the deformation area
R_a	Arithmetical average of roughness height
$P_{Contact}$	Asperity contact pressure

$P(t, \omega)$	Energy intensity at time t and frequency
Re	Reynolds number
Rq	Root mean square roughness
T	Duration of the AE signal
U_{AE}	AE energy released by acoustic emission sources
\dot{U}_{AE}	Rate of AE energy released
\dot{U}_f	Frictional acoustic emission signal rate
\dot{U}_{fT}	Total acoustic emission energy signal arte
U_{iAE}	AE energy released by a single asperity
V	Sliding speed
\bar{V}	Sliding velocity on the mean face diameter
V_E	Measured Electrical voltage
V_{rms}	RMS value of AE signal
V_w	Volume of wear
W	Contact load in asperity collision
$W(f)$	Function of frequency response of AE sensor
X	Displacement vector of a material point
a	Radius of circular contact area
a_f	Proportionality factor
$a(t)$	Recorded AE signal
b	Width of the seal face
c	Phase velocity
f_w^*	Complex conjugate of the wave signal
$f(t)$	Input signal to AE sensor
$g(t)$	Output signal of AE sensor

\bar{h}	Average film thickness
g	Gravitation force
l_s	Displacement of the free end of one asperity
m	Mass of a vibrating system
n	Number of asperity deformation in any unit area
n_i	Wave normal vector
s	Sliding distance
t	Time
$w(t)$	Transfer function of AE sensor
$w_a(t)$	Transfer function of amplifier
$w_f(t)$	Transfer function of filter
\bar{x}	Mean value
x_i	Data at each discrete point in time.
$z(x)$	Height of surface profile
$G(f), F(f), W(f)$	Fourier transforms of $g(t), f(t)$ and $w(t)$
Δ	Displacement of free end of a vibrating system
ΔL_i	Total spring compression
ΔL_w	Height worn away from the seal face
ΔP	Pressure drop across the seal
$\phi(z^*)$	Standard height distribution
ε	Normal stains in an asperity due to applied stress
ε_y	Yield strain of asperity material
ε	Strain
η	Dynamic viscosity
λ	Lambda elastic constant
μ	Fluid absolute viscosity

μ_L	Rigidity modulus
α	Positive constant determined by the size of sealing gap
β	Constant determined by the number of contact asperities
ν	Poisson's ratio
ρ	Density
σ	Standard deviation/ Normal stress
γ	Constant determined by sliding distance between asperities
σ_y	Yield stress of asperity material
σ^2	Variance
τ	Shear strength
φ	Phase of wave displacement
ω	Angular frequency
ω_n	Natural frequency of a vibrating system

CHAPTER ONE;

INTRODUCTION

This chapter provides an overview of the academic work in this thesis and gives a general background to the area of research. It first introduces an overview of seals highlighting different types and parts of mechanical seals. Then the range of commonly-encountered mechanical seal faults is explained with a view to identifying those which might reasonably be monitored using acoustic emission technique. Then the research background including the necessity and challenges for condition monitoring of mechanical seals is presented. This is followed by a brief review on different techniques that have been applied for monitoring the condition of mechanical seals. Finally, the motivation, research aim and the remaining structure of the thesis are outlined.

1.1 An Overview of Mechanical Seals

Seals are used throughout the world influencing on the reliability of pumps, compressors, turbines, mixers and etc. A seal is a device placed between two surfaces to prevent or reduce to a minimum acceptable level leak of gas or liquid from one region to another. They also prevent dirt from entering through those surfaces. Seals fall broadly into two categories, static and dynamic seals. Static seals such as gaskets are used when the mating surfaces are not subject to relative movement. A dynamic seal is a mechanical device used to control leakage of fluid when there is rotating or reciprocating motion between the sealing surfaces. Since the seal is designed to fit around the shaft or some part connecting to the shaft, dynamic seals are often called shaft seals. An example of static and dynamic seal application is shown in Figure 1.1.

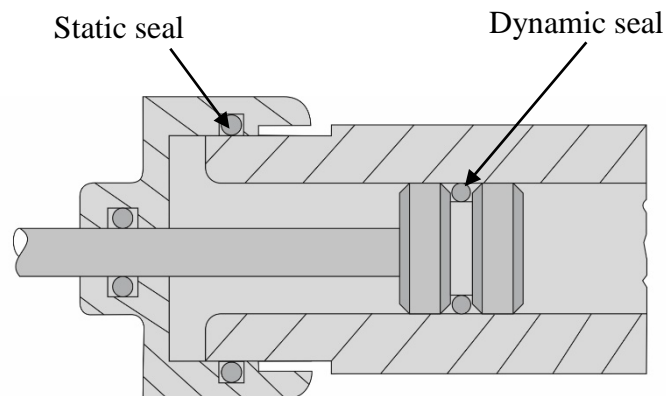


Figure 1.1 Static and dynamic seals

Dynamic seals can be classified into the contact seals where make contact with the moving part under positive pressure, and clearance seals which operate with predetermined positive clearance. The majority of dynamic seals such as mechanical seals come in the former category, where rubbing surfaces are separated and lubricated by a thin lubricant film [1].

Mechanical face seals known generally as mechanical seals or face seals have increasingly been used for sealing rotating shafts during last decades. Mechanical seals contain two annular faces that fit around a rotating shaft. One face known as runner or rotor which is attached to and rotates with the shaft (it is also called rotating face), and the other is attached to the device housing and is stationary. This face is known as the seal ring or the stator. Together they form the seal faces, which are very smooth, very flat and perpendicular to the shaft. One face is flexibly mounted and can be the "floating face" in the axial direction, usually with a spring, such that it can travel along the shaft axis to allow small relative motion in the axial or angular direction and hence to provide the flexibility for misalignment

between the parts, and the other face is fixed. The axially mounted spring on the shaft sealing assembly serves a fixed sealing force to the faces and hold them together to provide the static loading on the sealing gap.

Either the stationary ring or the rotating ring is rigidly mounted and the other is flexibly mounted, the floating face is also defined as the primary ring and the rigidly mounted one is referred to as the mating ring. These basic seal parts are shown in Figure 1.2

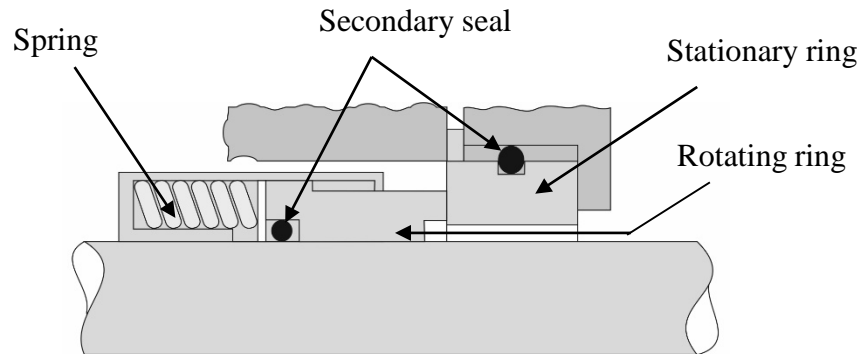


Figure 1.2 Schematic illustration of face seals

The seal faces restrict leakage by operating in close proximity to one another, so that any leakage through the seal assembly must be through the interface between the two faces, known as the face gap (the average distance between the two seal faces) or sealing gap. The seal face gap is of the same magnitude as the surface roughness (asperity contact).

Based on the Figure 1.2, there are also secondary seals in the assembly of mechanical seals. For example, O-rings are used between the rotating component and shaft or sleeve and between the stationary ring and gland plate. Secondary seals physically block gaps between the shaft, the housing, and the respective seal faces mounted to each preventing leakage by those routes and retain the sealing integrity. They also help to maintain close proximity between the annular seal rings under all operating conditions. The secondary seal can have a wide variety of different shapes and mechanism in addition to O-rings. Also, many seals contain anti-rotation pins to prevent the seal faces from rotating in undesirable directions.

Another important characteristic of a seal system is coning angle, or the taper of the face gap from the inner diameter of the seal ring to the outer diameter. This concept is beyond the scope of the present study and has been extensively discussed in the literature [2, 3].

Mechanical seals are divided into three very broad categories [4]: Elastomer-bellows seals, pusher seals, metal-bellows seals. In this thesis the primary interest is on pusher cartridge mechanical seals as shown in Figure 1.3.



Figure 1.3 Pusher type of mechanical seals

1.2 Failure Modes of Mechanical Seals

The reliability and performance of mechanical seals depends to a very large extent on its ability to maintain a thin fluid film that separates the stationary and rotating rings while simultaneously minimizing the duration and extent of mechanical contact between the mating surfaces. Too much contact force may cause dry running and overheat the face materials which increases wear rate and reduces seal life, not enough contact force may cause high leakage rate as shown in Figure 1.4. Based on the work of Summers-Smith [5], the existence of at least one of the following situations is an indication of mechanical seal failure:

- Excessive loss of fluid from the system being sealed;
- Excessive reduction of pressure within the system being sealed;
- Excessive addition of barrier fluid into the system being sealed (double seal installations).

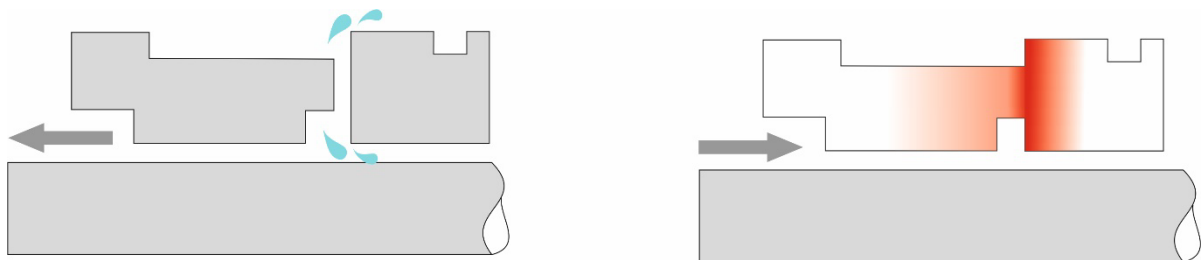


Figure 1.4 Effect of seal gap can produce leakage (left), or excessive contact (right)

Lebeck [1] classified more than 60 direct or contributing failure causes into three broad groups: environmental factors, design and manufacture, operation and installation. The environmental group includes all of the causes that may naturally occur in a mechanical seal environment as a consequence of the process itself. For instance, sealed fluid with very low or high viscosity are classified into the environmental group. The design and manufacture group consists of factors that may lead to seal failure due to incorrect design and errors during manufacture. All of the deviations from expected operation that might be encountered and directly lead to failure, such as excessive radial or axial vibration of shaft or abrasive particles in the operational system, are classified into the operation and installation group. Therefore each of the individual components of the mechanical seal may contribute to a potential failure, Figure 1.5

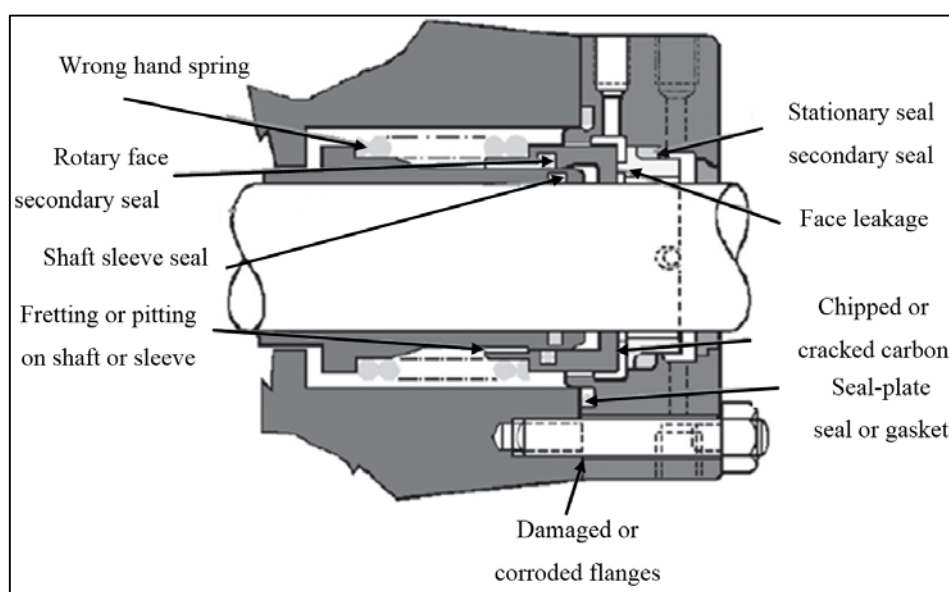


Figure 1.5 Examples of the common types of faults in mechanical seals[4]

The interaction of the failure causes often occurring in practice makes the failure even complicated [4]. Moreover, mechanical seals are exposed to widely varying operating conditions (temperature, sealed fluid pressure and rotational speed), sometimes operating conditions change to become quite different from the specific conditions for which the seal was intended. For instance, mechanical seals may experience transient conditions at start-up and shutdown, opening and closing of a valve, weak lubrication system, fluctuations of pressure, temperature and flow, fluid transient vaporization, high sealed pressure conditions and structural deflections because of pipe loads or thermal expansions etc. The chart shown in Figure 1.6. is an example of the reasons for seal failures. The survey reveal that dry

running and wear, which normally cause the damage of the seal faces, are the main reasons that can lead to failure of mechanical seals.

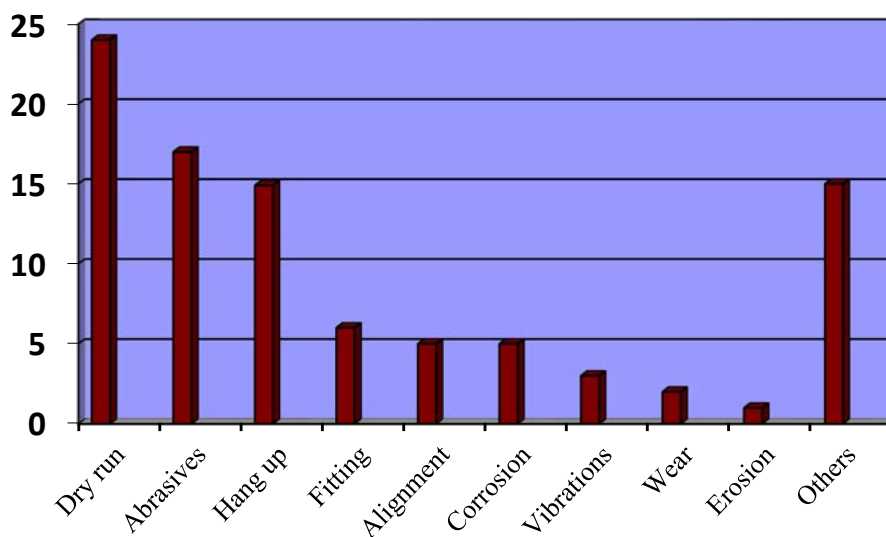


Figure 1.6 Causes of mechanical seals failure [6]

Therefore, to a large extent mechanical seal failures are attributed to mal operation of machinery (i.e. allowing pump to run dry) which are not potentially a fault with the seal itself. The view is widely held that the risk of failure is smaller when operating conditions are certain [6]. Hence the investigation of the effect of different operating conditions on the tribological behaviour of mechanical seals is of high importance to make sure that the mating faces continue to perform the functions for which they were intended.

1.3 Research Background

Although mechanical seals were originally designed to lend a greater sealing capability than could be achieved using common packing, they are now the most common type of seal found on centrifugal pumps, propeller shafts in ships and submarines, compressors, liquid propellant rocket motors in aerospace industry and in similar applications. A review of sealing technology [7] reiterated the important role of mechanical seals in rotating machines. For instance, about 95 % of the rotating equipment used in chemical processes adopts the mechanical seal for preventing leakage between shaft and shell [8]. The reason for such a popularity arises from the fact that mechanical face seals can protect against leakage across much higher pressure differences than the other types of dynamic seals. According to another statistic [9], among the sealing devices of rotary machines in industrially advanced countries,

mechanical seals account for about 90% of all sealing devices. For instance in China, mechanical seals are adopted in 80%-90% of centrifugal pumps [9].

Due to wide range application in industry, seal failures may cause direct (such as leakage and loss of fluid) as well as indirect (downtime and maintenance cost) losses. Moreover, failure of sealing devices directly affects the working status of a machine and has a great impact on the reliability of the whole system. A well-known example of this is the disaster of the space shuttle Challenger that occurred in 1986, claiming the lives of the all crew members. Subsequent investigations determined the cause of the accident was the failure of an O-ring in the solid rocket booster that was unable to seal a critical gap [10].

In 1999, Semple [11] claimed that the failure of pumps directly related to seals could drop from 52% to 9% if proper selection and engineering of the seal system were carried out. It has been shown that 52% of pump failure is caused by seals [11] and approximately 70% of pump maintenance cost in the refining industry is estimated to be related to mechanical seals [6]. Such seal failures indicating the role of monitoring the operational condition of mechanical seals if properly achieved can significantly reduce the maintenance costs.

The industry looks forward to techniques that can predict the failure of mechanical seals so as to avoid emergency shutdowns, improve performance of seals and reduce maintenance costs. Condition monitoring has received considerable and wide spread attention throughout most of the industries employing rotating machines [12]. It is increasingly becoming common in industry because of the needs to prolong machine life, increase reliability and decrease possible loss of production due to machine breakdown.

Different condition monitoring techniques are researched to predict seal life and to avoid premature failure. However, progress in the field of condition monitoring has been less than in design and manufacture. This is due to the fact that mechanical seal faces unlike motors, bearings, gear boxes and other types of rotating machinery has a wide diversity of working conditions. The environment is variable and is influenced by many factors such as changes to the pump flow rate, changes in fluid property and changes in mechanical vibration due to misalignment, bearing or coupling wear and dynamic balance.

The situation may get worse because the seal faces are low power consumption components (although it is an advantages itself), this property makes the signals from mechanical seals very weak compared to the signals from other components in rotating

machinery. Moreover, face seals are separated by extremely thin lubricating film and it is difficult to measure signals that can adequately represent their critical lubrication condition.

Since the phenomena of heat transfer, mechanical and thermal distortion, surface topography effects as well as tribology science are mixed together [13], the reliable condition monitoring program of face seals should include all these complex variables as shown in Figure 1.7.

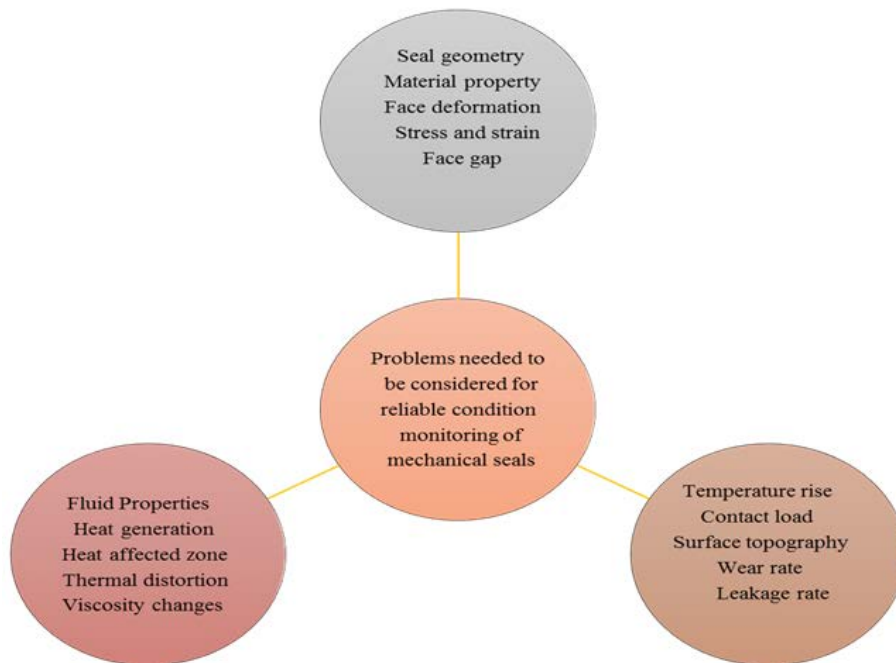


Figure 1.7 The interactive nature of a mechanical seal system

1.3.1 Condition Monitoring of Mechanical Seals

On the basis that a “significant change is indicative of a developing failure” [14], condition monitoring is a monitoring process or a sensitive tool that focuses on early detection of faults and failures of machinery by employing combinations of sensors and signal processing equipment that provide continuous indications of component to minimize downtime and maintenance costs [15].

Since run-to-failure maintenance is the most economic strategy under some low or even medium severe working condition of mechanical seals [16], the development of reliable condition monitoring is of high importance to avoid emergency shutdowns and great loss of production, especially in industry process applications, which is generally very high compared to the value of the seal itself.

Many condition monitoring techniques can be applied to evaluate the integrity and monitor the condition of industrial components. In the case of mechanical seals, different monitoring techniques based upon vibration analysis[16], eddy current [17, 18] and ultrasonic method [19, 20] have been used. Table 1.1 summarizes some limitations related to the mentioned methods. This is discussed extensively in Section 4.1.

Table 1.1 Summary table for limitations of mechanical seals CM

Applied method	Limitation(s)
Vibration analysis	<ul style="list-style-type: none"> ● Influenced more by the shaft speed rather than the frictional state of sealing gap
Eddy current	<ul style="list-style-type: none"> ● Cannot be used to monitoring of mechanical seals operating in the mixed or boundary lubrication regimes. ● Require modifying the device structure
Ultrasonic testing	<ul style="list-style-type: none"> ● Unable to evaluate the severity of contact. ● Cannot be used when the rings are fully separated due to the hydrodynamic lubrication

1.3.2 Acoustic Emission Condition Monitoring of Mechanical Seals

Materials naturally release elastic energy when they are deformed, which is known as acoustic emission (AE) or stress wave emission [21]. During the recent years, many researchers have investigated the development of AE applications for monitoring the condition of rotating machines such as bearings [21, 22], wind turbines [23] and gearboxes [24]. The principles and fundamentals of this technique is discussed in Chapter 3.

Studies on the AE condition monitoring of contacting mechanical face seals dates back to the 1960s. In his pioneering work, Orcutt applied AE technology to investigate the sealing breakdown (leakage) of mechanical seals, however, it was not able to distinguish the signals generated by the contact of the faces from the strong background noises [25]. Technically, the barrier for a successful AE condition monitoring is the difficulty in distinguishing signals generated by the seal itself from those by other sources and from background noise, as pointed out by Anderson et al. [26]. This requires an appropriate experimental procedure and signal processing method.

Later on with progress in the signal processing techniques, F.Y Edward et al. applied an effective algorithm to extract monitoring information from the AE signals measured from the contact of the seal faces under very noisy conditions such as the presence of particles in pump fluids [27]. They integrated high order statistics with the multiple signal classification algorithm to improve the ability of suppress signal noises. In 2015, Xiaohui Li et al. developed a new approach based on generic particle filter with auto regression and hypersphere support vector machine to reduce the background noises in AE monitoring of mechanical seals [28]. They claimed that this method can effectively restrain the background noises and make the signal energy more stable.

Since the energy of AE signals carry information about the details of frictional contact between seal faces, acoustic emission energy method has been proved to have promising potential for detecting incipient failures of mechanical seals such as leakage and dry running. Few researches are available in this area with positive outcomes [29-32]. Although not all researchers have equal success identifying the mentioned faults, the main difficulty with such investigation is that seal damage is needed to be simulated on test rig under realistic condition. Moreover, most of the previous studies have been undertaken in laboratories with non-ceramic materials samples [33-35], the application of results to the modern ceramic seal faces in industrial applications must be undertaken with caution as stated by Sikorska and Mba [36].

Whilst the effectiveness of acoustic emission measurements for mechanical seal diagnosis is well established (Table 1.2), the application of this technique in the field of tribology and early fault detection in mechanical seals is still in its infancy (Table 1.3). Based on the above understandings it is clear that the AE features which may help to explore the tribological behaviour of mechanical seals are needed to be more investigated in the real applications. To achieve this, the proper frequency range related to dominant AE sources is needed to be identified and analysed using theoretical models and associated signal processing methods.

At present some difficulties in fault generating in a controlled environment caused inconclusiveness in development of a strong diagnosis and prognosis for mechanical seals [36]. AE technology has also been proved to be a sensitive indicator of lubrication conditions and changes in the lubricant properties [37, 38], however, as a primary phase for accurate seal monitoring, the identification of different tribological regimes in mechanical seals has not been reported yet.

Table 1.2 Summary table for AE condition monitoring of mechanical seals

Reference	Major contribution
Orcutt. F, 1969 [25]	Detect failure of mechanical seals (defective seal).
Kataoka.T et al., 1987 [29]	Investigate the dependency of AE levels on the integrity of the mechanical seals.
Miettinen.J. and V. Siekkinen,1995 [30]	Diagnosis the leakage, dry running and cavitation.
Holenstein. A.P,1996 [32]	AE in time domain (RMS and energy) is used for diagnosis damage.
Anderson. D et al., 2000 [26]	Demonstrate the difficulty in distinguishing between signal and noise.
Mba. D. et al., 2006 [31]	Detecting the onset and duration of seal-to-seal contact.
Fan. Y.E, 2007 [16]	Modelling AE energy in terms of seal working parameters, AE features in time domain, frequency domain and time frequency domain are studied.

Table 1.3 Summary table for major limitations in previous works

Reference	Major limitation(s)
Orcutt. F, 1969 [25]	Low signal to noise ratio
Kataoka.T et al., 1987 [29]	No clear trend in AE level is reported in case of leakage
Miettinen.J. and V. Siekkinen,1995 [30]	Not realistic faults especially in leakage test by creating radial groove in face, tests are not carried out under near isothermal conditions.
Holenstein. A.P,1996 [32]	It is not proved that the AE level increases with the growing damage of the seal.
Mba. D. et al., 2006 [31]	Low sealed pressure (atmospheric conditions), tests were not carried out under near isothermal conditions, only commence of contact is studied.
Fan. Y.E, 2007 [16]	Lubrication regimes are not considered, direct asperity contact is studied under hydrodynamic lubrication regime.

1.4 Research Motivation

Mechanical seals have become the most popular sealing devices for rotating machines because of low leakage rate and long life under proper operating conditions. However, unpredictable seal failures with the seal life equal to two days to two months have been observed in some processes. This failure frequency is so high that they are even regarded like the fuse in an electrical system. Such unpredictable life of the same seal may occur due to improper design, wrong assembly, and diversity of operating parameters or incomplete operating instructions. For this reason, the need for reliable monitoring the condition of mechanical seals increases constantly. The conclusion drawn from previous works can be summarized as following:

- Progress in the field of condition monitoring of mechanical seals has been slow due to wide diversity of their working environment that can be variable and influenced by many factors.
- The available methods such as eddy current and ultrasonic testing can't be efficiently used in industry for reliable on-line condition monitoring of mechanical seals. Some of them require modifying the device structure, others have very expensive cost.
- Most of the available methods can only measure commence of contact at the sealing gap and hence, they cannot be used efficiently to distinguish different lubrication regimes in face seal.
- AE has been proved to be a sensitive indicator of lubrication conditions and changes in sealed fluid properties, however the application of technique for identification of lubrication regimes in mechanical seals has not been reported yet.
- AE has been applied for detecting the faults in mechanical seals. However, the development of a robust detection and prognosis system for mechanical seals is being thwarted by difficulties in generating failures in a controlled, but realistic environment.
- Despite a lot of published work, the application of AE technology to monitoring the integrity of mechanical seals has been slow to develop and has not been well documented.

- Direct asperity contact has been modelled, however the lubrication state in sealing gap as well as fluid borne AE signals have not been considered yet.

This thesis will add to the methods listed above, monitoring the tribological behaviour of mechanical seals by the use of non-intrusive AE measurements for the purpose of fault detection at early stages.

1.5 Aims and Objectives

The aim of this research is to develop a novel effective technique based on the acoustic emission measurements for condition monitoring of mechanical seals. This includes monitoring different lubrication regimes, investigate dominant AE sources based on tribological behaviour of sealing gap and apply this information to detect the premature failures of mechanical seals. It is clear however that occurs in a wide variety of operating parameters (especially rotational speed and sealed fluid pressure) and failure modes. Therefore, it is necessary and essential to concentrate on a certain area to make the research more effective. Studies in this thesis will focus on the failure of the mating and primary rings as well as sprig fault; the failure of secondary seals will not be covered.

The direct asperity friction, elastic deformation of asperities due to stress field of lubricant fluid and viscous friction in the sealing gap will be highlighted. These are strong acoustic emission sources in sealing gap and has critical influence on the tribological behaviour of mechanical seals. The AE sources will be mathematically modelled and verified. The developed models will be valid for a wide variation in film thickness covering some of the boundary, mixed and hydrodynamic lubrication regimes.

To overcome the deficiencies of aforementioned researches, a comparative experimental program has been designed and carried out to identify the proper frequency band that can present the tribological behaviour of mechanical seals. Moreover, the project will develop advanced signal processing techniques based on MATLAB post-process computational analysis.

In summary, this thesis will focus on three key topics: developing novel acoustic emission techniques, monitoring tribological behaviour of sealing gap and early fault detection in mechanical seals. The following objectives are identified:

Objective 1: To perform a literature review and establish the theory, evidence and knowledge gaps in relation to nonlinear tribological behaviour and condition monitoring of mechanical seals.

Objective 2: To carry out a comprehensive literature review and provide a theoretical basis for monitoring the tribological behaviour of rotating machines based on AE measurements.

Objective 3: To improve the performance of and design and construct new parts for available mechanical seal test rig to simulate wide range of operating parameters and desired faults.

Objective 4: To model the acoustic emission level caused by different AE sources at the sealing gap in terms of operating speed, load and other working parameters.

Objective 5: To develop MATLAB codes for processing the data outputs from the sensors.

Objective 6. To design a comparative experimental program to find the proper frequency band that can present the tribological behaviour of sealing gap.

Objective 7. To design and carry out an experimental program that simulates different lubrication regimes in the operation of mechanical seals.

Objective 8. To extract of the effective AE features to monitor the tribological behaviour of mechanical seals

Objective 9. To implement experiments to replicate common faults in the mechanical seals.

Objective 10: Study and verification of developed mathematical models to investigate tribological behaviour of mechanical seals and for detecting faults.

Objective 11: To provide future researches in condition monitoring of mechanical seals with a new and different idea for further work.

1.6 Organization of Thesis

The thesis is organized into nine chapters including the present chapter. The basic outline of the thesis is as follows:

Chapter 2: Presents a literature review on the tribological behaviour of mechanical seals highlighting lubrication regimes, friction, wear and heat transfer considerations.

Chapter 3: Describes the basic principles of the acoustic emission and its applications for condition monitoring of rotating machines as well as a brief discussion on propagation of elastic waves.

Chapter 4: Explain a summary of the state of knowledge of the areas relevant to the condition monitoring of mechanical seals using AE measurements and other methods. This chapter mainly presents a critical discussion of the different monitoring approaches applied to mechanical seals so far. This assists in avoiding replication of previous works.

Chapter 5: Presents the mathematical models to explain AE energy released from different sources at the sealing gap. The model is used to study the influence of different operating conditions on the elastic energy generated by AE sources.

Chapter 6: Details the test facility used for the study and lists the equipment used together with specifications and operating principles of the rig. Test procedures and faults seeding are also detailed in this chapter.

Chapter 7: Provides an in-depth discussion of the results of the experimental research on the tribological behaviour of mechanical seals using AE measurements. The main body of this chapter is related to investigate the AE features under different lubrication regimes. The discussion also compared the test results with the AE model developed in Chapter 5.

Chapter 8: Discusses the results of a fundamental investigation on the potential of the AE technology for the purpose of fault detection in mechanical seals. The main objective of this chapter is the comparison and discussion of the results of base line tests against the faulty seal.

Chapter 9: presents conclusions based on the findings and outlines recommendations for future work.

Chapter Two;

Tribological Behaviour of Mechanical Seals

This chapter reviews the material in relation with the tribological behaviour of mechanical seals from the literature. It first introduces the principles of mechanical seals. An understanding of their operation is presented along with constructional details and key characteristics. Then the tribology concept is presented. Focus is paid to the lubrication regimes of mechanical seals as well as dimensionless parameters usually used to characterize the tribological regimes of the sealing gap. This is followed by the concept of surface metrology, friction, wear and heat transfer in mechanical seals. All mentioned concepts are closely related to tribological behaviour of mechanical seals. Finally, the seal face material is discussed.

2.1 The Principles of Mechanical Seals

Mechanical face seals are used throughout the world as a key component of many rotating machines. Since the reliability and performance of the face seals is of high importance to prevent emergency shutdowns and reduce maintenance costs, understanding of their nonlinear tribological behaviour is a crucial consideration for the purpose of condition monitoring. This section deals with the principles of mechanical seals as well as design parameters that are usually discussed in connection with the tribology of the sealing gap.

2.1.1 Internal vs. External Pressurized Mechanical Seals

Mechanical face seals can be installed in two different ways, depending on whether the seal is mounted inside or outside the seal chamber:

1. Inside mounting: In this configuration the pressurized fluid is sealed on the outer periphery of the sealing gap, which is called an outside (or forward) pressurized seal, see Figure 2.1 (a). This is the most common arrangement, here the pressurized fluid acts with the spring load to keep the seal faces in contact.
2. Outside mounting: In this configuration the fluid under pressure is on the inside of the seal as shown in Figure 2.1 (b) and the seal is called inside (or reverse) pressurised. This configuration is used for low pressure applications [2]. It should be noted that all discussions in this thesis are for outside pressurized mechanical seals.

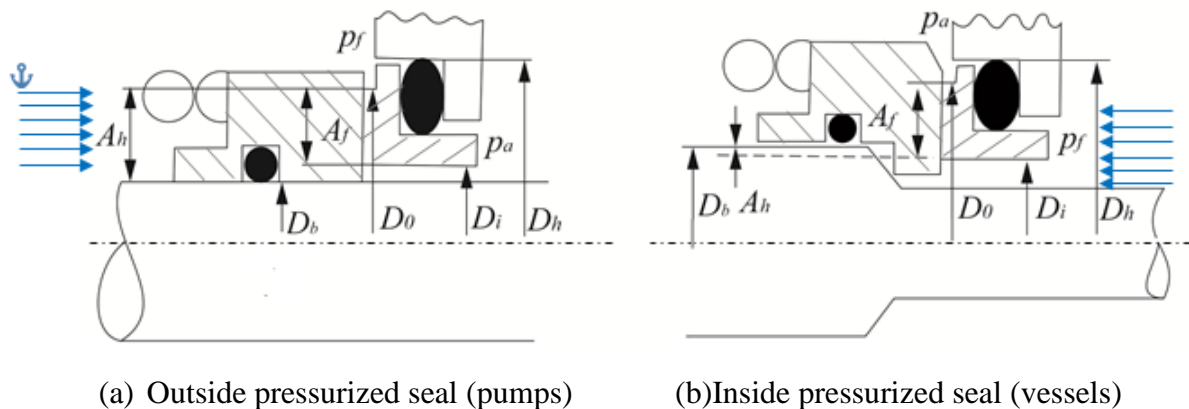


Figure 2.1 Interval vs. external mechanical seals

where:

P_f is the absolute sealed fluid pressure [bar]

P_a is the pressure to be protected, for most seals is the atmospheric pressure [bar]

A_h is the net hydraulic loaded face area [m²]

A_f is the sealing interface area [m²]

D_o is the outside diameter of sealing interface [m]

D_i is the inside diameter of sealing interface [m]

D_b is the balance diameter [m]

D_h is the hole (chamber) diameter [m]

2.1.2 Balanced VS. Unbalanced Mechanical Seals

An important seal design parameter, widely used term in the sealing industry is the balance ratio. It is often used to describe the relationship between the net hydraulic loading (closing) area and the sealing interface (opening) area and refers to the difference between the pressure of the sealed fluid and the contact pressure between the seal faces. The balance ratio controls the axial load acting on the sealing gap and determines how effective the mating faces matched. For an outside pressurized seal the balance ratio is defined as [2, 3, 16] :

$$B = \frac{A_h}{A_f} = \frac{D_o^2 - D_b^2}{D_o^2 - D_i^2} \quad (2.1)$$

When balance ratio is greater than 1, the seal is called unbalanced or over-balanced, while a balanced seal has a balance ratio value lower than 1, Figure 2.2. Based on Equation (2.1), if the sealing interface area is held constant and the hydraulic loaded face area is decreased the seal would be balanced. In practice it is achieved with a shoulder on a sleeve or seal hardware to reduce the net hydraulic loaded area. Consequently, the effective face contact pressure is always less than the fluid pressure which helps to reduce the friction, wear and heat generation at the sealing gap. In an unbalanced seal the sealed fluid pressure is not relieved by the face geometry and the seal faces withstand full system fluid pressure in addition to spring pressure.

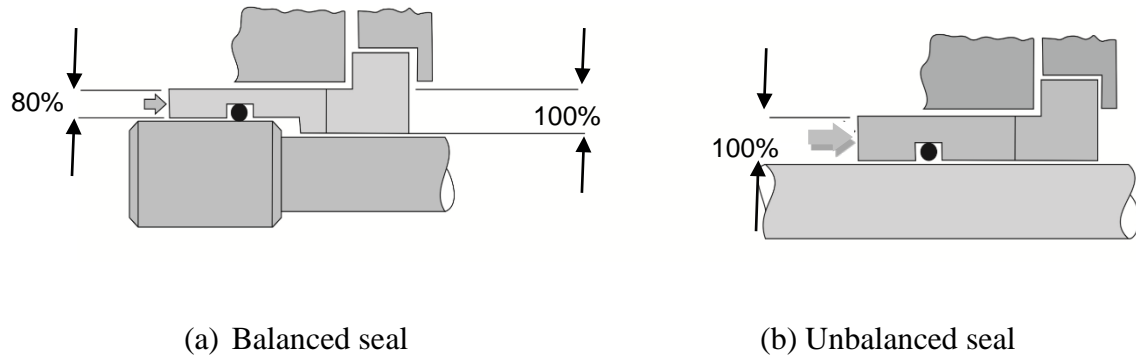


Figure 2.2 The concept of balance ratio

2.1.3 Closing Force VS. Opening Force

A useful theory of face seals operation can be developed by considering some simplifying assumptions. Assuming constant physical properties, laminar and incompressible flow, the leakage rate in face seals, Q_L , is directly proportional to the average film thickness cubed as well as the pressure drop across the seal, and is inversely proportional to the fluid viscosity as depicted in Equation (2.2) [3]:

$$Q_L \propto \frac{\Delta P \times (\bar{h})^3}{\mu} \tag{2.2}$$

As discussed in Section 1.1, the success of the seal depends on maintaining a very small sealing gap between the rotating and stationary rings. Since forces on the primary ring determine its axial location, in order to assure a small gap, the opening forces should balance the closing forces as shown in Figure 2.3. It should be noted that forces act to close the sealing gap are closing forces and forces that widen the sealing gap are opening forces.

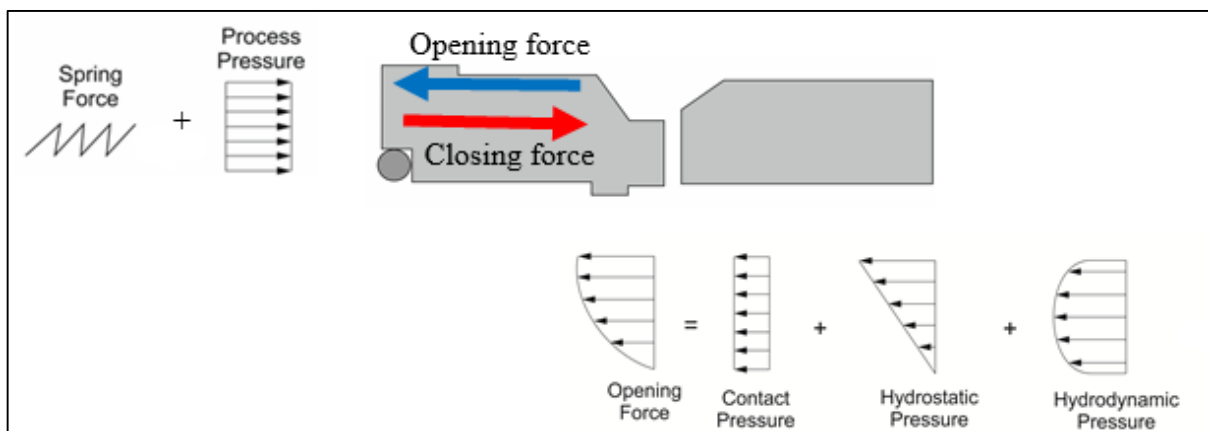


Figure 2.3 Forces acting on sealing gap [39]

As illustrated in Figure 2.3, the closing force has two components. The sealed pressure acts on the backside area of the seal face along with the spring force that acts to insure positive closing force at low pressures as well as during assembly. Thus the total closing force on the primary ring is the sum of the spring force and the hydraulic force produced by the sealed pressure:

$$F_c = F_s + F_h \quad (2.3)$$

where:

F_s is the spring force

F_h is the hydraulic force

The hydraulic closing force is obtained from Equation (2.4) [16]:

$$\begin{aligned} F_h &= A_f \times B \times P_f + A_f \times (1 - B) \times P_a \\ &= A_f \times (B \times \Delta P + P_a) \end{aligned} \quad (2.4)$$

For moderate to high pressures, the closing force exerted by the springs is often negligible when compared with the hydraulic forces. However in low pressure applications the spring pressure is of the same magnitude as the hydraulic pressure [16].

The closing force is simple to obtain for a specific seal design and is generally constant during seal operation. However, since any pressure force on the sealing interface area tends to open the faces and it varies during seal operation, it is difficult to calculate opening force. Considering the fact that the sealing gap is of the same magnitude as the surface roughness height, the opening force can be expressed based on sealed pressure, P_f , and asperity contact pressure, $P_{Contact}$:

$$F_o = \int_{A_f} P_f dA + \int_{A_f} P_{Contact} dA \quad (2.5)$$

One of the main assumptions made here is that the sealed pressure enters in the sealing gap due to radial pressure gradient between pressurized fluid and the atmospheric pressure and

distributes itself such that the average value of the hydrostatic fluid pressure in the face gap is proportional to the sealed pressure. It means seal faces will quickly reach a point of equilibrium where the closing force will be balanced by the opening force. If the closing force was the only force acting on the seal faces, there would be little fluid film and the faces would run hot and eventually fail. Thus the total closing pressure has to be supported by the mean hydrostatic pressure in the sealing gap. The mean hydrostatic pressure is defined as the integral of the pressure drop factor, K , times the sealed fluid pressure, P_f , over the face sealing interface area, Equation (2.6). Pressure drop factor is discussed in next Section.

$$P_{hys} = \int_{A_f} K P_f dA \tag{2.6}$$

When the mean hydrostatic fluid pressure is not capable of supporting the closing force, the rest of load has to be supported by both hydrodynamic pressure and the direct asperity contact pressure. In general, the pressure within the sealing interface can be classified into hydrostatic and hydrodynamic pressure according to the generation mechanism, these concepts are discussed in Section 2.1.5. Thus the total opening force can be expressed as:

$$F_o = \int_{A_f} P_{hys} dA + \int_{A_f} P_{hyd} dA + \int_{A_f} P_{Contact} dA \tag{2.7}$$

2.1.4 Pressure Drop Factor

The pressure drop (gradient) factor, K , is a function of the pressure profile at the sealing interface and its value greatly affects the contact pressure. Since the seal faces move relative to one another, the ratio of the inlet to outlet face opening changes. This is why the concept of pressure drop is arguably the most unpredictable parameter in Equation (2.6). Figure 2.4 shows different K values for different pressure profiles at the sealing gap [1, 40]. As it is illustrated, in a divergent pressure profile the pressure distribution falls off rapidly while in a convergent distribution the pressure falls off slowly.

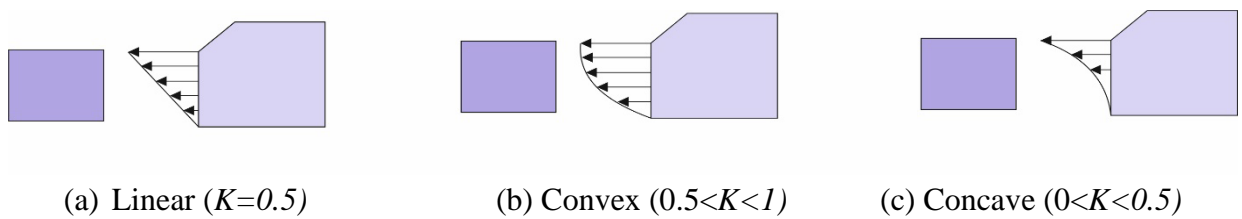


Figure 2.4 Pressure drop factor configurations

Linear pressure profile is approximately achieved when the faces are parallel and flat, the seal gap and geometry are axisymmetric, the pressure differential is low and the effects of compressibility are small. Depending on the design, under specific operating conditions of extreme temperature or pressure gradient, the seal faces often lose conformity and cease to run parallel [1].

2.1.5 Hydrostatic Vs Hydrodynamic Pressure Distribution

A lot of research has been carried out on the lubrication of mechanical seals during last 50 years. As discussed in Section 2.1.3, the generation of fluid pressure between the seal faces can be divided into two main mechanisms: hydrostatic lubrication and hydrodynamic lubrication.

In general, hydrostatic lubrication means that the pressure distribution in the sealing gap is derived from only the sealed pressure and does not directly depend on the relative motion of the seal rings. Several works have been published on the mechanism of hydrostatic pressure generation by e.g. [1, 41] and it is well understood. However, hydrodynamic lubrication of mechanical face seals is a difficult area and needs to be further investigated.

Several mechanisms have been proposed by different researchers to describe hydrodynamic pressure distribution, an extensive literature survey has been given in [42, 43]. Theoretically Reynolds equation derived from the Navier-Stokes equations is applied to describe hydrodynamic pressure generation as detailed in [2]. It was also believed that surface topography in seal faces, pressure gradient, thermal distortion, viscosity wedge, asperity to asperity collision and micro asperity lubrication, as well as anti-rotation devices such as drive pins used in the seal design have an influence on how the hydrodynamic film develops between the sliding surfaces.

Lebeck evaluated various proposed theories and confirms that the evidence of hydrodynamic load support is clear, however most of the previously proposed sources are inadequate to produce such load support [43]. He showed that residual waviness and misalignment which are the most important deviations from ideal parallelism of faces have the strongest effect on hydrodynamic fluid pressure [43]. The effect of surface texture is further discussed in section 2.3.

2.2 Tribology Concept

Tribology is defined as the science of interacting surfaces in relative motion dealing with the technology of lubrication, control of friction and prevention of wear. The word itself was first used in England the 1960's and comes from the Greek word “tribos” meaning “to rub” and from the suffix, “ology” means “the study of” [44]. Science and technology of tribology provide industry with design tools for failure analysis and developing beneficial maintenance and monitoring schedules. An improvement in the engineering practice of tribology through better understanding of contact mechanics problem may involve savings in the millions of Pounds. Textbooks usually discuss the economic impact of tribology in their introductions, an extensive literature review is found in [45].

2.2.1 Mechanical Seal as a Tribosystem

A mechanical seal is an assembly of a great number of systems in which surfaces operate under different lubricated conditions. The seal is made between the very smooth and flat faces of two annular rings, one is mounted on the shaft and rotates during operation and the other is mounted on the housing and is stationary. The structure of a typical mechanical seal is schematically shown in Figure 2.5. As illustrated, sealing interface is composed of two faces in relative motion which are interacting with each other under the lubricated conditions, therefore face seals can be considered as a tribosystem.

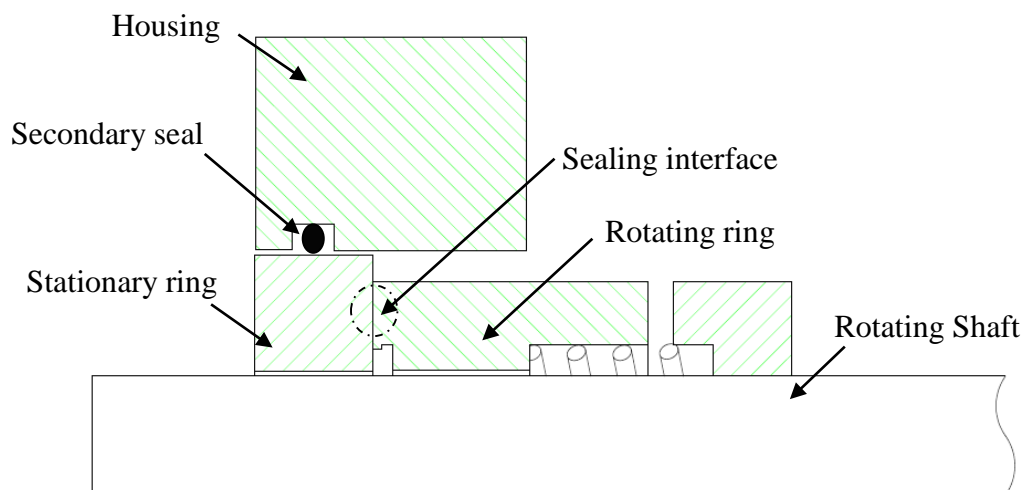


Figure 2.5 Schematic illustration of mechanical seals as a tribosystem

If the lubricant is not able to separate the mating faces, asperity contact takes place at the microscopic level, Figure 2.6. The severity of contact depends on the operational conditions such as load, sliding speed, temperature, type of lubricant as well as the surface roughness [46]. In time due to friction between the surface components, wear appears and changes the roughness and micro geometry which can finally result in the failure of the system. It should be immediately noted that the purpose of tribological studies in this research is to establish a scientific approach to predict friction state in mechanical seals based on acoustic emission measurements for the purpose of early failure detection in the operation of mechanical seals.

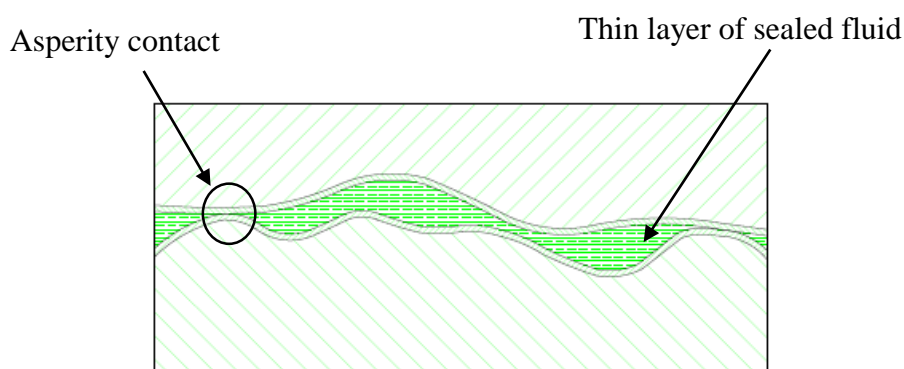


Figure 2.6 Schematic illustration of asperity contact in the sealing interface

2.2.2 Lubrication Regimes

Lubrication is defined as “the application of a suitable lubricant between two surfaces in relative motion for the purpose of reducing friction and wear” [44]. The lubrication condition between the rotating and stationary rings can be classified as dry friction, boundary lubrication (BL), mixed lubrication (ML) and hydrodynamic lubrication (HL) depending on the operational conditions as shown in Figure 2.7.

Before the fluid film is formed in the sealing gap, seal faces contact together. When the equipment starts to rotate, the sliding speed and film pressure is very low and the seal faces are not separated. Direct contact friction (dry friction) occurs between the faces where there is no lubrication film. In this case, there have serious friction losses, but small leakage.

At low values of sliding speed, the load is completely carried by the interacting asperities of the contacting surfaces and this is called boundary lubrication regime. This lubrication mode is the unwanted operating regime for mechanical seals, because it generates excessive friction, wear, and quickly damages to the mating faces. During the seals’ operating life, they face boundary lubrication during start-up, shutdown, low excitation speed, weak

lubrication system and high sealed pressure conditions. In the boundary lubrication regime friction and wear are controlled by the protective layers built on top of the rubbing surfaces.

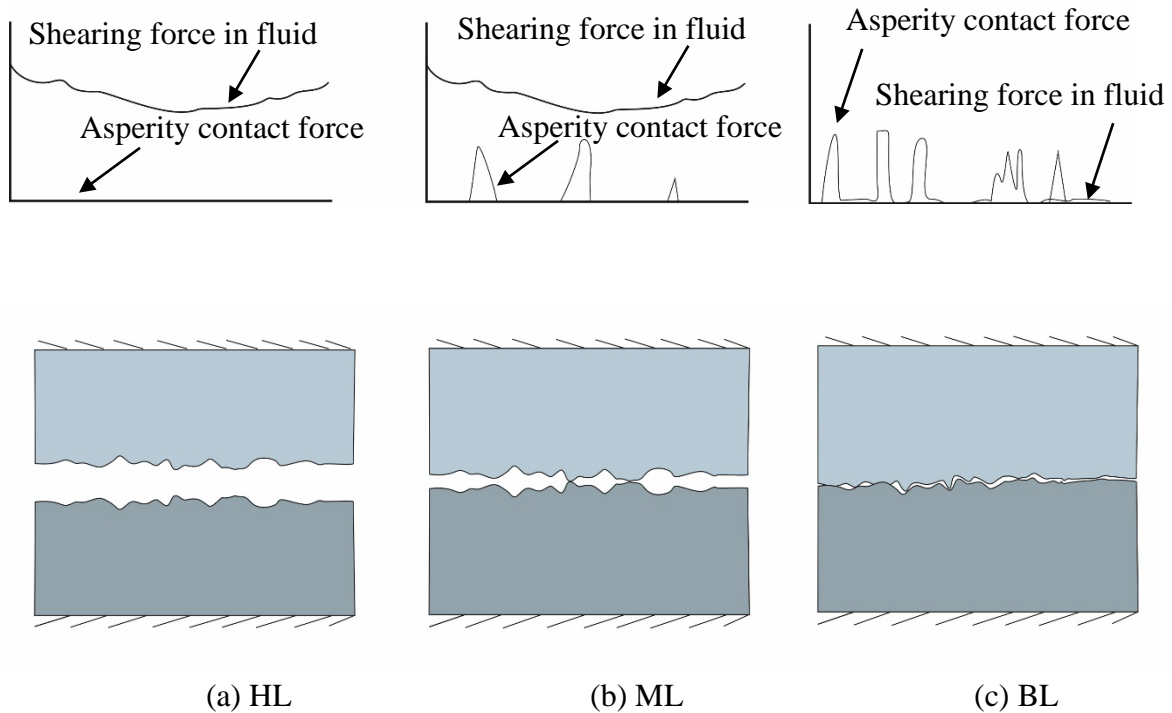


Figure 2.7 Asperity level illustration of Lubrication regimes

Under hydrodynamic or full film lubrication regime the faces do not contact each other and are fully separated by a fluid film due to hydrodynamic pressure build-up caused by rotational movement of mating faces. When the faces are hydro dynamically lubricated the load is transmitted by the lubricant and all shearing takes place in the fluid layers. Hydrodynamic lubrication maximizes seal life by eliminating wear caused by face contact during normal operation, but results in a higher leakage rate.

The last lubrication regime is mixed lubrication regime in which the fluid pressure is not capable of fully separating the seal faces and asperity contact will occur. This regime is considered to be a transition regime between boundary and hydrodynamic lubrication regimes, and hence the load on the faces is carried by both the fluid film and the asperities.

After his research on the bearing lubricity in 1900~1902, Stribeck was the first who masterfully reported the dependency of the coefficient of friction of a lubricated system as a function of rotational speed in the so-called Stribeck curve. In the generalized Stribeck curve, the coefficient of friction, f , is plotted as a function of operating parameters as schematically shown in Figure 2.8

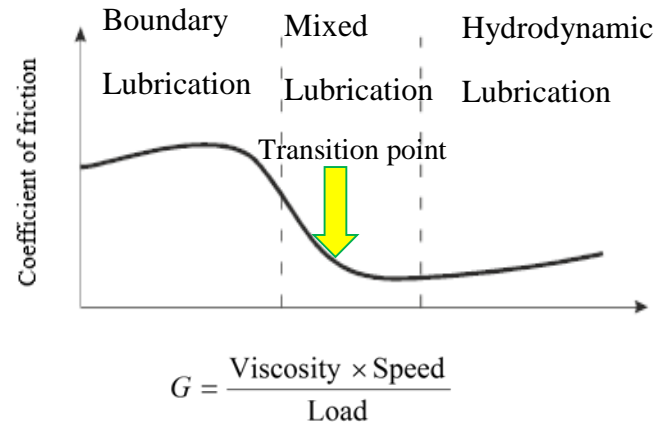


Figure 2.8 Stribeck curve

The horizontal axis in Figure 2.8 is referred to as the duty parameter, G , and the curve is also called f - G curve. The dimensionless duty parameter (analogous to the Sommerfeld parameter in bearing theory) characterizes the lubrication regime of face seals and usually is defined as the ratio of the viscosity force of the liquid film between the faces to the closing force as presented in Equation (2.8).

$$G = \frac{\eta \bar{V} b}{F_c} \quad (2.8)$$

where:

η is the dynamic viscosity of sealing fluid in [Pa.s]

\bar{V} is the sliding velocity on the mean face diameter in [m/s]

F_c is the net closing force acting on the seal in [N]

b is the width of the seal face in [m]

The minimum point of the Stribeck curve is a tribologically meaningful reference point where the leakage, friction and wear are minimized. An optimum operational region for face seals would be around the transition from mixed to hydrodynamic lubrication regime (see Figure 2.8). Consequently, mechanical seals ideally work near the transition from mixed to

hydrodynamic lubrication regimes where friction values depend on many parameters such as roughness height, seal face material, contact load and so on so forth [2, 47].

Several researchers performed friction measurements to judge lubrication state of the sealing gap by duty parameter in order to establish the transitions between the different lubrication regions. For instance Wei et al. [9] used the duty parameter to judge the lubrication state of sealing gap (see Table 2.1)

Table 2.1 Duty parameter in different lubrication regimes

Tribological regime	Duty parameter
Hydrodynamic lubrication	$G > 1 \times 10^{-6}$
Mixed lubrication	$5 \times 10^{-8} < G < 1 \times 10^{-6}$
Boundary lubrication	$2 \times 10^{-8} < G < 5 \times 10^{-8}$

In 1987, Lebeck plotted numerous friction measurements as a function of "duty parameter", Figure 2.9 [2]. To date most published work has shown that if the measured friction of a mechanical seal is presented as a function of the duty parameter, a typical Stribeck curve is obtained [47].

As shown in Figure 2.9, at low G -values a decreasing friction function is obtained corresponding to a mixed lubrication regime. This minimum value is reached after a certain threshold and then the friction starts rising with G , corresponding to viscosity drag in the hydrodynamic lubrication regime. In this thesis, new sources of friction will be introduced in Chapter 5 which may help to better explanation of friction rise under hydrodynamic lubrication regime.

Although duty parameter well describes the tribological regime of mechanical seals, the common characteristic observed for most of f - G plots is that the transition from a hydrodynamic to mixed lubrication regime occurred at different G values. As illustrated in Figure 2.9, the difference between G values for minimum point of the curve is remarkable which makes the comparison between different tribological characteristics of the mating faces to be quite random and unreliable as has been reported in the literature [2, 47].

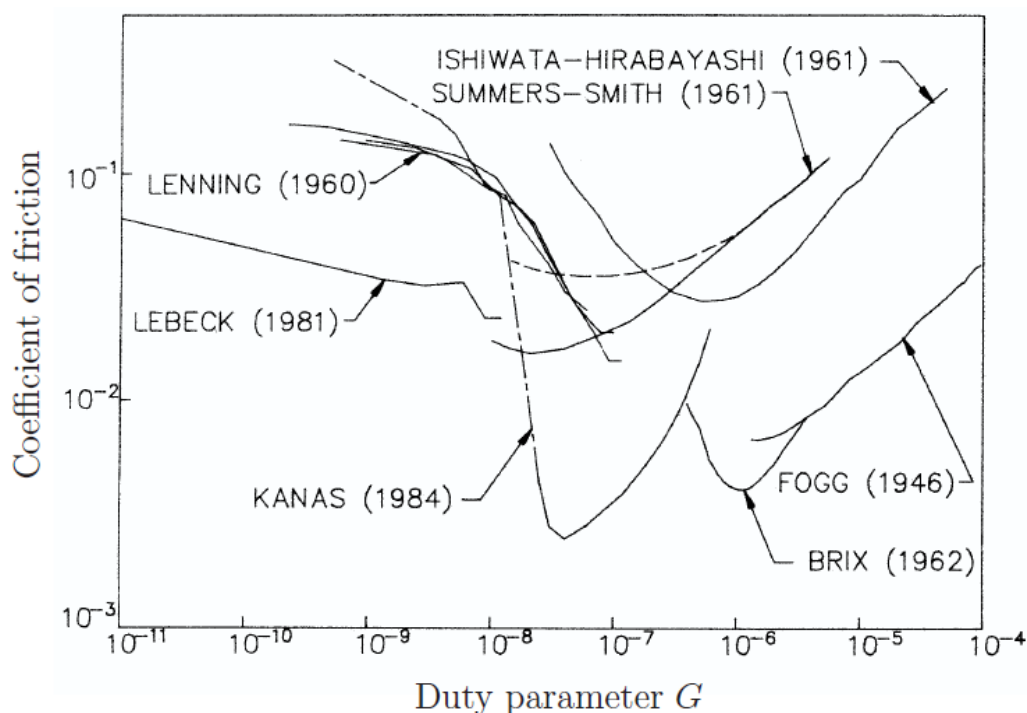


Figure 2.9 Stribeck curves obtained by different experiments [2]

2.3 Measurement of Surface Characteristics

As part from the tribology of the seal gap, surface metrology of face seals has an enormous influence on many important physical phenomena of sealing such as contact mechanics, friction, wear and seal life. To acquire low friction between seal faces, good surface roughness and flatness should be ensured. Typically the seal face is lapped to less than three helium light bands (slightly less than one micrometre) [48]. When the surfaces are not well lubricated, the faces tend to “stick” to each other. Then upon applying torque on the shaft, the stacked faces will make a sudden separation. This causes the actual rotating speed of the seal faces to fluctuate widely, that is called stick slip in tribology [49]. It may result in very severe vibration, which will damage the seal faces and cause excessive seal leakage indicating the importance of surface metrology on the reliable performance of mechanical seals.

2.3.1 Geometrical Features

Surface metrology refers to “the science of measuring small-scale geometrical features on surfaces: the topography of the surface” [50]. The geometrical features of a surface can be classified as roughness, waviness and form as described extensively in the literature[51].

Another widely used term in metrology, “surface texture”, refers to roughness and waviness features which are the deviations from the nominal surface with shorter wavelength than form error deviations. The typical surface texture of seal rings is a statistic distribution of micro scratches in all directions obtained by means of a lapping process. A shiny surface with a small roughness can be produced by lapping. However, where both seal rings are made of hard materials, one of the seal rings should have a dull finish to prevent the seal rings from sticking together during standstill. For a dull surface finish the running-in period may last several days [52].

The effects of surface texture on the lubricated contacts have been studied since 1991 [53]. During recent decades, several works have been published on the importance of surface roughness in mechanical seals, an extensive survey is found in the work of Mayer. E and B.S. Nau [54]. They report that in mechanical seals with parallel faces asperity contact normally exists and hence permeability of the interface to leakage is determined by the magnitude of the surface roughness.

The most common method of characterizing roughness is by an average value of the profile variation over a reference length as shown in Figure 2.10. This is known as centre line average (CLA) or arithmetical average (AA) commonly expressed as R_a . Centre line average is defined as the integral of the absolute value of the roughness profile height over the evaluation length based on Equation (2.9). It should be noted that the mean line is a datum line which allows the areas of the profile above and below it to be equal:

$$R_a = \frac{1}{L} \int_0^L |z(x)| dx \quad (2.9)$$

Where:

L is the sampling length

$Z(x)$ is the height of the surface profile from the mean line

Another method of characterizing roughness is root mean square (RMS) roughness or R_q . This parameter which is defined as the root mean square average of the roughness profile, Equation (2.10), ordinates plays an important role to characterize the contact of two engineering surfaces, see Section 5.5

$$R_q = \sqrt{\frac{1}{L} \int_0^L z^2(x) dx} \quad (2.10)$$

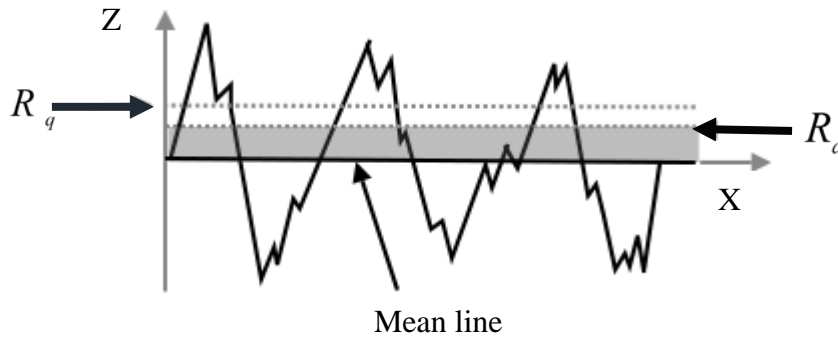


Figure 2.10 Illustration of a surface profile element [55]

Waviness is another surface parameter which has strong effect on tribological behaviour of face seals. It is believed that the waviness has strongest effect on the hydrodynamic lift off generation at the sealing gap [43]. Seal faces contact lightly at wave peaks and fluid enters wave valleys to establish hydrodynamic lift pressure which leads to increase load support and reduce heat generation as schematically shown in Figure 2.11. This pressure increases the lubricating film thickness, resulting in a higher leakage rate, increase load support and reduce heat generation. The effect of waviness on the hydrodynamic pressure distribution is further discussed in [52].

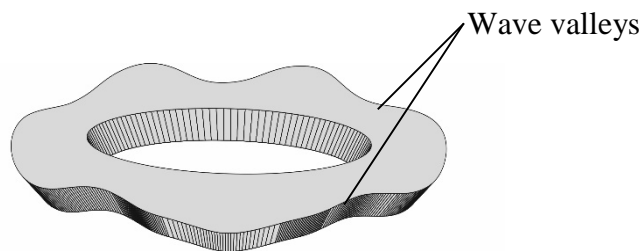


Figure 2.11 The effect of waviness on hydrodynamic pressure generation

Same as roughness, waviness is characterized by some parameters. Total waviness height is the maximum peak to valley height of the levelled and filtered waviness profile from roughness, Figure 2.12

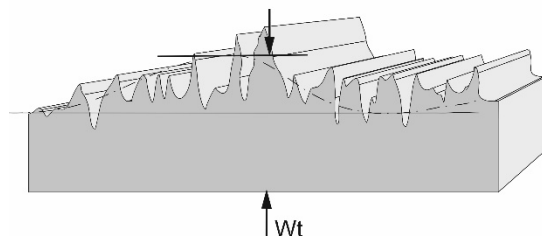


Figure 2.12 Total waviness height representation

2.3.2 Surface Roughness Considerations for Sealing Performance

Mechanical face seals ideally operate at the transition point from mixed to hydrodynamic lubrication regime where hydrodynamic lubrication and asperity contact both occur, with an average surface distance as thin as a few tenths of a micron [56, 57]. Under these conditions surface roughness height has a great effect on the tribological behaviour of face seals such as friction and hydrodynamic lift-off.

Since the effect of surface roughness on the formation of the lubricant film is complicated [54], analytical prediction of the mechanical seal performance is usually used to aid the design and troubleshooting of mechanical seals. Hence, the tribological behaviour of mechanical seals is modelled based on three different analytical approaches: deterministic, stochastic and multi scale approaches.

In the stochastic approach the influence of surface roughness height on the lubrication state of sealing gap is related to statistical parameters using two different theories. The first hypothesis is calculating the pressure as a sum of the asperity contact pressure and hydrodynamic lift pressure. Second, the Reynolds equation with flow factors is solved to include the surface roughness effects. This method has been widely used, however since the roughness effect is averaged with stochastic approach, it is not possible to generate hydrodynamic lift off with nominally flat surfaces as occurred in mechanical seals [58].

In the deterministic approach the surface texture is accurately described by a very fine mesh, which allows solving the regular Reynolds equation. Recently, Minet et al. used this approach to study mixed lubrication in mechanical seals [59]. They showed that surface roughness is able to generate a hydrodynamic lift-off above a velocity threshold to fully separate the surfaces even if they are nominally flat and parallel. In another work, Minet et.al have investigated the influence of working conditions in terms of friction and separation distance for different surface topographies [57]. Their model which is also able to produce

Stribeck curves demonstrates that transition from a mixed to hydrodynamic lubrication regime is surface dependent

The main principle of the multi scale approach is to solve as accurately as possible problems in the macroscopic scale, while including the effect of the micro-scale parameters such as roughness. In 2012 Nyemeck et.al presents a multi scale approach for the numerical calculation of the pressure distribution in mechanical face seals under mixed lubrication condition [58]. They concluded that the macroscopic pressure provides comprehensive information explaining the roughness-induced pressure generation, which is not easily obtained with a full deterministic solution.

2.4 Friction

Friction is one of the most fundamental physical phenomena and is defined as the resistance to motion during sliding or rolling that is experienced when one solid body moves tangentially over another with which it is in contact [60]. Friction and contact affect the operation of many machines in daily life; examples range from brakes of the automobiles to the motion of the knee-joint [61]. Sometimes friction is useful, without friction walking is impossible, however usually it costs money in the form of energy dissipation. Recent research in the US states that 57.5% of all generated energy is not only wasted by transport losses, but also by friction losses [62].

2.4.1 Friction Laws and Origin of Friction

The history of the study of friction dates back to ancient times, Dowson and Tichy et.al present an entertaining history of the field that is summarized below [45, 63].

Our ancestors started to think about reducing friction by using wheels or lubricants, e.g. the earliest record of using wheels was from 3500 BC and the earliest record of using lubricant was in 1880 BC approximately, by the Egyptians. More than 1000 years later in 350 BC, Thermistius found that the friction for sliding is greater than that for rolling. This finding led to the understanding in modern terms that the static friction coefficient is greater than the kinetic coefficient of friction, however, the detailed scientific understanding was not set up then.

The pioneer work in the field of friction was conducted by Leonardo Da Vinci, a poly math (1452-1519), who for the first time proposed the concept of friction and specially introduced the idea that friction force is proportional to the normal load. Many years later Guillaume Amontons (1663–1705), a French scientist, presented a paper to the French academy and proposed the two well-known friction laws in 1699:

The 1st friction law: Friction force is proportional to the normal force between the surfaces in contact.

The 2nd friction law: Friction force is independent of the apparent contact area.

In 1781, a French physicist, Charles-Augustin Coulomb summarized da Vinci and Amontons’s work and contributed the 3rd friction law. A short historical overview of Coulomb’s works is found in [64]. Coulomb’s law for dry friction states that the ratio of the friction force, F_f , to the normal force acting on the surface, W , is constant. This constant is the coefficient of friction, f , given by [61]

$$f = \frac{F_f}{W} \tag{2.11}$$

It is worthy to note that the coulomb law of friction is usually not sufficient to describe the friction characteristics of lubricated systems. In many instances the behaviour of the lubricant film leads to a decreasing friction coefficient when the sliding speed is increased. That is why the Stribeck curve is so popular in tribological studies. On the other hand, in most dynamic systems contact parameters between two sliding surfaces continually change, and the normal contact force does not stay constant. As a result, friction force becomes time dependent and its estimate requires detailed measurements of the system response and an understanding of the system dynamics.

Moreover, some researchers have shown that the laws of friction are only approximately valid in evaluating the frictional state of mating surfaces and are not generally applicable for direct asperity contact in boundary lubrication condition [61, 65, 66]. The idea is held that Equation. (2.11) provides an extraordinarily simple phenomenological friction law, although the nature of the friction force is not well-understood. The friction force generated between the mating faces is the combined result of friction forces which are present in a very large

number of micro-scale asperity contacts and maybe affected by too many complicated mechanisms.

However, most analyses of dynamic systems represent friction with a constant coefficient or with a function that depends on such parameters as sliding speed or infrequently temperature. The use of such phenomenological expressions gives acceptable results, particularly when modelling a continuous relative motion, as in rotating machinery [67].

Several works have confirmed that the laws of friction are applicable for a variety of combination of materials and operating conditions [68]. In recent years many researchers have investigated the origins of friction which can be attributed to different mechanisms such as formation and break-down of asperity junctions [69], ploughing of hard asperities over the softer surface [70], entrapment of hard wear particles [71] and adhesive force due to chemical reaction or inter-atomic diffusion [72].

2.4.2 Friction Components

The chart in Figure 2.13 describes the processes by which kinetic energy of a relative motion converts into oscillations representing thermal energy that eventually dissipates to the surroundings.

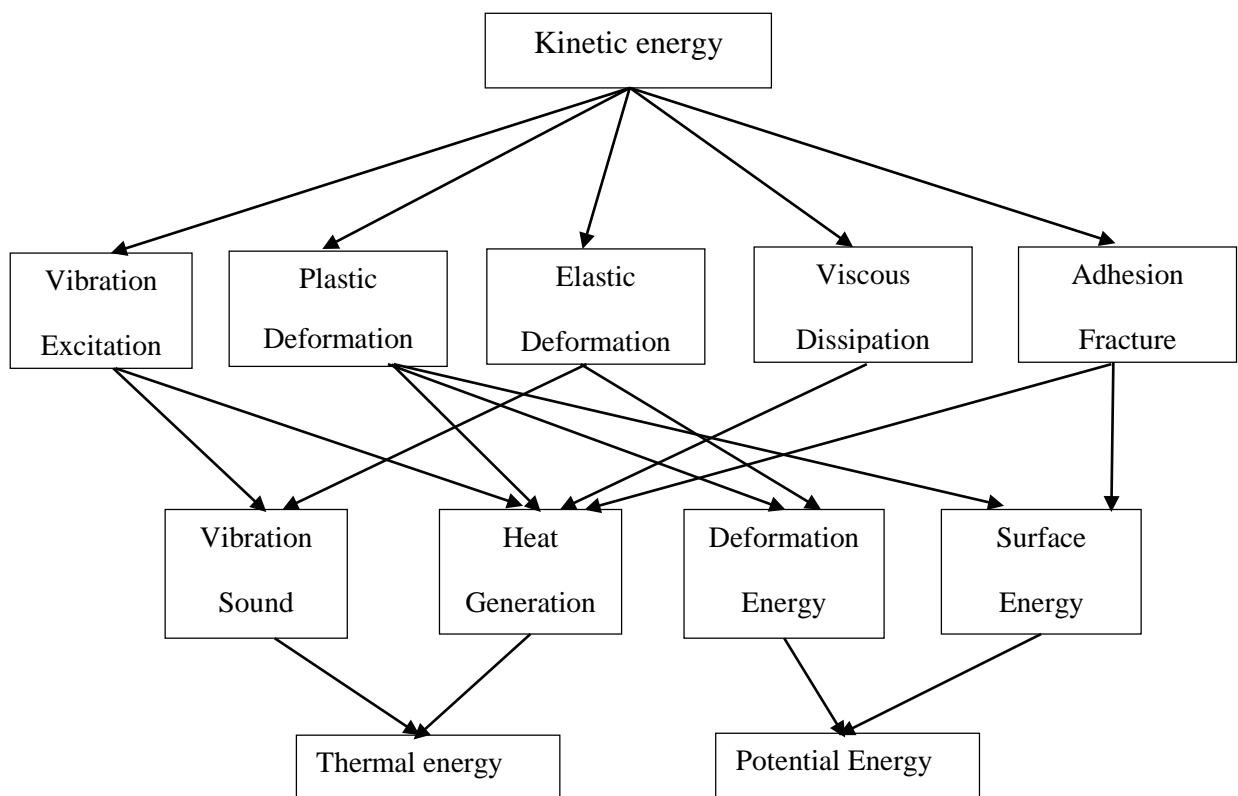


Figure 2.13 A description of energy path during friction [67]

During sliding contact part of the kinetic energy produces waves and oscillations in the bodies, and part of it leads to plastic and an elastic deformation of asperity tips. Some energy expends through viscous dissipation, and the balance through adhesion and fracture. Distribution of energy conversion through these processes varies for different applications. The same phenomenon occurs during passage of a sound wave in a solid when some of its energy converts to thermal energy [67].

A significant, but often overlooked, aspect of friction and the waves it causes relates to the feedback relationship between friction and the resulting structure-borne acoustic field. This interaction of vibration and friction at the continuum scale forms the basis for a feedback loop between friction and vibrations. Because friction is an intrinsic part of a dynamic system, accurate models to describe friction-excited vibrations must account for the coupling of system dynamics and the simultaneous development of friction during relative motion. One approach that combines system dynamics with the development of friction relates reactions at asperities to relative motion in terms of the elastic deformation of asperities [67], this is discussed in details in Section 5.5.

2.4.3 Mechanical Seal's Friction

The friction of face seals is a key parameter in the working process of mechanical seals, and is also the most important factor to characterize the lubrication state at the sealing gap as discussed in Section 2.2.2. The frictional characteristics of face seals is used to predict their operating life, to decide sealing performance [9], frictional power lost, frictional heat generation, and temperature rise of the end faces [73].

Frictional behaviour of the sealing gap is a complicated non-linear phenomenon that have been investigated during previous decades [74, 75] and is simply characterized by using the coefficient of friction. It has been reported that the friction factor of face gap changes from 0.03 to 0.3 and generally it is found to be around 0.1 for most applications [76]. The coefficient of friction is generally computed based on measurements of heat generation and mechanical torque. A certain load is assumed and the friction factor is computed [77]. This method is extensively used in the literature. For instance, Yu et al. [78] have conducted an experimental research on the frictional characteristics of laser textured mechanical seals with a porous face by measuring the friction torque developed between the stationary and rotating ring, see Figure 2.14. They concluded that compared with the conventional mechanical seals,

the temperature rise and friction torque of the laser textured mechanical seals is much lower [78].

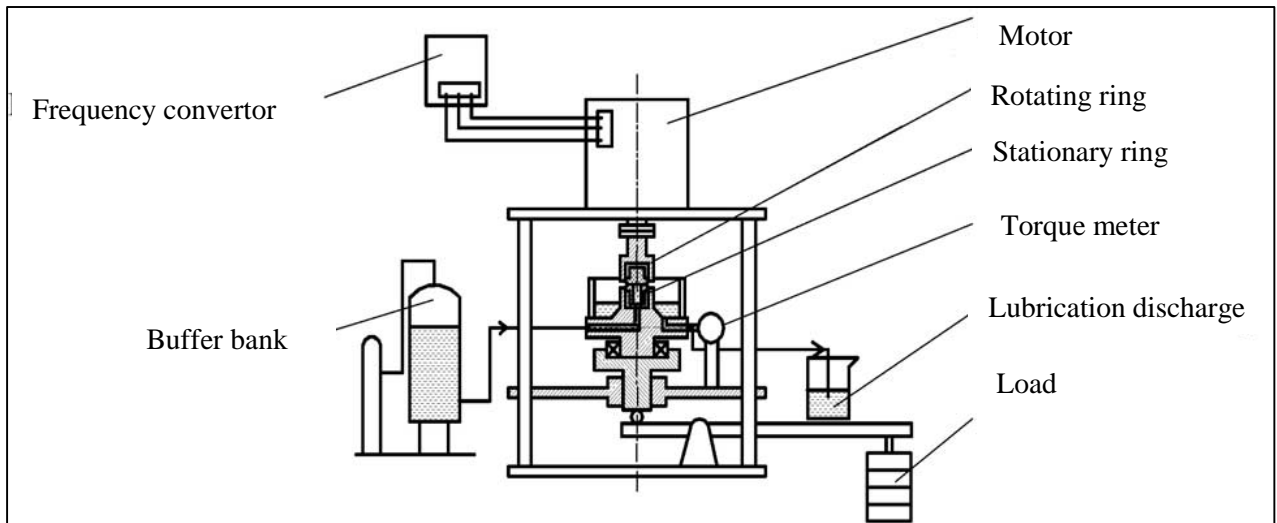


Figure 2.14 Schematic representation of the rig to measure frictional torque [78]

In 1981 Mayer, in his pioneering work [79], presented the friction factors of the different lubrication regimes which are listed in Table 2.2. This method is unlikely to be used to judge the lubrication state of a sealing gap due to significant amounts of data scatter that exists around the transition point as discussed in Section 2.2.2. Moreover, the fluctuations of friction state of the face gap have been observed by many previous studies on the sliding of mechanical seals

Table 2.2 Coefficient of friction in different lubrication regimes [79]

Tribological regime	Friction factor
Hydrodynamic Lubrication	$f < 5 \times 10^{-3}$
Mixed Lubrication	$5 \times 10^{-3} < f < 3 \times 10^{-2}$
Boundary Lubrication	$3 \times 10^{-2} < f < 15 \times 10^{-1}$

Currently, theoretical calculation methods of friction factor at the sealing gap are mainly either analytical or the weighted average method [73]. Both of them divide friction into viscous shear friction of the lubricant film and contact friction of the asperities. However, using these methods the predicted results of friction factor have no uniqueness. Hence it is

necessary to develop the measurement systems that can produce reliable results on the frictional state of sealing gap.

Recently Wei et al. established a friction factor fractal model based on asperity contact for mechanical seals which expresses the relationships among the friction factor and operating parameters, structural parameters, surface topography fractal parameters, material characteristic parameters and average temperature between the end faces [73]. Also, they mention that operating parameters have a great effect on the friction factor of the sealing gap for mechanical seals. The friction factor goes up with the increases of spring pressure when the end face is coarse (fractal dimension of the end face profile of the soft ring is smaller, and characteristic length scale of the end face profile of the soft ring is larger), and it decreased slightly with the increases of spring pressure when the end face is smoother. Friction factor increases with the decreases of sealed medium pressure, and which approximate linearly increase with the increases of rotating speed (Figure 2.15).

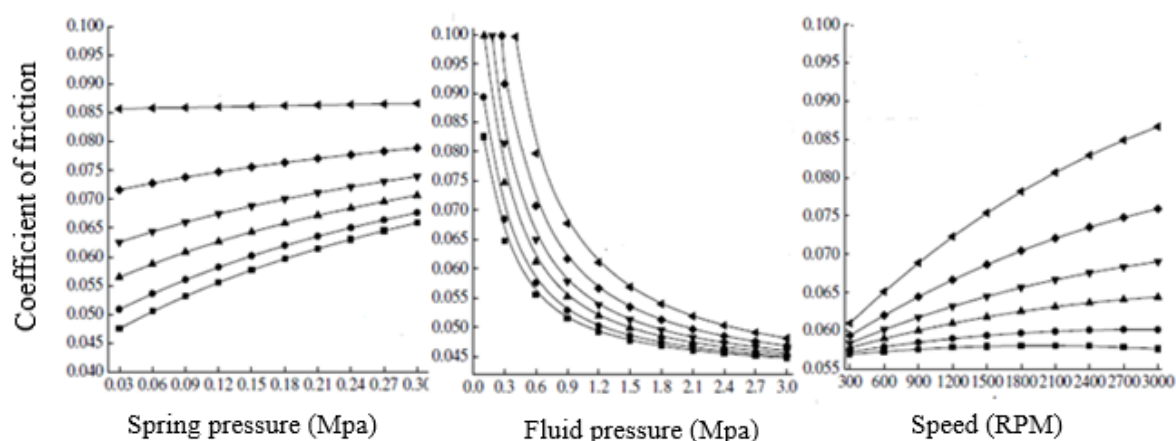


Figure 2.15 The effect of seal working parameters on friction factor

Tabor [80] lists the following three basic elements contributing to the dry friction of mating faces: (1) the real contact area between the sliding surfaces; (2) the type and the strength of the bond at the contact interface; and (3) the shearing and rupturing characteristics of the material in and around the contact regions. These basic elements can be strongly affected by various factors such as the presence of oxide films, the contact size of individual asperities, and temperature effects [80]. Thus it becomes important to study how the frictional behaviour and topographical properties of mating surfaces contribute to measurement of AE signals from the sealing gap. This will be discussed further in Chapter 5 where the elastic deformation of asperities is modelled.

2.5 Wear

Wear is a system response and depends on the characteristics of the materials in contact (hardness, thermal conductivity), the environment (lubrication regimes, temperature, lubricant) and working conditions (sliding speed, contact pressure) [81]. In general, “Mechanical wear”, “chemical wear” and “thermal wear” are terms used to describe wear with scientific expressions. In this thesis the word wear only refers to mechanical wear.

Wear is defined as progressive damage and material loss from interacting surfaces as a result of relative motion [82]. This phenomenon which is one of the reasons for mechanical seals failure (see Section 1.2), has far reaching economic consequences it involves not only the costs of replacement but also the expense involved in machine downtime and lost production. Statistics show that the cost of failures due to wear in industry is remarkable [83]. As a result, considerable efforts have been expended on the development of theories and deterministic models to predict wear rate of tribosystems. For Instance Meng and Ludema have identified nearly 200 wear equations involving an enormous spectrum of material properties and operating conditions [84], but even the best one has a very limited use [85]. Most of them cannot predict wear rate properly based only on material property data and contact information. The complexity of phenomenon and the large number of working parameters influencing the outcome are the primary reasons for this situation [86].

The earliest contributions to the wear constitutive models were made by Holm (1946) as reported by Zmitrowicz [87]. Holm established a relationship for the volume of the material removed by wear based on sliding distance and related it to the true area of contact. In 1953 J.F. Archard published an equation for the volume of wear of material, V_w , which is now a common starting point in the analysis of wear and known as Archard law of wear, Equation (2.12). A comprehensive survey on Extensions of Archard's law of wear can be found in [87].

$$V_w = K_w \cdot \frac{F_N}{H} \cdot s \quad (2.12)$$

where:

V_w is the total wear volume of the specific component in [mm³]

K_w is the dimensionless wear coefficient

F_N is the normal load in [N]

H is the hardness of the softer contact surface

s is sliding distance in [m]

Minimizing the wear on seal faces is one of the main issues in the seal design. Typical mechanical seals have a ‘nose’ on the carbon or other ‘wearing’ face of approximately 3-mm depth. In a low-viscosity liquid such as water, the typical wear rate of a standard design of conventional flat-face seal will be of the order of 0.25 μm per hour or less [4, 88].

The values for wear rates of metallic materials in sliding contact under different lubrication regimes are presented in the literature [89]. In the hydrodynamic lubrication regime, the separation between the surfaces is sufficient to prevent asperity contact, however it does not completely reduce the appearance of wear and is characterized by low values of wear rate. Depending on the lubricant properties in the boundary lubrication regime, the values for the wear rate increase. If the operational conditions become severe and sliding contact occurs between unlubricated surfaces, then the values of wear rate may become greater.

It is relatively unusual for seals to continue to operate until the wear out life is achieved. They more usually will have suffered one of the random-event failures discussed in the Sections 1.2. Wear out can be considered to have occurred if the seal nose has worn to a very shallow height, from an initial 3 mm, and there is no indication of overheating or wear grooves. To achieve a longer seal life will usually require attention to the seal-face loading to prevent breakdown of the film [4].

2.6 Wear Mechanisms

Wear can be classified as a function of the physical mechanism which causes damage by material removal to three main categories i.e. adhesive wear, abrasive wear and fatigue wear. which are discussed in this section briefly, interested readers may refer to [49, 89] for more details.

2.6.1 Adhesive Wear

Adhesive wear occurs when the mating faces slide against each other due to misalignment or severe operational conditions [89]. Since the two faces contact at the asperity peaks, high

local friction causes high shear stresses at the points of contact. Due to micro scale size of asperities the local stresses can reach one or both of the materials' yield stress very rapidly causing plastic deformation. This plastic deformation along with high local stress at contact locations may result in "cold welding" junctions and hence adhesion occurs between some of contact asperities.

Wear particles are fractured and detached from one of the asperities in the welded junction and will either attach themselves to another asperity or become loose particles, the particles may transfer back and forth between two materials or come out of the rubbing area [49]. Adhesive wear which can lead to the lubricant's breakdown is the most common wear mode in mechanical seals [89].

2.6.2 Abrasive Wear

Abrasive wear is a form of a face damage occurs where the asperity material is harder than the material surface or particles sliding on a softer surface and fracture at the interface. Two modes of abrasive wear may occur: two body abrasive wear and three body abrasive wear. The former can be understood in the situation that the asperities of the harder surface is hard enough to be considered as a cutting tool which removes the chip from softer material. The latter occurs when the harder surface is a third body, which is usually a small particle of abrasive or hard removed particles in the contact area, and is hard enough to scratch one or both of the faces [49, 89].

2.6.3 Fatigue Wear

The last type of wear, fatigue wear, is defined as a mechanism in which removal of wear particles detached by fatigue arising from cyclic stress fluctuations. The fatigue loading is originated from sliding at the sealing gap. The sliding can cause repeated loading and unloading cycles in certain areas of sealing gap as well as some asperities, which will induce the formation of cracks on the sliding surface or subsurface. Fatigue wear occurs when the number of cycles goes beyond the critical point, this may lead to initiation and propagation of subsurface cracks. The material in the crack area will break up into particles leaving small pits on the seal faces and resulting in a progressive loss of material [49, 89].

2.7 Face Pressure-Velocity Product

A rule of thumb factor in design of dynamic seals is the pressure-velocity product. This parameter is defined as the maximum PV value that the material of a mechanical seal can sustain before it degrades by frictional heating and excessive wear. The pressure-velocity product is characterized as the frictional power lost, N_f , per unit area with a coefficient of friction of unity [90]

$$PV = \frac{N_f}{A_f} \quad (2.13)$$

where A_f is the net hydraulic loaded face area. In mechanical seals pressure-velocity product is useful in estimating seal reliability when compared with limit values developed by manufacturers as a measure of adhesive wear. If a seal face operates beyond its PV limits, a seal may wear at a rate greater than desired and become non-uniform. Table 2.3 shows the comparison of seals' PV duty limits of some typical materials with balanced and unbalanced structure [91]. The operating PV limits are much greater for balanced seal than unbalanced ones. Another example of such a table is found in [48, 92]. The PV limit of Silicon carbide against carbon (which is used in this research) is slightly more than Tungsten carbide against carbon, however in some researches their values are approximately considered as equal [93].

It should be noted that for different operational conditions (sealed pressure, speed, viscosity and face material combinations), tabulated values of tribological parameters such as coefficient of friction, duty parameter and pressure velocity product are less useful than might be expected. This is because mechanical seals operate most of the time in the hydrodynamic or mixed lubrication regimes. The mentioned parameters therefore vary with the many complex factors that determine hydrodynamic lift pressure in the sealing gap. Values also vary between seals because of interactions between design and material change face deformations [56]. For instance, a value of PV is sometimes quoted for a specified fluid at a specified temperature. These are not general constants and are useful means of comparing frictional state of sealing gap especially when tests are repeated under similar conditions.

Table 2.3 PV limits of material pairs [91]

Face materials	Water and Aqueous solutions.10 ⁵ (Pa m/s)		Other fluids.10 ⁵ (Pa m/s)	
	Unbalanced seals	Balanced seals	Unbalanced seals	Balanced seals
Stainless steel/Carbon	5.5	-	30	-
Lead bronze/Carbon	23	-	36	-
Stellite/Carbon	49	85	52	580
Chrome oxide/Carbon	70	440	-	-
Alumina ceramic/Carbon	36	250	88	420
Tungsten carbide/Tungsten Carbide	44	500	71	420
Tungsten carbide/Carbon	70	700	88	1225

2.8 Heat Transfer Consideration in Mechanical Seals

In spite of the fact that the phenomena of transition from hydrodynamic lubrication to the mixed lubrication regime along with surface roughness effects have as much influence as frictional heating of the fluid film, the performance of a mechanical seals is greatly influenced by thermal effects [1]. The frictional heat is generated as the primary ring and mating ring slide against each other. Heat is also generated through viscous shear of the fluid film between the faces and around the rotating components. Zhu reports that there are at least three heat sources in a sealing system: interface friction, fluid churning at a high shaft speed and process fluid temperature [13]. For low viscosity fluids, most of the heat is generated by the rubbing of mating faces. In this case the coefficient of friction for the primary ring and mating ring pair determines the heat generation [77]. For viscous fluids there may be no direct contact of faces, but viscous shearing may generate about the same amount of heat as rubbing. An important difference is that the wear rate is likely to be much greater when low viscosity fluids are between the seal faces [76]. In his book [1], Lebeck described the basic nature of the thermal system for a seal as shown in Figure 2.16.

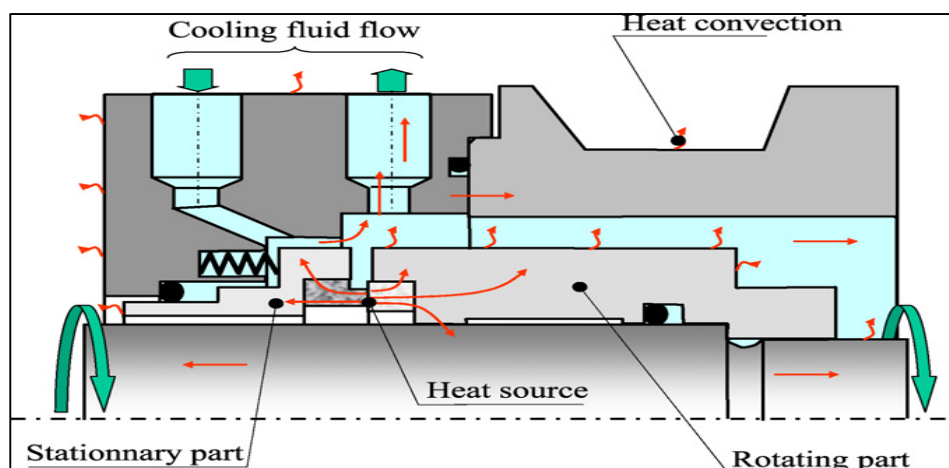


Figure 2.16 Heat Generation in a Mechanical Seal [1]

Both conduction and convection heat transfer mechanisms are significant. The major part of the heat generated flows from the mating faces of the seal rings and then immediately out to the surrounding fluid by convection [77]. Some of the heat passes through other parts of the seal and may exit through the shaft or out the housing.

Since the heat transfer in mechanical seals is a complex problem which involves many parameters, a lot of simulation work has been reported in recent decades. For instance, Zhu conducted a comparative computer based model for simulating mechanical seal operation [13]. He coded his model into a mechanical seal package CSTEDYSM which is a personal computer based software developed by John Crane EMA. He reported that the temperature distribution is non-uniform, predominantly in the radial and axial directions leads to radial tapering.

In 2009, Brunetière and Modolo studied both numerically and experimentally the heat transfer phenomena in mechanical face seals [94]. Their Test rig was designed to validate numerical models of the frictional behaviour through infrared temperature measurements and was thus quite different from industrial mechanical face seals. They performed the simulations by means of the computational fluid dynamic code (CFD) in Fluent and modelled the heat produced in the sealing interface by a uniform volumetric heat source being applied in a thin solid layer between the rotating ring and the stationary ring. The main conclusions drawn from their research are follows:

- a. The temperature has the maximal value in the contact area between the stationary and rotating ring.

- b. The temperature in the solids decreases progressively as the distance from the heat source rises and appears to be uniform in the fluid (oil).
- c. The thermally influenced zone has a length of approximately twice the contact width (i.e. the difference in contact radius) on either side of the sealing interface.

To date most published work, Z Liu et al. carried out the simulation of mechanical seal with ANSYS finite element method [95]. They mainly investigated the influence of sealed fluid pressure (water) and rotational speed of shaft on the mechanical seal performance. They pointed out that local contact situation of the mechanical seals is closed to the outside edge of the sealing gap, and both maximum contact pressure and temperature are too, Figure 2.17.

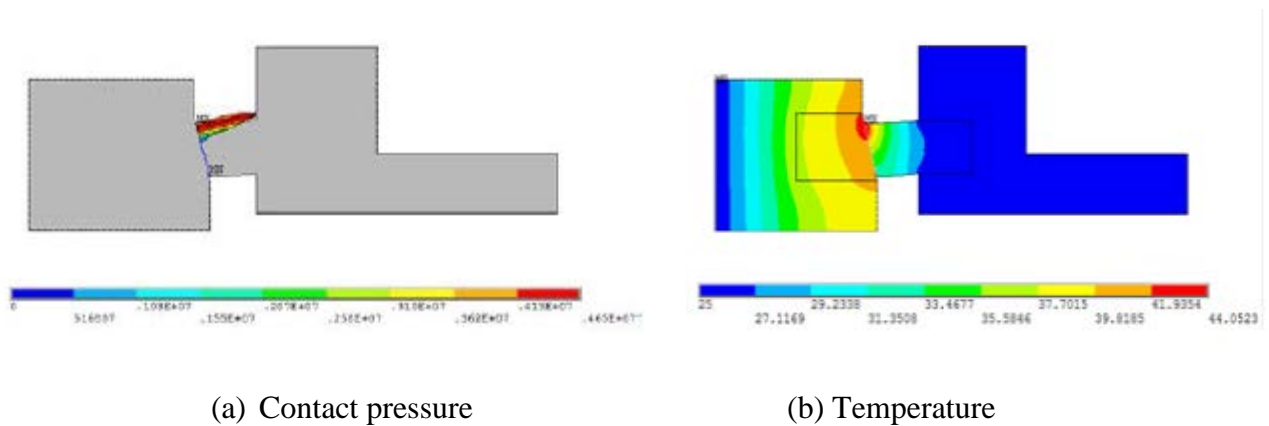


Figure 2.17 Predicted contact pressure and temperature distribution[95]

The Frictional effects tend to have a pronounced influence on the performance and reliability of mechanical seals. Frictional heat changes not only the seal geometry but also the fluid viscosity [96], consequently the lubrication conditions are modified because of fluid viscosity variation and thermal distortions of the seal rings and cause gaps which can increase the leakage rate. It can also cause material changes that can significantly increase the seal face wear rate.

Furthermore, sealed fluids may vaporise at higher temperatures. Evaporation of fluid film from the sealing gap (dry running) is one of the main failure causes of mechanical seals as discussed in Section 1.2. Frictional heat may have different consequences on tribological behaviour of mechanical seals. The most important are summarized in Table 2.4.

Table 2.4 Thermal effects on sealing gap

Thermal effect	Consequence(s)	Cause(s)
Thermally induced radial taper	The hotter face expands more than the colder one	large change of average temperature across the radial dimension
Thermally induced waviness	Variable expansion of the same end face at different spots	Circumferential variation in temperature
Heat checking	Multiple radial cracks on one of the seal faces	Poor liquid lubrication, high speeds, high loads, and the use of certain materials
Hot spotting	Some regions of an interface that develop a much higher temperature than the average	Thermo elastic instabilities

2.9 Seal Face Materials

The seal faces are the most critical part of a mechanical seal assembly; the main requirements are tribological. High quality seal face materials are necessary for industrial applications, in order to withstand rubbing against each other at different combinations of operating parameters (i.e. sealed fluid pressure, rotational speed and viscosity). Moreover, the seal rings are exposed to chemical attack by a wide range of fluids during their service life. The structural behaviour of seal components also plays a crucial role in determining performance. This is because of the extremely thin lubricating film in the sealing gap, the thickness being typically in the range 0.1-1.0 μm [56, 57]. Thus any deflection at this size of scale directly affect the reliability and performance of seal.

When seal rings contact each other, the tribological characteristics of the face material combination determine survival or failure of the seal. Proper mating face materials must be matched so that excessive heat is not generated from the relative sliding motion of the seal faces. The best seal face materials have low friction, high hardness differences, not soluble in each other, good corrosion resistance, good bearing properties, good machining ability and high thermal conductivity[49, 97]. Table 2.5 lists some examples of thermal conductivities and some other properties of seal face materials [77].

Table 2.5 Typical Properties of seal face materials

Typical property	316SS	Carbon Graphite	Tungsten Carbide	Silicon Carbide
Modulus of elasticity, Pa× 10 ⁹ (Mpsi)	193 (28)	20.7 (3)	586 (85)	414 (60)
Compressive strength, MPa (Kpsi)	207 (30)	207 (30)	4483 (650)	462 (67)
Tensile strength, MPa (Kpsi)	207 (30)	483 (7)	1380 (200)	310 (45)
Coefficient of expansion, m/m °K ×10 ⁶ (in/in °F × 10 ⁶)	16 (8.9)	4.5 (2.5)	6.1 (3.4)	4.5 (2.5)
Thermal conductivity, W/mK (BTU/hr ft °F)	16.2(9.4)	8.7 (5)	86.5 (50)	138.4 (80)
Hardness (Vickers)	155	40-100 (Depends on percentage of Carbon)	Approximately 2600	Approximately 2800

It has been shown that a mechanical face seal with some design or manufacturing errors but made from a good material has often longer life than one made from a worst material but with no errors of any kind [16]. Material pairs used in face seal combinations are usually different in order to maintain an optimum operation result in terms of friction and wear. The selection of the material pairs for modern mechanical seals is made according to the following considerations [49]:

- a. A soft material and a hard material referred to as “hard face” and “soft face” are often used. The hardness difference between two materials is usually 20%. The softer material is worn by the harder one.
- b. Low friction coefficient between rotating material and stationary material is needed to decrease the heat generation at the interface and thus reduce thermal expansion.
- c. The two materials should have high modulus of elasticity difference so that the stiffer material will be able to run into the softer one to make good sealing.

Wide varieties of materials are used as seal face materials in practice. An extensive survey can be found in [98]. Nowadays metals and metal alloys, metallic-ceramic materials and metallic carbides are used for face seals. For “hard faces” plain stainless steel, lead bronze, Ni-resist to tungsten carbide and silicon carbide are usually used. The counter-face materials are mostly made of carbon composites with metal or resin filler normally referred as carbon.

A carbon seal face run against a hard face has proven to be the optimal face combination for many industrial applications [16]. For instance, silicon carbide when paired with carbon offers the lowest coefficient of dry friction of any face material combination. Because of this silicon carbide will generate less heat and the heat that it does generate will be conducted away more quickly. These characteristics of silicon carbide makes it to be one of the most widely used mechanical seal face materials. Sometimes metal alloys (such as stainless steel and Ni-resist cast iron) are selected to run against carbon to reduce the manufacture cost. However, compared with carbides metal alloys have poor tribological properties.

2.10 Main Findings

The design parameters which influence the tribological behaviour of mechanical seals are geometrical features of the sealing gap, balance ratio and pressure drop factor. These parameters along with the force equilibrium on the face gap determines the frictional state of mechanical seals. The tribological behaviour of mechanical seals is usually characterized by dimensionless parameters such as the coefficient of friction or duty parameter.

Since mechanical seals are applied under a wide variety of working conditions, the lubrication condition of sealing gap is modified because of fluid viscosity variation that may lead to the increase of the wear and leakage rate. Furthermore, sealed fluids may vaporise at higher temperatures and lead to dry running that is one of the main failure causes of mechanical seals.

To overcome this situation, the best seal face materials have low friction, high difference of hardness between the faces, good corrosion resistance and high heat conductivity. The selection of the material pairs for modern mechanical seals should include “hard face” and “soft face” combination. Silicon carbide as the hard face when paired with carbon offers the lowest coefficient of dry friction of any face material combination.

Chapter Three;

Acoustic Emission Technology

In this chapter the history of acoustic emission and its applications for condition monitoring of rotating machines are first presented. The chapter also includes general description of the acoustic emission technology used in the present investigation. The details of the acoustic emission measurement installation and the technical data of the measurement devices are given in chapter 6. This is next followed by a general discussion on the propagation modes of stress waves under different boundary conditions which mathematically show the complexity of the acoustic emission phenomenon. Finally, the characteristics of acoustic emission waves in real measurement highlighting the attenuation and distortion of wave-form are presented. Full understanding of these characteristics is necessary for successful condition monitoring of mechanical seals.

3.1 History and Background of Acoustic Emission

From the beginning of humankind, people were observing acoustic emission when they heard cracking of stones, fracturing of bones, crackling of wood in the fire and so on so forth. The first documented observation of the phenomenon which later came to be called acoustic emission was made by an Iranian philosopher and chemist, Jabir ibn Hayyan (721-815 A.D), which was published in Latin in the year 1545. Jabir wrote that tin gives off a "harsh sound" or "crashing noise" and iron "sounds much" during forging [99]. This "sound" probably comes from twinning of pure tin during plastic deformation and martensitic transformation during forging process of iron which are nowadays considered as the important source of acoustic emission in metallurgy and metal forming. A survey on the history of the subject can be found in [100, 101].

In 1936 Friedrich Forster, German scientist, was the first who measured the acoustic emission phenomena that occurred during martensitic transformations in steel through very small voltage changes owing to resistance fluctuations [102]. However, AE began to be more investigated thoroughly in the middle of the 20th Century.

In the period of 1950-1967, significant improvements were made in researches regarding the fundamentals of acoustic emission phenomena and studying of acoustic emission behaviour during deformation of different materials. At the beginning of this period, Joseph Kaiser published his Doctoral dissertation on his investigations on different engineering materials which is considered the genesis of current acoustic emission technology [103]. He discovered the irreversibility phenomenon of acoustic emission which is simply about the effect of the absence of acoustic emission in materials under stress levels below those previously applied on that material. This effect is nowadays known as the Kaiser effect and is one of the basic phenomena of acoustic emission. Kaiser presented also the division of the acoustic emission into two parts: continuous emission and burst emission (see Section 3.3.1).

Another major effort in the acoustic emission research area was introduced by Bradford Schofield (in the U.S, 1954) consists of basic reports published entitled "Acoustic Emission under Applied Stress" [104]. In the 1960s the level of research activity in this area became so high that international AE symposia were held all over the world [105].

In 1963 Harold L. Dunegan started a comprehensive research on AE which directly influenced the inception of major efforts in acoustic emission research in the U.S,

particularly at a number of U.S. atomic energy commission facilities as Purarjomandlangrudi and Nourbakhsh reported [101]. Several other research projects have been carried out during this period which accelerated work throughout the world.

In the 1960s, in parallel, in different countries the use of AE technology for practical non-destructive testing was proposed. For instance, acoustic emission techniques drew a great deal of attention for the inspection of pressure vessels in the U.S [105]. Consequently the golden age of acoustic emission was initiated in the late 1960s by organizing the acoustic emission working groups and continued to the decade of the 1970s. One of the major areas of research followed during this period was the study of dislocations being the source of acoustic emission [101].

The third stage in development of acoustic emission can be considered from (1980-present) [101]. During this period, acoustic emission technologies have been developed for new fields of application. In this stage the waveform-based analysis has produced a revolution in signal analysis, source characterization and source location [106]. It has been claimed that the first result obtained with scientifically planned acoustic emission experiment was published by T. F. Drouillard during this period [107], he reported the creaking of timber before breaking. Today the application of acoustic emission is vast in research and industry especially in the area of condition monitoring of rotating machines which is very well documented and will be discussed briefly in next section.

3.2 Application of AE Condition Monitoring to Rotating Machines

Application of acoustic emission technique to condition monitoring of rotating machines started in the late 1960s [108], where AE is a term used for transient elastic waves generated due to a rapid release of strain energy caused by the interaction of two media (i.e. the interaction of surface asperities) in relative motion. Tan. I et al. reported that impacting, cyclic fatigue, frictional wear, cavitation, leakage and dry running are the important sources of acoustic emission in rotating machines [109]. Today the application of acoustic emission in the area of condition monitoring of rotating machines is very well established. While vibration monitoring, the traditional technique for rotating machines fault detection, measures the response of the structure to the developing fault (e.g. a change in surface roughness, clearance reduction or developing spall), AE sensors measure the actual degradation mechanism itself. Therefore it is not surprising that literature extensively reports

acoustic emission as offering superior early detection capabilities over vibration analysis for monitoring the condition of rotating machines [36].

Acoustic emission condition monitoring of mechanical seals has been discussed briefly in Section 1.3.2 and will be discussed extensively in next chapter. Here, the application of AE measurements for the purpose of condition monitoring of other rotating machines is briefly outlined.

3.2.1 Rolling Element Bearings

The impact of inner and outer races in the rolling action of the bearing elements and sliding between damaged mating surfaces within the bearing generates various failure modes such as flaking, fluting, pitting, and seizures. A lot of researches has been reported on the detection of both localized and distributed defects in rolling element bearings, the former has drawn the attention of a great number of researchers. From a literature review carried out by Tandon and Choudhury on the vibration and acoustic measurement techniques for the detection of defects in rolling element bearings, it is concluded that the emphasis is on vibration measurement methods [110].

Acoustic emission measurements have also been used successfully for detecting defects in rolling element bearings. Some studies indicate that these measurements are better than vibration measurements. For instance to monitor the outer race defects, acoustic emission has proved to be more effective than vibration especially in low bearing speeds (less than 100 rpm) where the transmitted vibration energy is too small for successful detection [111]. Furthermore, because of the sensitivity of acoustic emission to surface roughness, researchers have found that even the lengths of the outer race defect can be estimated from AE measurements [112].

The same overwhelming success has not been reported for inner race defect detection. This is probably because of the complex and continuously varying transmission path between the inner race defect and sensors mounted on the bearing casing [36].

3.2.2 Journal Bearings

Since vibration responses are well related to asperity contact [113] as well as viscous friction effects [113], vibration monitoring can be considered as an effective tool to detect internal surface defects in journal bearings. However, most of the works reported in this area are

directed to novel signal processing algorithms rather than discussing the effect of vibration sources. The application of high frequency AE measurements for monitoring the condition of journal bearings has been extensively reported in the literature. The research in this area include identification of lubrication regimes [38], investigation of the effect of working parameters (e.g. load, rotational speed and viscosity) [114, 115] and fault detection in journal bearings [113].

The location of acoustic emission sensors is one of the common challenges associated with the monitoring of journal bearings to capture the signals whilst reducing background noises such as electromagnetic and fluid flow noises as well as from rotational movement of the drive shaft.

3.2.3 Gearboxes

AE technique seems superior in detecting faults (e.g. tooth pitting and cracking) in the earlier stages and giving significant indications to the monitored parameters, something that was not observed for the vibration monitoring or wear debris analysis of gearboxes [116-118].

Previous researches indicate that, as a disadvantage of acoustic emission technique, under non-isothermal conditions acoustic emission features are also affected by load and speed which may complicate diagnosis in an industrial environment. These features do not change when temperature is kept constant [36, 119]. Another major conclusion drawn from the literature is the difficulty of mounting the AE sensor close to the source of the signal. Attenuation of acoustic emission signal (see Section 3.6.1) in a gearbox is significant due to a large number of sound interfaces which attenuate the energy of acoustic emission waves [120]. The situation may get worse by different transmission paths travelled by the signal to the detector.

3.3 Principals of AE Testing

All materials can be compressed or strained under external loading. The higher the deformation the higher is the energy released during the loading and releasing process. This rapid release of transient energy which may be observed both in highly elastic as well as brittle materials is called acoustic emission. AE is structure-borne and fluid-borne waves generated by the release of strain energy in the widest range of natural events, from seismic events which are the largest-scale acoustic emissions to the microstructural changes that

occur in a material. The latter one is like an earthquake at the acoustic emission source but in microscopic dimensions. The waves generated are in the ultrasonic range between 20 kHz and 1 MHz.

The instabilities or the source mechanisms of acoustic emission are mainly divided into material sources and pseudo sources [121]. Crack formation and extension, dislocation movement and phase transformation are examples of the first type, while pseudo sources include phenomena such as leakage [122, 123], mechanical impact [124], turbulent fluid flow and fluid cavitation [125, 126], wear and friction [127, 128].

The high frequency acoustic emission waves propagate through the solid and on the surface in all directions. When the stress waves reach to the surface of the material, the vibration and displacement of these waves is measured and converted into electrical AE signal using an acoustic emission sensor as shown in Figure 3.1. The amplitude (and consequently, the energy) of the stress pulse generated can vary drastically depending on the nature of the acoustic emission source and the dynamics of the source process [129].

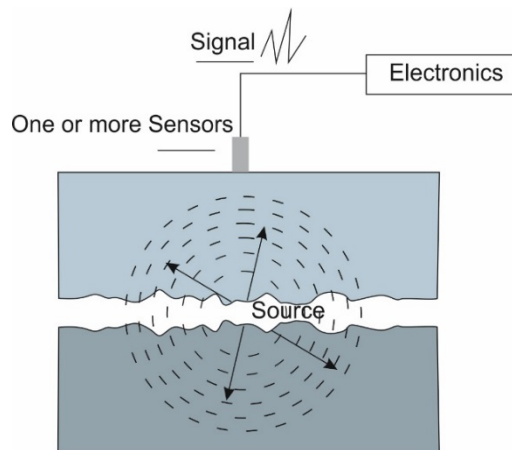


Figure 3.1 Principles of AE wave propagation

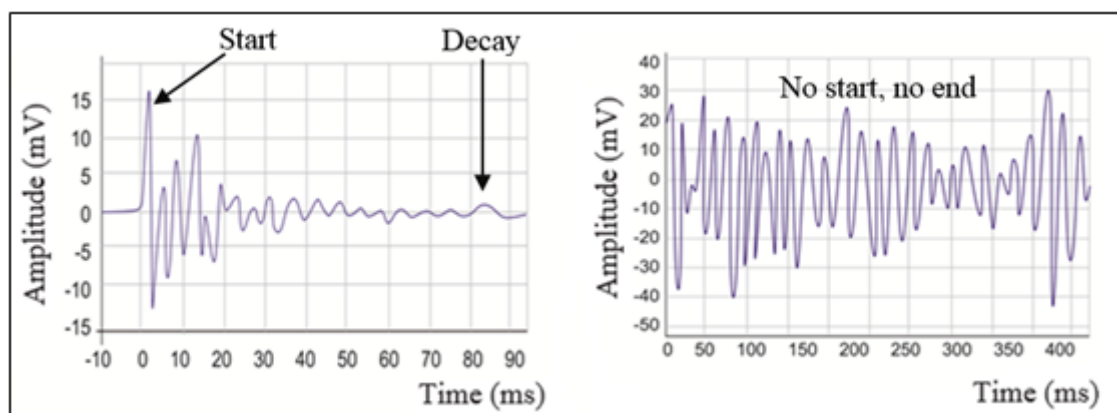
The AE system processes the recorded signal, converts it into featured data and displays them graphically and numerically in real time. Real time monitoring has a unique advantage and is one of the main reasons for this technique to come in to the forefront of condition monitoring of rotating machines. Real time analysis of the recorded signal can provide continues information about the nature of the source and permits on line condition monitoring. AE differs from most other non-destructive testing methods (NDT) methods in two major respects. First, the signal has its origin in the material itself, not in an external source, as in radiographic or ultrasonic testing. Second, Acoustic emission is a dynamic test

method which detects existing geometrical discontinuities and provides a response to discontinuity growth under imposed structural stress. This ability is in contrast to other NDT methods which depend on prior knowledge of the location and orientation of the discontinuity to direct a beam of energy on a path that will properly intersect the area of interest [130].

3.3.1 Transient vs. Continuous AE Signal

The sources of acoustic emission signal can have widely varying characteristics due to significant differences in the source signal. Basically, an acoustic emission signal can be classified into:

- a. Transient signal (bursts): these signals have definite start and end points deviating clearly from background noise, Figure 3.2 (a). This type of acoustic emission signal rises very quickly and decays slowly which is useful in industrial applications such as monitoring large pressure vessels where this type of signal indicate crack growth leading to failure.
- b. Continuous signal: If there is a high rate of occurrence, the individual burst-type signals interfere with each other to form a continuous emission. Continuous waves are produced by rapidly repeated processes such as machine vibrations, fluid flow and continuous friction between surfaces. Monitoring of continuous acoustic emissions can be used to control the operation of machines such as in on line condition monitoring of rotating machines. Continuous signals have varying amplitudes and frequencies but never end as shown in Figure 3.2 (b).



(a) Transient signal

(b) Continuous signal

Figure 3.2 Different types of AE signal

It should be noted that continuous emissions produced for instance in rotating bearings show very different signal characteristics when compared to burst signals caused by the spontaneous release of energy during cracking [131]. Since the AE signal in rotating machines is often a mixed type between transient and continues emissions, it is necessary to identify the source of burst type and continuous type of AE signal in a system before interpreting and analysing the signal [132].

3.3.2 AE Signal Measurement Parameters

The signal features that are commonly used to characterize the acoustic emission source mechanisms are briefly described in this section. It should be noted that in Figure 3.3 features are indicated based on the number reference in the following discussion.

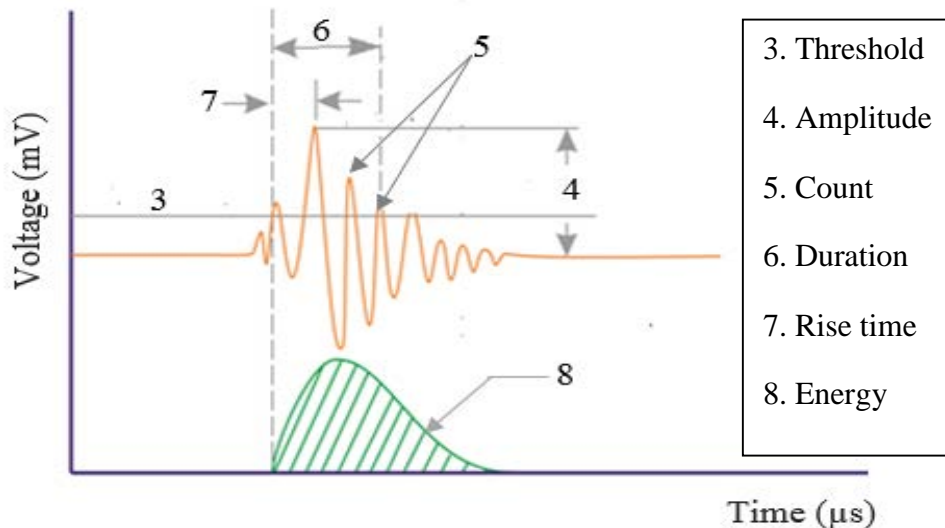


Figure 3.3 Definitions of AE signal parameters

1. **Hit:** A hit is defined as the detection and measurement of an individual acoustic emission signal on an individual sensor channel. This parameter can be used to quantify an acoustic emission activity.
2. **Event:** An event is defined as a local material change giving rise to acoustic emission, a single event may result in multiple hits (at one or more sensors).
3. **Threshold level:** AE condition monitoring is usually carried out in the presence of background noise. Hence, a threshold detection level is set slightly above this background level and serves as a reference for several of the simple waveform features. The threshold level may be user-adjustable, fixed, or automatically floating

and is defined as the voltage level on an electronic comparator such that signals with amplitudes larger than this level are recognized.

4. **Signal amplitude:** is defined as the magnitude of the peak voltage of the largest excursion attained by the signal waveform from a single emission event. This is very important parameter because it directly determines the detectability of the AE event. AE amplitudes are directly related to the magnitude of the source event and they vary over a wide range from micro-volts to volts. The amplitudes of AE signals are customarily expressed on a decibel scale in which 1 μV at the transducer is defined as 0 dB, 10 μV as 20 dB, 100 μV as 40 dB and so on. Recently the amplitude of AE signal has been used to distinguish different wear mechanisms [133].
5. **Count:** is defined as the number of times the AE signal exceeds a present threshold during any selected portion of a test and sometimes is called ring-down. This parameter has been used in some previous tribological studies. For instance Lingard et al used the AE count rate (count rate denotes the number of counts per unit time) to indicate the variation of friction coefficient in different lubrication regimes [134]. In another study, Hase et al reported that AE count rate is proportional to the surface damage at a friction interface [135].
6. **Signal duration:** It is the length of the first and the last time the detection threshold was exceeded by a burst signal, or in a simpler way it can be defined as the time interval between AE signal start and end. Duration is measured in microseconds. It is valuable for noise filtering and other type of signal qualification.
7. **Signal rise time:** is defined as the time interval between AE signal start and the maximum peak amplitude of that AE burst signal.
8. **Signal energy:** Energy of the signal is another parameter that conveys information about the strength of AE source. Various ways of expressing energy exist such as the area under the amplitude curve, root mean square (RMS) value of AE signal (see Section 4.3.1) and etc. Energy as the measured area under the rectified signal envelope is preferred over AE counts because it is sensitive to amplitude as well as duration. Moreover, energy is less dependent on the threshold setting and operating frequency.

In modern AE systems these parameters are known as feature data and are captured by signal processing software. This is achieved by extracting the value of these parameters from waveform data. AE signals can be analysed by correlating one feature to the others or to other parameters such as load, rotational speed or time.

3.4 AE Sensor Considerations

The process of acoustic emission condition monitoring is made possible using an appropriate AE sensor and data acquisition system. When the AE elastic waves reach the surface at a frequency in the approximate range of 100 kHz to 1.2 MHz, dynamic elevations at the surface of material occur in the nanometre range which are detected by sensitive AE sensor. Then the detected mechanical motion is converted into electrical signals.

The majority of all commercially available AE sensors use piezoelectric elements. AE piezoelectric sensors have proven to be sufficiently sensitive and robust to be used in a variety of environments. The piezoelectric transducers are made by using a special ceramic (PZT) that provide the best combination of low cost, high sensitivity, ease of handling and selective frequency responses, Figure 3.4.

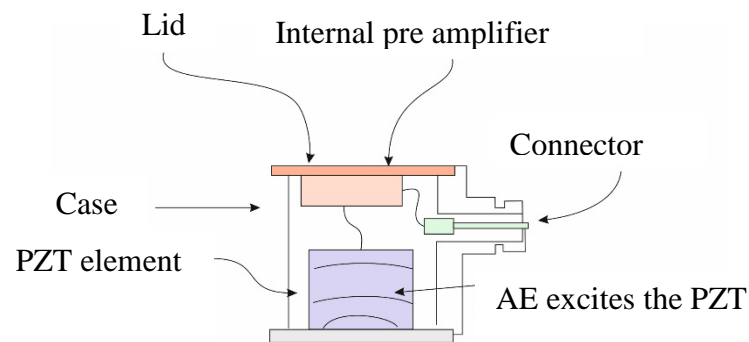


Figure 3.4 Schematic view of a piezoelectric sensor

AE sensors can be divided into two groups: Broadband sensors and resonant sensors. As the name suggests, resonant sensors detect signals are recorded in the frequency range where they are very sensitive. Broadband sensors are highly damped sensors which are operated outside their resonance frequencies allowing a broadband detection (up to 1–2 MHz). Since the acoustic emission frequency depends on the material involved, broadband sensors ideally respond with similar sensitivity to all frequencies in this range. Therefore broadband sensors are usually applied for collecting AE signals from rotating machines [36].

3.4.1 Sensor and System Response

The AE signals measured at the sensor is indirect and is influenced by many factors. To gain understanding of sensor and system response, it is beneficial to formulate the system response by a linear system as shown in Figure 3.5.

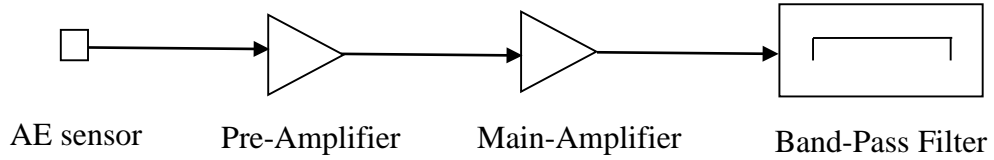


Figure 3.5 AE detection system [131]

The above system can be presented mathematically as shown in Figure 3.6.

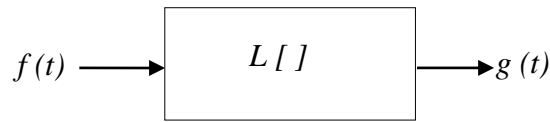


Figure 3.6 A linear system[131].

The AE detection system presented above is characterised by Equation (3.1) as following:

$$g(t) = L[f(t)] \tag{3.1}$$

As discussed in [131], using Dirac's delta function $\delta(t)$, Equation. (3.1) becomes (The symbol * represents the convolution):

$$g(t) = L[f(t) * \delta(t)] = f(t) * L[\delta(t)] \tag{3.2}$$

The function $L[\delta(t)]$ is the response of the system due to the input of the delta function. Setting $L[\delta(t)]$ as $w(t)$ and using the convolution integral it is possible to show that [131]:

$$G(f) = F(f) W(f) \tag{3.3}$$

Here $G(f)$, $F(f)$ and $W(f)$ are Fourier transforms of $g(t)$, $f(t)$ and $w(t)$, respectively. $w(t)$ and $W(f)$ are named the transfer function and the function of frequency response respectively. The signals measured using acoustic emission sensor are very weak and have to be amplified to be detected and recorded. All of these influences can be assigned

by different transfer functions as can be found in [131]. Consequently, the recorded acoustic emission signal $a(t)$ can be mathematically represented as

$$a(t) = w_f(t) * w_a(t) * w(t) * f(t) \quad (3.4)$$

where $w_f(t)$ and $w_a(t)$ are transfer functions of the filter and the amplifiers respectively. The frequency response of both the filter, $w_f(f)$, and the amplifier, $w_a(f)$, are known to be fairly flat or almost constant in the frequency domain. As a result, it is found that the frequency response, $W(f)$, or the transfer function, $w(t)$, of AE sensor significantly affects the frequency contents of AE signals.

3.4.2 Calibration

It would be always useful to confirm the condition of the measurement devices from the point of view of sensitivity, repeatability and accuracy which is technically called calibration. As defined by the British standard number BS EN 45003, calibration is "a set of operations that establish, under specified conditions, the relationship between values of quantities indicated by a measuring instrument or measuring system, or values represented by a material measure or a reference material, and the corresponding values realized by standards"[136]. Based on the understandings from Section 3.4.1, the calibration of AE sensor means quantitative estimation of the frequency response $W(f)$ or the transfer function $w(t)$ of the sensor.

AE Sensors are tested by accredited laboratories to recognized international standards and are initially supplied with their frequency response curves [36]. As an example figure 3.7 shows how sensor sensitivity varies with frequency [131]. Two different types of AE sensors are presented. Although both sensors respond irregularly, the sensitivity of the broadband type is lower than that of the resonant type. This fact is so general that selection of AE sensors should be based on either the sensitivity (resonance type) or the flat frequency response (broadband type) [131]. These curves are of high importance in practical AE applications. For a given sensor type, the calibration curves of the individual sensors should be closely matched. The shapes of these curve is of the characteristics of the sensor type and vary widely in their sensitivity and frequency response.

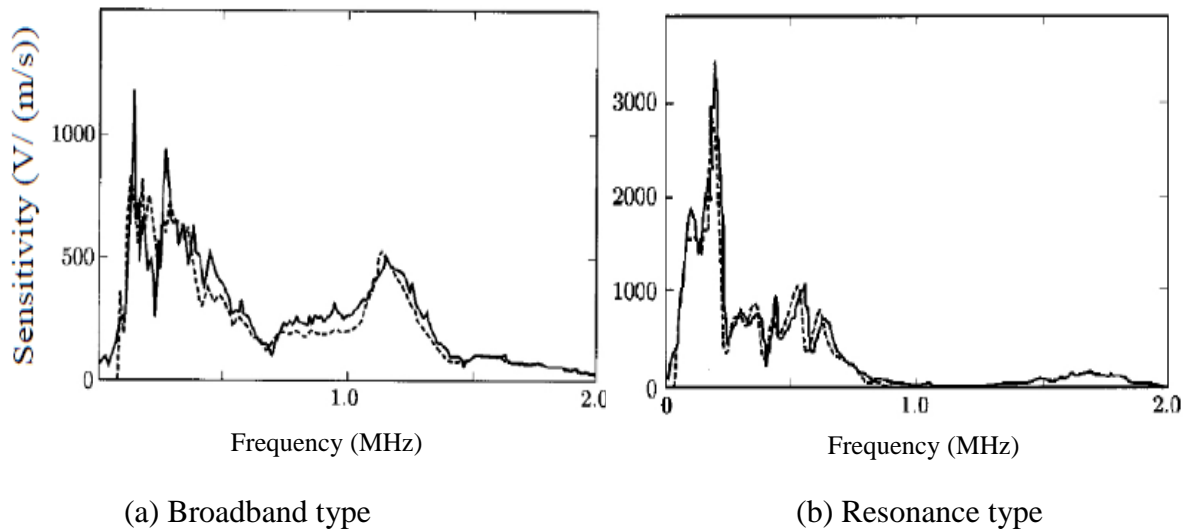


Figure 3.7 Calibration curves of commercial AE sensors [131].

In this research the absolute values of the acoustic emission activity were not under examination, more over the sensors have been calibrated initially at the manufacturer company. Hence there was not a need to calibrate the sensors again.

However, the condition of the AE sensors can be always confirmed by testing the measurement chain before and after measurements. The test method is the simple "Pencil Lead Break" method according to the ASTM standard number E 976-84. In the method a pencil lead is broken against the surface where the sensor is mounted. The breaking generates an acoustic emission burst signal for testing the measurement chain. The lead is supported by a special guide ring during fracture, as shown schematically in Figure 3.8. This method can provide a way of characterizing a sensor reproducibly and discriminatingly that is low cost, and provides a very simple calibration [99].

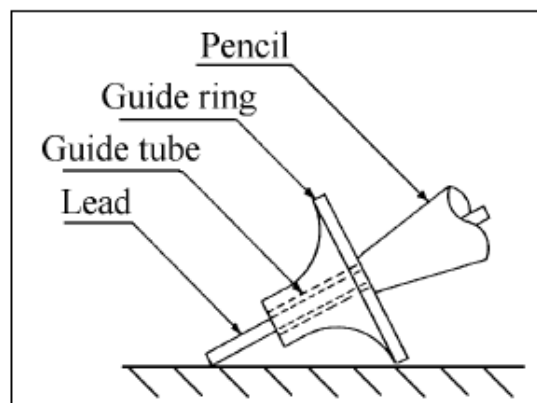


Figure 3.8 AE "Pencil Lead Break" method [99].

3.5 Propagation of Stress Waves

The propagation of ultrasonic waves in bounded elastic solids is very complex (see e.g. [132]) and beyond full consideration in this thesis. In general, the term “wave propagation” illustrates the propagation of waves through gaseous, liquid, and solid mediums and the term “elastic wave propagation” which is usually used to define AE wave form (see Section 3.2) implies that stresses in the solid obey Hooke’s law. The wave particle directions in a propagating wave depend on the boundaries of the medium, and here is discussed briefly. For a homogeneous isotropic elastic solid the differential equation of motion in terms of displacements is expressed as [137, 138]:

$$(\lambda + \mu_L)\nabla\nabla.X + \mu_L\nabla^2X + \rho F_b = \rho\ddot{X} \quad (3.5)$$

Where X is the displacement vector of a material point. The mass density per unit volume of the material is ρ and F_b is the body force per unit mass of material. The elastic constants for the material are the lambda elastic constants λ and rigidity modulus μ_L , which maybe expressed in terms of the other elastic constants [99].

3.5.1 Waves in Infinite (Unbounded) Medium

To investigate the conditions under which plane waves may propagate in an infinite elastic solid, a plane wave can be expressed by [137, 138]:

$$X_i = A_i f(\varphi) \quad (3.6)$$

Where A_i denotes the amplitude of particle displacement along the plane of the wave and φ denotes the phase which is equal to

$$\varphi = n_i x_i - ct \quad (3.7)$$

where n_i and C denotes the wave normal and phase velocity respectively as shown in Figure 3.9

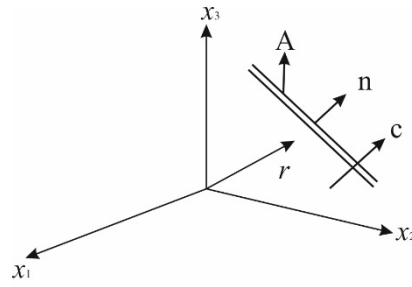


Figure 3.9 Plane wave propagating in three dimensions.

Substituting Equation (3.6) into tensor form of the Equations (3.5) (with body forces zero), three homogeneous equations in the amplitude components A_1 , A_2 and A_3 is obtained (see [137] for discussion and proof). Upon expanding the determinant of the coefficients, there results:

$$(\lambda + 2\mu_L - \rho c^2)(\mu_L - \rho c^2) = 0 \quad (3.8)$$

Which has two roots:

$$c_1 = \sqrt{\frac{\lambda + 2\mu_L}{\rho}}, \quad c_2 = \sqrt{\frac{\mu_L}{\rho}} \quad (3.9)$$

Equations (3.9) indicates two different types of propagation models for the plane waves: the longitudinal plane wave, Figure 3.10 (a), which travels with velocity C_1 and the shear or transverse wave, Figure 3.10 (b), which travels with velocity C_2 .

As indicated in Figure 3.10, in the longitudinal wave the motion of particles will be in the direction of the wave motion. This behaviour is analogous to that of fluids. In transverse or shear wave the motion of particles is transverse to the direction of propagation. The simple behaviour of longitudinal and shear waves is widely exploited in ultrasonic testing method where the type of wave injected can be controlled by the type of transducer and simple ray-tracing can be used to interrogate the body for defects. However, in AE applications there is no control of the types of waves being generated or recorded, and generally no specific interest in locating internal reflectors [139].

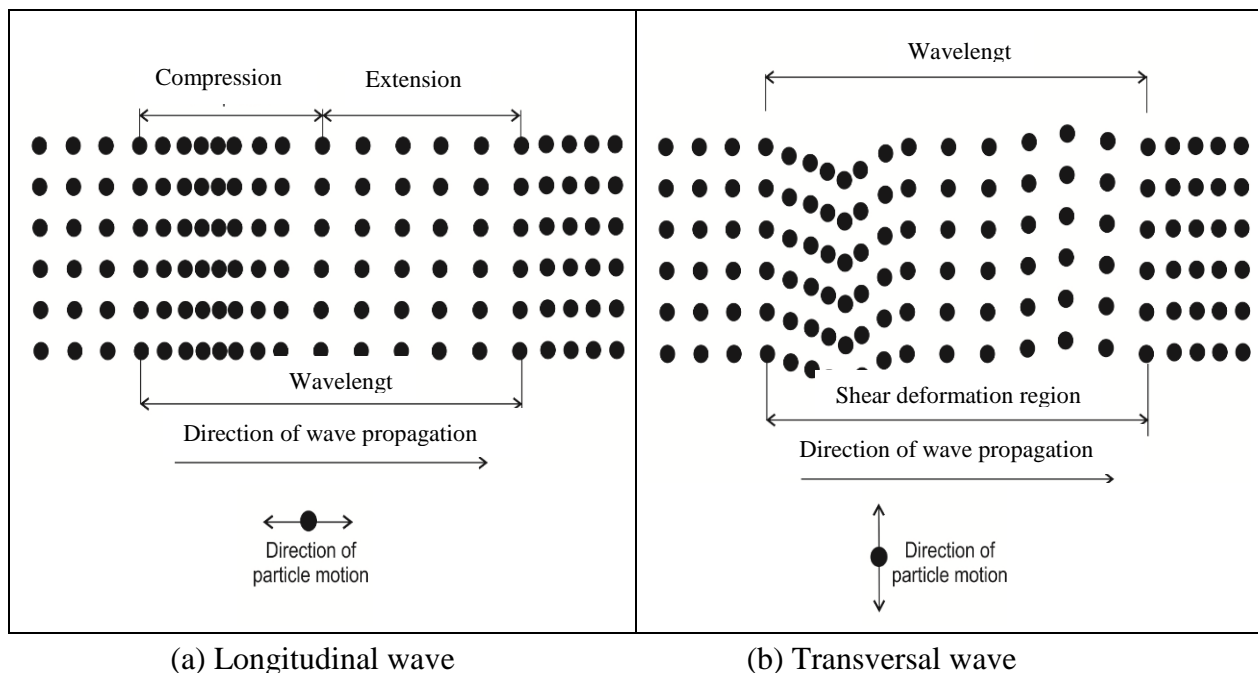


Figure 3.10 AE wave types in infinite media

3.5.2 Waves in Semi-Infinite Medium (One Bounding Surface)

As discussed in the Section 3.5.1, in an infinite elastic medium only longitudinal and transverse waves can be propagated. However when the medium is bounded by a half-space ($z > 0$) a third type of stress waves may appear whose effects are confined closely to the surface, Figure 3.11. These surface waves, first described by Lord Rayleigh in 1885, have been investigated in detail in seismology before finding applications in the ultrasonic frequency range for non-destructive testing discovered by Horace Lamb in 1917 [140].

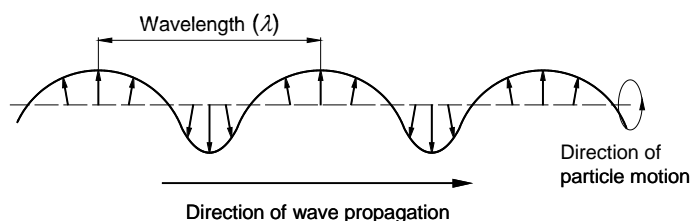


Figure 3.11 Surface wave or Rayleigh wave in the material [141]

Since AE sensors are surface mounted, it is common to assume that the acoustic emission energy is mostly carried in a surface wave for condition monitoring purposes. In Rayleigh waves particles vibrate in an orbital fashion, individual particles moving in an elliptical path, in much the same way as particles in water waves. Rayleigh waves include both longitudinal

and transverse motions that decay exponentially in the layers under the surface of the material.

In Table 3.1 values of density and longitudinal, transverse and Rayleigh wave phase velocities are given. Rayleigh waves have a speed slightly slower than shear waves, as demonstrated in the work of Graff. K.F [137] or other literature. The phase velocity of the Rayleigh wave as well as the phase velocities of the longitudinal and transverse waves are independent of the wavelength and therefore also independent of frequency [99].

Table 3.1 values of density and phase velocities for different materials and waves

Material	Density (kg/m ³) × 10 ³	Longitudinal wave (m/s) × 10 ³	Transverse wave (m/s) × 10 ³	Rayleigh wave (m/s) × 10 ³
Steel	7.8	5.9	3.2	3
Copper	8.9	4.6	2.3	2.1
Aluminium	2.7	6.3	3.1	2.9

3.5.3 Waves in Infinite Medium Bounded by Two Surfaces

Discovered by Horace Lamb in 1917, Lamb waves (plate waves) are the fourth important mode of the stress waves which appear in solid material. The development of this topic was driven essentially by its applications in the medical industry during World War II. Subsequently in 1961 Lamb waves were introduced as a means of damage detection for the purpose of non-destructive evaluation [142].

In an infinite medium bounded by two surfaces, such as a plate, wave propagation is more complicated due to interaction with the boundaries. When the wavelength is much smaller than the plate thickness the wave propagates on the surface as a Rayleigh wave. As the plate becomes thinner the surface wave begins to interact with the bottom boundary producing guided Lamb waves [139]. Thus a Lamb wave is defined as a plane elastic wave which is born in a material body with two boundaries where the material has a thickness of a couple of wavelengths of the stress wave [99].

There are two classes of Lamb waves which are essentially coupled surface waves, one where propagation involves compression and rarefaction (symmetric (*S*) modes or

extensional waves) and the other involving bending motions (asymmetric (A) modes or flexural waves), Figure 3.12 [143].

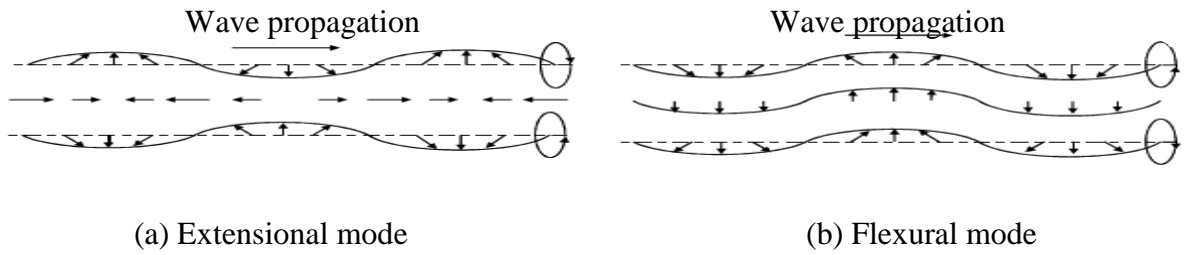


Figure 3.12 Two classes of Lamb wave

The extensional mode has a lower amplitude than the flexural component and occurs as a small amplitude precursor to the larger flexural wave, Figure 3.13[144].

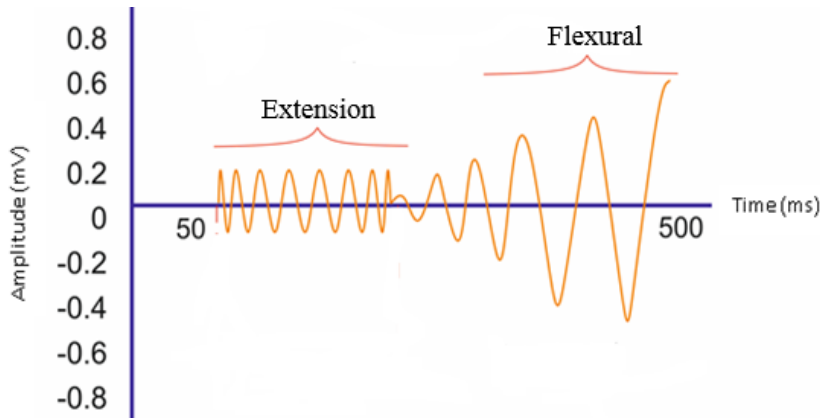


Figure 3.13 Extensional vs. flexural wave

Lamb waves differ from longitudinal, transverse and Rayleigh waves in that the phase velocity of Lamb waves depends on its wavelength and frequency. Both lamb wave modes propagate at various speeds which are dependent on both frequency and plate thickness. Generally, Lamb wave speeds C_p , fall between those of longitudinal and shear waves [145]:

$$C_p = C_2 \sqrt{\frac{2}{1-\nu}} \tag{3.10}$$

Where ν is Poisson’s ratio. The movement of the surface of the material (surface waves), that is measured in the acoustic emission method consists mainly of waves which are “like” Lamb waves [99]. However, in practical situations, the acoustic emission energy is carried in one or more mode and each mode can be converted to another at boundaries. Thus it is not common to treat AE waves as pure modes (i.e. Lamb mode). For many applications the

AE wave can be considered as a packet of mixed frequency propagating at a specific group velocity.

3.6 AE Waves in Real Measurements

The types of sound wave described in the previous section resulted from the wave equation using idealised boundary conditions and idealised source functions. On operational machines it is often only practical to take AE measurements from nonrotating members such as the bearing housing or seal cartridge. Consequently, AE signals originating from the mating surfaces will incur significant changes across the transmission path to the receiving AE sensor and are seldom as regular and predictable as is assumed in theory of elastic wave propagation. Moreover, materials can contain non-homogeneities which means that elastic properties are different from point to point. This may result in distortion of AE wave front during its propagation through the medium. Possible distortion sources include reflection, refraction and attenuation. Moreover, different sources and structures lead to different amplitude, frequency, damping and dispersion characteristics of wave fronts.

Neither the medium nor the boundaries nor the source is simple. Material dimensions are not infinite and the way from the source point to the measuring sensor can contain boundaries where the travelling stress wave is affected and thus several changes can occur. Depending upon the geometry of the solid and the nature of the stimulus, AE waves can propagate in a number of different ways. Unlike in ultrasonic testing method the propagation paths of AE waveform are generally beyond the control of the researcher [139].

The signal received by the acoustic emission sensor has little resemblance to the original signal and this adds to the complexity of non-intrusive AE measurements and makes interpretation of results more difficult. In this section the most important deviations from ideal propagation of the wave form are briefly reviewed.

3.6.1 Wave Attenuation

Acoustic emission response is directly affected by the loss of energy as waves propagate through a medium. The amplitude of an AE signal detected by a sensor is considerably lower than the intensity that would have been observed in close proximity to the source, a phenomenon normally referred to as attenuation [146, 147].

Attenuation occurs both in the near field and far field. Near field attenuation is the loss of amplitude in close proximity to the source while the loss of amplitude further from the source is described as far field attenuation. The four main causes of attenuation are; geometric spreading, scattering and diffraction, internal friction (absorption) and attenuation from velocity dispersion [139, 145]. Among the four main causes of attenuation, it has been suggested that geometric spreading dominates the attenuation for all kinds of structures over small distance (near field) [139, 145]. For long distances (far field) internal friction dominates [148].

The main concern with application of the external AE measurements is the attenuation of the signal during propagation, as such the AE sensor has to be as close to its source as possible. This limitation may pose a practical constraint when applied to certain rotating machinery as stated by Mba et al. [31] where interfaces play a more important role. In 2007, F.Y Edward evaluated the AE signal attenuation on a purpose built mechanical seal test rig [16] as shown schematically in Figure 3.14. He compared the signals from the AE sensor located at the back of the stationary ring with that from the sensor on the seal cartridge. The attenuation of the AE signal was significant and some of the characteristics were lost during the propagation.

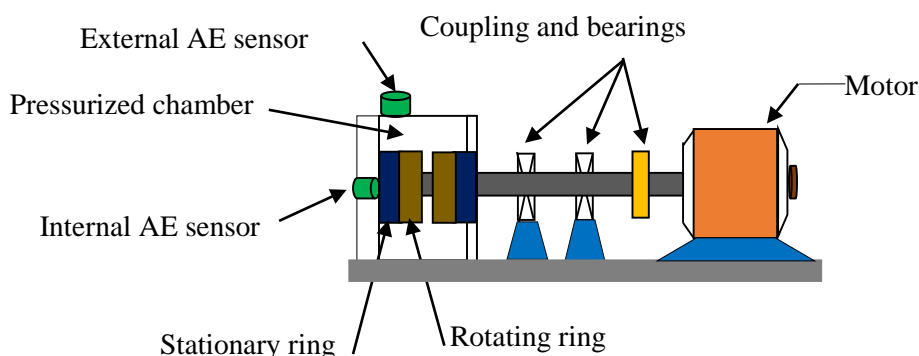


Figure 3.14 Schematic representation of mechanical seal test rig

In another study Mba and Hall have investigated the attenuation of AE signals on a large industrial gas turbine [149]. They state that AE signatures can propagate across a turbine at distances of up to 2 m, Figure 3.15. This indicates that AE is a viable tool for detecting seal and blade rubbing even for the far distances from the AE source. However, its success is considered to be dependent on the fully understanding the background noise received by the sensor on an operational turbine unit.

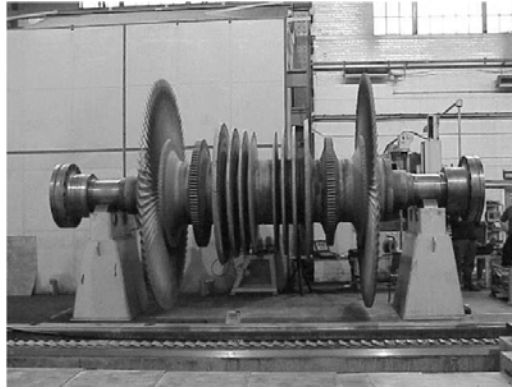


Figure 3.15 Turbine unit investigated by Mba and Hall [149]

In another study Nivesrangsan et al [150] studied the attenuation and the propagation of AE signals on the cylinder head of a diesel engine and reported that the attenuation increases with distance from the source and that more complicated transmission paths and geometries give higher attenuation factors.

3.6.2 Wave Reflection and Refraction

Although ultrasound waves are fundamentally different to light waves, the law for reflection of both wave types is similar. When a wave reaches an interface of two different media, some of the wave energy is transmitted into the other medium, some is reflected and some will propagate along the boundaries. Reflection, refraction and mode conversion can all occur when waves encounter boundaries. The reflection and refraction of waves depends on the angle of incidence (Snell's law) as well as the acoustic impedance of material [139]. Acoustic impedance determines the percentage of energy transmitted and reflected between two infinite media of different acoustic impedance, Z_1 and Z_2 , the acoustic impedance can be used as given by Equation (3.11):

$$E_r = \frac{(Z_1 - Z_2)^2}{(Z_1 + Z_2)^2} \quad (3.11)$$

Therefore, an essential requirement in mounting a sensor is sufficient acoustic coupling to remove any air from the interface introduced due to the surface roughness of the two contacting surfaces. The surface of acoustic emission sensor should be smooth and clean, allowing for maximum couplant adhesion. Application of a couplant layer should be thin so that it can fill gaps caused by surface roughness and eliminate air gaps to ensure good acoustic transmission [131]. This is crucial to the transmission of ultrasonic energy. The

acoustic impedance with an air gap is around 5 orders of magnitude lower than that of the two contacting surfaces, allowing for very little transmission of acoustic energy at the typical frequencies of acoustic emission. There are a number of couplant types to choose from typically liquid, gel or grease such as propylene glycol, silicon grease, ultrasound jell, grease and so on so forth. The effectiveness of a given couplant depends on its acoustic impedance, acoustic absorption, application thickness and viscosity. Each of these can have a strong influence on the sensitivity response of the sensor and can ultimately change the way the sensor responds to different wave modes [151].

3.7 Summary

Today the application of AE is growing especially in the area of condition monitoring of rotating machines e.g. mechanical seals that is very well documented. The source mechanisms of AE are mainly divided into material sources and pseudo sources. AE events generated by these source mechanisms are recorded at their moment of occurrence (real time monitoring) that is a unique advantage for condition monitoring of rotating machines. Based on the nature of source mechanism, an AE signal can be classified into transient and continuous type which is very useful in industrial applications to differentiate healthy and faulty conditions.

From the differential equation of motion, ultrasonic wave propagation can be considered under three different boundary conditions: waves in infinite medium, waves in semi-infinite medium and waves in infinite medium with two boundaries. The two latter one's result in surface waves (Rayleigh wave) and plate waves (Lamb wave).

However, in practical situations the AE energy is carried in one or more mode and can be considered as a packet of mixed frequency propagating at a specific group velocity. This wave form is affected by attenuation and distortion and thus the signal received by acoustic emission sensor has little resemblance to the original signal. Before starting experimental tests, full understanding of these elements is necessary for successful application of acoustic emission measurements to monitor the condition of mechanical seals.

Chapter Four;

Condition Monitoring of Mechanical Seals, a Literature Review

This chapter aims to provide a summary of the state of knowledge of the areas relevant to the condition monitoring of mechanical seals using non-intrusive AE measurements and other methods. The review is divided into three main parts, commencing with a critical discussion of the conventional condition monitoring approaches applied to mechanical seals so far. This is followed by an outline of AE technology applied for monitoring the tribological behaviour of mechanical seals and detecting faults at early stages is present. Finally, a review on the role of the AE data acquisition systems and signal processing techniques highlighting the time domain, frequency domain, and time-frequency domain methods is presented.

4.1 Mechanical Seals Condition Monitoring and Diagnostic

Condition monitoring as a widely used term is considered to be any system for providing an assessment of a machine's condition based on collecting sensor data, and analysing it with regard to any deviations from its normal operating conditions that could affect the service life of the machine. Based on the British Standard BS ISO 13372, condition monitoring is defined as "Detection and collection of information and data that indicate the state of a machine" [152]. Here the meaning of 'condition' is clear. It is not meaningful to consider a machine to be in 100% condition or 0% condition [101]. Consequently, condition monitoring instruments evaluate the related characteristics (i.e. vibration, temperature, ultrasonic sound propagation, heat generation and so on) which can differentiate between healthy and faulty conditions of a machine.

Condition monitoring is a pioneer concept for the purpose of on-line monitoring of rotating machines offering sustainable improvement in machinery performance and reliability. Modern diagnostic systems are based on advanced signal processing approaches. Remarkable amounts of data are recorded including complex time series signals such as acoustic emission alongside more conventional and less rapidly changing signals, such as temperature, pressure and speed in order to identify the effect of operating parameters on the machine's condition. The application of condition monitoring techniques allows earlier diagnosis and prompt repair of any malfunction and avoidance of breakdown caused by faulty components, which is most critical for process plant and machinery [141]. A successful monitoring system will have the potential to minimise the cost of maintenance, improve operational safety, and reduce the incidence of in-service machine failure or breakdown.

The main general methods which have been established for condition monitoring of mechanical seals such as vibration analysis, eddy current and ultrasonic testing are briefly discussed in this section in preparation for a comparison of their strengths and weaknesses compared with what is currently known about AE condition monitoring of mechanical seals.

4.1.1 Vibration Analysis

Vibration analysis is one of the most widely used condition monitoring techniques especially for rotating machines [153, 154]. All rotating machines components produce a wide range of vibration frequencies due to changes in mass, stiffness and damping properties of the

system, the total spectrum of frequencies being referred to as the machine's signature. If a fault produces a signal at a known frequency then the magnitude of this signal is expected to increase as the fault develops [155]. Vibration monitoring has been widely applied to monitor and diagnose faults in rotating machines such as journal bearings [156], centrifugal pumps [157] and gearboxes [158].

Since vibration analysis can only detect a signal in the sonic frequency range and cannot detect signals in the ultrasonic frequency range, it is unlikely to be applied for monitoring the rubbing of the seal faces. F.Y. Edward [16] carried out a lot of experiments on a purpose built test rig to monitor the condition of mechanical seals using vibration analysis. He reports that vibration is more likely to be influenced by the change of shaft speed rather than the severity of the elastic deformation of asperities in the sealing gap. This indicated that it is not efficient to monitor the condition of mechanical seals by vibration analysis.

4.1.2 Eddy Current Testing

The eddy current method has proved to be useful for monitoring the condition of mechanical seals by Constantinescu and Etsion [17]. They experimentally observed the dynamic behavior of a non-contacting seal by means of proximity eddy current probes monitoring the motion of the flexibly mounted stator. In the later studies Green applied this technique to monitor the seal clearance (sealing gap) and the relative angular misalignment between the stationary and rotating rings [18]. To date most published work, Zhang and Li used the data from eddy current sensors to direct the processing of the acoustic emission signal using principle component analysis and artificial neural network [159] due to the fact that the thickness of the fluid film can't be monitored by the acoustic emission signal directly. In their apparatus two steel rings are inlaid in the silicon carbide seal rings and are ground on the two end faces. An eddy current sensor is put through a small hole drilled on the steel ring, while the acoustic emission sensor is mounted on the bottom of the stationary seat as Figure 4.1 shows. With water as the sealed fluid, they carried out tests under a wide range of operating conditions. During the tests water pressure changes from 0.5~10 MPa and the spindle speed varies in the range of 0~1500 rpm. They reported that the film thickness increased with water pressure, but scarcely was affected by spindle speed. Also they mentioned that the attenuation of the acoustic emission signal is a big restriction.

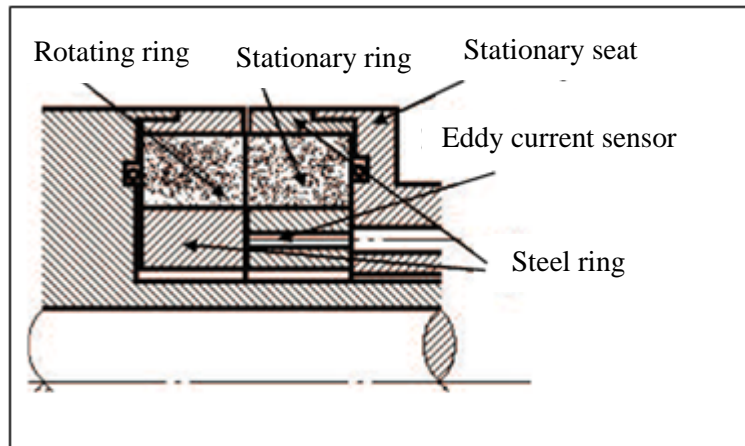


Figure 4.1 Mechanical seal test rig for eddy current testing principle [159]

All previous work in this area is based on the dynamics of non-contacting mechanical seals and cannot be extended to the condition monitoring of contacting mechanical seals, due to the fact that contacting face seals usually operate in the mixed (or even boundary) lubrication regime which makes it very difficult to evaluate the condition of lubrication due to the very small gap between the seal surfaces.

4.1.3 Ultrasonic Testing

The ultrasonic method has been applied by Anderson, Jarzynski et al. [160] to monitor the onset of contact between seal faces. An ultrasonic transducer mounted on the back of stationary ring such that it sent a pulse and received the shear wave reflection, as Figure 4.2 shows. Shear wave propagation through a liquid is negligible, hence the shear wave reflection is only increased by the existence of contacting seal faces. Therefore, when contact between the seal rings starts the reflection coefficient of shear waves goes up.

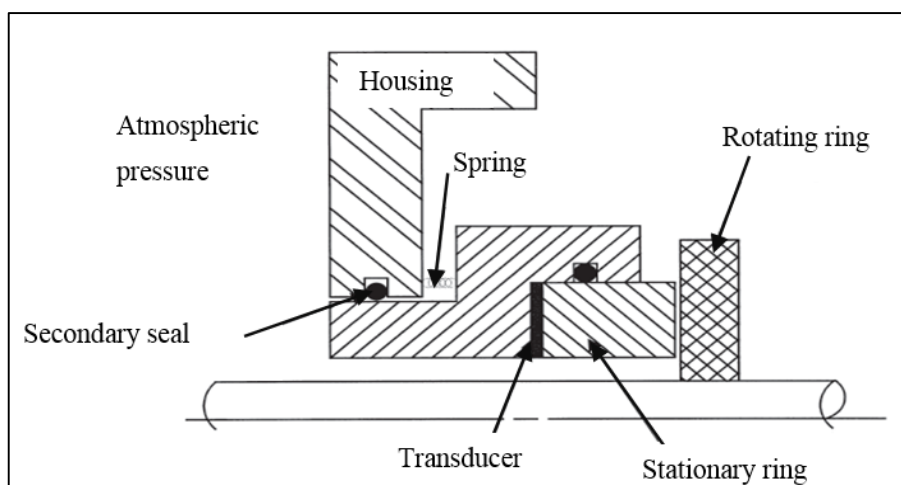


Figure 4.2 Illustration of film collapse detection using ultrasonic waves [160]

Later on Reddyhoff et al. [20] also estimated the film thickness over a range of loads and rotational speeds based on the same procedure as shown in Figure 4.3. They reported that while the rig is stationary the film thickness varied noticeably with the load. When rotating however, the lubricant film remained relatively stable around 2 μm . It is clear however the ultrasonic technique can detect the face contact as a qualitative tool, but is unable to evaluate the severity of contact. Moreover, this method cannot be used to measure the changes in the sealing gap (leakage rate) when the rings are fully separated due to the hydrodynamic lubrication established. These disadvantages hinder the practical application of ultrasonic method to monitoring the condition of mechanical seals.

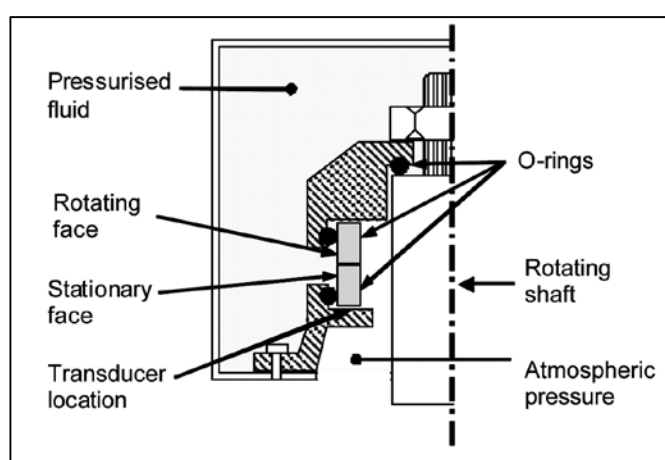


Figure 4.3 Basic concept of film collapse detection using ultrasonic waves [20]

4.2 Literature on the AE Condition Monitoring of Mechanical Seals

Acoustic emission is an effective technique for detecting incipient failures of mechanical seals in a wide variety of rotating machines from small pumps to large-scale turbine units. In all cases, by investigating the AE features, the failure modes as well as the effect of operational conditions on tribological behaviour of mechanical seals has the potential to be monitored. For instance in a review of monitoring techniques applied to steam turbine units [161], AE was identified as a condition monitoring technique that might detect the sliding contact between mating faces. However, at present some difficulties in fault generating in a controlled environment caused inconclusiveness in development of a strong diagnosis and prognosis for mechanical seals [36]. On the other hand, the high sensitivity of acoustic emission makes the interpretation difficult. Moreover previous researches widely reported that AE signals taken from different types of mechanical seal are affected by ambient noises [25-27]. Noise is widely defined as ‘any unwanted part of the signal (or data set)’ and therefore to ensure valid analysis conclusions, needs to be eliminated (or quantified) at the

time of data collection or during post-processing. Sikorska and Mba [36] report that when collecting AE data from machines, noise can originate from several external sources such as steady background noise from electronic components, Quasi-periodic transient events such as rubbing of seals or bearing faults and so on.

Separating the acoustic emission associated with a defect condition from noise is problematic. This is why a variety of techniques have been developed over the past 20 years to de-noise condition-monitoring data, with varying degrees of success when applied to acoustic emission signals. The present study aims to introduce a novel AE based experimental research for the purpose of condition monitoring of mechanical seals based on simple signal processing techniques. Attempt is paid to identify the noises based on an extensive experimental program which is further discussed in Section 6.5.

4.2.1 Traditional Acoustic Emission Sources at Seal Faces

The generation of AE waves during the sliding motion of two mating surfaces is attributed to different mechanisms such as adhesion, contact and deformation of asperities. The deformation and movement of a single asperity does produce an AE stress wave, but it is not large enough to be detected as an isolated process. However, when millions of asperities are combined and move at the same time, the individual stress waves overlap and superimpose to give a detectable result. It has been shown that the strength and rate of AE activity is dependent on sliding speed, friction coefficient of mating surfaces, contact pressure and the height of surface roughness [161]. Traditional process which may lead to AE wave generation are schematically presented in Figure 4.4. Interested readers may refer to work of Fan for a detailed discussion. [16]

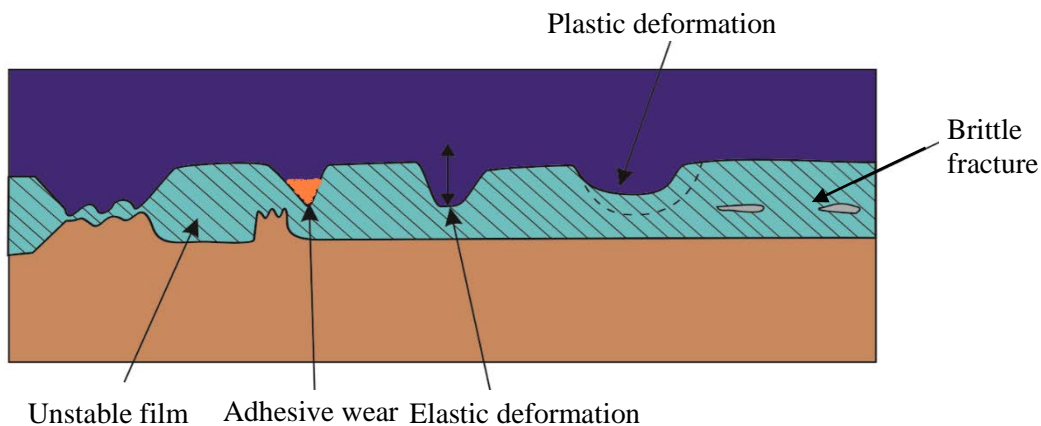


Figure 4.4 Illustration of acoustic emission sources in mechanical seals

4.2.2 Application of Acoustic Emission to the Sliding Contact

Acoustic emission has proven to be an effective tool to monitor the sliding contact and changes in lubricant properties [37, 38, 162]. For instance Asamene and Sundaresan experimentally observed acoustic emission signals generated by friction between two dry flat steel surfaces under several conditions of surface roughness, normal pressure, sliding speed and time duration [163]. They reported that friction related AE signals were distinguishable from other sources of acoustic emission.

The correlation between AE and wear variables in sliding contact have been well documented [7, 33, 133, 164, 165], although not all researchers have equal success quantifying all variables. For instance Hase et al examined the AE signals generated during the two main types of wear (i.e. adhesive wear and abrasive wear) using a pin-on-block micro-sliding friction tester, Figure 4.5. They stated that during adhesive wear, burst-type AE signals are produced as a result of the generation of wear elements and transfer of particles while in abrasive wear burst-type AE signals are generated by cutting and ploughing of material [133].

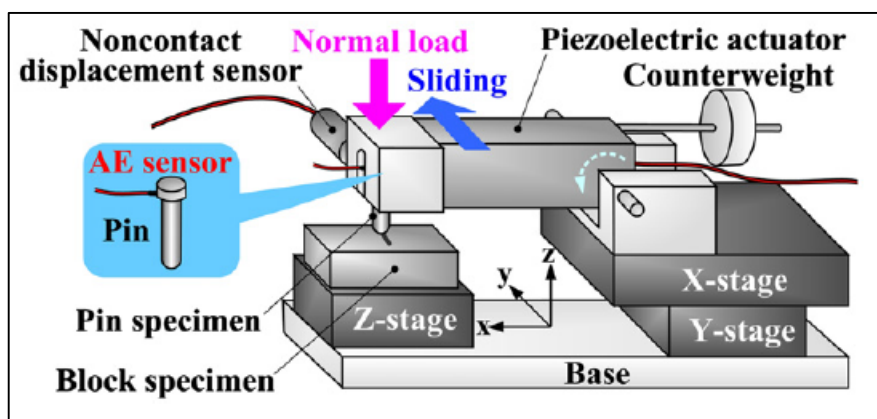


Figure 4.5 Illustration of pin-on-block-type test rig [133]

As most of the previous studies have been undertaken in laboratories with non-ceramic materials in the form of pin on disk, block or cylinder samples [33-35, 134], the application of results to modern ceramic seal faces in industrial applications must be undertaken with caution [36]. For instance Hase, Wada et al. have investigated AE signals generated by tribological actions under repeated dry rubbing on a pin on cylinder rig [135]. Different non ceramic materials such as Brass, Phosphor Bronze, Steel, Aluminium and Copper have been examined to study the formation and removal of wear particles. They stated that the AE

method can detect tribological phenomena such as the removal of transfer particles that cannot be detected from measurement of the coefficient of friction.

In another study, Benabdallah investigated friction, wear and acoustic emission properties of some plastic materials in the form of a stationary ball against a rotating flat disc of silicon nitride [166]. He showed that integrated acoustic emission energy ($\int AE dt$) increases with an increase in the wear volume. However, direct use of such studies in industrial applications may face some challenges.

Few studies using ceramic materials have been performed [33-35] which clearly shows that the application of AE measurements to explore the frictional characteristics of face seals in real applications are needed to be investigated further.

Since the energy of the AE signal is sensitive to high frequency events caused by frictional interactions it carries information about the details of such processes. Acoustic emission energy method can be used for detecting incipient failures of mechanical seals such as leakage and dry running. However, one or two researches are available in this area with positive outcomes. For instance in 1987, Kataoka et al. [29] stated that acoustic emission measurements could be applied to monitoring mechanical seals without interfering with its operation. Furthermore, it was stated that AE could monitor seals in real applications such as pumps. A correlation between AE levels and the mechanical integrity of the seals was determined based on laboratory and field tests by taking measurements on the actual seals and on their casings. In a subsequent study, Miettinen and Siekkinen studied the AE response to the sliding contact behaviour of a mechanical seal on the 15 kW centrifugal pump under different working conditions [30]. It was concluded that AE amplitude values of a leaking seal were on average 25% lower than in normal running conditions. The authors also stated the possibility of detecting dry running and cavitation in mechanical face seals. For instance, in case of dry running test, an even higher level of AE amplitude has been reported, however this study was only limited to a simple time domain analysis.

One year later, Holenstein et al. applied acoustic emission measurements for detecting deterioration of seals. A pilot system was developed and installed in a thermal power plant [32]. They applied different data analysis methods to correlate operating parameters and absolute wear. It was shown that a rise in AE levels was due to deformation of the seal surfaces and periodic contact. They stated that the main difficulty with the investigation is

that seal damage needs to be simulated on a test rig under realistic condition. Later on, Mba et al. confirmed that acoustic emission signals can be successfully used to monitor the onset and duration of seal-to-seal contact [31].

Another complication reported with AE condition monitoring of mechanical seals is that some failure modes result in a decrease in the signal amplitude or energy, contrary to expected trends [29, 30, 33]. This may be due to an increase in the lubricating film causing leakage, but decreasing wear and thus AE levels as pointed out by [36]. Alternatively, in ceramic materials, an oxide layer might be formed due to high temperatures at the sealing interface area. When this occurs, acoustic emission levels have been observed to decrease despite an increase in wear rate [33].

Despite the published work, the application of AE technology to monitoring the integrity of mechanical seals has been slow to develop and remains in its infancy especially for the purpose of fault detection.

4.3 Literature on AE Signals and Signal Processing Methods

The efficiency of condition monitoring techniques relies upon two basic elements: the number and type of sensors as well as the associated signal processing methods that are applied to extract useful information from the recorded signals [23]. In the case of AE condition monitoring, the extraction of important features from the recorded signal usually involves a number of confounding problems such as contamination from noise, interference from structural vibration, confusion of multiple modes and bulkiness of sampled data [142]. Bechhoefer et al. believe that from the signal processing perspective, acoustic emission has a number of perceived disadvantages [167]:

- AE signals are relatively high frequency; thus the sample rates must be high.
- Processing of the data, needed for feature extraction, is made more difficult because of the high sample rates and large volume of data that must be processed.
- Typical AE analysis is limited in its “action ability”, meaning that its can detect or count AE events, but does not tie the event to a component of the system.

The role of signal processing techniques is of high importance to present a proper interpretation of the captured signals. Various signal processing and identification

techniques can be applied for fault detection and failure diagnosis by analysis of the AE data obtained from the data acquisition system as schematically shown on Figure 4.6

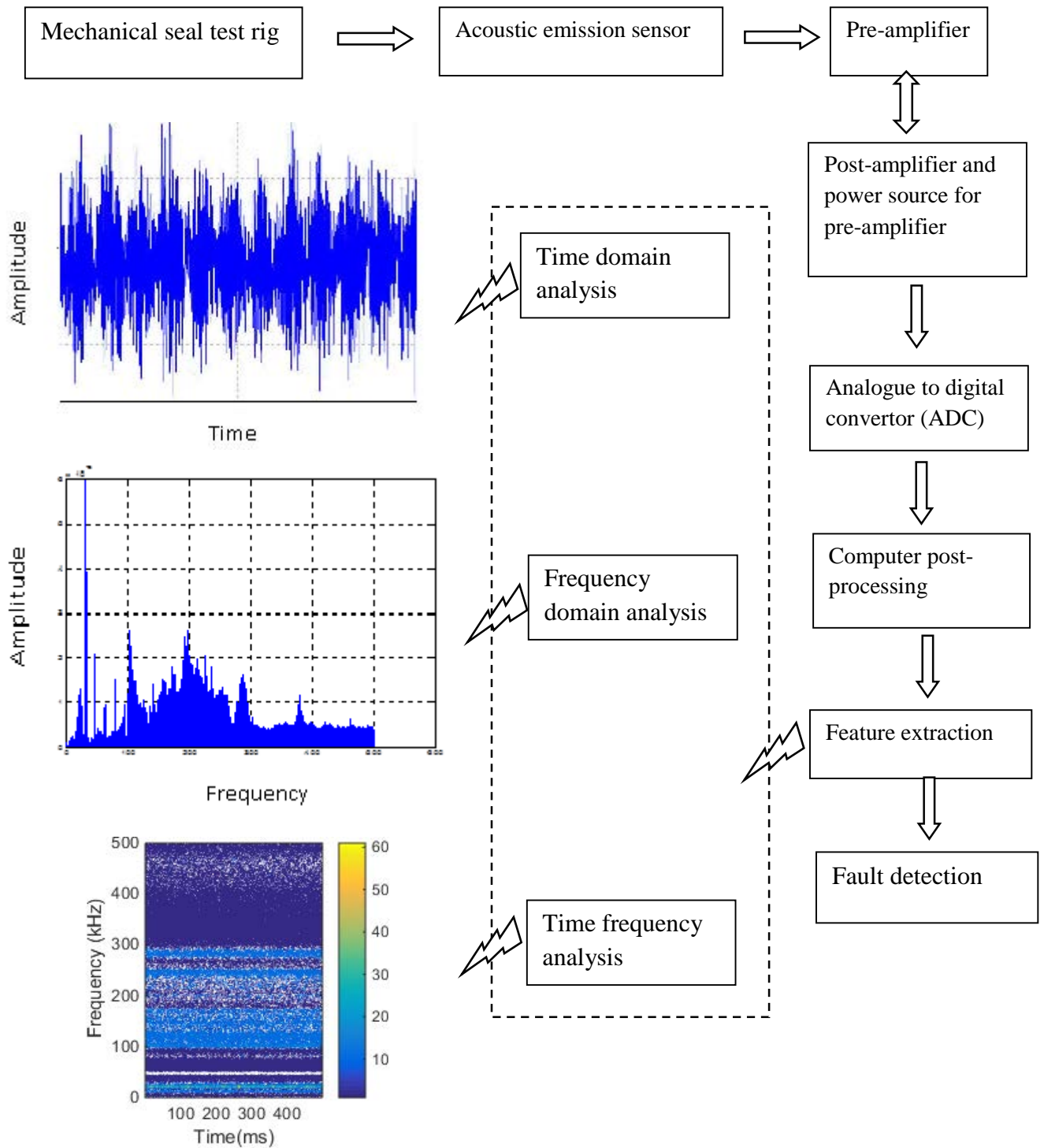


Figure 4.6 Overview of fault diagnosis based on AE signals

4.3.1 Time Domain Analysis

AE features extracted from the AE waveform are widely used for the purpose of condition monitoring and fault diagnosis, these features have been introduced in Section 3.3.2. Also the type of AE signal (i.e. continuous and transient signal) is used to evaluate the acoustic emission sources as discussed in Section 3.3.1.

Time domain statistical parameters are another area of research which are usually used for signal processing and drawing different features of signals. The statistical parameters are only based on the distribution of AE signals with the time series treated as a random variable. Extracting these features from raw AE signals is considered as a first level of signal processing. Using these statistical parameters researchers are able to summarize the data to extract meaningful and useful features.

Normally, time features such as mean value, standard deviation, root mean square (RMS), and peak value are used to describe characteristics of time series data from random, stationary, erratic and continuous processes. When damage occurs, a pickup in these values is usually observed. Among these features, RMS value of AE signal has been extensively discussed in the literature (see Section 5.2) and has been reported to be a measure of AE activity that can be related to the energy of emission or area under the signal curve. Table 4.1 summaries a typical set of time-based features and the information they convey about the source event where the time signal, $x(t)$, having N data points.

In AE applications mean value of the AE signal varies in a narrow band around zero. It arises due to the symmetry of AE time domain data. Hence the standard deviation sees approximately the values close to the RMS value. Therefore, to interpret the results in time domain, RMS and standard deviation are usually considered as an identical feature.

Due to variation of the mean value of AE signal in a narrow band around zero, skewness sees randomly the negative and positive values. This makes some difficulties in analysis of the results. Moreover, a clear physical concept for the skewness has not been reported yet. However, kurtosis is more interesting feature due to the fact that it only gets positive values. F.Y Edward [16] tried to correlate the kurtosis with the severity of contact in mechanical seals, but it was not completely successful. A novel physical concept for kurtosis is proposed in Section 7.3.3 which has good agreement with the tribological behaviour of the sealing gap.

Table 4.1 Summary of typical statistical parameters used for continuous signals [101, 141]

Feature	Summary description
<p>Mean value (\bar{x}) or the first moment of amplitude distribution function</p> $\bar{x} = \frac{1}{N} \sum_{i=1}^N x_i \quad (4.1)$ <p>where</p> <p>N is the number of data points;</p> <p>x_i is the data at each discrete point in time.</p>	<ul style="list-style-type: none"> Measures the central distribution of discrete time series data. For AE signals is zeros in theory. In measured signals may have very small values which is arise from measurement system.
<p>Root mean square (RMS) value</p> $RMS = \sqrt{\frac{\sum_{i=1}^N x_i^2}{N}} \quad (4.2)$	<ul style="list-style-type: none"> Measures square root of mean square in the density probability function. Indicates energy contained in continuous AE data.
<p>Variance or the second moment of the amplitude distribution function.</p> $\sigma^2 = \frac{1}{N} \sum_{i=1}^N [x_i - \bar{x}]^2 \quad (4.3)$	<ul style="list-style-type: none"> Indicates the spread or dispersion or distribution of the density probability function.
<p>Standard deviation</p> $\sigma = \sqrt{\frac{1}{N} \sum_{i=1}^N [x_i - \bar{x}]^2} \quad (4.4)$	<ul style="list-style-type: none"> Indicates the spread or dispersion or distribution of the density probability function.
<p>Skewness or the third moment of amplitude distribution function.</p> $Sk = \sum_{i=1}^N \left[\frac{x_i - \bar{x}}{\sigma} \right]^3 \quad (4.5)$	<ul style="list-style-type: none"> Measures the extent of the asymmetry distribution of the density probability function. $Sk = 0$ represents normal distribution such as AE signals. For, $Sk < 0$ the left tail of distribution is heavier than the right tail and the opposite for $Sk > 0$.
<p>Kurtosis (Kt) or the fourth moment of amplitude distribution function.</p> $KT = \sum_{i=1}^N \left[\frac{x_i - \bar{x}}{\sigma} \right]^4 - 3 \quad (4.6)$	<ul style="list-style-type: none"> Demonstrates the flattening of the density probability function near the average value. $KT > 0$ represents a peaked distribution. $KT < 0$ represents a flat distribution.

4.3.2 Frequency Domain Analysis

Frequency domain Analysis is a method applied to analyse data and refers to analysing a dynamic signal with respect to frequency. The advantage of spectral analysis over time domain analysis is its ability to identify and isolate certain frequency components of interest. The main idea is to either look at the whole spectrum or look closely at certain frequency components of interest and then extract desired features from the signal [168].

The Fourier transform (FT) is usually used for the conversion of a recorded signal from the time domain into one in the frequency domain. The FT transforms mathematically a time-dependent AE wave signal, $f(t)$, into the frequency domain by [141, 142]:

$$F(\omega) = \int_{-\infty}^{\infty} f(t) e^{-j\omega t} dt \quad (4.7)$$

where ω and j are the angular frequency and unit complex, respectively. $F(\omega)$ is the Fourier counterpart of $f(t)$. From the point of view of mathematics, frequency domain analysis is mostly used on signals that are periodic over time. Originating from the Fourier transform but with enhanced ability, the fast Fourier transform (FFT) is able to speed up this transform. The fast Fourier transform is widely used for AE wave signal analysis [168] and to identify the frequency features of dynamic signals [169].

Spectral analysis can generally indicate machinery faults better than time domain features because characteristic frequency components such as resonance of a component or particular frequency component correspond to particular states (e.g. fault-free, defective components) and it is relatively easily detected and matched to the faults [23]. This can be implemented by considering the fact that the useful information provided by the frequency spectra is often the change of the frequency components and their amplitudes for different working conditions. For instance Hase et al reported that different mechanisms of wear (i.e. adhesive and abrasive wear) can be recognized from the features of the AE frequency spectrum such as frequency peak and frequency band [133].

AE spectral analysis is more affected by noise rather than time domain or time-frequency analysis. Most of the noise has specific frequency components with constant amplitudes. Filtering can be used to separate the noise from the signal, thus improving the signal-to-noise ratio (Nashed 2010). However, some sources of AE can sometimes be masked by noise.

Analysing the AE signal in the frequency domain is more effective if it can characterise the signals under noisy conditions. For instance Sato used the spectrum of the envelope AE waveform to monitor seal rubbing on an operational 350 MW steam turbine under real noisy industrial condition [170]. It has been reported that the rub source location could be effectively determined using the time or phase difference between the AE modulated signals from two sensor channels. Furthermore, Sato stated that rotational frequencies of the turbine were generated with rubbing. Wang and Chu carried out the same analysis but on a test-rig in the lab [171]. It was stated that due to the influences of impacting, structural characteristic, oil film and noise, a conventional frequency domain technique was unable to aid identification of the rub source. The situation sometimes get worse to identify effective features for fault diagnosis in the frequency spectra due to the other limitations mainly caused by the nature of AE events, attenuation, dispersion, multiple reflections and the non-linear character of AE signal during its propagation [16]. Moreover, a spectral peak at a particular frequency may have several possible causes.

The techniques were also applied by calculating correlation or logarithmic value of transformation parameters. For example, the power spectrum, as a second order spectrum, whose amplitude is the square of the amplitude of the spectrum is an effective method to diagnose machinery faults [172, 173]

The higher order spectra, bispectrum and trispectrum, can be applied to fault diagnosis in rotating machines [174] as well. For instance Ibrahim et al. used the bispectrum to develop pre-processing procedures for bearing condition monitoring because of its ability to provide improved diagnostic capability (i.e. suppression of noise) compared with conventional power spectrum analysis [175]. In another work, Gu et al developed a novel method for fault diagnosis of planetary gearboxes based on an accurate estimation of residual sidebands using a modulation signal bispectrum method [176].

4.3.3 Time-Frequency Analysis

A number of studies have investigated the use of time domain and frequency domain in processing the AE signals from rotating machines such as mechanical seals [31, 32, 177] and journal bearings [115]. However, the signals collected from many rotating machines are non-stationary random signals where the background noise level is fluctuating significantly with the time. It can be caused by several reasons such as fault development or even periodic changes in the operational parameters (rotational speed and load) of the system within a single rotation cycle [172]. This means that the shorter the time waveform used to calculate statistical parameters, the greater the likelihood that the parameter does not accurately describe the underlying signal. Even an average of the parameter, calculated from a large ensemble of waveforms, may not be particularly useful as it does not describe the spread of a parameter's values [36]. During the past decades, various joint-time-frequency methods have been studied and applied to machinery fault diagnosis due the deficiencies of either time- or frequency-domain analysis of the non-stationary signals. Most time–frequency algorithms can be generalized as [142]:

$$P(t, \omega) = \frac{1}{2\pi} \int_{\beta} \int_{\alpha} \int_{\theta} e^{-i\theta t - i\alpha \omega - i\theta \beta} \varphi(\theta, \alpha) f_w^* \left(\beta - \frac{t}{2}\right) f_w \left(\beta + \frac{t}{2}\right) d\beta d\alpha d\theta \quad (4.8)$$

where $P(t, \omega)$ is the energy intensity at time t and frequency ω , f^* denotes the complex conjugate of the wave signal, f_w , and $\varphi(\theta, \alpha)$ is a function depending on $f(t)$.

In practice, rather than direct time–frequency analysis, some variants of Equation (4.8) are more popular e.g. short-time Fourier transform (STFT), Winger-Ville distribution (WVD), and wavelet transform (WT). The former is applied in this research and others are beyond the scope of present study.

Short-time Fourier transform (STFT) analysis, introduced by Dennis Gabor in 1946, was developed to improve the efficiency of the Fourier transform or Fast Fourier transform for non-stationary signals [142]. STFT is the simplest time-frequency decomposition of a signal and may be considered as a method that breaks down the non-stationary signal into many small segments around a specific time window ('short time'), which can be assumed to be locally stationary, and applies the conventional fast Fourier transform to these segments.

Continuously moving this short time interval along the time axis, STFT can map a time-dependent wave signal into a 2D representation. Preliminary time frequency analysis techniques, windowed Fourier transform [178] and Short time Fourier transform [179, 180] were applied to monitoring the condition of rotating machines.

4.4 Main Findings

Many condition monitoring techniques can be applied to evaluate the integrity and monitor the tribological behaviour of mechanical seals. Among them the eddy current and ultrasonic methods have been widely used. Some of these methods require modifying the mechanical seal structure, others involve with expensive cost.

Whilst the effectiveness of AE measurements for mechanical seal condition monitoring is well established, the application of this technique in the field of tribology and early fault detection in mechanical seals is still in its infancy. Among the AE features extracted from the waveform in the time domain, root mean square (RMS) value is widely used for the purpose of condition monitoring and fault detection. At present difficulties in generating faults in a controlled environment caused inconclusiveness in the development of a strong diagnosis and prognosis for mechanical seals.

Chapter Five;

Mathematical Modelling

In this chapter the investigation develops a comprehensive mathematical model which can predict the energy of an AE signal under different tribological regimes. This is of high importance to monitor the sealing gap and detect faults at the early stages. This chapter starts with the introduction of theories on acoustic emission source modelling which includes both empirical and mathematical models. This is followed by a general literature review on the application of the AE energy methods for condition monitoring of tribosystems. Then new sources of acoustic emissions in tribosystems are introduced which includes the direct asperity contact between two rough surfaces, the viscous friction between fluid layers and elastic deformation of asperities due to hydraulic induced pressure and shearing effects of the moving lubricant. This is followed by an introduction to the characterisation of solid surfaces and the contact between asperities. Then the behaviour of asperity contact at the sealing gap is explained based on the Greenwood-Williamson model and Hertz theory. Finally, the AE sources are mathematically modelled based on the working parameters of seals. These models may explain nonlinear tribological behaviour of mechanical seals compared with those available in literature.

5.1 Background of AE Source Modelling

Modelling of the stress waves that are generated by acoustic emission sources has played a major role in condition monitoring and fault diagnosis applications. AE source modelling includes three major area of research, empirical models, mathematical models and finite element models (FEM). The latter is beyond the scope of this research and has been discussed extensively in the literature [181, 182].

5.1.1 Empirical AE Models Related to Friction

To gain an understanding of the relations between the characteristics of AE signals and the process parameters, empirical models are first developed. In 1990 Jiaa and Dornfeld [183] have investigated the frictional AE signal rate on a pin-on-disk test rig. They simulated experimentally dry sliding contact and proposed the empirical relation as bellow:

$$\dot{U}_f \propto (\tau_s A_s V)^{K_m} \quad (5.1)$$

where τ_s is the shear strength of the interfacial layer, A_s is the actual area of a contact, V is the sliding speed and K_m is a constant determined by the material system and the detection equipment and can be assumed to be 1.0 [99]. In a consequent study Mullins et al. reported that with stronger interfacial film layers or with increasing sliding speed, the average frequency and amplitude of AE signals increase that leads to a non-linear increase in the energy detected by the AE sensors [184]. They mentioned that the total acoustic emission energy release rate can be expressed as:

$$\dot{U}_{fT} = \int_A a_f (\tau_s A_s v_s)^{\frac{m}{2}} dA_{tot} = \int_A a_f (F_f v_s)^{\frac{m}{2}} dA_{tot} \quad (5.2)$$

where

a_f is a proportionality factor

A_{tot} is the total contact area

F_f is the friction force

5.1.2 Mathematical AE Models

Mathematical modelling of AE sources is widely used in condition monitoring of tribosystems. This offers benefits in evaluating the performance of machines, studying how operating parameters of a system work and improving diagnosis of frictional processes. In this research area, mathematical modelling mainly includes modelling of AE source mechanisms as well as signal propagation and transmission paths to pave the way for effective condition monitoring and early fault detection.

Since direct asperity contact is considered conventionally as the main cause of all failures in sliding contact of mating surfaces [16, 61], Figure 5.1, contact modelling becomes an essential part of any AE friction model. It consists of two related steps. First, the equations representing the AE generated in contact of a single pair of asperities are extracted. Second, the cumulative effects of individual asperities are determined. Considering the first step, AE signals generated during frictional process are modelled mathematically using two general approaches.

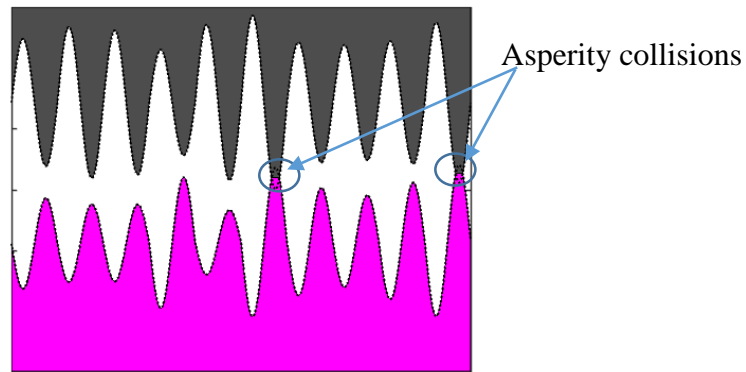


Figure 5.1 Schematic illustration of direct asperity contact

The first approach is integrating the friction force over sliding distance $\int F_f ds$, where S is sliding distance and defined as the distance that a pair of asperities move over each other in the direction of sliding. Assume that the circular contact area (with radius of a) is formed during asperity contact, Figure 5.2, the sliding distance can be defined as:

$$S = 2a + 2a = 4a \quad (5.3)$$

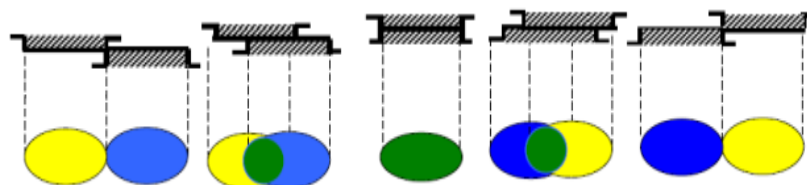


Figure 5.2 The concept of sliding distance in asperity contact

This method has been used by Benabdallah [166] and Towsyfyan et al. [185] to model the frictional energy released during direct asperity contact. The same idea is found in pioneering work published by Archard in 1953 [186], however he assumed that the total distance of contact is the sum of the individual asperity contact area. For micro scale contacts the effect of adhesion on the contact area is important [61] that is not considered in this approach and for that reason has been used less frequently.

Another approach for modelling acoustic emission in frictional process is based on strain energy released during elastic deformation of the asperities. F.Y.Edward et al. [187] used the integration of contact load over elastic deflection of the asperities ($\int W d\delta$) to model the stored strain energy during sliding contact of mating surfaces. In 2017, Sharma and Parey used this approach to model the stored elastic energy for the asperities contact between the surfaces of inner race-rolling element and outer race-rolling element [188]. The idea behind such models considers every asperity as a spring under axial loading. Hence continuous compression and release of asperities in sliding contact generates AE waves which is proportional with contact load, W , and elastic deflection of asperities, δ , in the direction of the applied load, Figure 5.3.

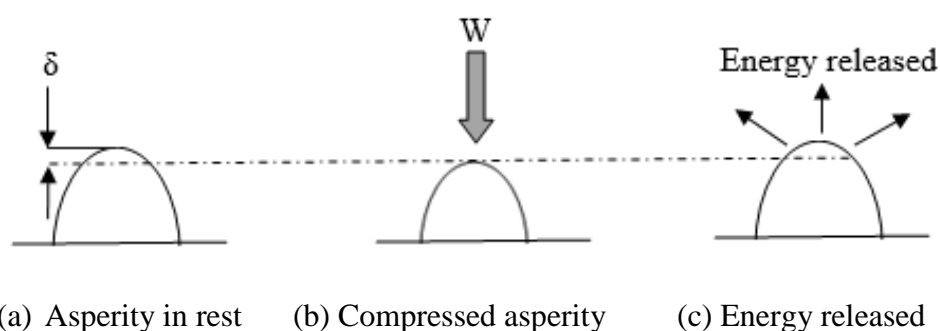


Figure 5.3 The concept of strain energy released in sliding contact

However, based on the above idea it is not possible to explain why continuous and burst type AE signals are generated during the contact of mating faces. F.Y.Edward [16] states that ‘The asperity contact between seal faces is not always continuous during the operation of

mechanical seals. When the contact load is light, asperity contact only last for a short time in one rotational period and burst-type acoustic emission is observed. When contact load increases, the asperity contact will last longer. If the asperity contact is enough, the generated bursting emissions will overlap each other and continuous AE signal will be observed'. Primary investigations in this research shows that both continuous and burst type AE signals are generated during different operating condition of mechanical seals, whether the contact is light or massive, therefore some improvements in the model developed by F.Y.Edward [16] is necessary that can explain the phenomena more clearly.

In this thesis attempt is made to model the strain energy released during the dynamic bending of asperities which is more consistent with the physics of sliding contact in mechanical seals and can proposes logical explanation for existence of both type AE responses in the time domain signal, see Section 5.8. The bending of asperities occurs due to collision and interaction of asperities in the boundary and mixed lubrication region, while in the hydrodynamic lubrication region the stress field of moving fluid can cause bending of asperities when a pair of asperities approach each other and then release when they leave the interaction area as will be discussed further in Section 5.6.

5.2 Quantifying of AE Energy Released in Frictional Process

Most of the work related to AE condition monitoring of tribosystems commonly use the root mean square (RMS) value of the AE signal to quantify the energy of frictional process. For instance, Boness et al. [189] investigated the RMS value of AE signals obtained from sliding metallic contacts. They showed that RMS measurements are able to differentiate between different wear mechanisms occurring in both dry and lubricated contacts from the tests carried out on a ball-on-cylinder test apparatus. One year later they established a direct empirical relationship between integrated RMS signal and wear volume removed in the sliding contact [34].

In 2007 F.Y.Edward reported that RMS value of AE signal is not affected by signal distortion and transmission paths [16]. He showed experimentally that RMS value of external AE measurements could keep the signal trend obtained by the internal measurements (see Section 3.6.1). Since his work has been carried out on a mechanical seal test rig, it gives an encouraging motivation for this research to monitor the condition of mechanical seals using external measurements.

Research has been reported in the literature showing that a strong relationship exists between the RMS value of AE signals and the friction state of mating surfaces in sliding contact [35, 190]. For instance Huang et al. [191] investigated the frictional behaviour and characteristics of the AE signals recorded from a pump dry gas seal. They reported that expressing the AE energy level using the RMS value by an appropriate frequency band not only traces the friction state of mating faces but also can effectively reduce the interference of noises.

Whilst the effectiveness of RMS value of AE signals for condition monitoring of the mating faces is well developed, the application of RMS based mathematical models to explain the tribological behaviour of mechanical seals based on dominant AE sources is still in its infancy. In general, the energy released by AE source mechanisms in any desired time interval can be expressed as:

$$U_{AE} = \int_0^{\infty} \dot{U}_{AE} dt \quad (5.4)$$

where \dot{U}_{AE} is the acoustic emission energy release rate during the interaction between two media. Assume that the acoustic emission sensor converts the collected ultrasonic energy to electrical voltage, the energy of the acoustic emission signal in terms of measured electrical voltage can be expressed as:

$$U_{AE} = G_E \int_0^{\infty} V_E^2(t) dt \quad (5.5)$$

where G_E is the electrical conductance of the AE measuring circuit. Considering Equations. (5.4) and (5.5) the RMS value of AE signal is given by:

$$V_{rms} = \sqrt{\frac{G_E}{T} \int_0^T V_E^2(t) dt} = \sqrt{\frac{1}{T} \int_0^T \dot{U}_{AE} dt} \quad (5.6)$$

where T is the selected duration of the AE signal. Assuming the sliding between two surfaces is stable, the RMS value of AE signal based on the acoustic emission energy release rate can be expressed as follow:

$$V_{rms} = \sqrt{\dot{U}_{AE}} \quad (5.7)$$

From Equation. (5.7) and assuming that the frictional behaviour of the seal faces is stable, it can be concluded that a theoretical relationship exists between the RMS value of the AE signal and the energy excited by the multiple interactions between the acoustic emission sources.

In 2010, F Y Edward et al. [187] developed a mathematical model for direct contact of asperities and pointed out that the level of AE signals depends on the sliding speed, the load supported by contact asperities, the number of asperity contacts and surface topographic characteristics. Based on this model the AE RMS has a square root relationship with sliding speed and contact load. However, they failed to validate the model and reported that based on their experimental study, the relationship between AE RMS value and contact load is linear. Hence, it seems necessary to find more accurate equations that can clearly predict the level of acoustic emission excitations in sliding contact of face seals.

Furthermore, either previous empirical relationships or theoretical models predict the level of AE signals due to direct asperity contacts. However, based on the tribological behaviour of mechanical seals the mating surfaces maybe well separated because of the hydrodynamic lubrication established. Thus it is necessary to propose a comprehensive model which can explain the tribological behaviour of the mechanical seals especially in mixed and hydrodynamic lubrication regimes where they are supposed to work ideally. Consequently, it is expected that the model can estimate the frictional energy generated from acoustic emission sources under different lubrication regimes. This may explain why frictional energy changes under different lubrication regimes which could be useful for the purpose of fault detection in tribosystems.

5.3 Novel AE Source Mechanisms

The amount of acoustic emission energy released during the frictional process depends primarily on the source of the generated stress energy. The traditional acoustic emission sources have been discussed in the Section 4.2.1. It is unlikely possible to explain the acoustic emission signal recorded under different working condition of mechanical seals based on traditional source mechanisms. Hence it is necessary to model dominant acoustic emission sources by which the tribological behaviour of face seals can be explained under both healthy and defective conditions. Based on the operational conditions, three main

mechanisms may contribute to acoustic emission energy release in mechanical seals as shown schematically in Figure 5.4.

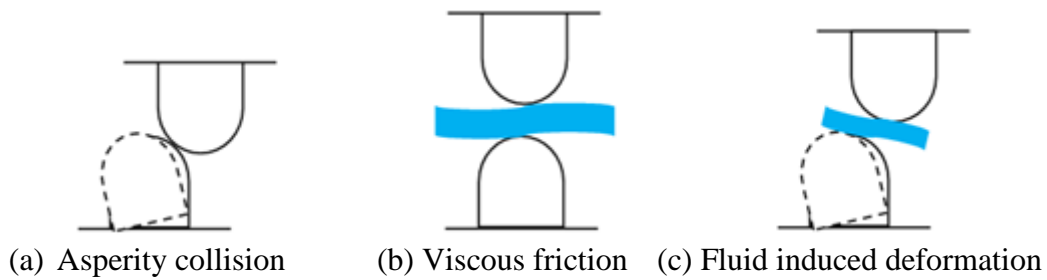


Figure 5.4 Schematic illustration of AE generating mechanisms at sealing gap

In a properly maintained hydrodynamic lubrication regime, the main sources of acoustic emission are the viscous friction due to shearing lubricant at sealing interface and deformation of asperities due to hydraulic pressure induced by relative motion of asperities. The latter type of acoustic emission source can be understood to be the effect of fluid stress field that cause an alternation between asperity elastic deformation and recovery as moving asperities approach and leave the stationary asperities, Figure 5.5. Further details are given in Section 5.3.2.

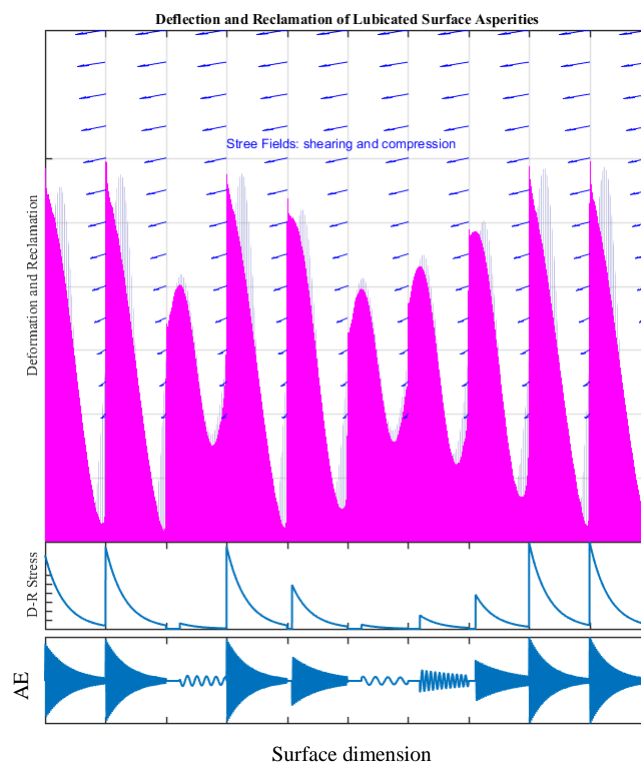


Figure 5.5 AE signal generated due to fluid induced asperity deformation

Fluid stress field changes due to the fact that fluid pressure increases when the asperity is approached and decreases when the asperity is left behind, this phenomenon is called micro asperity lubrication in the literature [42, 43]. Under this condition ideally no asperity contact occurs, however the compression and recovery of asperities may produce high frequency AE waves due to the micro-scale size of asperities and high fluid flow, Figure 5.5. These deformations may generate fatigue crack in the mating faces.

By reducing the duty parameter (increasing the load or reducing the speed) to the mixed lubrication regime, the interaction and collision between asperities generates high frequency AE signals that is well documented in the literature [16]. In the meantime, similar to the effect of fluid shearing, the alternation of deformation and recovery by the collision of asperities produces AE responses. In this region same as hydrodynamic lubrication region, viscous friction between fluid layers generates AE waves. This mechanism can be understood to be the effect of resultant force excreted from the mating asperities to the lubricant fluid that generates high frequency AE waves due to shearing in lubricant layers, Figure 5.6. Further details are given in Section 5.3.3.

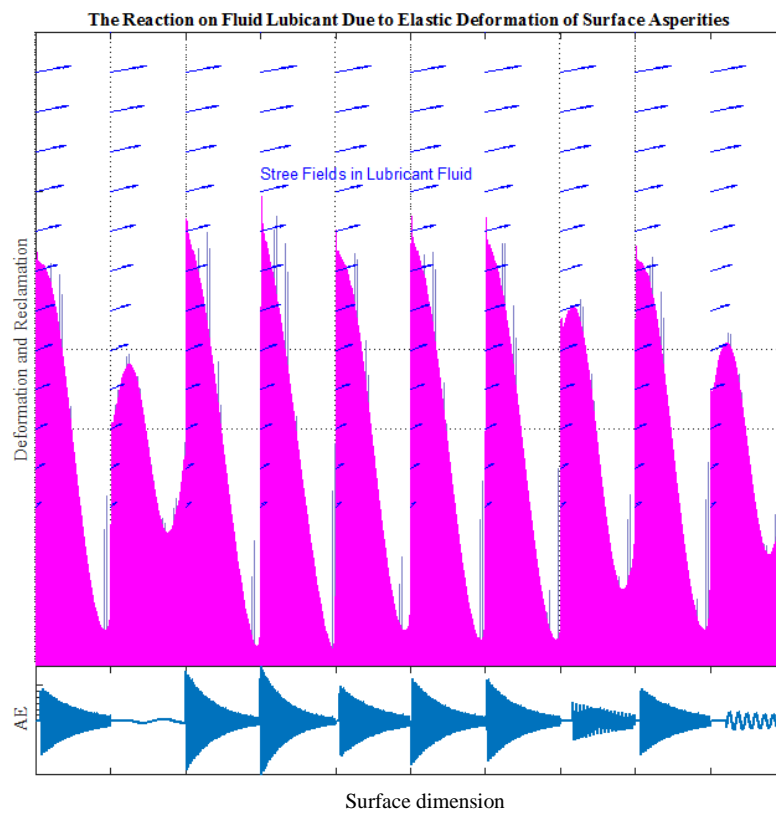


Figure 5.6 AE signal generated due to shearing in the lubricant fluid

5.3.1 Asperity Collision Induced Emissions

As discussed in Section 5.2, direct asperity contact is one of the main sources of AE excitations in the sealing gap and not only for mechanical seals [16] but also for other rotating elements such as journal bearings [192] has been well documented.

As schematically shown in Figure 5.7, the sliding movement of mating faces causes a bending load on contact asperities when a pair of asperities approach each other and then release when they leave the interaction area. This compression and release generates high frequency vibration responses. As long as the contact load stays light, dynamic-response stress distribution is confined to an area near the interface. At higher contact loads, the stress field around each true contact spreads and starts to interact with the stress fields of the other contacts, eventually developing into a full stress field in the body. Because the system is dynamic, these contact stresses lead to waves in the bodies and transport some of the energy away from the contact areas [193].

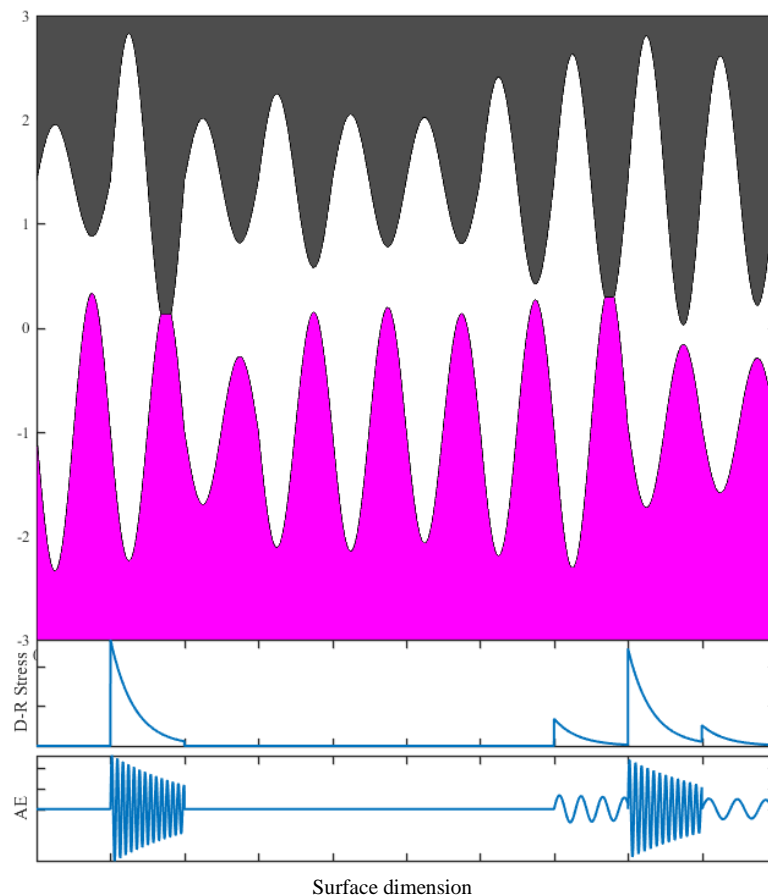


Figure 5.7 AE wave generated due to bending of asperities in direct contact

5.3.2 Flow Induced Emissions in Asperities

The purpose of this section is to describe analogies between fluid-asperity friction and asperity-asperity friction. Focus is paid to explain how the hydraulic force caused by the lubricant flow leads to the development of a vibratory behaviour in the surface asperities.

Fluid flow over a rough surface exhibits an analogous behaviour with direct asperity contact where local pressure fields develop around the asperities on a surface. At low Reynolds (Re) numbers, the influence of pressure fields remains local. As Re increases by increasing the rotational speed of shaft, the pressure field around each asperity spreads and starts to interact with the pressure fields around the others [67]. It should be immediately noticed that F.Y. Edward [16] calculated the Re number for different rotational speeds of shaft. Based on his calculations the Re at rotational speed of 1500 RPM is 239557 and hence the fluid flow in this research is laminar, however some turbulences accrue locally around the asperities due to development of boundary layer.

In spite of the above analogies, the nature of contact of a fluid flow over a rough surface differs from that between two solids. In solids actual contact takes place between crests of waves or tips of asperities while at the fluid interface, contact develops everywhere. In the case of a fluid, boundary layers develop and carry momentum into the free-stream flow that may cause flow induced vibration (FIV). Flow induced vibration is a wide area of research itself and can be generated due to different source mechanisms. These mechanisms are beyond of the concept of this thesis, interested readers may refer to references [194, 195] for a comprehensive review and detailed discussion.

Historically the first attempts to suppress flow induced vibration are found in the civil engineering design of chimneys and suspension bridges [196]. Recently, following the exploration of oil in deep waters, it became a real concern for the offshore industry [194]. Flow induced vibration also may happen in internal flow. As an example flow of a fluid through a pipe that can impose pressures on the walls of the pipe causing it to deflect under certain flow conditions. This deflection of the pipe may lead to structural instability and vibration of the pipe [197].

The evidence of flow induced vibration has been well documented [194, 195]. However, the effects of stress field of lubricant flow on the AE excitation of micro scale size asperities has not been reported yet.

Based on the above understandings, it is not difficult to imagine that a type of flow induced vibratory behaviour can also take place in the asperities of the sealing gap. To explain this,

three different position of interacting zone are considered to explain the changes in the fluid velocity as schematically shown in Figure 5.8.

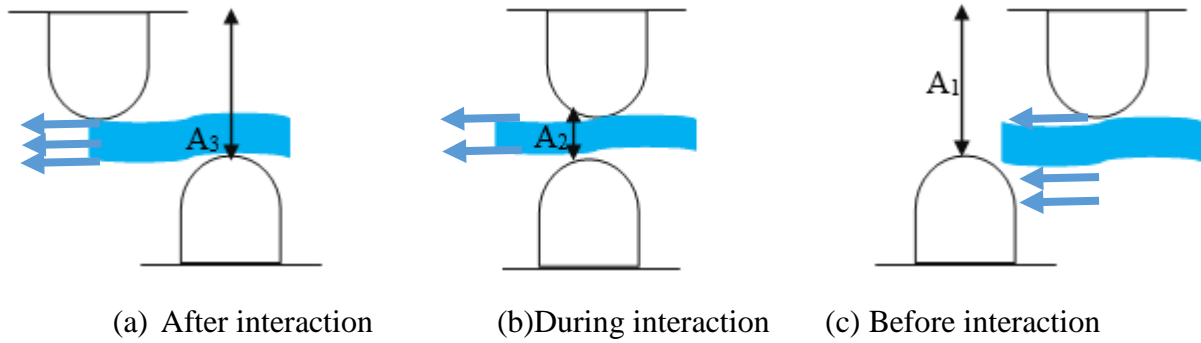


Figure 5.8 The changes in fluid passing area confined between asperities

Since the flow rate of lubricant flow, Q , is constant (as long as sealed pressure is constant) hence:

$$Q_1 = Q_2 \rightarrow A_1 V_1 = A_2 V_2 \rightarrow V_2 > V_1 \quad (5.8)$$

$$Q_3 = Q_2 \rightarrow A_3 V_3 = A_2 V_2 \rightarrow V_3 < V_2 \quad (5.9)$$

Based on Equations (5.8) and (5.9), the velocity of flow first increases and then decreases since asperities approach and left each other. Considering the Bernoulli Equation as follow:

$$P + \frac{1}{2} \rho V^2 + \rho g h = cte \quad (5.10)$$

Where P and ρ are fluid pressure and density respectively, it is easy to conclude that

$$P_2 < P_1 \text{ and } P_3 > P_2 \quad (5.11)$$

Having demonstrated the changes in fluid velocity and pressure caused by the relative movement of asperities, the changes in fluid forces can be explained. Two component of fluid flow are considered, viscous friction (drag) force, F_D , and pressure force, F_p . Figure 5.9 shows schematically how these forces change during interaction of asperities with flow fluids. The resultant force, F_R , is shown by red colour. The value of drag force depends on sliding speed while the pressure force is a function of pressure.

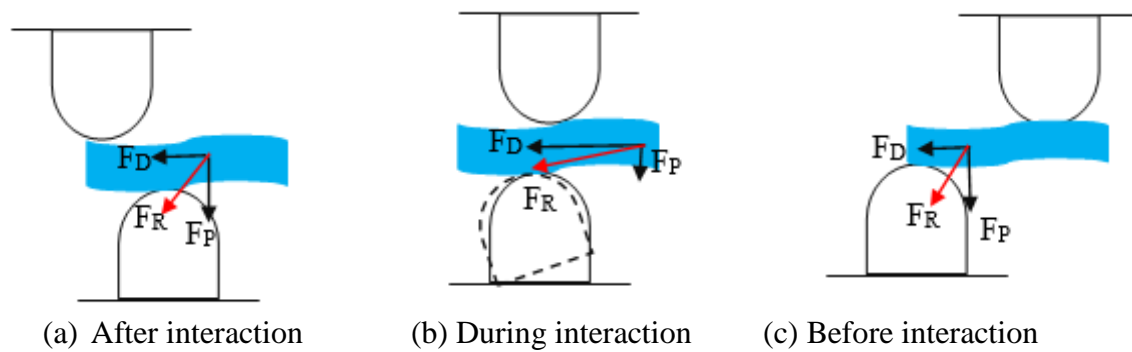


Figure 5.9 The changes in the fluid forces exerted into asperities

Considering asperities as free end cantilever beams, the change in the value and direction of resultant force exerted on every single asperity may cause a bending moment. Consequently, the deflection and recovery of asperities may produce high frequency acoustic emission waves that is modelled in Section 5.6. This energy is then directly converted into heat as it is absorbed into the random motion of the molecules by viscosity [66].

5.3.3 Friction Induced Emissions in Fluid Lubricant

The purpose of this section is to explain the mechanism of friction-induced emissions in the lubricant film that is confined between the mating surfaces. In general, few researches are available in the field of fluid borne sound [198], consequently the interest of this section emerges from the lack in literature of studies focused on the acoustic emission signals generated from such vibrations.

As has been discussed in Chapter 2, the tribological behaviour of fluid film varies under different lubrication regimes. In the boundary lubrication regime, a thin fluid film is confined between the mating faces and shows specific properties that strongly differ from those of the hydrodynamic lubrication regime. These changes have been extensively studied in the literature [199, 200].

The friction response of such confined layers under shear stress can be complex and depend on the operating conditions, the nature of the surfaces and their mechanical and topographic characteristics, as well as the nature and shape of the confined fluid molecules [201, 202]. These responses transmit energy from the flow to the surrounding solids as well as dissipates the kinetic energy of the flow as viscous shear stresses perform work.

The mechanism studied most widely to investigate the friction induced vibration is often called the mechanism of the falling friction characteristic as shown in Figure 5.10 [60, 203, 204].

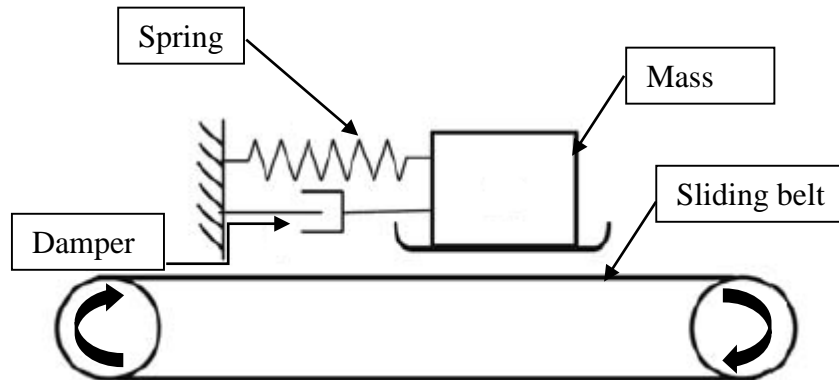


Figure 5.10 Single degree of freedom friction drive oscillator

This system composed of a mass held against a moving band with a confined lubricated interface that is considered a viscoelastic medium. During shear in fluid layers the contact area consists of some independent adhesive junctions. At any time of shear, individual junctions are continuously formed and broken incoherently. Each junction remains in the bonded state until it is elastically stretched under shear, up to a yield distance beyond which it becomes free as schematically shown in Figure 5.11. It should be immediately noted that a critical sliding velocity is needed at the junction becomes free under shear. As a result of alternative forming and breaking the junctions, an integrated water film is difficult to form or being destroyed on the point of forming. This generates vibration in the spring and mass system as has been reported by Sinou et. al [203].

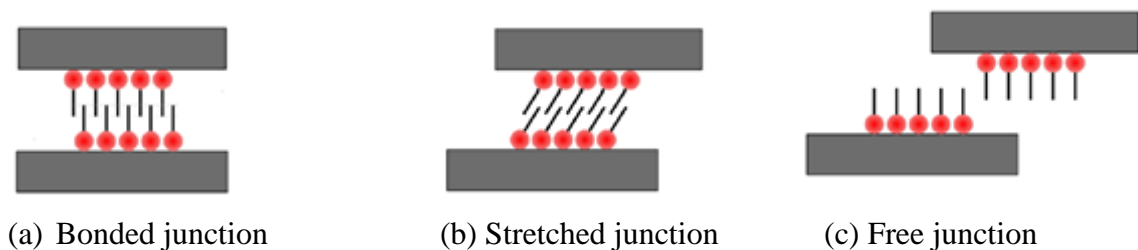


Figure 5.11 Shear induced vibration [203]

In case of fluid layers confined between the mating faces in the sealing gap, the changes in the value and direction of resultant force (excreted from the mating faces to the lubricant layers) may cause a vibratory behaviour in fluid that generates high frequency acoustic emission waves as has been shown in Figure 5.6. Various models have been proposed in the literature to characterize this type of fluid induced vibrations [203], however no work has been published on modelling the AE signals generated by this mechanism.

5.4 Contact Mechanics of Randomly Rough Surfaces

Greenwood and Williamson [205] pioneered the so called “asperity-based model”. Based on this approach the contact of two engineering flat surfaces with roughness Rq_1 and Rq_2 can be estimated by converting it into the contact between two surfaces; one is assumed smooth and the other is a rough surface with equivalent roughness $Rq = \sqrt{Rq_1^2 + Rq_2^2}$. The model assumes that: (1) the rough surface is isotropic; (2) the rough surface covered with a large number of asperities with spherical summits distributed with a density D , i.e. the number of summits per unit area; (3) all the asperity summits have equal and constant radius of curvature while the asperity heights vary randomly; (4) there is no interaction between neighbouring asperities; and (5) there is no bulk deformation. The existing literature shows extensions of the Greenwood and Williamson model over the last three decades. These models differ in their assumptions related to surface and asperity geometry and material properties, a great review is found in [206].

Of particular interest to the modelling goal of this thesis is the surface model in which asperities are allowed to form contact on both tips and shoulders. In the derivation of the equations for such a contact, the behaviour of the asperities is initially elastic. As the contact load is increased the elastic behaviour continues to describe the deformation until a critical interference is reached. At this critical load and beyond, the asperity deforms as a purely plastic body [205]. However F.Y. Edward [16] evaluated the degree of plastic deformation of the mechanical seal faces employed in this work and reports that the plastic deformation of asperities is just about one in one thousand asperity contacts. Hence to model the asperity contact it is logical to assume that the asperity deformation is pure elastic in this thesis.

Based on Greenwood and Williamson model the probability that a particular asperity has a height between z and $z + dz$ above the reference plane is defined as $f(z)$. Based on Figure 5.12 if two surfaces come together until their reference planes are separated by a distance d then there will be a contact (shaded in Figure 5.12) and the load is supported by those asperities whose height are originally greater than d . Thus the probability of making contact at any given asperity of height z is [206, 207].

$$p(z > d) = \int_d^{\infty} f(z) dz \quad (5.12)$$

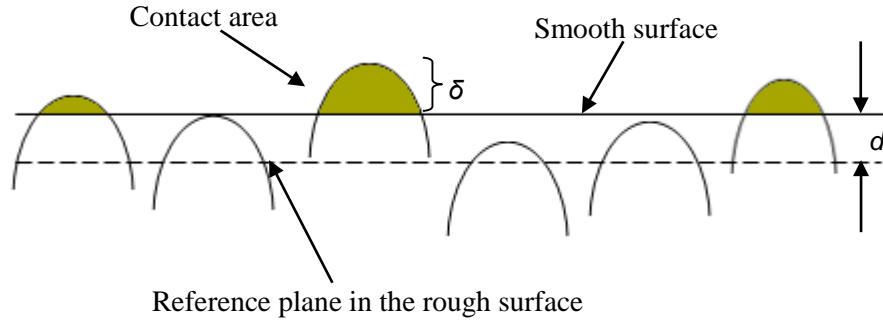


Figure 5.12 Greenwood and Williamson for contact model

It was assumed that the number of asperities per unit area is D , thus the expected number of contacts in any unit area is:

$$n = D \int_d^{\infty} f(z) dz \quad (5.13)$$

The well-known solution for the single contact between two elastic bodies was developed in the late nineteenth century by Hertz. Hertz theory describes the contact between two elastic spherical bodies (radius R_1 and R_2 , respectively) with perfectly smooth surfaces. The assumptions for what has become known as the Hertz contact theory are: (1) the contact area is elliptical; (2) each body is approximated by an elastic half-space loaded over an elliptical contact area; (3) the dimensions of the contact area must be small compared to the dimensions of each body and to the radius of curvature of the surfaces; (4) the strains are sufficiently small for linear elasticity to be valid; and (5) only a normal pressure is transmitted and the contact is frictionless in the direction of normal pressure.

Assume that the spheres are squeezed together by the normal force W , the deformation field in the solids can be determined by minimizing the elastic deformation energy [207]. The radius of the circular contact region, a , and the maximum deflection in the contact area, δ , are given by Equations (5.14) and (5.15) respectively [205, 207].

$$a = \left(\frac{WR}{E} \right)^{\frac{1}{3}} \quad (5.14)$$

$$\delta = \frac{a^2}{R} \rightarrow \delta = \left(\frac{W^2}{RE^2} \right)^{\frac{1}{3}} \quad (5.15)$$

where W is the normal load supported by a single asperity, R and E are the radius of the curvature in the contact area and the Hertzian contact modulus (composite Young's modulus of elasticity) respectively given by:

$$\frac{1}{R} = \frac{1}{R_1} + \frac{1}{R_2} \quad (5.16)$$

$$\frac{1}{E} = \frac{3}{4} \left(\frac{1-\nu_1^2}{E_1} + \frac{1-\nu_2^2}{E_2} \right) \quad (5.17)$$

where:

E_1 and E_2 are the Young's modulus of the two sphere materials respectively

ν_1 and ν_2 are the corresponding Poisson's ratio

R_1 and R_2 are the radius of contact asperities

The rest of this chapter aims to model strain energy released based on novel acoustic emission sources at the sealing gap i.e. asperity collision, fluid induced deformation and viscous friction as previously discussed. The two formers are modelled based on the dynamic bending of asperities which is more consistent with physics of such a sliding contact rather than previous works [187] where asperity deformation was considered simply in the direction of the contact load. Viscous friction is also modelled based on tangential viscous friction force acting in the sliding direction of the mating faces.

5.5 Modelling Asperity Collision

Conventionally the friction force in the direction of sliding between a pair of contact asperities is defined by [2]:

$$F_f = \iint_{A_s} \tau_s dA \quad (5.18)$$

where A_s and τ_s are the actual area of a contact and shear stress at the asperity contact respectively. Thus if the friction stress is constant, the friction force is proportional to the

real area of contact and will be roughly proportional to the normal load. Therefore, the coefficient of friction of a single asperity, f , can be expressed as:

$$f = \frac{\tau_s}{P_s} \quad (5.19)$$

where P_s is the normal stress in a single asperity contact. It should be immediately noted that recent experimental evidence shows that the friction stress τ_s is scale dependant. Consequently there is a significant change in the friction stress as the contact area changes and this difference is greater than an order of magnitude [61]. Therefore it is not logical to substitute τ_s from Equation (5.19) into Equation (5.18) unless it is assumed that the contact radius is smaller than a critical value as presented in the work of Hurtado and Kim [208]. Therefore, rearranging the integral in Equation (5.18), the tangential friction force acting between a pair of contact asperities will be:

$$F_f = \iint_{A_s} \tau_s dA = \iint_{A_s} f P_s dA = f W \quad (5.20)$$

where W is the normal contact load between a pair of asperities. Assuming asperities behave like an end-loaded cantilever beam, the elastic strain energy released during bending of a single asperity can be expressed as (see Appendix A for details and proof) :

$$U_{iAE} = \frac{F_f^2 \delta^3}{6EI} \quad (5.21)$$

where F_f is the friction force between a pair of asperities, δ is the maximum deflection in the contact area, E is the Hertzian contact modulus and I is the area moment of inertia, (see Figure 5.13):

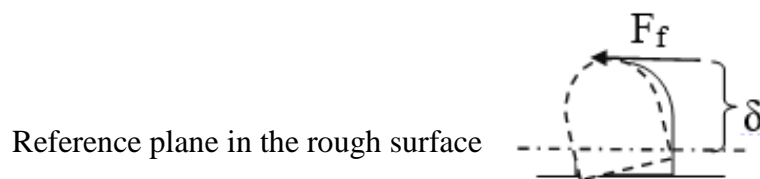


Figure 5.13 Schematic of the bending of an asperity during sliding contact

Substituting friction force, F_f , from Equation. (5.20) into Equation. (5.21) results in:

$$U_{iAE} = \frac{f^2 W^2 \delta^3}{6EI} \quad (5.22)$$

Since $\delta = z - d$ (see Figure 5.12), thus the mean frictional acoustic emission strain energy released in a single asperity contact is

$$\bar{U}_{iAE} = \frac{f^2 W^2 \int_d^{\infty} (z-d)^3 f(z) dz}{6EI \int_d^{\infty} f(z) dz} \quad (5.23)$$

The total strain energy released in the asperity contacts U_{AE} can be expressed as

$$U_{AE} = A n \bar{U}_{iAE} \quad (5.24)$$

where A is the apparent asperity contact area and n is the number of contacts in unit area given by Equation (5.13). Substituting Equation (5.23) into Equation (5.24) and considering n from Equation (5.13), the total frictional energy is:

$$U_{AE} = AD \frac{f^2 W^2}{6EI} \int_d^{\infty} (z-d)^3 f(z) dz \quad (5.25)$$

If the sliding speed of the moving surface is V , then the time needed for the release of individual asperity contact can be calculated based on the radius of contact area, see Equation (5.3):

$$t = \frac{S}{V} = \frac{4a}{V} = \frac{4\sqrt{\delta R}}{V} \quad (5.26)$$

where, a , δ , R and s are the radius of contact area, elastic deflection and equivalent radius of the curvature in the contact area respectively described by Equations (5.14) to (5.16) respectively. Thus substituting δ with $z-d$, the mean elastic discharge time is:

$$\bar{t} = 4 \frac{\int_d^{\infty} \sqrt{R(z-d)} f(z) dz}{V \int_d^{\infty} f(z) dz} \quad (5.27)$$

Dividing Equation. (5.25) by Equation. (5.27), the rate of strain energy released can be expressed as:

$$\dot{U}_{AE} = \frac{U_{AE}}{\bar{t}} = \frac{A D f^2 W^2 V \int_d^{\infty} (z-d)^3 f(z) dz \int_d^{\infty} f(z) dz}{24 EI \int_d^{\infty} \sqrt{R(z-d)} f(z) dz} \quad (5.28)$$

The total number of asperity contacts between two surfaces can be defined as:

$$N_{tot} = AD \int_d^{\infty} f(z) dz \quad (5.29)$$

It would be convenient to standardize the probability density function using a standardized variable $z^* = \frac{z}{Rq}$ where Rq is the standard deviation of asperity height distribution. Then

the standard separation is equal to $d^* = \frac{d}{Rq}$. Moreover, an auxiliary function can be defined

as follows. This function has been used extensively in the literature [186, 187, 205]:

$$F_n(d^*) = \int_{d^*}^{\infty} (z^* - d^*)^n \phi(z^*) dz^* \quad (5.30)$$

where $\phi(z^*)$ is the standard height distribution. Suppose that a portion k_e of the elastic strain energy is converted to AE pulses and the gain of the AE measurement system is k_g , using Equations (5.28) to (5.30) the rate of AE energy release can be expressed as:

$$\dot{U}_{AE} = K_e K_g \frac{N_{tot} f^2 W^2 V F_3(d^*)}{24 EI \sqrt{R} F_1(d^*)^{\frac{1}{2}}} \quad (5.31)$$

Substituting Equation (5.31) into Equation (5.7), the relationship between AE RMS and the strain energy released during direct asperity contact can be expressed as:

$$V_{rms} = fW \sqrt{K_e K_g \frac{N_{tot} V F_3(d^*)}{24 E I R^2 F_1(d^*)}} \quad (5.32)$$

This Equation is important because it helps to estimate the contact load supported by asperities from non-intrusive acoustic emission measurements, which is a critical parameter to evaluate lubrication conditions in industrial applications. The model presented in Equation (5.32) is completely fitted with the experimental work of F.Y. Edward et al.[187], they reported that the relationship between AE RMS value and the contact load is linear with a coefficient of determination close to unity ($R^2=0.99$), Figure 5.14. However, their theoretical model is not able to truly predict this trend. In their work, the contact load supported by a mechanical seal face was calculated using the well-established mechanical performance calculation software available at John Crane UK.

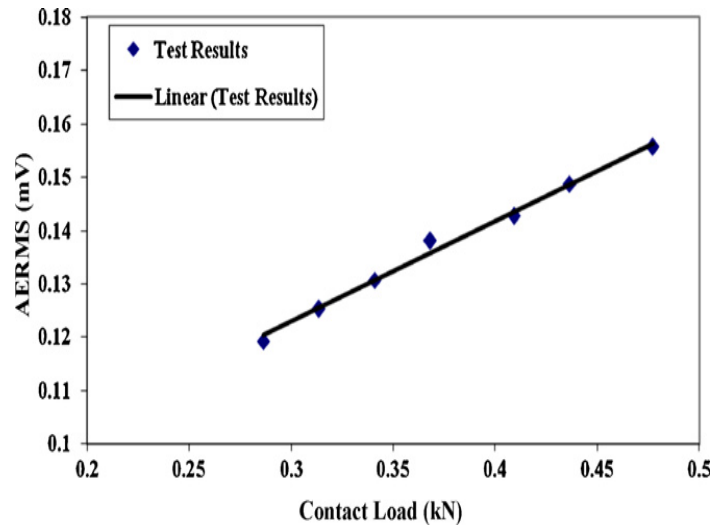


Figure 5.14 AE from mechanical seals running with different contact loads [187]

5.6 Flow Induced Asperity Deformation Model

Since this type of acoustic emission source does not include direct asperity contact, the traditional form of contact mechanics of rough surfaces is not applicable. Hence the Greenwood and Williamson theory of contact model is adopted for fluid induced asperity deformations.

Based on Figure 5.15, if the sealing gap is filled with the lubricant fluid that rotates with the speed of V and two surfaces come together until their reference planes are separated by a distance d , there will be the potential of some fluid induced asperity deformations (shaded in Figure 5.15). This causes an alternation between asperity elastic deformation and recovery in moving asperities whose height are originally greater than d . This means that elastic deformation of those asperities whose height are less than d is not considered, see Figure 5.5 as well.

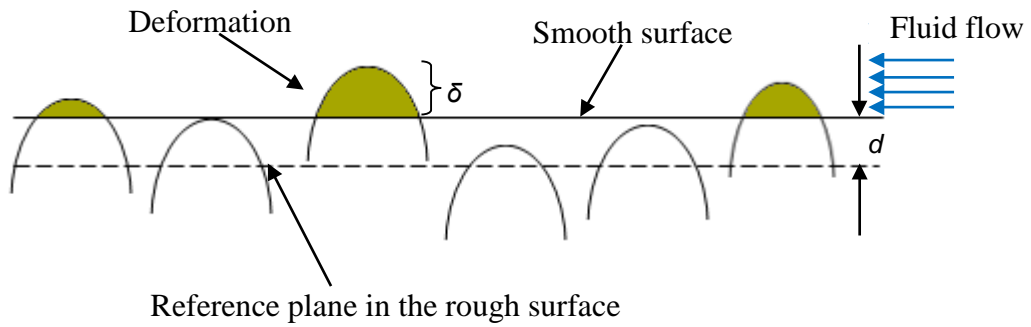


Figure 5.15 Contact model adopted for fluid induced asperity deformation

Hence the Equations (5.12) and (5.13) can be applied with the new definition. Here P is the probability of asperity deformation due to fluid flow at any given height of asperity and n is the expected number of fluid induced asperity deformations in any unit area.

According to Newton's viscos law, the tangential stress acting on the free end of an asperity due to the fluid stress field can be expressed as Equation (5.34). It should be noted that the elastic deformation, δ , is approximately equal to the lubricant film around the asperities:

$$\tau = \mu \frac{V}{\delta} \quad (5.33)$$

The fluid induced tangential friction force is given by:

$$F_f = \iint_{A_0} \tau dA \quad (5.34)$$

where A_0 is the fluid induced asperity deformation area of a single asperity from the top view. It is assumed that the deformations in the shape of this area due to bending moment is negligible. Substituting Equation (5.33) into Equation (5.34) gives the fluid induced tangential friction force:

$$F_f = \mu \frac{V}{\delta} A_0 \quad (5.35)$$

Assuming asperities behave like end-loaded cantilever beams, the elastic strain acoustic emission energy released during bending of a single asperity can be expressed as (see Appendix A for details and proof)

$$U_{iAE} = \frac{F_f^2 \delta^3}{6EI} \quad (5.36)$$

Substituting Equation (5.35) into Equation (5.36) and assume that the released strain energy is significant for asperities whose height is larger than the average height of asperities, the mean energy release of one asperity deformation is

$$\bar{U}_{iAE} = \frac{(\mu V A_0)^2 \int_d^\infty (z-d) f(z) dz}{6EI \int_d^\infty f(z) dz} \quad (5.37)$$

The total strain energy released U_{AE} can be expressed as:

$$U_{AE} = A n \bar{U}_{iAE} \quad (5.38)$$

where A_0 is the total deformation area and n is the number of fluid induced deformations in unit area given by Equation (5.13). Substituting Equation (5.37) into Equation (5.38) and considering n from Equation (5.13), the total frictional energy yield:

$$U_{AE} = A D \frac{(\mu V A_0)^2}{6EI} \int_d^\infty (z-d) f(z) dz \quad (5.39)$$

If the sliding velocity of the surface is V , then the time needed for the elastic deformation of an individual asperity can be expressed as:

$$t = \frac{2l_s}{V} \quad (5.40)$$

Where l_s is estimated by the displacement of the free end of one asperity (see Figure 5.16):

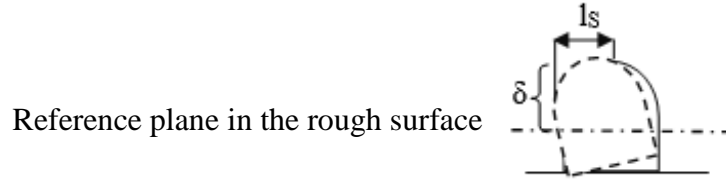


Figure 5.16 Illustration of sliding distance in fluid induced deformation of asperities

Based on the theory of deformation of beams, the displacement of the free end loaded cantilever beams can be expressed as [209]:

$$l_s = \frac{F_f L^3}{3EI} \quad (5.41)$$

Where L is the length of beam. Substituting F_f from Equation (5.35) into Equation (5.41) and set $L=\delta$, the displacement of free end of each asperity is:

$$l_s = \frac{\mu V A_0 \delta^2}{3EI} \quad (5.42)$$

Substituting l_s from Equation (5.42) into Equation (5.50) and set $\delta=z-d$, the mean energy release time during the asperity deformation is:

$$\bar{t} = \frac{2}{3} \frac{\mu A_0}{EI} \frac{\int_d^{\infty} (z-d)^2 f(z) dz}{\int_d^{\infty} f(z) dz} \quad (5.43)$$

Dividing Equation. (5.39) by Equation (5.43), the rate of energy release can be expressed as:

$$\dot{U}_{AE} = \frac{U_{AE}}{\bar{t}} = \frac{A A_0 D V^2 \mu \int_d^{\infty} (z-d) f(z) dz}{4 \int_d^{\infty} (z-d)^2 f(z) dz} \int_d^{\infty} f(z) dz \quad (5.44)$$

The total number of asperity deformations between two surfaces can be defined as:

$$N_{tot} = AD \int_d^{\infty} f(z) dz \quad (5.45)$$

Suppose that a portion k_e of the elastic strain energy is converted to AE pulses and the gain of the AE measurement system is k_g , using Equations (5.30) and (5.45), the rate of energy can have rewritten as:

$$\dot{U}_{AE} = K_e K_g \frac{A_0 N_{tot} V^2 \mu F_1(d^*)}{4 F_2(d^*)} \quad (5.46)$$

Substituting Equation (5.46) into Equation (5.7), RMS voltage of AE signal generated by flow induced asperity deformation in terms of sliding speed and viscosity can be expressed as:

$$V_{rms} = \frac{V}{2} \sqrt{\frac{K_e K_g A_0 N_{tot} \mu F_1(d^*)}{F_2(d^*)}} \quad (5.47)$$

Based on Equation (5.47) sliding speed, deformation area of asperities, the number of asperity deformation, viscosity of the sealed fluid and surface topographic characteristics influence the energy of the AE signal generated by fluid induced deformation.

5.7 Viscous Friction Model

Friction between fluid layers consists of three components i.e. sliding component, rolling-or- squeezing component and a geometrical component. Because of the simple sliding movement of the seal faces the last two friction components are negligible and only become of interest in the case of pure rolling [2]. Hence in this thesis the tangential viscous friction caused by shear of the lubricant at the sealing gap is modelled.

In 1991 Lebeck [1] used a finite volume of fluid bounded within two arbitrary surfaces to characterize general lubrication theory at the sealing gap, Figure 5.17.

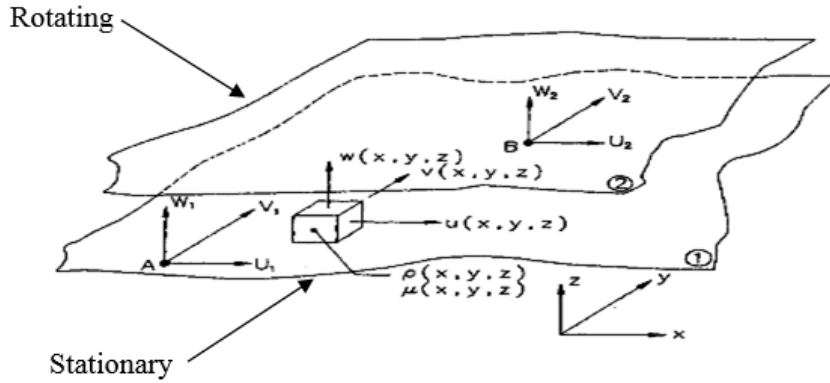


Figure 5.17 Cartesian geometry for general lubrication theory [1]

where:

ρ is fluid density

x, y, z are Cartesian coordinates

g is gravitation force in direction (x, y and z) indicated [m/s^2]

P_f is sealed pressure [Pa]

μ is absolute viscosity [Pa/s]

v, u, w are components of velocity along x, y, z Cartesian coordinate directions [m/s]

Considering the Cartesian geometry, the Navier-Stokes equations can be applied to describe the pressure and fluid motion at the sealing gap. The structure of Navier-Stokes equations is as follow:

$$\begin{aligned}
 \rho g_x - \frac{\partial p_f}{\partial x} + \mu \left(\frac{\partial^2 u}{\partial x^2} + \frac{\partial^2 u}{\partial y^2} + \frac{\partial^2 u}{\partial z^2} \right) &= \rho \frac{du}{dt} \\
 \rho g_y - \frac{\partial p_f}{\partial y} + \mu \left(\frac{\partial^2 v}{\partial x^2} + \frac{\partial^2 v}{\partial y^2} + \frac{\partial^2 v}{\partial z^2} \right) &= \rho \frac{dv}{dt} \\
 \rho g_z - \frac{\partial p_f}{\partial z} + \mu \left(\frac{\partial^2 w}{\partial x^2} + \frac{\partial^2 w}{\partial y^2} + \frac{\partial^2 w}{\partial z^2} \right) &= \rho \frac{dw}{dt}
 \end{aligned} \tag{5.48}$$

Lebeck used some simplifications and assumption to simplify the equations, these assumptions which are matched logically with the physics of sliding motion at the siling gap can be expressed briefly as [1]:

- 1- The first term (ρg) in each equation represents gravitational force and could be neglected.
- 2- The term on the right hand side of each equation represents the inertia effect and could be neglected in comparison with viscous forces.
- 3- The fluid flow is laminar because the lubrication film is thin compared with other dimensions.
- 4- Fluid is considered to be Newtonian (because the shear stresses in the lubricant are relatively low).
- 5- If z axis is aligned with the thin direction of the lubrication film then the velocity gradients of u and v with respect to z are much larger than all other velocity gradients.

Using all of these simplifications plus that ($\frac{dp_f}{dz} = 0$, for thin film), the Equations (5.48)

can be rewritten as:

$$\frac{\partial p_f}{\partial x} = \mu \frac{\partial^2 u}{\partial z^2}$$

$$\frac{\partial p_f}{\partial y} = \mu \frac{\partial^2 v}{\partial z^2} \quad (5.49)$$

$$\frac{\partial^2 w}{\partial z^2} = 0$$

Considering the boundary conditions, the components of fluid velocity in x and y directions can be expressed as (see [1] for details and proof):

$$u = \frac{1}{2\mu} \frac{\partial p_f}{\partial x} (z^2 - zh) + U \frac{z}{h} \quad (5.50)$$

$$v = \frac{1}{2\mu} \frac{\partial p_f}{\partial y} (z^2 - zh) \quad (5.51)$$

For the basic acoustic emission model being derived in this section, only a very simple velocity field is needed. Hence assuming a linear pressure profile between atmospheric pressure and sealed pressure, the pressure gradient in the radial direction would be constant:

$$\frac{dp}{dx} = \frac{dp}{dy} = C \quad (5.52)$$

Differentiating Equation (5.50 and 5.51) with respect to z read:

$$\frac{\partial u}{\partial z} = \frac{C}{2\mu} (2z - h) + \frac{U}{h} \quad (5.53)$$

$$\frac{\partial v}{\partial z} = \frac{C}{2\mu} (2z - h) \quad (5.54)$$

Thus (based on Newton's viscous flow law), the components of shear stress acts in the sliding direction (τ_{zx}) and y direction (τ_{zy}) (see Figure 5.18) can be expressed as Equations (5.55) and (5.56) respectively:

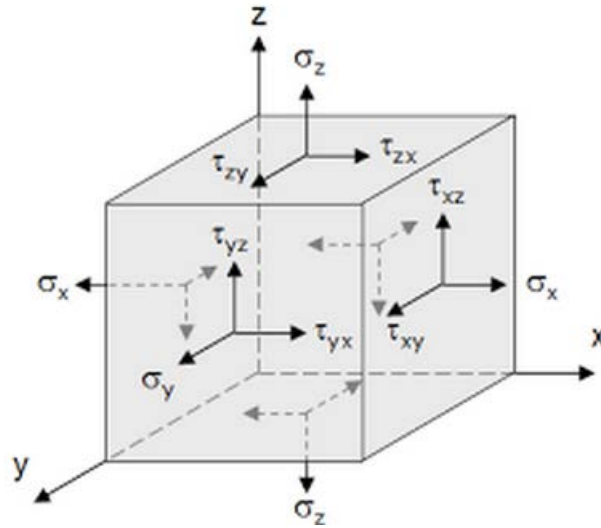


Figure 5.18 Stress components acting on a differential element of fluid

$$\tau_{zx} = \frac{C}{2} (2z - h) + \mu \frac{U}{h} \quad (5.55)$$

$$\tau_{zy} = \frac{C}{2} (2z - h) \quad (5.56)$$

Due to the extremely thin sealing gap that exists between mating faces, it is logical to claim:

$$\frac{C}{2} (2z - h) \ll \mu \frac{U}{h} \quad (5.57)$$

Therefore only the shear stress component that acts in the sliding direction (τ_{zx}) is considered and Equation (5.56) can be ignored. Based on Equations (5.55) and (5.57) shear stress component acting in the sliding direction can be rewritten as:

$$\tau_{zx} = \mu \frac{U}{h} \quad (5.58)$$

The component of viscous friction force acting on any arbitrary differential element of fluid is (Figure 5.19):

$$dF_x = \tau_{zx} dA \quad (5.59)$$

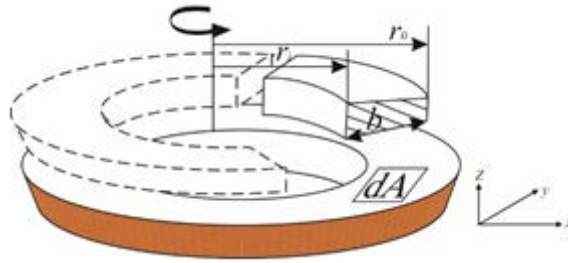


Figure 5.19 Differential elements in viscous friction model

Where b is the seal width. Suppose that a portion k_e of the elastic strain energy is converted to AE pulses and the gain of the AE measurement system is k_g , the acoustic energy release rate (power) at the mentioned differential element of fluid is given by:

$$\dot{U}_{AE} = K_e K_g \iint u dF_x \quad (5.60)$$

Substituting dF_x from Equation (5.59) and considering the maximum velocity component at sliding direction as U , integrating Equation (5.60) will result in:

$$\begin{aligned} \dot{U}_{AE} &= K_e K_g \int_{r_i}^{r_0} \int_{r_i}^{r_0} U \mu \frac{U}{h} dx dy \\ &= 2\pi \mu \frac{U^2 r_m b}{h} \end{aligned} \quad (5.61)$$

Where r_m is the mean radius of seal face area. Substituting Equation (5.61) into Equation (5.7) reads:

$$V_{rms} = \sqrt{2\pi K_e K_g \frac{\mu r_m b}{h}} U \quad (5.62)$$

This Equation can explain the AE activities generated from viscous friction of the lubricant. Equation (5.44) shows clearly that the fluid shearing induced AE is greater when rotational speed and lubricant viscosity are higher. However, this type of excitation has little connection with sealing pressure.

To connect the AE activities with waviness of mating faces, the film thickness for an outside pressurized seal with coning angle equal to zero is defined as follows [1]

$$h = h_{min} + A(1 + \cos(k\theta)) \quad (5.63)$$

where h_{min} is the minimum film thickness, A the amplitude of the waviness, k the number of waves on the circumference and θ is an angle in polar coordinates which covers from 0 to 2π , see Figure 5.20.

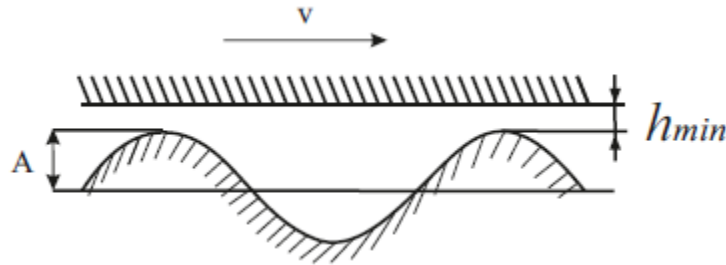


Figure 5.20 Waviness amplitude

Substituting Equation (5.63) into Equation (5.62) results in (it should be noted that in this thesis the sliding speed of mating faces is noted by V , that is why U in Equation (5.62) is substituted by V in below Equation):

$$V_{rms} = \sqrt{2\pi K_e K_g \frac{\mu r_m b}{h_{min} + A(1 + \cos(k\theta))}} V \quad (5.64)$$

5.8 The Effect of Source Mechanisms on the AE Signal

This section aims to explain the effect of acoustic emission source mechanisms on the type of generated AE signals based on the tribological behaviour of mechanical seals.

To connect the future results with developed models, two types of asperity deformation (whether it is in direct contact or caused by fluid flow) are defined in this thesis, peak asperity deformation and massive asperity deformation. The former refers to the situation that elastic deformation happens in some peak asperities which those heights are greater than the average value of all asperity heights (hatched in Figure 5.21). Peak asperities are typically few in number and are generated with comparative ease using process including grinding [210]. The latter refers to deformation of those asperities that their heights are around the average value of all asperity heights, that is why the term 'massive' is used.

Peak asperity deformation in direct contact may happen at lower speeds and before mating faces come to the contact in boundary or mixed lubrication regimes. By increasing the sealed pressure (which means reducing the sealing gap) more asperities come to contact and massive asperity contact occurs, Figure 5.21. In this situation burst type responses are generated due to contact of peak asperities while the asperities whose heights are around the average generate continuous type responses. This can be better understood by considering Equations (5.22). In peak asperity deformation more deformation energy is released in every rotational period of shaft due to bigger values of δ (maximum deflection in the deformation area). Hence the generation of burst type responses is expected.

By increasing the speed to the transition point, seal faces become separated gradually and hence fluid induced deformation occurs in those asperities whose heights are around the average of asperity heights (massive deformation) that generates continuous responses. In the meantime, some direct asperity contact still occurs in the tips of peak asperities due to the fact that seals are not fully separated, this generates burst type responses.

As the speed increases gradually, the mating faces become fully separated and flow induced asperity deformation happens in peak asperities as well as massive ones. In this situation burst type responses are generated due to deformation of peak asperities, Equation (5.36), while the asperities whose heights are around the average generate continuous type responses.

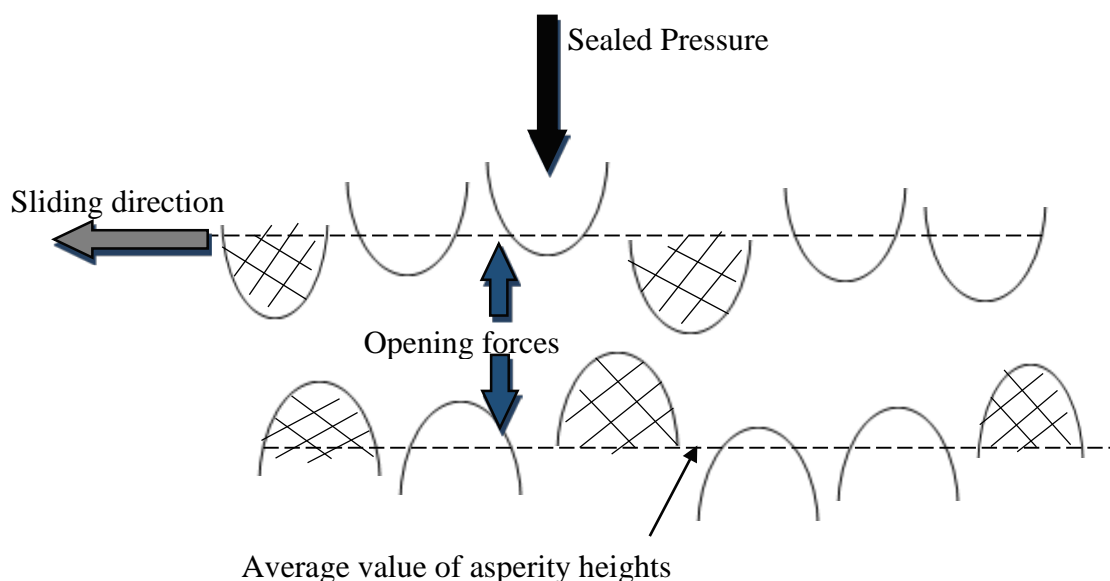


Figure 5.21 The concept of peak and massive asperity deformation

5.9 Main Findings

This chapter proved an approach to mathematical modelling of strain energy released during the deformation of asperities as well as shearing of the sealed fluid in the sealing gap. The deformation of asperities occurs due to collision and interaction of asperities in the boundary and mixed lubrication region, while in the hydrodynamic lubrication region the flow induced effects of moving fluid can cause bending of asperities when a pair of asperities approach each other and then release when they leave the interaction zone.

Based on the mathematical models developed in this work, in direct asperity contact the root mean square (RMS) value of AE signal is linearly proportional to the coefficient of friction and contact load. Also it is proportional to the square root of sliding speed. In viscous friction and flow induced deformations, the effect of sliding speed is dominant. In both models the root mean square of AE signals increases linearly with sliding speed, also it is proportional with square root of viscosity. In all models topography of the contact zone as well as asperity height distribution play an important role.

Chapter Six;

Experimental Set up Facilities

This chapter details the test facilities employed for studying the condition monitoring of mechanical seals. The Chapter has four main parts. The first part provides the design objectives as well as the limitations of the previous structure of the test rig. The second part discusses the development of new test rig for the purpose of condition monitoring of face seals. This includes the main body of the rig and auxiliary fluid circulating system. This is followed by the third part where the arrangement of the sensors is discussed along with the data acquisition system. In the last part, the test procedure and fault simulation program applied in this work is discussed.

6.1 Introduction

In order to verify the theoretical models developed by the author in practical applications, experimental data i.e. Stribeck-like friction curves are required. In the literature most of the studies related to tribological AEs have been undertaken in the form of pin on disk or pin on cylinder in laboratories (as discussed in Section 4.2.2). Since mechanical seals operate under quite different conditions in industrial application, it is impractical to study the tribological behaviour of mechanical seals using these test facilities.

Little information on condition monitoring of mechanical seals using industrial test rigs are available. Very often important information on seal design, fluid temperature, operational conditions, sensors configuration and set up is left out. Also most of the previous research has major limitations (e.g. realistic faults has not been simulated) as discussed in Section 1.4.2. Therefore, this thesis designed and constructed a new mechanical seal test rig for condition monitoring research purposes. The rig will be used for developing appropriate data analysis methods to extract useful information for early fault detection and diagnosis.

The test rig was based on preliminary design by F.Y Edward, see [16]. However, a number of modifications were made to allow accurate measurements and realistic fault simulation.

6.1.1 Limitations of the Primary Design

One of the major limitations in the work of F.Y. Edward [16] is that he tried to prove his direct asperity contact model based on the data that has been recorded mainly under the hydrodynamic lubrication regime. He focused on a fairly small range of low pressures and relatively high speeds, once the test rig operates outside that range the mathematical model diverges. The main limitations of the primary design of the mechanical seal test rig are:

1. Two mechanical seals were employed, this may lead to cross talk from dummy seal. Moreover, this configuration is unlikely to be similar to that in a real pump.
2. It was very difficult to inspect or change the driven end mechanical seal as well as the shaft itself and the supporting bearings.
3. The designed circulating system needs to exchange the frictional heat which is a limitation due to available space in the lab.

4. To simulate different tribological regimes seals are needed to be tested under different speeds and loads, the employed electrical motor is not convenient from the point of view of heat transfer. There was always a risk of breakdown due to overheating of the motor when running at low speeds. The proper electrical motor needs to have better cooling arrangement to insure adequate heat transfer is available.
5. To simulate boundary lubrication regime, very low rotational speeds are needed which was difficult to achieve due to misalignment in the original rig configuration. In addition, the micro scale deformations of the drive shaft and bearings may intensify the misalignment. Changing the parts or adjusting the alignment was difficult as two seals had to be aligned with in $\pm 0.025mm$ (Maker's data).

6.1.2 Design Objectives of the Test Rig

Hence it is necessary and essential to examine the developed models on a wide range of pressure and velocity combinations so that it can simulate different lubrication regimes. Once the effectiveness of the mathematical models is proved, then any deviation from normal working conditions may be considered as a developing fault. Based on the above discussion, the design objectives of the test rig are as follows:

1. To ensure the test rig replicates the usual seal arrangement in practical applications such as pumps, real industrial mechanical seals rather than just pairs of face seal materials were employed. To get stronger acoustic emission signals, larger mechanical seals for larger pumps were selected.
2. To ensure that the acoustic emission method developed in this thesis is easily applicable for industrial parts, only one acoustic emission sensor was employed. The acoustic emission sensor is mounted externally on the cartridge of the seal as it is the easiest place to access.
3. To avoid the effect of radio frequency emissions and electrical noises on the sensors, the rig was grounded carefully to the earth.
4. To pressurize the face seals in the chamber, a nitrogen vessel was used. For the health and safety of operation, the test rig did not use explosive or flammable sealed fluid to avoid the risk of fire and explosion.

5. To reduce the effects of frictional heat on the acoustic emission measurements to a minimum acceptable level, a cooling system is used to reduce the thermal effects on the measurements.
6. To simulate different lubrication regimes and investigate the relationship between acoustic emission signals and the change of the operating parameters, the rotating speed of the mechanical seals and the pressure of the sealed fluid were all adjustable. The electrical motor was controlled by an inverter so that variable sliding speed of mechanical seal faces could be achieved. The load on the mechanical seals were adjusted by changing the water pressure in the sealed chamber.
7. The test rig could simulate several types of faults such as spring faults, misalignment, dry running, thermal shock and leakage.
8. Both balanced and unbalanced mechanical seals can be easily mounted on the drive shaft of the rig. It gives a promising potential for future studies to use unbalanced seals for simulating higher rates of friction and wear with no need to modify the rig.

6.2 Development of the New Test Rig Facilities

This section aims to explain the advantages of new design of the rig. This includes both the main rig and the auxiliary circulating system as shown in Figure 6.1.

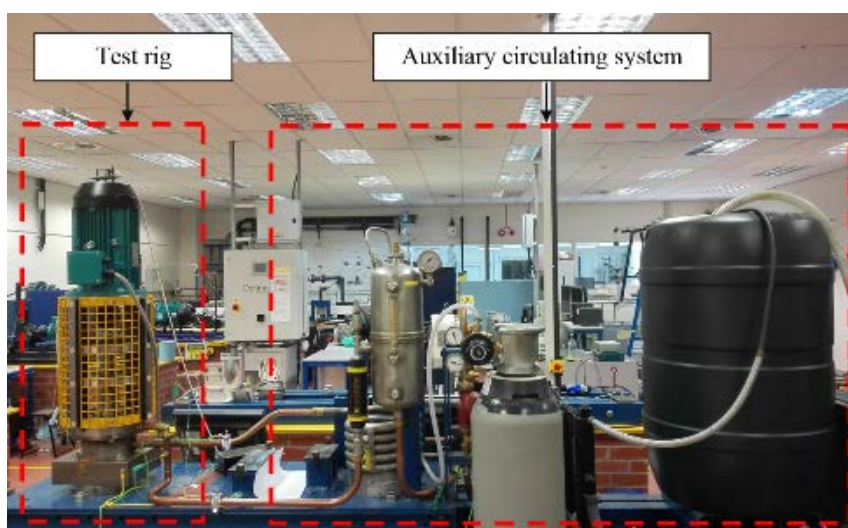


Figure 6.1 New design of the mechanical seal test rig

6.2.1 Test Rig Construction and Components

Figure 6.2 shows the general view of the main body of the test rig designed for the condition monitoring of mechanical seals. It consists of seven major parts; mechanical seal, stainless steel tube, body of the rig, test rig shaft, deep groove ball bearings, coupling and electrical motor. Some of the main dimensions of the new design are presented in Appendix C. The new design of the rig gives several advantages to the system:

1. Test rig replicates usual seal arrangement in industrial applications such as pumps.
2. Control of alignment is assured.
3. Single seal that eliminates cross talk from the dummy seal.
4. Seal and bearing changes are simplified, few minutes compared to hours.

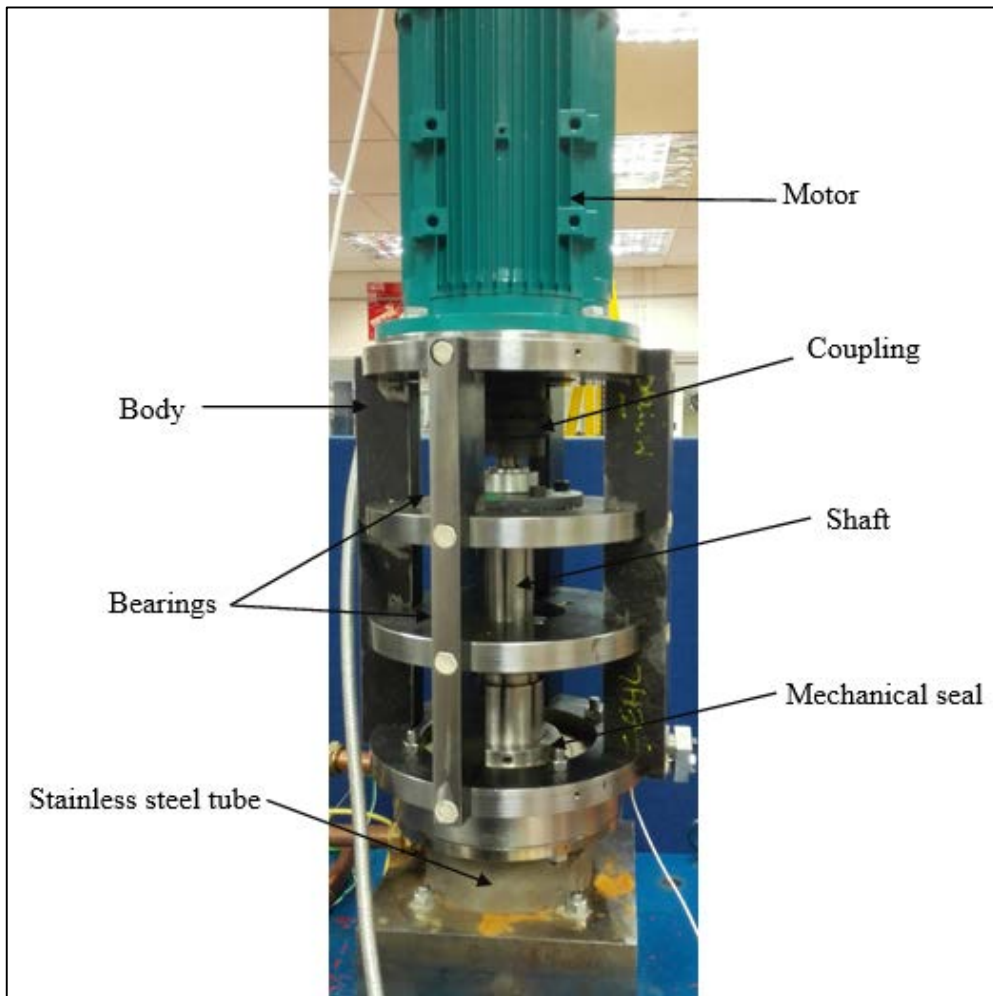


Figure 6.2 The main components of the test rig

Each part has been designed to do a specific function. A pusher cartridge mechanical seal and a stainless steel tube formed a pressurised chamber. The shaft of the test rig was supported by two deep groove ball bearings; ANI 6208 and ANI 6210. These bearings are used to transmit unbalanced axial force from rotating parts to body of the rig with minimum friction loss and compensate for shaft misalignment. In addition, low cost bearings allow possibility of investigating the effects of bearing damage on seal performance for future studies. The specifications of these bearings are presented in Table 6.1.

Table 6.1 Specifications of deep groove ball bearings

Bearing	Bore diameter(mm)	Number of balls	Diameter of balls (mm)	Pitch line (mm)
6208	40	9	11.91	60.00
6210	50	10	12.7	70.00

The driven shaft is connected to a 3 kW three-phase electrical induction motor. Instead of a low cost electric motor as has been employed in the preliminary design, a high quality high power electric motor with better heat transfer was chosen for this research. This gives better heat control and hence it is more convenient for tribological studies. Some specifications of electrical motor used in this research are presented in Table 6.2.

Table 6.2 General specifications of the electrical motor

Manufacturer	Type	Number of poles	Power (kW)	Connection	RPM at 50 Hz
Brook Crompton	P-DA100LA-D	2	3.0	Star	2913

The electric motor is mounted on the body of the rig. This part has a very important role and was designed to prevent small misalignments due to the micro scale deformations of the shaft and bearings. These deformations are generated by the weight of the shaft and may decrease the accuracy and repeatability of acoustic emission measurements. The weight of the electric motor is supported completely by this body.

Another major difference between current research and the work of F.Y Edward [16] is the experimental program and test procedure. F.Y. Edward designed an experimental study to

demonstrate the potential of acoustic emission technique to monitor the condition of mixed lubricated mechanical seals. These experiments were conducted at five different speeds: 600 rpm, 900 rpm, 1200 rpm, 1500 rpm and 1800 rpm. At each speed, 9 tests were carried out under different pressures: 1 bar, 1.5 bar, and 2-8 bar with an increment of 1 bar. The main challenges for such a test procedure are listed as follow:

1. It is difficult to simulate mixed lubrication regime in the mentioned range of speed. The primary investigations in current research shows that the transition from mixed to hydrodynamic lubrication occurs around 600 rpm (see Section 7.3). Hence much lower speeds are needed to simulate different lubrication regimes, especially to investigate direct asperity contact.
2. From the theoretical understanding gained in Chapter 5, the effect of rotational speed is more important to generate acoustic emission signals. To investigate the tribological behavior of mechanical seals, it is more effective to keep the pressure constant and increase the speed from low values to relatively high values. This may insure that boundary, mixed and hydrodynamic lubrication regimes are simulated.

In this thesis, the incremental increase in speed is used under constant pressure. To achieve this, a speed controller is required. A Park 690 AC drive with Siemens Micro Master Controller was installed so that the electric motor could be run at different speeds. The essential advantage of an AC drive is that it offers practically unlimited induction motor speed control. The Siemens Micro Master Controller was installed on the rig and proved easy to use and was able to deliver torque and speeds accurately. Adjustment is conducted using a set-up panel screen that includes number of steps, time of operation (minute), and AC motor speed (%), Figure 6.3

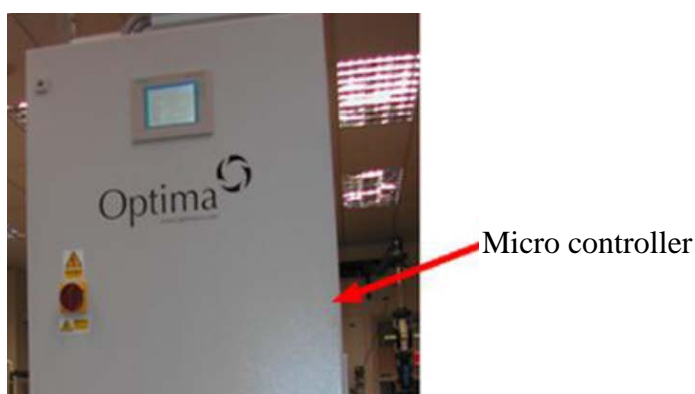


Figure 6.3 Siemens Micro Master Controller system

To match the specifications of electrical motor with the drive, a software is available as shown in Figure 6.4. Also it is possible to trace the speed and electrical features of motor using this software.



Figure 6.4 Siemens Micro Master data acquisition system

To reduce the effect of radio frequency emissions from AC drive and electrical noises on the sensors, the rig was grounded carefully to the earth, Figure 6.5.

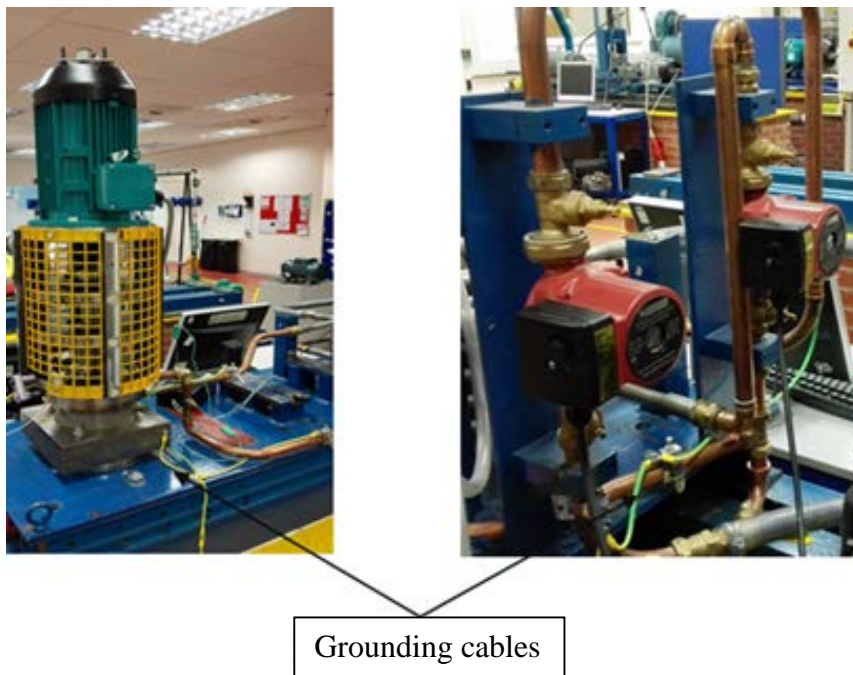


Figure 6.5 Grounding cables on different components of the test rig

The mechanical seal employed in this research is John Crane Type 1648 MP pusher single cartridge seal fitting for a shaft of 70 mm in diameter, as shown in Figure 6.6. This along with a stainless steel tube (to resist possible corrosion) formed a pressurised chamber.



Figure 6.6 John Crane type 1648 MP cartridge seal

The specifications of Type 1648 mechanical seal used in this study are given in Table 6.3. The rotating ring is made of antimony carbon and the stationary ring is reaction bonded silicon carbide.

Table 6.3 The specification of John Crane Type 1648 mechanical seal

Description	Notation	Unit	Value
Maximum service pressure	/	bar	≤69
Operating speed	/	m/s	≤25
Operating temperature	/	°C	-40 to 260
Inside diameter of sealing interface	D_i	mm	80.42
Outside diameter of sealing interface	D_o	mm	90.58
Balance diameter	D_b	mm	82.55
Outer periphery diameter of the rotating face	D_s	mm	104.78
Bore diameter of the seal chamber	D_{Sc}	mm	163.00
Length of the rotating component	L_r	mm	52.40
Spring force	F_s	N	320
Face width	b	mm	5
Maximum rubbing speed	/	m/s max	25
Length of shaft	L	mm	340
Axial force from max service pressure	/	N	9315

6.2.2 New Design of the Auxiliary Circulating System

Figure 6.7 shows the auxiliary circulating system of the mechanical seal test rig. It consists of several components as illustrated in Table 6.4. The function of this system is to generate pressure in the sealed chamber, circulate the working fluid (plain water in this research) and take away the friction heat produced in the sealing gap.

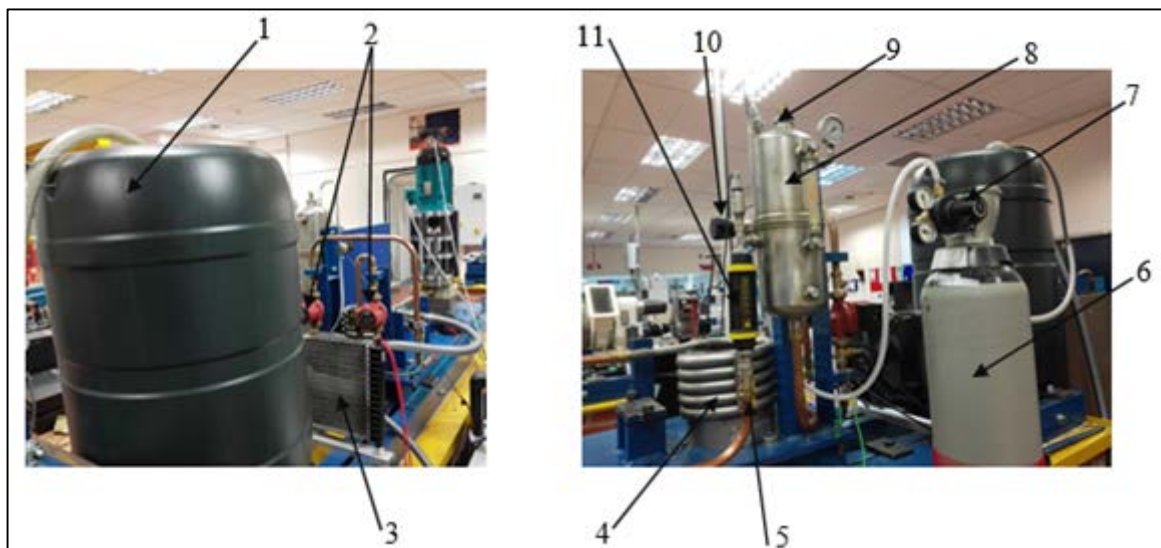


Figure 6.7 Different components of the auxiliary system

Table 6.4 Main parts of the auxiliary circulating system

Item number in Figure 6.7	Description
1	Water container
2	Circulating pumps
3	Radiator
4	Heat exchanger
5	Valves
6	Cylinder of nitrogen gas
7	Regulator on nitrogen cylinder
8	Pressurized vessel
9	Pressure relief valve
10	Regulator on pressurized vessel
11	Flow meter

The capacity of water container is 100 litres. For all experiments in this research, the container was filled with approximately 75 litre of plain water. The outlet valve of the water container is directly connected to one of the pumps. This pump is called cooling pump which supplies the fresh water for outer line of the heat exchanger as shown in Figure 6.8.

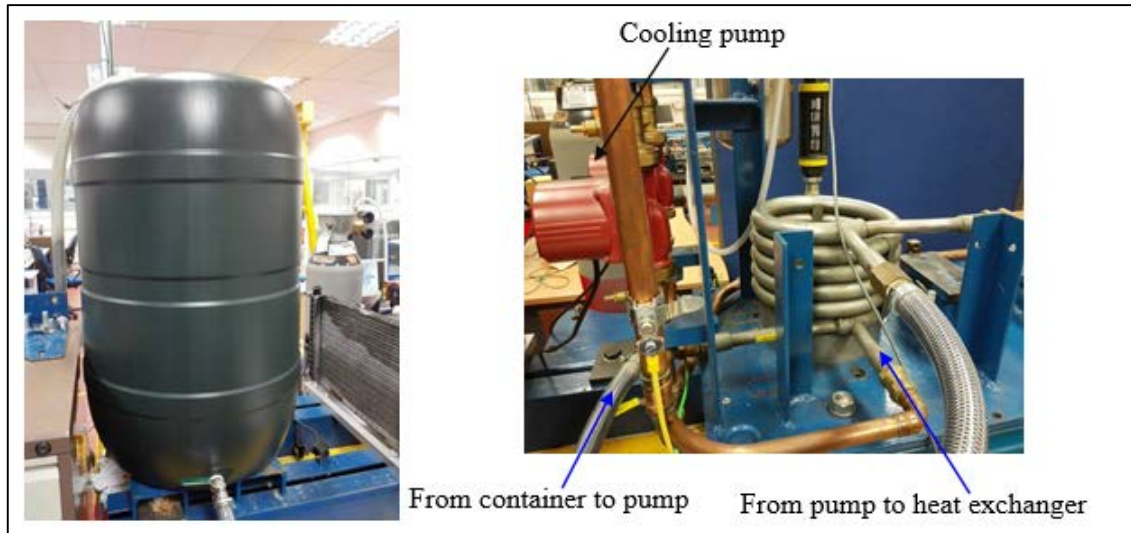


Figure 6.8 The system for supplying fresh water to the heat exchanger

Having transferred the heat with internal line of the heat exchanger (which is pressurized water coming from sealing gap), the water is feed into a radiator as shown in Figure 6.9. This circulating path of water is called external circulation and is not connected to the process fluid.

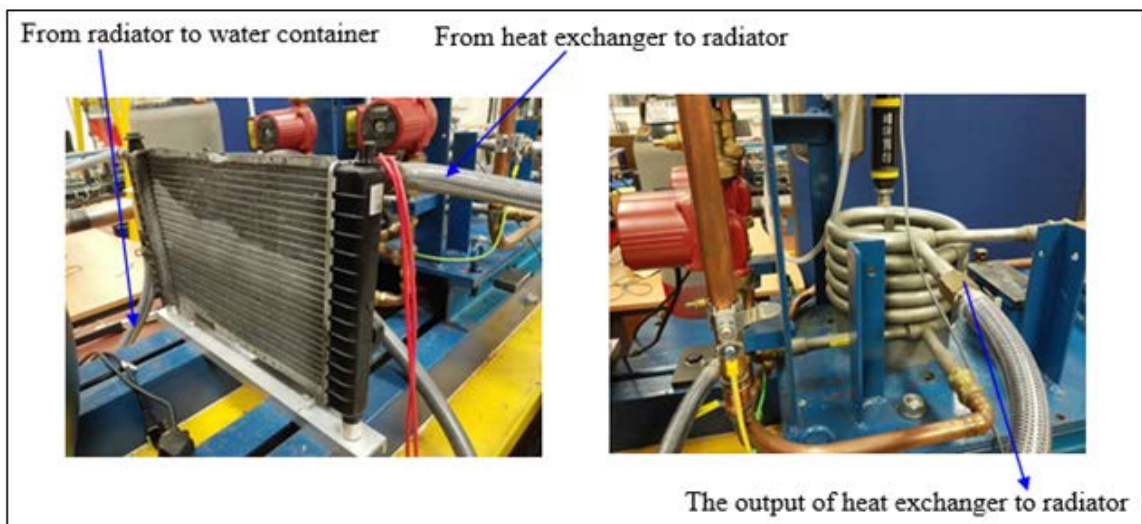


Figure 6.9 Connections to the radiator

During the primary investigations in this research, it has been found that the heat exchanger employed in the test rig is not able to keep the temperature near isothermal condition, especially when its external line is connected to a container with 100 litre capacity of plain water. Since in tribological studies on mechanical seals the temperature rise around 35 to 90 degrees has been reported in the literature [47], keeping the temperature near isothermal condition is a difficult task. Hence a radiator was added to the basic design which not only gives more area of heat transfer to the circulating fluid but also blows the heat exchanger by its fan. Using this system the changes in temperature is so small (the temperature of working fluid was kept around $26 \pm 2^\circ\text{C}$ during tests) that it can be considered as a near isothermal conditions, Figure 6.10. The fan of radiator is directly connected to a battery. The battery is charged frequently by a battery charger.

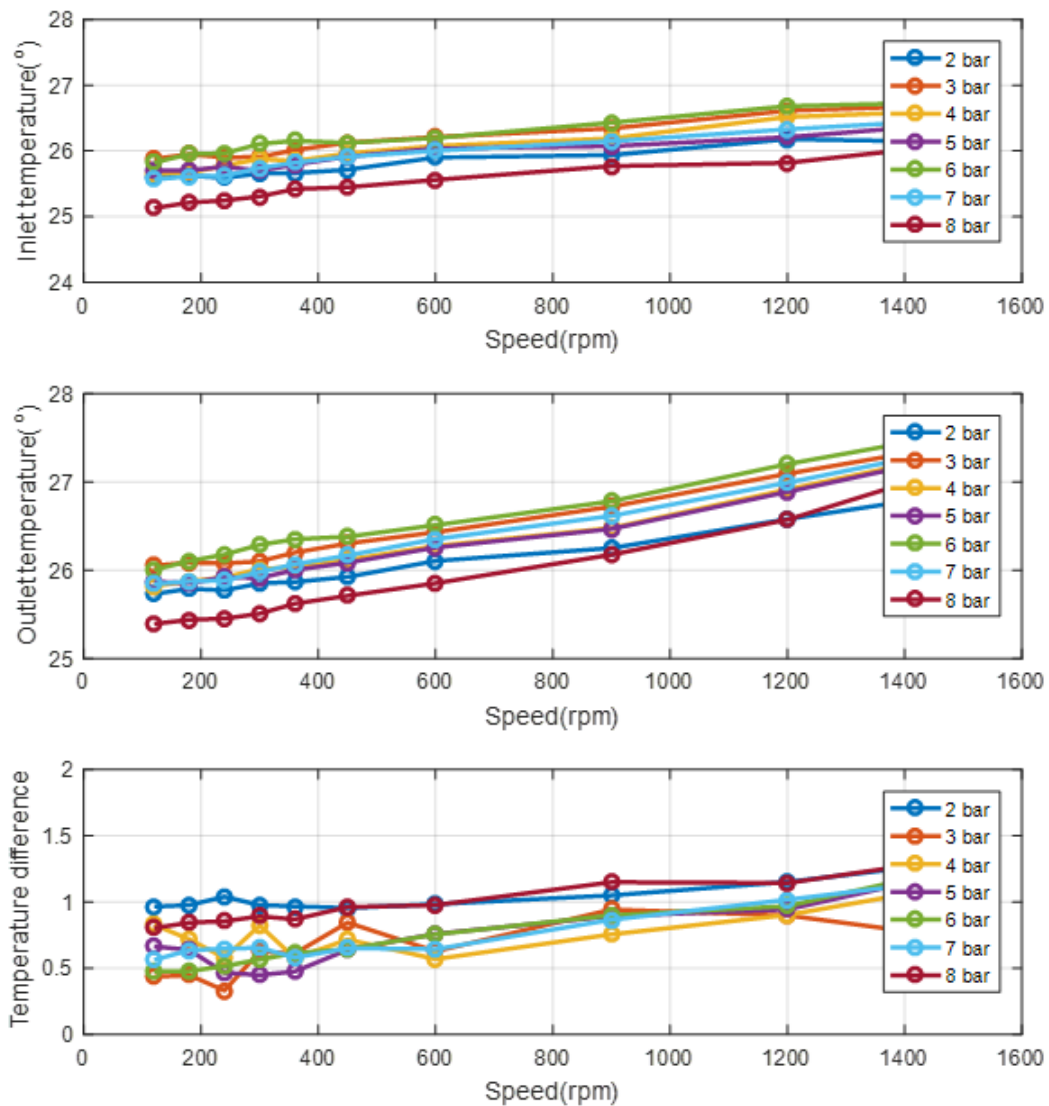


Figure 6.10 The temperature change in a test

The sealing gap is pressurised by the nitrogen gas above the water in the pressurized vessel and the pressure is controlled by the pressure regulator connected to the pressurized vessel. The maximum operational pressure of the system is up to 10 bar due to safety issues in the lab. The inlet pressure from the nitrogen cylinder to the operating system is controlled using an accurate multi stage regulator, Figure 6.11.



Figure 6.11 Multistage regulator mounted on the nitrogen cylinder

The second pump is used to circulate the process fluid, this pump is called circulating pump. The process fluid from pressure vessel was pumped to the internal line of heat exchanger, which took away the heat generated by the friction of mechanical seals as shown in Figure 6.12.

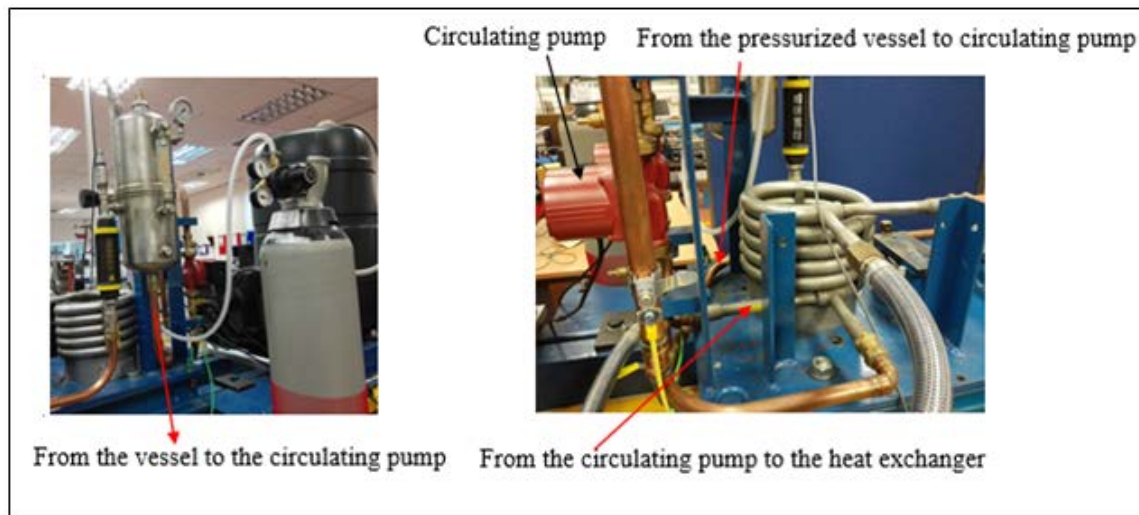


Figure 6.12 Connections to the radiator

The output of the heat exchanger is connected to the sealed chamber through the hole in the middle of the chamber and then the process fluid goes back to the pressurized vessel through flush holes in the seal cartridge, Figure 6.13. The inlet and outlet of process fluid in the pressurized chamber was inverse in the previous design of the rig. It means that the process

fluid coming from heat exchanger was connected to the flush holes. This configuration may lead to a thermal attack on the seal material as well as increase the fluid noises that are recorded by acoustic emission sensor.



Figure 6.13 Connections from and into the chamber

Both cooling and circulating pumps are the same, they operate like the heart of the auxiliary circulating system and can provide three selections of flow rate: 1.8, 2.3 and 3.3 m³/h as listed in Table 6.5 and shown in Figure 6.14. For all experimental work in this research the flow rate of pump was set to 3.3 m³/h.

Table 6.5 The general specifications of pump

Manufacturer	Type	Electrical specifications	Flow rate (m ³ /h)	Power consumption(w)
Prima flow	IP44 class H	230v~ 50hz Single phase shielded	1.8, 2.3, 3.3	55, 70,100



Figure 6.14 The pump employed in circulating system

6.3 Signal Measurement

To investigate the tribological behavior of the sealing gap, monitoring the working parameters of mechanical seals is necessary. This provides reliable data to correlate AE signals with working conditions of mechanical seals. Three main parameters are monitored accurately in this research; temperature, pressure and sliding speed of the mating faces as listed in Table 6.6

Table 6.6 The parameters measured in the experiments

Description	Sensor type	Range
Water temperature at the inlet and outlet of the sealed chamber	K Thermocouple	-100 to 8100°C
Pressure of the circulating system	Pressure gauge	0 to 25 bar
AE sensor	WD S/N FQ36 (peak frequency 263.67 kHz)	100 to 300kHz
Shaft speed	Encoder	

Developing reliable data acquisition systems for online monitoring of these working parameters will increase the chance of controlling them in an acceptable range. This may enhance the reliability of the tests and gives a guarantee that the results are achieved by off line analysis of the data that have been recorded under the same operating conditions. Hence a scientific comparison between different working conditions of mechanical seals would be possible either in the healthy or faulty case.

The sensors are connected to two data acquisition systems, the configuration of the measurement system is shown in Figure 6.15. In this section the general specifications of the sensors and the data acquisition systems applied in the experimental research is presented.

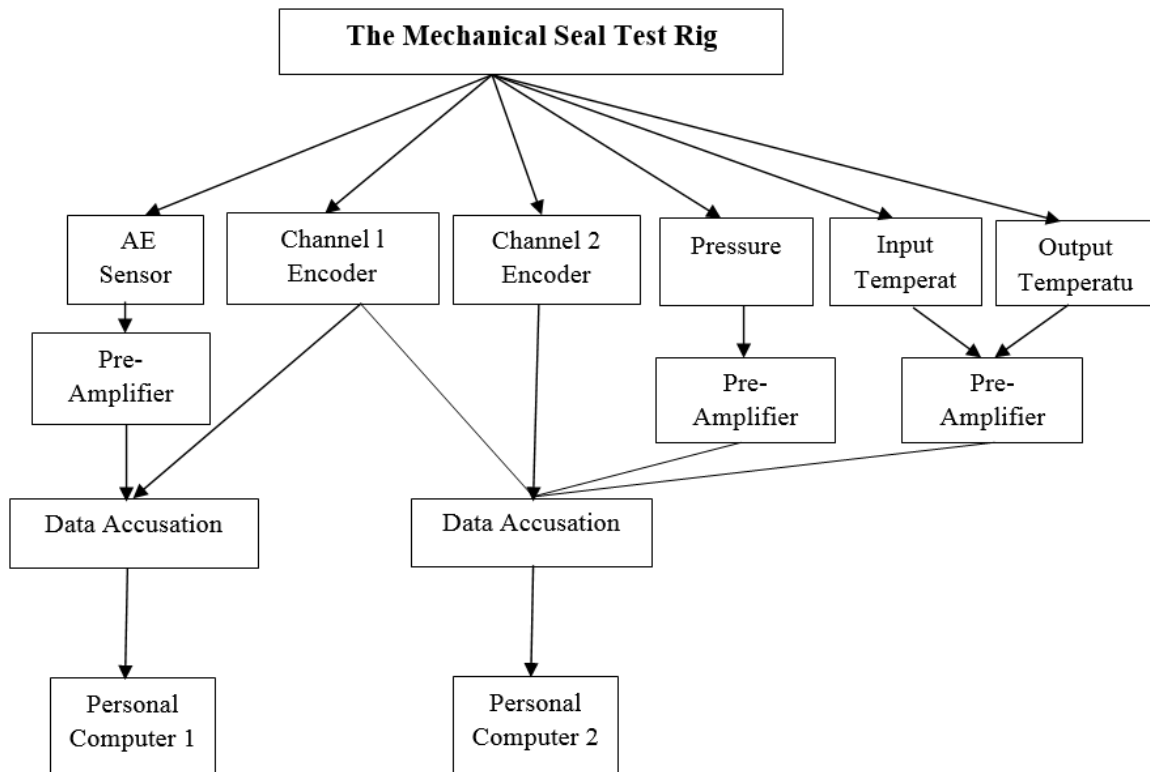


Figure 6.15 Sensor configuration and data acquisition

6.3.1 Data Acquisition System

Data acquisition will involve measuring the required variables (e.g. pressure, temperature, voltage, current, rotational speed) and turning them into electronic signals. To do so effectively will involve judicious choice and placement of the right type and number of sensors and conditioning may be necessary to reduce the susceptibility of the signals to

interference. Conditioners are employed for performing basic operations including amplification, filtering, linearization, and finally modulation/demodulation [23]

Data acquisition systems and cards have developed significantly in the last 20 years. Before that acoustic emission events were investigated on oscilloscope monitors or recorded on tape. A few seconds of recorded signal needed many meters of tape and triggering the recording was complicated. With the continued development of analogue-to-digital converters data recording has become much faster. Today's AE systems are able to acquire multiple channels simultaneously channels can be monitored continuously and stored. The new generation systems also enable extensive post processing possibilities. Huge amounts of data can be stored on hard drives and accessed for signal processing afterwards. Complete acoustic emission systems with integrated data acquisition cards, special software and data storage are available but many systems, especially those for research purposes, are PC based with high speed data acquisition cards.

Two data acquisition system (DAS) are employed in this research. The first one is a multiple channel analogue to digital convertors (ADC) with associated software for collecting operational parameter's data such as rotational speed of shaft, temperature and sealed fluid pressure. The second one is a two channel acoustic emission data acquisition system, channel one is used for collecting AE data and channel two is used for collecting encoder data. So the encoder data is collected from both data acquisition systems because of the important role of measuring the real rotational speed of the shaft in this research

For the operational parameters, the data acquisition system was a Sinocera YE6230B, a 16-channel high speed data acquisition system which recorded all the measurements data at a sampling rate of 96 kHz, see Figure 6.16. This figure clearly shows that the first channel of data acquisition was connected to two cables, one of them coming from the encoder and another is used for connecting the encoder data to the AE data acquisition card.



Figure 6.16 Sinocera YE6230B

The data acquisition system is supported by general purpose YE76000 software for data acquisition, conditioning and analysis as part of the data acquisition system. The software allows data acquisition with different triggering modes, which is convenient for viewing the data in real time and saving data to the hard drive, Figure 6.17.

It also possesses efficient data storage and fast data conversion to MATLAB format; 16 bit with 16 channels. Also it is possible for selection of different acquisition modes: oscilloscope, manual continuous and triggered. The specifications of the Sincocera YE6230B are presented in Table 6.7.

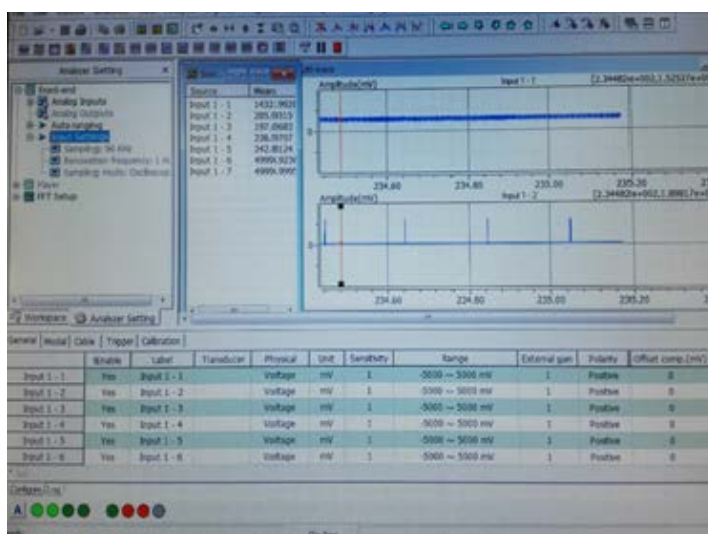


Figure 6.17 Operational condition control system

Table 6.7 Technical specifications of the Sinocera

Manufacturer	Sinocera YE6230B
Number of Channels	16 channels, selectable voltage
A/D conversion resolution	16 bit
Sampling rate (maximum)	100 kHz per channel parallel sampling
Input range	±5V
Gain	Selectable, either 1, 10 or 100
Filter	Anti-aliasing filter
Interface	Anti-aliasing filter
Software	YE7600

A PAC PCI-2 commercial data acquisition system has been employed for acoustic emission sensor. The PCI-2 AE System is a 2-channel data acquisition and digital signal processing system on a single full-size 32-bit PCI-Card as shown in Figure 6.18

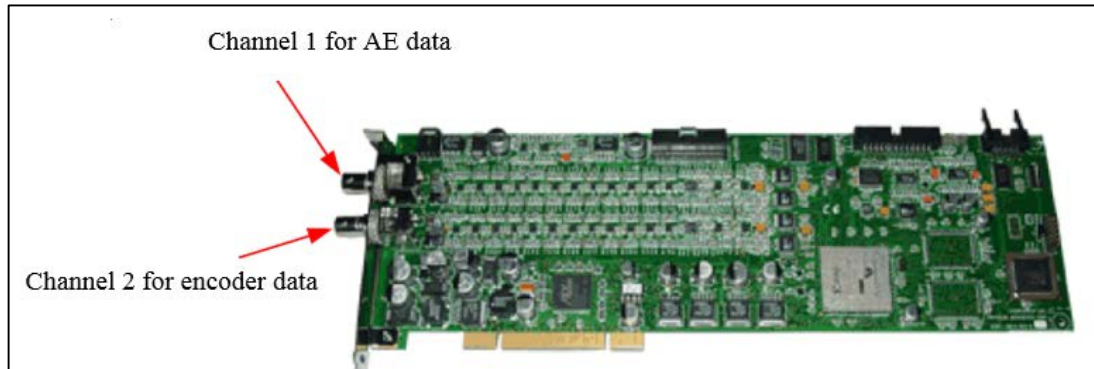


Figure 6.18 PCI-2 AE System board

During data acquisition, the waveform is transferred and processed by PAC Windows platform consisting of AEwin™. The sampled AE waveforms can be continuously transferred and saved to the hard disk of computer depends on its capacity. The PCI-2 AE system specification is shown in Table 6.8.

Table 6.8 Technical specifications of the PCI-2 AE system

Manufacturer	Physical Acoustic Corporation
Number of inputs	2 channels
Input impedance	50 ohm or 1000 ohm
Minimum noise threshold	1kHz-3MHz
ADC Type	18bit 40 MSPS per channel maximum
Dynamic range	>85dB
Sample rate	100 kS/s to 40 MSPS
Operating temperature	5°C to +45°C
DC Power	12 Volt, 1.0 amps
Minimum noise threshold	17dB

The configuration of the AE signal and streaming data system is shown schematically in Figure 6.19.

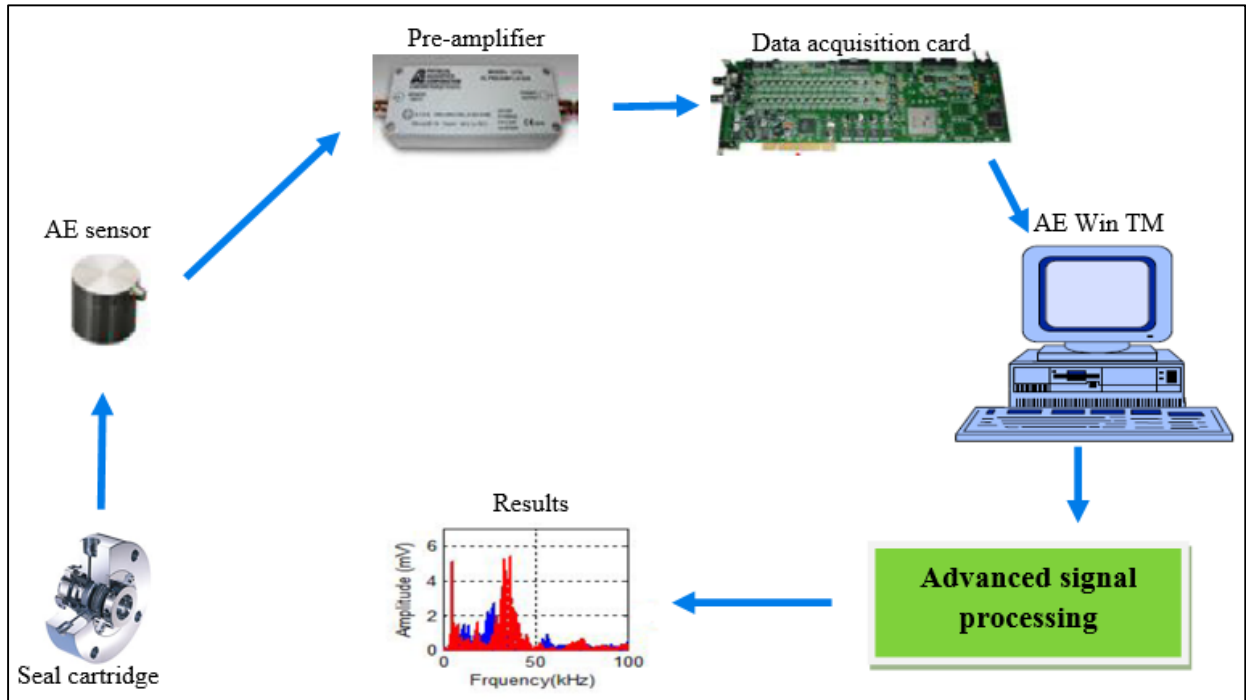


Figure 6.19 AE signal measurement and data streaming system configuration

6.3.2 Temperature Sensor

The fluid temperature at the inlet and outlet of the pressurized chamber were measured using two TC Ltd commercial type K thermocouples. The positions of the thermocouples are indicated in Figure 6.20. These are miniature (1.5 mm diameter) mineral insulated thermocouples with miniature flat pin plug connected to the data acquisition system through a preamplifier and distributor Figure 6.20 (c). The specifications of the thermocouple are shown in Table 6.9.



(a) Inlet temperature

(b) Outlet temperature

(c) Amplifier

Figure 6.20 The position of temperature sensors

Table 6.9 Thermocouple specifications

Manufacturer	TC Ltd
Type	K
Sheath diameter	1.5 mm × 250 mm
Sheath material	321 Stainless Steel
Operating range	-100 °C to 800 °C
Accuracy	±1.3 °C

6.3.3 Pressure Sensor

Pressure of the circulating system is measured using a pressure gage and a pressure transducer, Figure 6.21. The range of the pressure gage applied in this work is between 0-25 bar. The pressure transducer used to measure the pressure of the circulating system is a GEMS 2200 SGB 100 1F3DA strain gauge pressure sensor. The strain gauges are small components that are fixed to a surface that is strained. The change in length of the element caused by external pressure or external force produces change in the electrical resistance. The electrical resistance change is processed and converted into a voltage. The specification of the pressure transmitter is presented in Table 6.10.

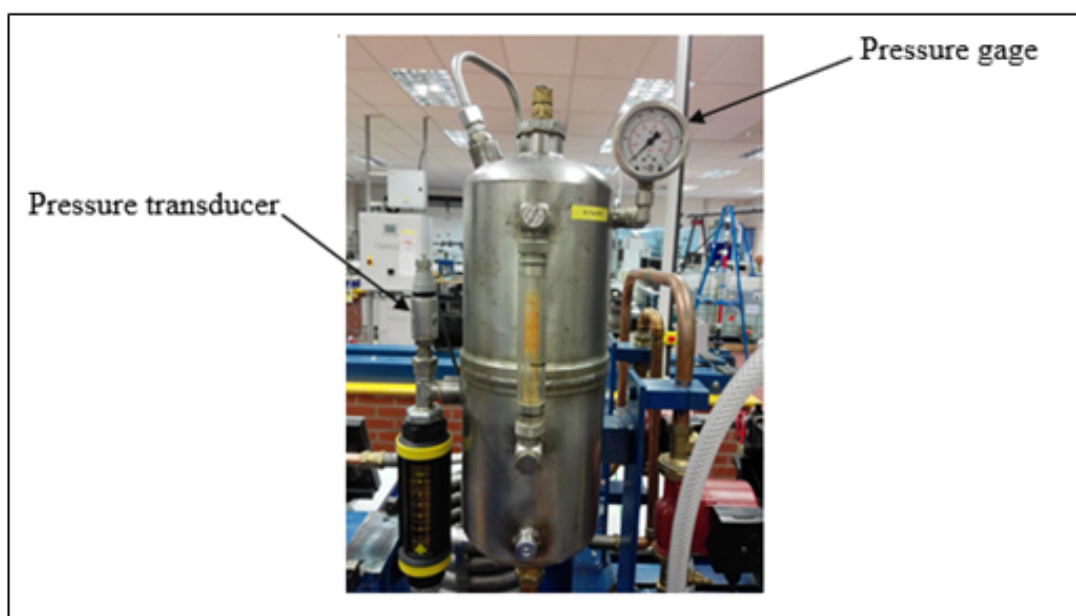


Figure 6.21 The position of the pressure gage and pressure transducer

Table 6.10 Pressure sensor specifications

Manufacturer	GEMS
Type	2200 SGB 100 1F3DA
Supply	D.C 11.5 to 35 V
Output	0 to 10 V
Operating range	0 to 10 bar

6.3.4 Acoustic Emission Sensor

The acoustic emission sensor used in this research is a wide band model WD S/N FQ36 transducer with an operating frequency range from 100 kHz to 1MHz to obtain the AE signals, allowing high frequency events due to frictional process to be monitored. The sensor has been mounted in the radial direction on the seal cartridge, since this is the closest place to the sealing gap with the least possible interfaces as shown in Figure 6.22. This may guarantee that the wave distortion is reduced to a minimum possible level.

The electrical signal from AE sensor is usually very weak. It needs to be amplified otherwise it would attenuate rapidly when it travels over the relatively long distance to the data acquisition card. The pre-amplifier must be located close to the transducers to eliminate signal loss from the connecting cable, usually within one meter of wire length. Sometimes pre-amplifiers are integrated into the sensor housing. The signal is usually amplified by 20 dB to 60 dB, which is between 10 and 1000 times the input signal voltage. Some pre-amplifiers are also fitted with analogue filters to eliminate and reject the noise from outside of sensor operating range, especially low frequency noise.

The specification of the AE sensor is as shown in Table 6.11. The calibration certificate of the acoustic emission transducer is presented in Appendix B. The output signal from AE-sensor was pre-amplified by 40 dB through a preamplifier 20/40/60 dB gain. In this research the gain was set to 40 dB. The signal from amplifier is acquired by a 2 MHz high speed data acquisition system with 16 bit resolution as discussed in Section 6.3.1.



Figure 6.22 AE sensor mounted on the seal cartridge

Table 6.11 AE sensor specifications

Manufacturer	Physical Acoustic
Type	Wideband AE Sensor
Model	WD FQ 35
Peak sensitivity	64.50 dB ref 1V/ μ bar
Frequency response	Peak frequency 263.67 kHz
Frequency range	100 kHz to 1 MHz
Operating range	-45 °C to 125 °C

6.3.5 Shaft Encoder

Encoder or speed transducer is widely used for measuring the output speed of rotating machines such as electrical motors. This sensor is coupled and installed to the end of the electrical motor shaft and generates electrical signals due to rotation of the shaft, Figure 6.22. The encoder used is economic for small devices, has a long life and very small torque ball bearings. Specification of the encoder is shown in Table 6.12.

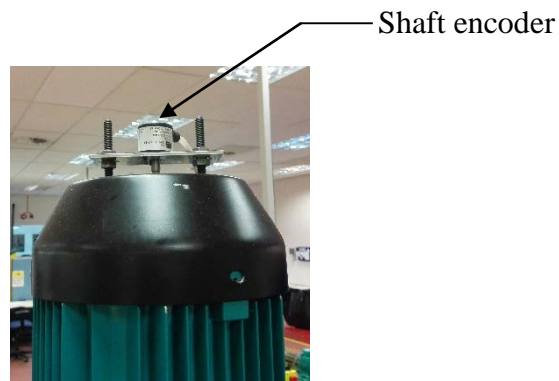


Figure 6.22 Shaft encoder

Table 6.12 Shaft encoder specifications

Manufacturer	HENGLER
Type	RI 32
Mounting	Round flange
Number of pulse per revolution	50
Maximum speed	6000 rpm
Operating temperature	-10 to 60 °C
Supply voltage	DC 10 to 30V

6.4 Surface Roughness Measurement

The mechanical seal applied in this research is not brand new. Thus it is necessary to measure the roughness and waviness of the mating faces to insure that the surface topography of sealing gap meet the manufacturer's requirements of John Crane before the test. To achieve this, a Taylor Hobson Form Talysurf series 2 has been employed to examine the surface topography of the mating faces before and after the test, Figure 6.23. Form Talysurf Series 2 is a comprehensive range of high performance hardware and software that offers precision evaluation of different surface topography parameters of mating faces.



Figure 6.23 Taylor Hobson Form Talysurf applied in this research

Before and after the tests, both rotating and stationary faces were examined. Eight different samples have been selected on the mating faces. The attempt was paid to pick up the data from the same samples before and after the tests. To achieve this, a reference point has been selected on both stationary and rotating rings. Then the periphery of both rings has been divided to 8 different samples. The first data point was approximately matched on the reference point. After that the specimen was rotated clock wise to reach the next sample.

This procedure has been carried out for both rings. The data length and the speed of Talysurf probe were set to 4.8 mm and 1 mm/s respectively. An example of surface profiles obtained during the measurements is presented in Appendix D. The results of the surface measurements are presented in Appendix E.

6.5 Test Procedure and Fault Simulation

To investigate the tribological behaviour of mechanical seals and prove the potential of acoustic emission measurements to detect the faults at early stages, a comprehensive experimental program is needed. The experimental study in this thesis includes two main programmes: investigate the tribological behaviour of mechanical seals which is the base line analysis in this research and then fault simulation. The former includes four different tests; sealed free test, static test, transient test and test under different speed and pressures. The main objective of these tests is to find a proper frequency range that can present the tribological behaviour of sealing gap. As discussed in Section 5.3, the novel AE sources introduced in this study include fluid friction, deformations of asperities due to direct asperity contact, and fluid induced asperity deformation. The difficulty of the research lies in the highly interacting influence of deformations of different AE sources on the generation of acoustic emission signals during the operation.

Since there is neither experimental proof nor theoretical model to prove which of the mentioned acoustic emission source mechanisms plays a dominant role, this experimental program aims to examine how acoustic emission features changes by changing the operating conditions as well as proving the mathematical models presented in Chapter 5. This may demonstrate the potential of external AE measurements to monitor the lubrication state and frictional behaviour of mechanical seals under different operating conditions.

The fault simulation program includes three different tests; partial dry running test, spring fault test and defective seal test. The main objective of the fault simulation program is to understand how acoustic emission features change under fault conditions as well as performing a robust comparison against the baseline. This may pave away for early fault detection in industrial applications. Table 6.13 summarises the experimental program carried out in this this thesis. These tests are discussed further in the rest of this section.

Table 6.13 Summary of experimental program

Experimental program	Test	Operating parameters		Purpose
		Sealed pressure (bar)	Rotational speed (rpm)	
Base line tests	Seal free test	Not pressurized	120, 180, 240, 300,360,450, 600, 900, 1200 and 1600 rpm	Evaluating the noises of the test rig.
	static test	Not pressurized	The shaft was turned manually	Investigate the frequency range related to rubbing of faces.
	transient test	0 bar, 4 bar and 8 bar	1500 rpm	Investigate the frequency range related to AE events.
	Test under different speed and pressures	From 2 bar to 8 bar load with the step size of one bar	120, 180, 240, 300,360,450, 600, 900, 1200 and 1600 rpm	Investigate the changes in AE signal under different lubrication regimes.
Fault simulation	Partial dry running	Not pressurized	120, 180, 240, 300,360,450, 600, 900, 1200 and 1600 rpm	Fault simulation.
	Spring fault	From 2 bar to 8 bar load with the step size of one bar	120, 180, 240, 300,360,450, 600, 900, 1200 and 1600 rpm	Fault simulation.
	Defective seal	From 2 bar to 8 bar load with the step size of one bar	120, 180, 240, 300,360,450, 600, 900, 1200 and 1600 rpm	Fault simulation by scratching the stationary ring.

In general, the aim of this experimental study is to give some fundamental investigations to provide a solid base for the implementation of acoustic emission technique to the condition monitoring of mechanical seals. The objectives of the program are summarized as follows:

1. Test the hypothesis that the elastic deformation of asperities due to direct contact and due to fluid flow as well as friction between fluid layers are the dominant mechanism of acoustic emissions in the sliding of mechanical seal faces.
2. Find the AE frequency band that reflects the effect of different AE sources in the sliding of seal faces under both healthy and faulty conditions.
3. Investigate how the type of AE signal is affected by different AE sources as well as different operating conditions.
4. Extract the AE features that can represent the tribological behaviour of mechanical seals under both healthy and faulty conditions.
5. Investigate how the AE signal changes with changing the lubrication regime of face seals under both healthy and faulty conditions.
6. Compare the experimental results with the prediction of the AE model developed in Chapter 5.
7. Demonstrate the potential of external acoustic emission measurements for early fault detection in mechanical seals.

6.5.1 Seal Free Test

This test refers to idling of the test rig where the seal head assembly (including the rotating ring) was removed and consequently no acoustic emission signal was picked up from the sealing gap as schematically shown in Figure 6.24. During this test the seal was not pressurized, however other parts of the system such as circulating and supplying pumps were working as usual. For each test 10 different incremental speeds were adjusted; 120, 180, 240, 300, 360, 450, 600, 900, 1200 and 1600 rpm. For each speed the run time duration was 3 minutes, the data was recorded after approximately two minutes. The data recording duration

was selected as 8 seconds for the data acquisition system. Purpose to carry out this test was to evaluate the noises of the test rig. The efficiency of this test has been proved in previous works [191].

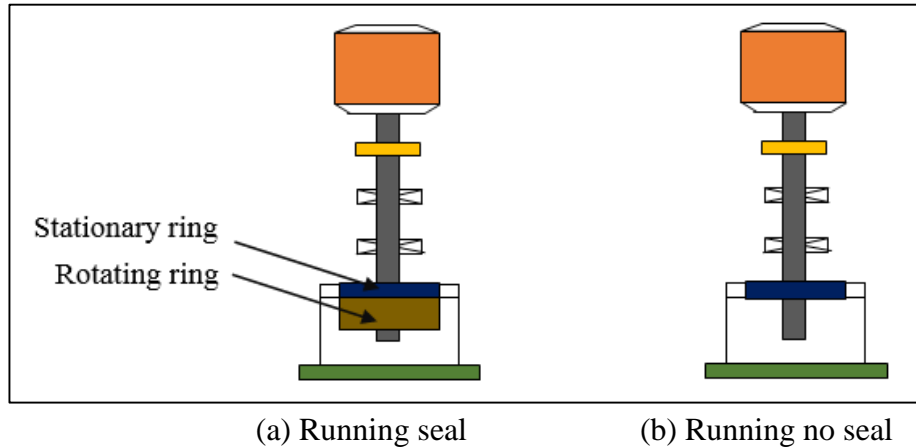


Figure 6.24 Schematic illustration of the seal free test configuration

6.5.2 Static Test

During this test the acoustic emission data acquisition system was kept on working and the shaft of the test rig was turned manually. Since it is impossible to turn the shaft manually when the chamber is pressurized, the tests were conducted under no sealed pressures. The time duration of each test is 8 seconds. Since it is impossible to generate vibration by just turning the shaft, the acoustic emission was likely caused by the sliding of seal faces rather than by the vibration of the test rig. Therefore, it can be concluded that the results of this test are related to the rubbing of mechanical seals.

6.5.3 Transient Speed Test

This test was carried out under three different loads; 0 bar, 4 bar and 8 bar (sealed pressure) and at speed of 1500 rpm. Since it takes around 16 seconds for the electric motor applied in this work to reach the speed of 1500 rpm, Figure 6.25, hence for each test the load is constant and speed increases automatically up to adjusted value of 1500 rpm (50% speed). Using this method different lubrication regimes (i.e. boundary lubrication, mixed lubrication and hydrodynamic lubrication regime) can be simulated during the start up to steady state condition of motor. The purpose to carry out this test is to identify the frequency range

that significantly reflects the characteristics of different acoustic emission sources and different lubrication regimes in the sliding of seal faces.

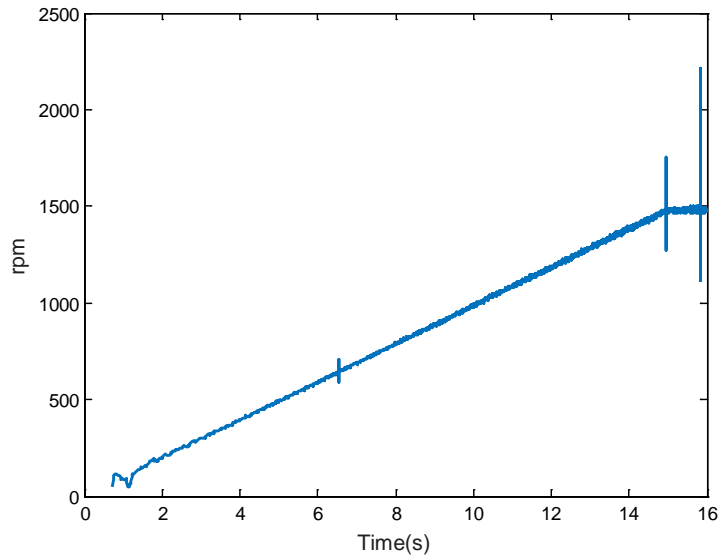


Figure 6.25 Motor speed variations up to 1500 rpm under 4 bar load

6.5.4 Tests under Different Operating Conditions

The aim of this experimental study is to demonstrate a correlation between AE signals and duty parameters that refer to different lubrication regimes. It means that the seal needs to be tested under a wide range of duty parameters. To achieve this, experiments were conducted at 7 different loads from 2 bar to 8 bar load with the step size of 1 bar ± 0.02 , Figure 6.26. At each load, 10 tests were carried out under different speeds 120 rpm, 180 rpm, 240 rpm, 300 rpm, 360 rpm, 450 rpm, 600 rpm, 900 rpm, 1200 rpm and 1500 rpm to simulate different Tribological regimes.

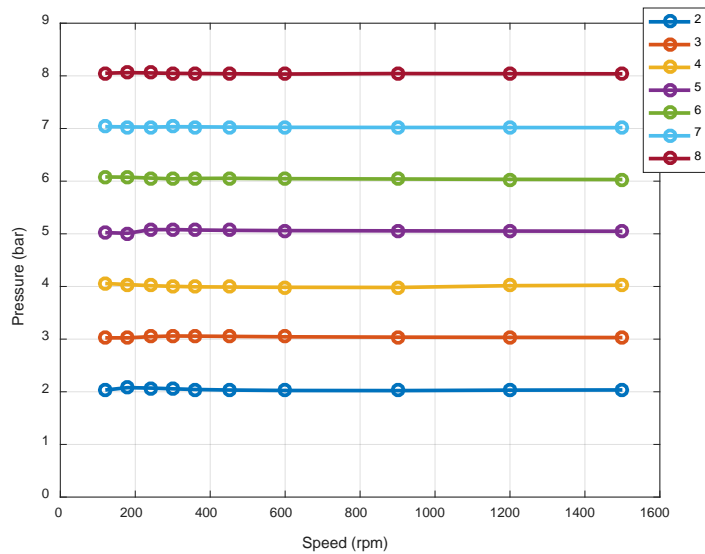


Figure 6.26 Operational conditions during the tests

These operating conditions can achieve a minimum duty parameter of 0.199×10^{-8} at which it is more convinced that the seal is under the mixed lubrication or boundary conditions according to Table 2.1. In the meantime, the maximum duty parameter of 5.211×10^{-8} indicate that the seal may operate under hydrodynamic regimes. Thus, it allows AE signals to be examined in wide lubrication conditions and henceforth develops effective AE based diagnostics. For each speed the run time duration was 3 minutes, the data was recorded after approximately two minutes. The data recording duration was selected as 8 seconds for the both data acquisition systems.

6.5.5 Partial Dry Running Test

Since the mechanical seals are hydrostatically lubricated, the lack of sealed pressure simulated the conditions under which partial dry running occurs. 10 tests were carried out under no pressure and different incremental speeds; 120 rpm, 180 rpm, 240 rpm, 300 rpm, 360 rpm, 450 rpm, 600 rpm, 900 rpm, 1200 rpm and 1500 rpm. For each speed the run time duration was 3 minutes, the data was recorded after approximately two minutes. The data recording duration was adjusted on 8 seconds for the both data acquisition systems. It should be noted that it is possible to drain the chamber and simulate dry running test, but it will damage the mating faces.

6.5.6 Spring Fault Test

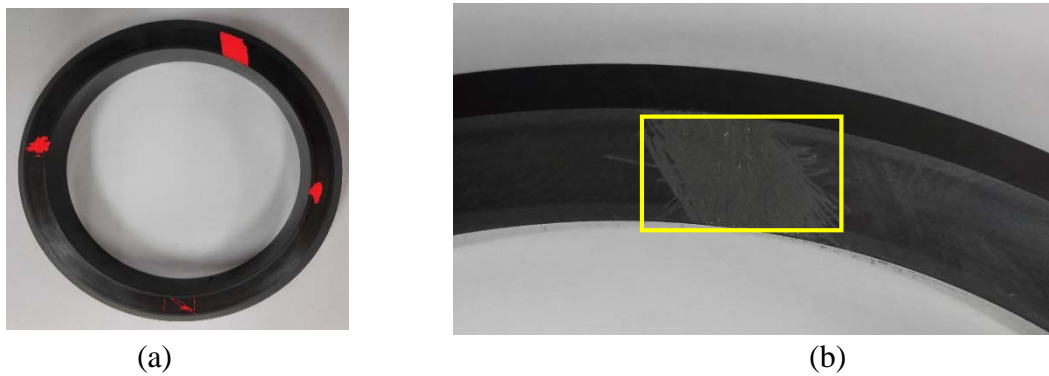
Spring fault is another common fault in the operation of mechanical seals. The test were carried out by taking off 2 springs out of 12 available springs in the seal head assembly, Figure 6.27. In theory, this provides approximately 16% reduction in the spring force, based on the design characteristics of seal and operating conditions, however its effect on the closing force is discussed in Section 8.3. Experiments were conducted at 8 different loads from 1 bar to 8 bar load with the step size of one bar. At each load, 10 tests were carried out under different speeds 120 rpm, 180 rpm, 240 rpm, 300 rpm, 360 rpm, 450 rpm, 600 rpm, 900 rpm, 1200 rpm and 1500 rpm to simulate different lubrication conditions. For each speed the run time duration was 3 minutes, the data was recorded after approximately two minutes. The data recording duration was selected as 8 seconds for the both data acquisition systems.



(a) Before assembly (b) After assembly
Figure 6.27 Seal head assembly in spring fault simulation

6.5.7 Defective Seal Test

The last test in this research is defective seal test. To do this test, four small radial superficial scratches were made on the mating ring as shown in Figure 6.28. The area of defects increases incrementally from the bottom one in the anti-clock wise direction. The smallest defect is only an artificially induced crack (approximately 6 mm length) and the biggest one has an approximately $7 \times 8 \text{ mm}^2$ dimensions.



(a) Damaged face (b) Scratches on stationary ring
Figure 6.28 Defective seal test

Since during the operation of defective seal the sealing action is not performed properly, hence different levels of leakage occurs depend on operational conditions. In general, the level of leakage increases by increasing the pressure and rotational speed of drive shaft. To avoid flooding the lab, the flushing port of the seal was connected to a small bottle, Figure 6.29. The maximum level of leakage occurred during the tests was recorded manually around 1 litre in three minutes for the maximum pressure and speed.

Experiments were conducted at 8 different loads from 1 bar to 8 bar load with the step size of one bar. At each load, 10 tests were carried out under different speeds 120 rpm, 180 rpm, 240 rpm, 300 rpm, 360 rpm, 450 rpm, 600 rpm, 900 rpm, 1200 rpm and 1500 rpm to simulate different lubrication conditions. For each speed the run time duration was 3 minutes, the data was recorded after approximately two minutes. The data recording duration was selected as 8 seconds for the both data acquisition systems.



Figure 6.29 Leakage during the defective seal test

6.6 Main Findings

This thesis designed and constructed a new mechanical seal test rig for the purpose of condition monitoring of mechanical seals. To ensure the test rig replicates the usual seal arrangement in practical applications such as pumps, real industrial mechanical seals rather than just pairs of face seal materials were employed. To get stronger acoustic emission signals, larger mechanical seals for larger pumps were selected.

To investigate the tribological behaviour of mechanical seals and prove the potential of AE measurements to detect the faults at early stages, a comprehensive experimental program has been developed. The experimental study in this thesis includes two main programmes: investigate the tribological behaviour of mechanical seals which is the base line analysis and then fault simulation. The former includes four different tests; sealed free test, static test, transient test and test under different speed and pressures. The main objective of these tests is to find different frequency ranges that can present the tribological behaviour of AE sources. Later, the fault simulation program, includes three different test; partial dry running test, spring fault test and defective seal tests. The main objective of the fault simulation program is to understand how acoustic emission features change under fault conditions as well as performing a robust comparison against the baseline. This may pave away for early fault detection in industrial applications.

Chapter Seven;

Experimental Study of AE from the Tribology of Mechanical Seals

This chapter aims to present the results of an experimental study on the tribological behaviour of mechanical seals using non-intrusive AE measurements. The study includes four groups of experiments: the seal free test, the static test, the transient speed test and the tests under different operating conditions (baseline test) as illustrated in previous chapter. The primary tests are conducted to find the proper frequency range of AE signals that can present the tribological behaviour of the sealing gap by analysing AE signals in time-frequency domain. While the latter test is used to study the tribological behaviour of mechanical seals. The main body of this chapter is related to the baseline test, where focus is paid to investigate the change of AE time domain and frequency domain features under different tribological regimes. The discussion is also made by developing novel equations that can explain tribological AEs based on the AE source models that have been detailed in Chapter 5. At the end of the chapter, conclusions are drawn on the basis of the information obtained in this experimental study.

7.1 Introduction to the Baseline Experimental Study

The promising potential of external AE measurements to monitor the tribological behaviour of mechanical seals has been demonstrated in previous studies [191]. The main limitations of the previous works can be summarized as followings:

1. A systematic test procedure is needed to distinguish AE signals from the background noises. There is no comprehensive experimental program in the literature to find proper frequency range of AE responses.
2. To investigate the tribological behaviour of mechanical seals, it is necessary to run the rig at very low speeds. Previous experimental researches have been carried out under relatively high speeds where mechanical seals work in the hydrodynamic lubrication regime. Under this working conditions viscous friction and fluid induced asperity deformation can be studied logically, however it is not possible to investigate the effects of direct asperity contact at high speeds.
3. The tribological aspects of mechanical seals such as the effect of sealed pressure and sliding speed on the AE features under different tribological regimes have not been studied yet.
4. Previous mathematical models only can predict the level of AE signals in direct asperity contact of asperities. No work has been published to explain tribological AEs, especially at transition point between mixed to hydrodynamic lubrication regime where mechanical seals are ideally and by definition operate.

This study aims to improve the previous works to pave a way for on line condition monitoring of mechanical seals. All experiments were conducted using the mechanical seal test rig presented in Chapter 6.

7.2 Identification of the Tribological AEs

In the industrial applications, AE signals are generated not only by rubbing of the mating faces, but also from noise sources [16, 26, 28]. For instance, Xiaohui Li et al. concluded that in AE monitoring of mechanical seals, spindle is the main noise source and signal to noise ration decreases with the increase of rotational speed of spindle [28]. Therefore, to monitor the tribological behaviour of the sealing gap, it is necessary to distinguish AE signals from the background noises that requires an appropriate test procedure and signal processing method. In this section the results of the three comparative program (the seal free test, the

static test, the transient speed test) are presented to find the proper frequency band that can represent the tribological behaviour of mechanical seals. To gain more effective details, AE responses are analysed in time frequency domain.

7.2.1 Results of the Seal Free Test

To do this test the primary ring was removed before running the motor. Then the drive shaft was turned manually and data was recorded simultaneously, see spectrogram in Figure 7.1. This test revealed that some noises are generated by every rotational period of the shaft. Two main frequency bands are observed: 0-40 kHz and 100-150 kHz.

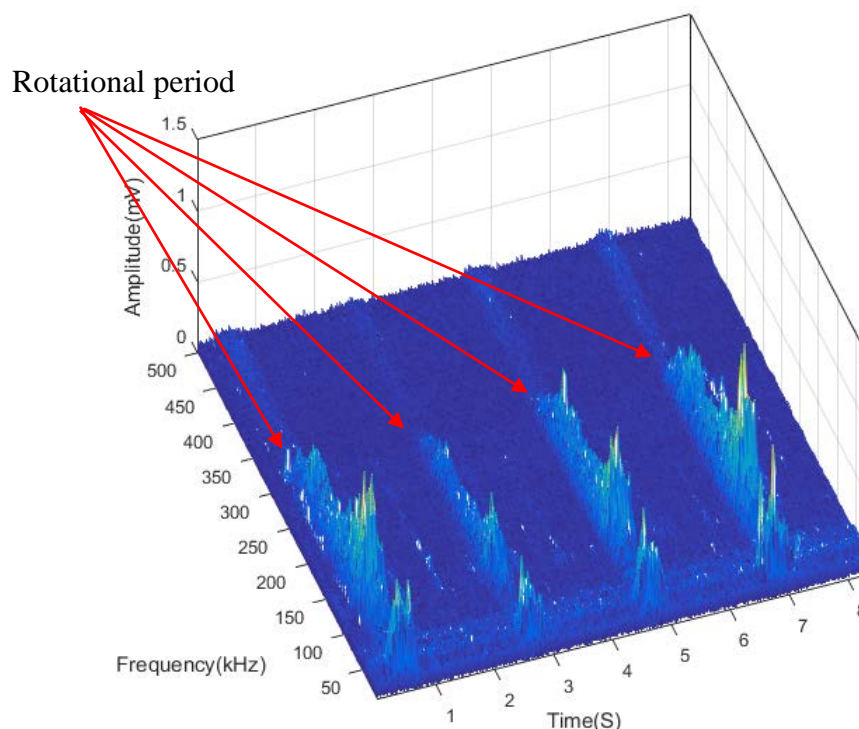


Figure 7.1 The spectrogram of the AE signal measured in manual turning of shaft

To get insight into the background noises, the results of seal free test (when electric motor is running) are presented in Figure 7. 2. The frequency bands that have been observed in manual rotation of shaft still exist in the spectrogram, however no time interval between the AE responses is distinguishable. This clearly shows that these peaks are generated due to the rotational movement of the shaft. Based on Figure 7.2, no remarkable change in the amplitude is observed by increasing the rotational speed of the shaft. These noises may be generated due to the vibration of the rig, rotational movement of shaft, electric noises from the inverter (or motor), resonant frequency of the sensor, natural frequency of stationary ring

or circulation of fluid in the sealed chamber. To get a solid conclusion on this, the results of the static test and the transient speed test are investigated in the rest of the this section.

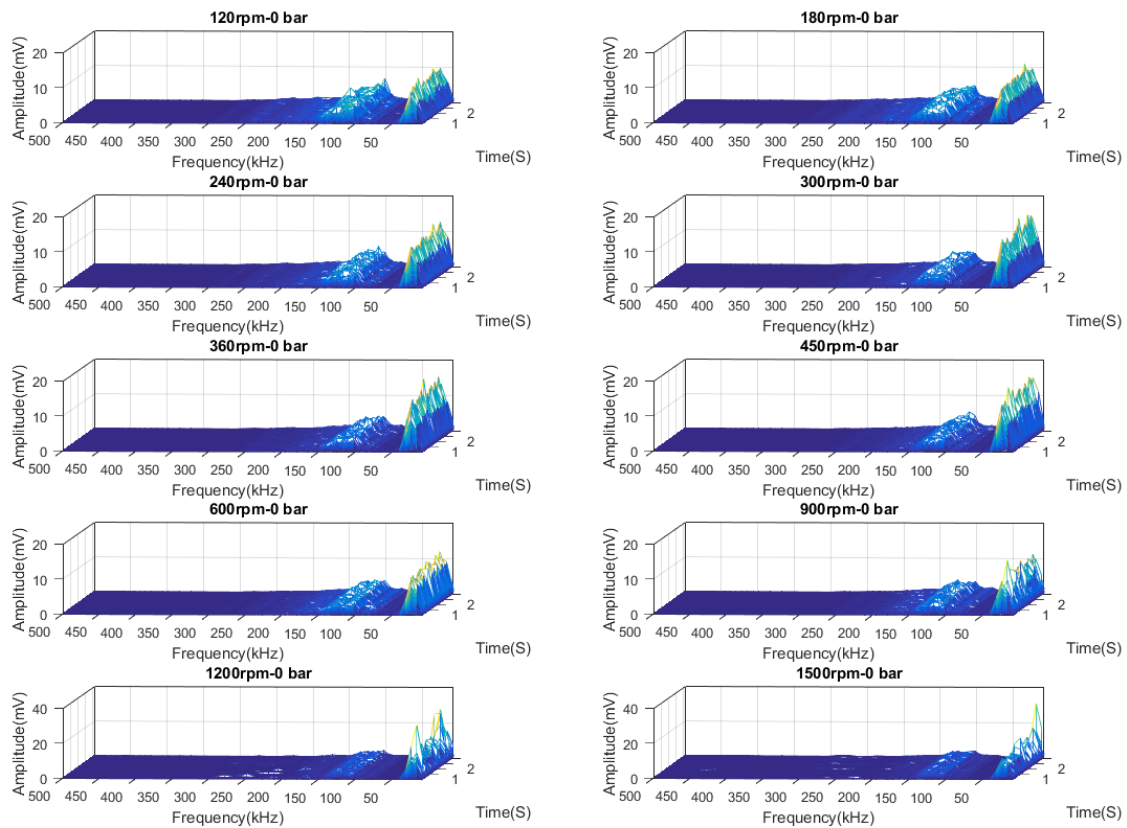


Figure 7.2 The spectrogram of the AE signal measured in seal free test

7.2.2 Results of the Static Test

During the static test both stationary and rotating rings were assembled and the shaft of the test rig was turned manually. Three tests have been carried out, the results of one of them is presented in Figure 7.3. Based on Figure 7.3, the amplitude of the low frequency events located in the range of 0-40 kHz goes down significantly. It is believed that the mentioned frequency range is related to electromagnetic field of the motor. Since in seal free test it was much easier to rotate the shaft manually, the amplitude of this frequency range was higher. In static test, manual turning of shaft is difficult due to rubbing of the mating faces. Consequently, the amplitude of the related noise decreases or even completely disappeared. Moreover, the resonant frequency of stationary ring is located in this frequency range (see Appendix F), thus the frequency band of 0-40 kHz is not related to the tribological AEs.

It is believed that the frequency band of 100-150 kHz that has been observed in all previous tests, whether in the seal free test or the static test, is intensified by the AE sensor and can be considered as one of the main noise sources in this research.

In addition to frequency range of 100-150 kHz, one more peak is observed in the range of 235 to 305 kHz. Based on Figure 7.3, the seals come to contact slightly before the 5th and 8th seconds of data recording time. Thus it can be concluded that the frequency range of 270 ± 35 kHz is caused by the rubbing of seal faces rather than by the noise sources of the test rig.

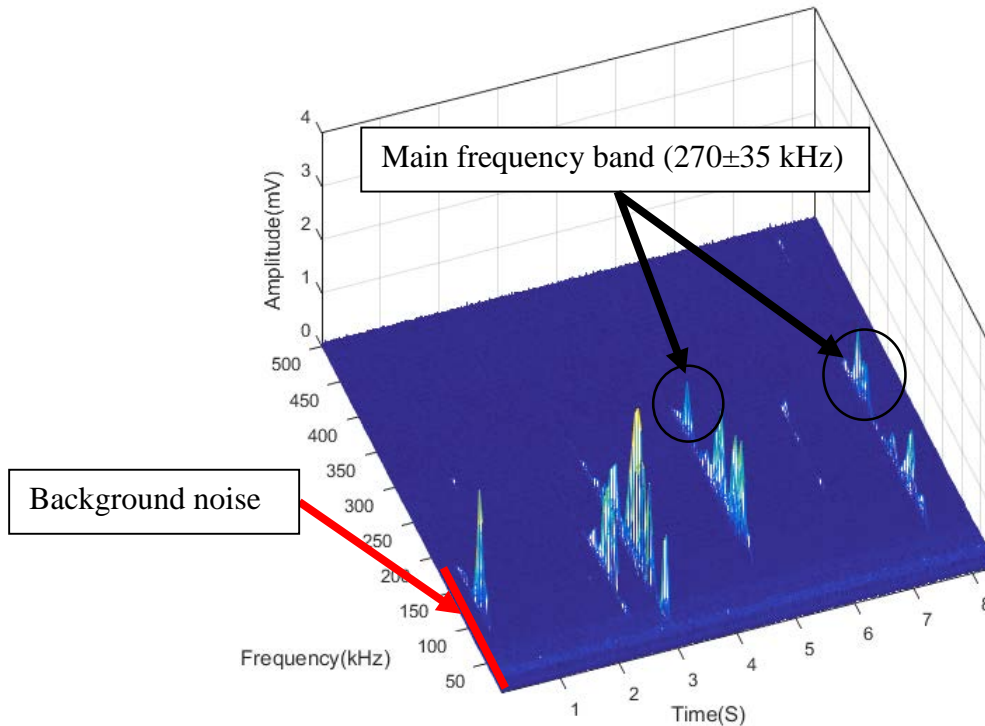


Figure 7.3 The spectrogram of the AE signal measured in static test

7.2.3 Results of the Transient Speed Test

As discussed in Section 6.5.3, the transient speed tests were carried out under three different sealed pressures, 0 bar, 4 bar and 8 bar and at a variable speed up to 1500 rpm. The data recording time was 16 seconds. The purpose to carry out this test was to investigate the changes in the amplitude of the AE signals (especially in the range of 270 ± 35 kHz) under different lubrication regimes.

Figure 7.4 shows the spectrogram when the seal chamber is not pressurized. Since mechanical seals are hydrostatically pressurized, the transient speed test under 0 bar gives the most possibility of direct asperity contacts. These asperity collisions generate high frequency emissions (in the range of 270 ± 35 kHz).

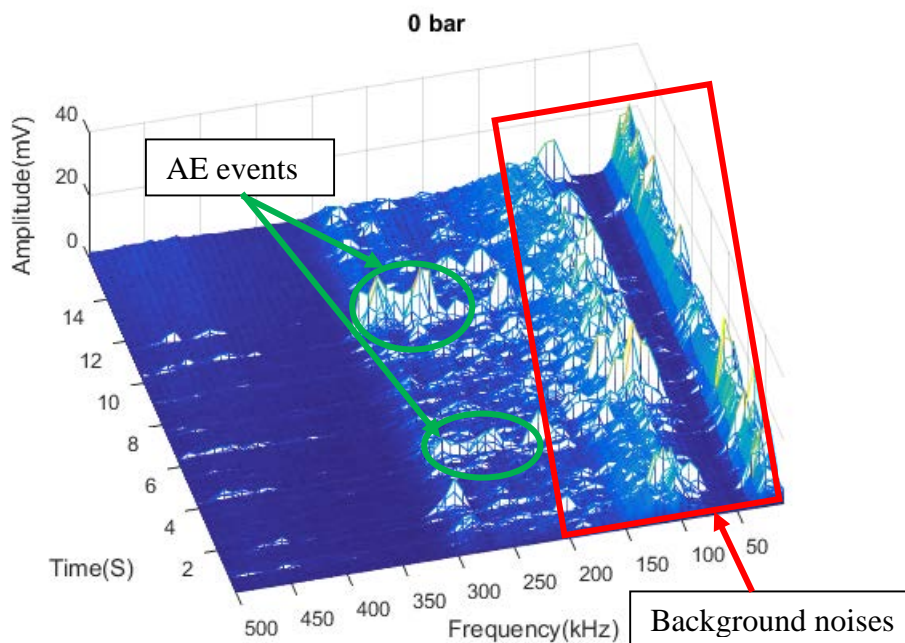


Figure 7.4 The spectrogram of the AE signal from transient speed test at 0 bar load

Figures 7.5 shows the results of transient speed test for 4 and 8 bar sealed pressures respectively. As it is observed at the beginning of the test, where boundary lubrication regime is dominant due to very low speeds of shaft, the amplitude of AE responses is higher. By increasing the speed gradually, the AE amplitude goes down due better lubrication condition in the mixed lubrication regime. At the end of data recording time, when the hydrodynamic lubrication regime is dominant, the amplitude of AE signals increases due to the viscous friction in the lubricant film as well as fluid induced asperity deformations.

Based on the above understandings, the AE amplitude in the frequency range of 270 ± 35 kHz changes with the lubrication regime change indicating that the mentioned frequency band is related to the tribological behaviour of mechanical seals and represents the tribological behaviour of seal faces applied in this research. It is noted that this frequency band does not shift under different operational conditions. Thus for the rest of this research, a band pass filter was designed using MATLAB codes and applied to analyse the data in the range of 270 ± 35 kHz.

More over as it is observed at higher speeds, the amplitude of AE signals increases by rotational speed increase. Since mechanical seals are designed to operate in the hydrodynamic lubrication regime at higher speeds, it can be concluded that other AE sources

mechanisms (i.e. viscous friction and fluid induced asperity deformation) are dominant in the hydrodynamic lubrication regime.

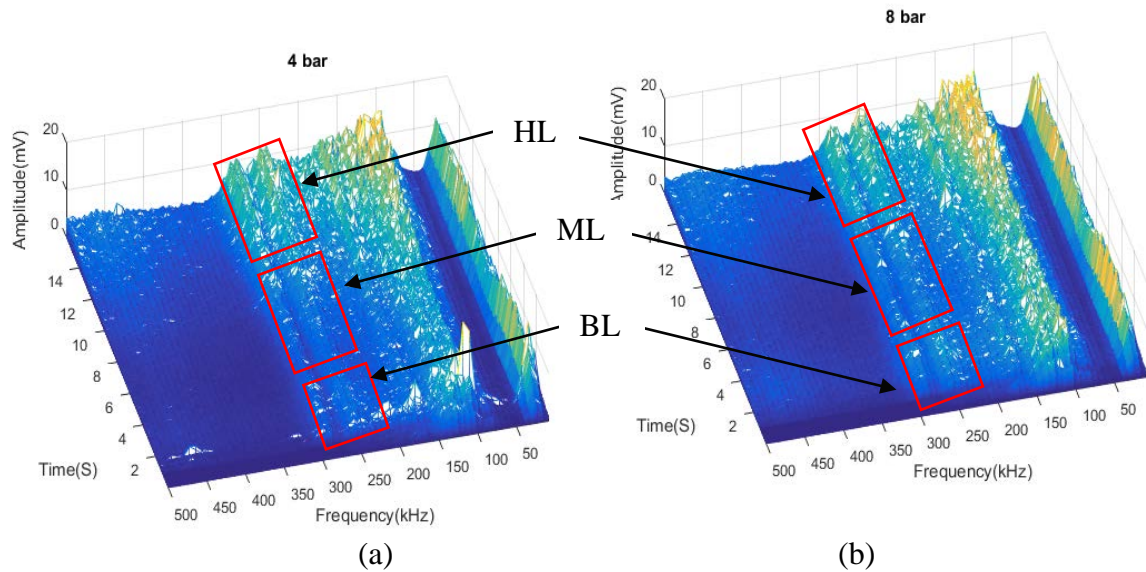


Figure 7.5 The spectrogram of the AE signal from transient speed test at different loads (a) 4 bar (b) 8 bar

Furthermore, based on Figure 7.5, the analysis in the time-frequency domain is not sensitive enough to indicate the mechanism of the frictional AE sources as well as severity of elastic asperity deformations in the sealing gap. As it is shown in the spectrograms, the AE amplitude does not show a good response to the change of operating conditions. Hence to get understanding of frictional behaviour of sealing gap under different lubrication regimes, for the rest of this thesis the raw AE signals are analysed in time domain and frequency domain that can provide much more details.

7.3 The Observation of Mechanical Seal's Tribological Behaviour

The results of test under different operating conditions (base line test) are presented in this section. This experimental program aims to investigate how AE features, generated by different AE sources that have been discussed in Chapter 5, change under different lubrication regimes. The results of analysis in time domain and frequency domain are presented for different load and speed settings so that it represents tribological AEs generated due to different lubrication regimes in the operation of mechanical seals.

7.3.1 AE Signal Characteristics in the Time Domain

To gain understanding of the tribological AEs, typical AE signals under different speed and pressure settings are presented. Figure 7.6 (a) and (b) show that AE amplitudes decrease with the speed increase (for all sealed pressures), indicating that asperity reactions are less with the speed increase and hence showing that either lubrication condition moves from the boundary to mixed lubrication or may be progress only in the mixed lubrication regime.

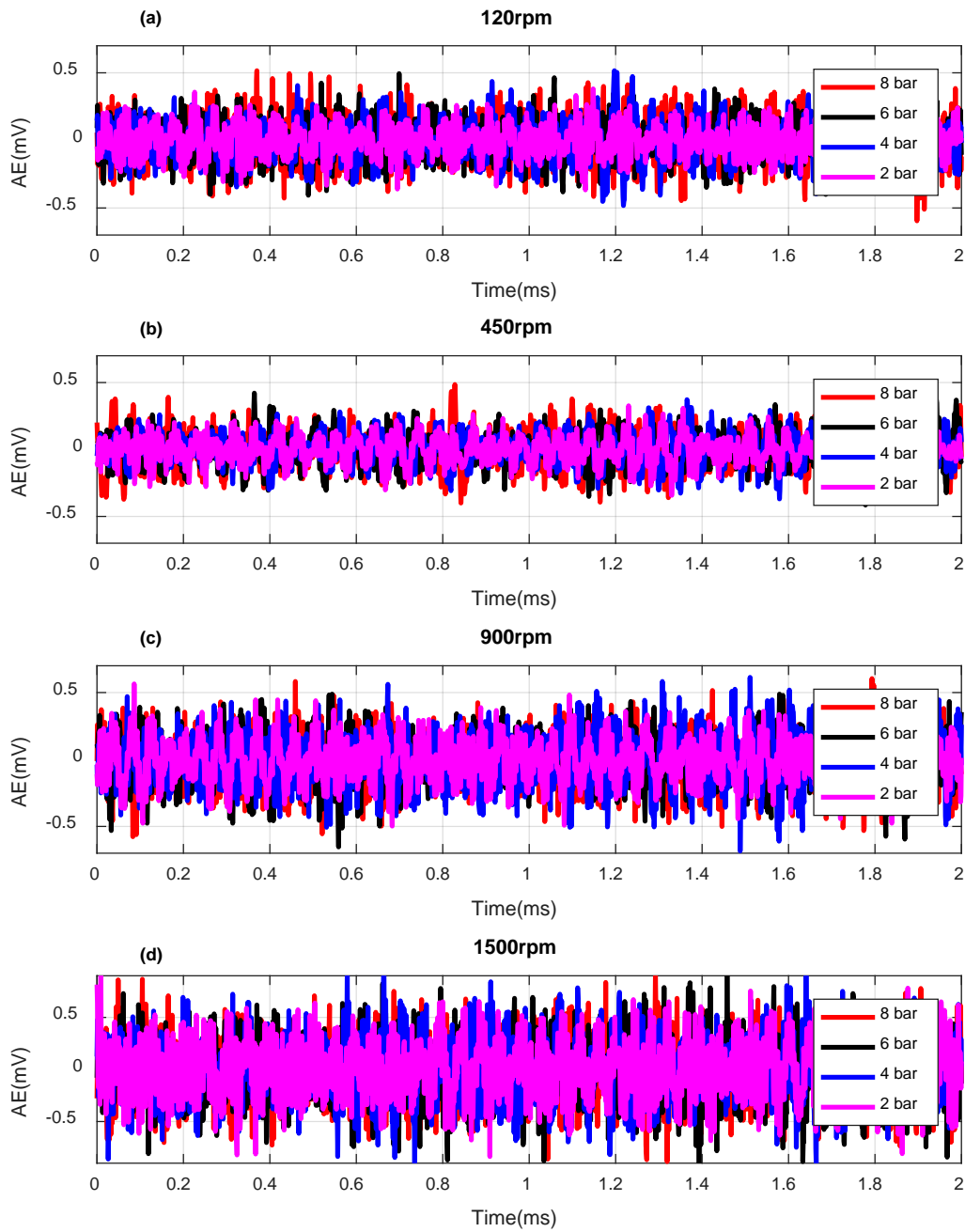


Figure 7.6 AE signal for different operating conditions

As the speed increases continuously, shown in Figure 7.6 (c) and (d), the amplitudes become larger gradually. This indicates more effect of viscous friction as well as flow induced asperity deformations and hence shows that the hydrodynamic lubrication regime is dominant. Therefore, this speed dependency allows different tribological regimes to be identified.

Moreover, the comparison of the AE responses between low and high sealed pressures shows that a clearer difference can be seen at the low speed whereas it is insignificant at the high speeds. This indicates that more asperity interaction due to increasing the load happen at the low speed, which is consistent with that predicated using Equation (5.32). On the other hand, at high speeds fully developed hydrodynamic lubrication regime helps to reduce or eliminate the effect of direct asperity collisions. Therefore, it has been demonstrated further that the AE responses will be dominated by the viscous friction i.e. speed but not the load as shown in Equation (5.47).

In addition, Figure 7.6 (a) and (b) show that burst type AE responses decrease with speed increase at lower speeds, indicating that peak asperity reactions are less with increasing in speed due to better lubrication condition in the mixed lubrication regime. By increasing the load at lower speeds, more asperities come to contact and massive asperity deformations happen in the mixed lubrication regime. Consequently, the number of burst type AE responses decreases while the AE amplitude goes up by the load increase.

In the hydrodynamic lubrication regime, shown in Figure 7.6 (c) and (d), the number of burst type AE responses goes up by the speed increase. As discussed in Section 5.8, by increasing the speed after transition point into the hydrodynamic lubrication regime, first massive asperity deformations happen due to stress field of fluid. This generates continuous type AE responses. By more increase in the rotational speed of shaft, the massive asperity deformation will be accompanied by peak asperity deformations simultaneously and hence generates more bursts. The more faces become separated (up to a threshold), the more flow induced deformations occur and hence the amplitude of AE signals goes up.

7.3.2 The Variation of AE RMS Value under Different Operating Conditions

As discussed in Section 5.2, a strong relationship exists between RMS value of the AE signals and the tribological behaviour of the mating surfaces in sliding contact [16, 35, 190]. To examine the connection between energy of the AE activity and tribological regimes of

the sealing gap, average RMS value of AE signals recorded during three different tests are calculated and presented versus the actual speed of shaft, Figure 7.7. The actual speed of shaft was calculated based on the encoder data that has been recorded by AE data acquisition system, see Section 6.3.1. For each curve the sealed pressure is constant and speed increases incrementally from 120 to 1500 rpm.

Based on Figure 7.7, for low speeds (less than 600 rpm) the RMS values go down first and then increase with the speed increase indicating that lubrication regime changes from the mixed to the hydrodynamic lubrication regime. The transition points are indicated by big brown circles as well as arrows. It is clear that for lower sealed pressure e.g. 2 bar the transition occurs at lower speeds.

Moreover, for the 8 bar sealed pressure the RMS value first increases and then decreases showing that the lubrication regime changes from the boundary to the mixed lubrication regime at lower speeds and higher loads. As the speed increases continuously the RMS value goes up indicating that the lubrication is in the hydrodynamic lubrication regime.

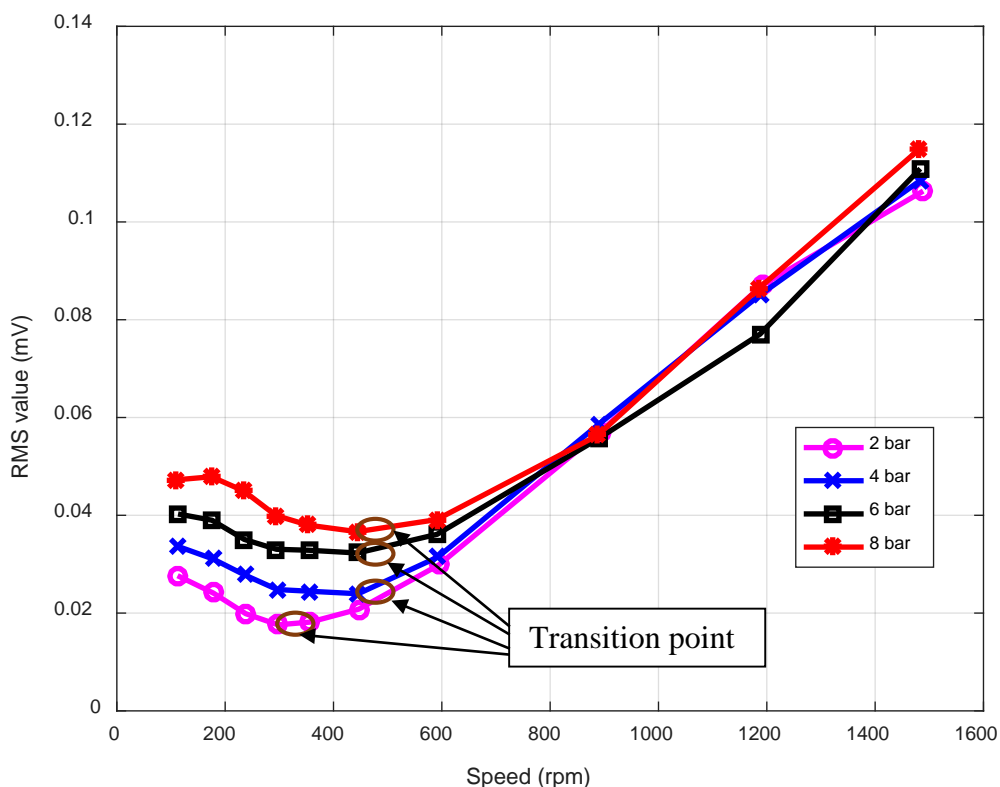


Figure 7.7 The AE RMS values under different speeds and pressures

Furthermore, for the experiments conducted at low speeds (before transition point) the level of AE energy goes up with the sealed pressure increase that is consistent with Equation (5.32). Based on Equation (5.32) the RMS value of AE signal increases linearly by increasing the contact load. However, for higher speeds, the effect of sealed pressure on the AE responses becomes insignificant and hence the curves cross each other randomly. This is consistent with Equation (5.47) that does not include any term related to the contact load. It should be immediately noted that increasing the sealed pressure to the higher values (the maximum working pressure of mechanical seals applied in this research is 69 bar, see Table 6.9) may lead to viscosity increase. However, compared to the temperature influence, liquids are influenced very little by the applied pressure. The reason is that liquids are almost non-compressible at low or medium pressures.

To make better separation between the curves in the hydrodynamic lubrication regime, RMS values of the AE signals are presented versus the dimensionless duty parameter G as shown in Figure 7.8. The duty parameter is calculated based on Equation (2.7). To achieve this, the actual sealed pressure was calculated based on the pressure sensor data. Based on Figure 7.7, the minimum point of the curves (indicated by big brown circles) fluctuates in a narrow transition region around 1.00×10^{-8} , a plausible explanation for scattering of the data is that enough data is not available around the transition point ($G = 1 \pm 0.1 \times 10^{-8}$). It is believed that the more data points are available around transition point, the closer would be the transition points. It should be immediately noted that the transition range achieved in this research is not consistent with Table 2.1. It is the common characteristic that transition occurs at different G values under different seal configuration as reported in the literature [2, 47], also see Figure 2.9. In addition, based on Equation (2.7), the closing force as well as the seal width affect the G values. Therefore, to use such tables, it is more logical to apply same mechanical seals as seal geometry as well as working parameters have significant effect on the duty parameter values. This clearly confirms the conclusion that has been made in Section 2.7 is valid. Based on the mentioned understandings, for different operational conditions (sealed pressure, speed, viscosity and face material combinations), tabulated values of tribological parameters such as duty parameter are less useful than might be expected. Therefore, the development of reliable online condition monitoring techniques that can estimate the tribological behaviour of mechanical seals is necessary and essential.

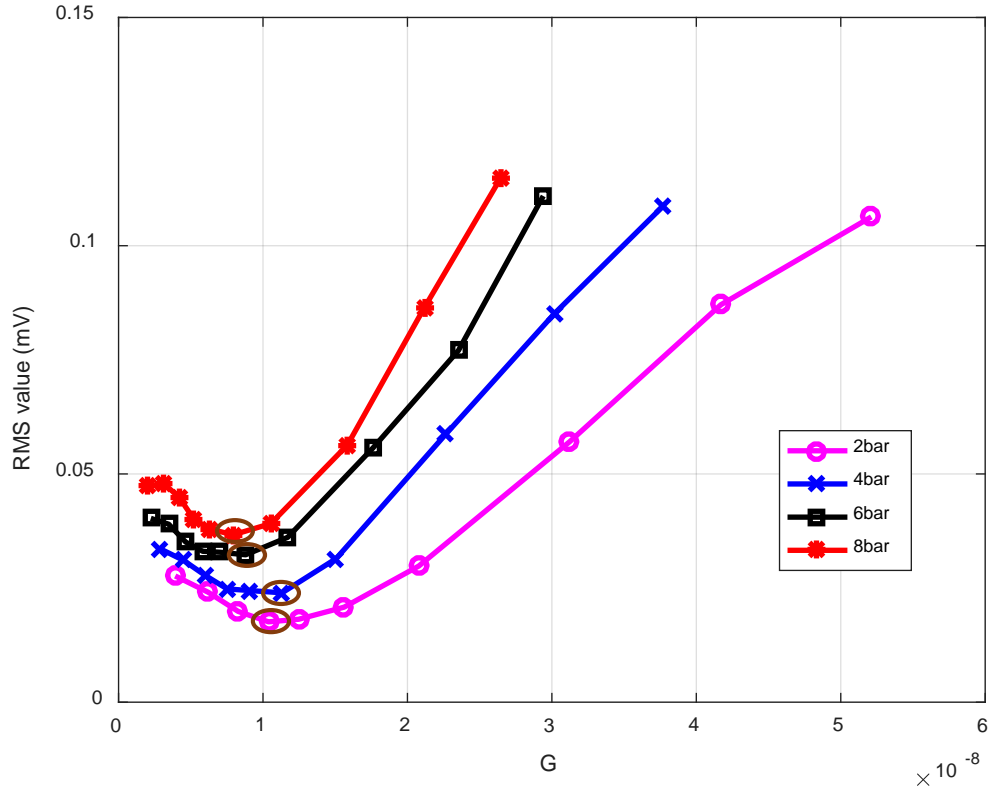


Figure 7.8 The AE RMS values in terms of duty parameter

7.3.3 The Variation of AE Kurtosis Value under Different Operating Condition

As discussed in Section 5.4, the height distribution of asperities is an important property to describe the characteristics of randomly rough surfaces. All of the equations that have been developed in Chapter 5 correlate with the height distribution of asperities. Moreover, it has a significant influence on the type of AE responses as discussed in Section 5.8. As it is assumed that AE only is generated by frictional process in the sealing gap, the distribution of AE signals will be an indication of the AE source mechanism. This gives a promising potential to interpret the changes of AE kurtosis value under different operating conditions using the distribution of AE signals. This might be useful for the purpose of condition monitoring and fault diagnosis in mechanical seals.

The height distribution of asperities usually follows the normal distribution [16], for a normal distribution data the probability density function (PDF) is defined:

$$P(x) = \frac{1}{\sigma\sqrt{2\pi}} e^{-\frac{(x-\mu)^2}{2\sigma^2}} \quad (7.1)$$

where

μ is the mean value.

σ is standard deviation.

x is the data at each discrete point in time.

To connect the concept of kurtosis of AE signals with the asperity height distribution, Figure 7.9 is presented. As illustrated, the value of kurtosis is greater than 3 if a distribution is more outlier-prone than Gaussian distribution while kurtosis is less than 3 if the distribution is less outlier-prone than Gaussian distribution. The more peak asperity deformation happens, the more outlier-prone is achieved that generates higher kurtosis values. The more massive elastic asperity deformation occurs, the more kurtosis of the AE signal generated is close to 3. It should be immediately noted that elastic asperity deformation in this thesis refers to either the dynamic bending of asperities in direct contact (boundary and mixed lubrication regimes) or fluid induced asperity deformations (hydrodynamic lubrication regime). This may happen in the form of peak asperity deformations or massive asperity deformations or even both of them simultaneously based on the operational conditions.

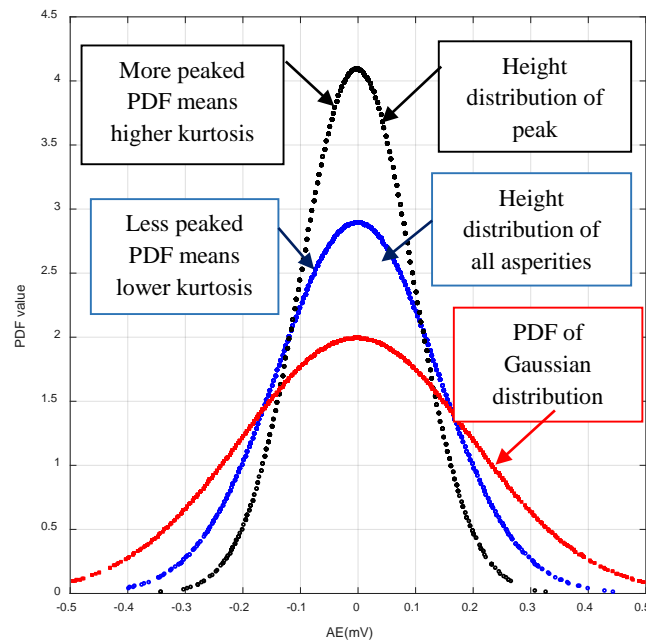


Figure 7.9 The distribution of AE signals against normal distribution

Figure 7.10 gives kurtosis of the AE signals measured during different operating conditions. It is noted that the value shown in this figure is the difference between the kurtosis of measured AE signal and Gaussian distribution. For the experiments conducted at speeds under 600 rpm (left hand side of transition point), kurtosis peaked under 2 bar and dropped to the lowest value under 8 bar. For instance, at the speed of 120 rpm kurtosis sees the high

peak for 2 bar pressure indicating that contact occurs only in some peak asperities. These asperities have such peaks that their heights are meaningfully larger than the average value of all asperity heights. Hence the standard deviation is lower (more peaked PDF) that leads to higher kurtosis values.

By increasing the sealed pressure, massive asperity contact happens. In massive asperity contact the standard deviation is higher (less peaked PDF) and hence kurtosis sees lower values. Consequently, the AE signal distribution becomes closer to the Gaussian distribution implies that massive asperity contacts occurs at higher sealed pressure.

By increasing the speed gradually up into the transition point, the improvement of lubrication condition between the seal faces would confine the severity of asperity contacts. However peak asperity contacts occur around the transition point due to the fact that faces are going to be separated. Therefore, kurtosis increases at rotational speed of 600 rpm. By increasing the rotational speed of shaft into the hydrodynamic lubrication regime, the seal faces become fully separated and viscous friction at sealing interface as well as flow induced asperity deformations generate more elastic deformations. Therefore, the distribution of AE signal gets closer to the Gaussian distribution and hence kurtosis dropped by increasing the speed in the hydrodynamic lubrication regime.

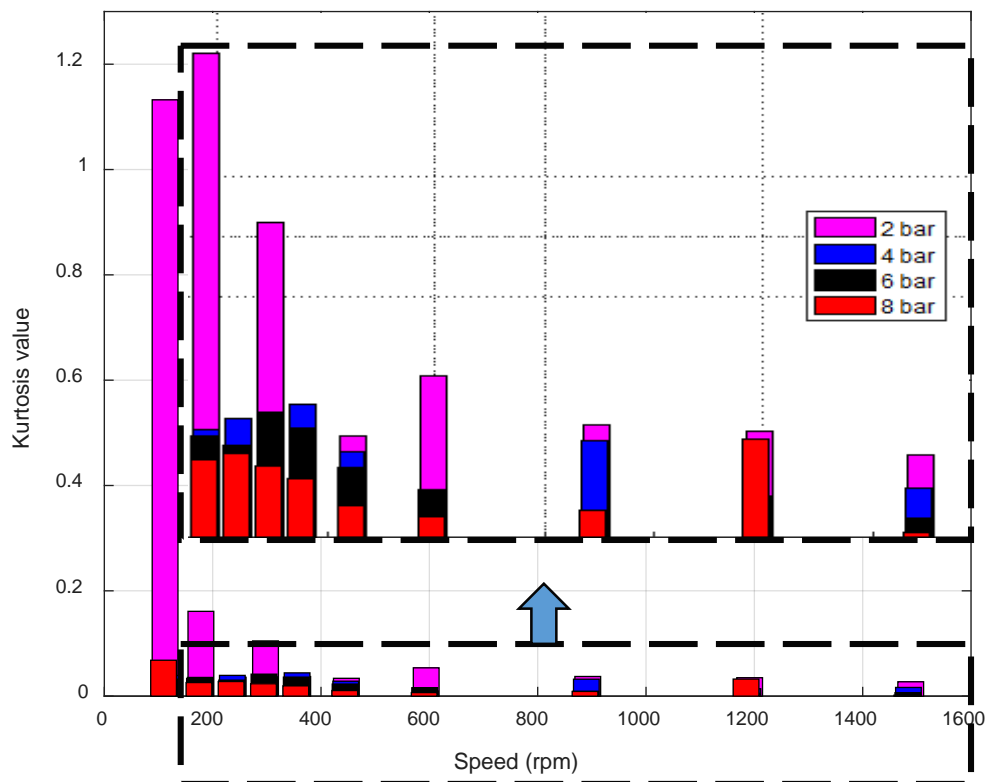


Figure 7.10 The AE kurtosis values under different speeds and pressures

In addition, in the hydrodynamic lubrication regime, the effect of sealed pressure becomes less significant which coincides well with the conclusion drawn from the analysis of RMS value of AE signals presented in previous section. Also, it is in very good agreement with the previous researches [16] where it has been claimed that the distribution of AE signals is not sensitive enough to the change of asperity contacts under well-lubricated conditions.

7.3.4 Frequency Domain Analysis

Figure 7.11 shows the spectra of AE signals when the seal operates under different speed and pressure settings.

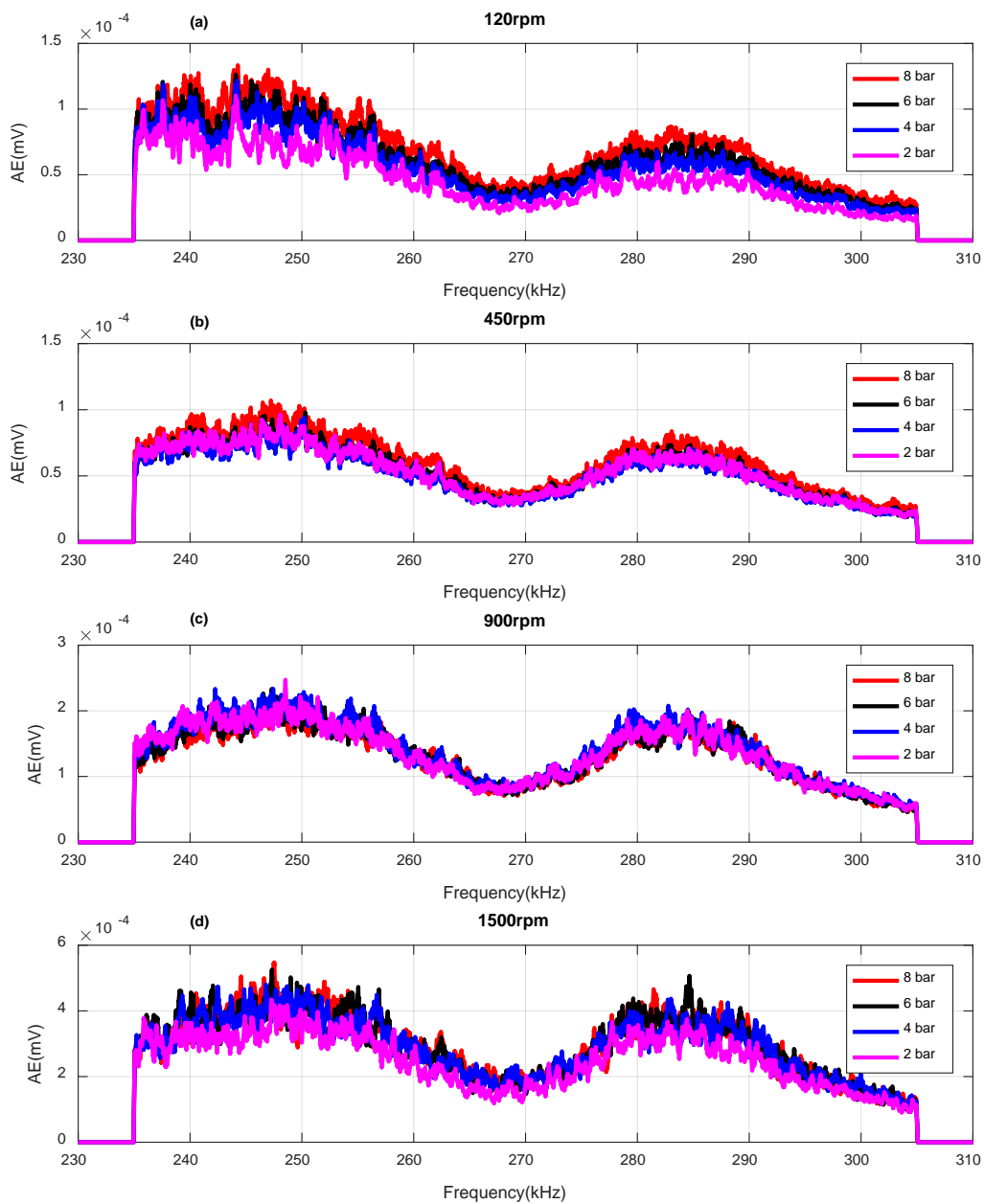


Figure 7.11 AE spectra for different operating conditions

Based on Figure 7.11 (a) and (b), the amplitudes of AE spectra decrease first with speed increase. Then, as the speed increases continuously, shown in Figure 7.11 (c)–(d), the amplitudes become larger gradually. On the other hand, by increasing the speed, the difference between the amplitude of AE spectra related to low and high load decreases gradually and finally in Figure 7.11 (d), changing the load has no significant effect on it. This indicates that when hydrodynamic lubrication is well established, the AE responses are more dominated by the fluid induced asperity deformations due to change in speed but not the sealed pressure as has been demonstrated in Equation (5.47). To get a solid conclusion on this idea, the AE spectra for mixed and hydrodynamic lubrication regimes are presented in Figures 7.12 and 7.13 respectively.

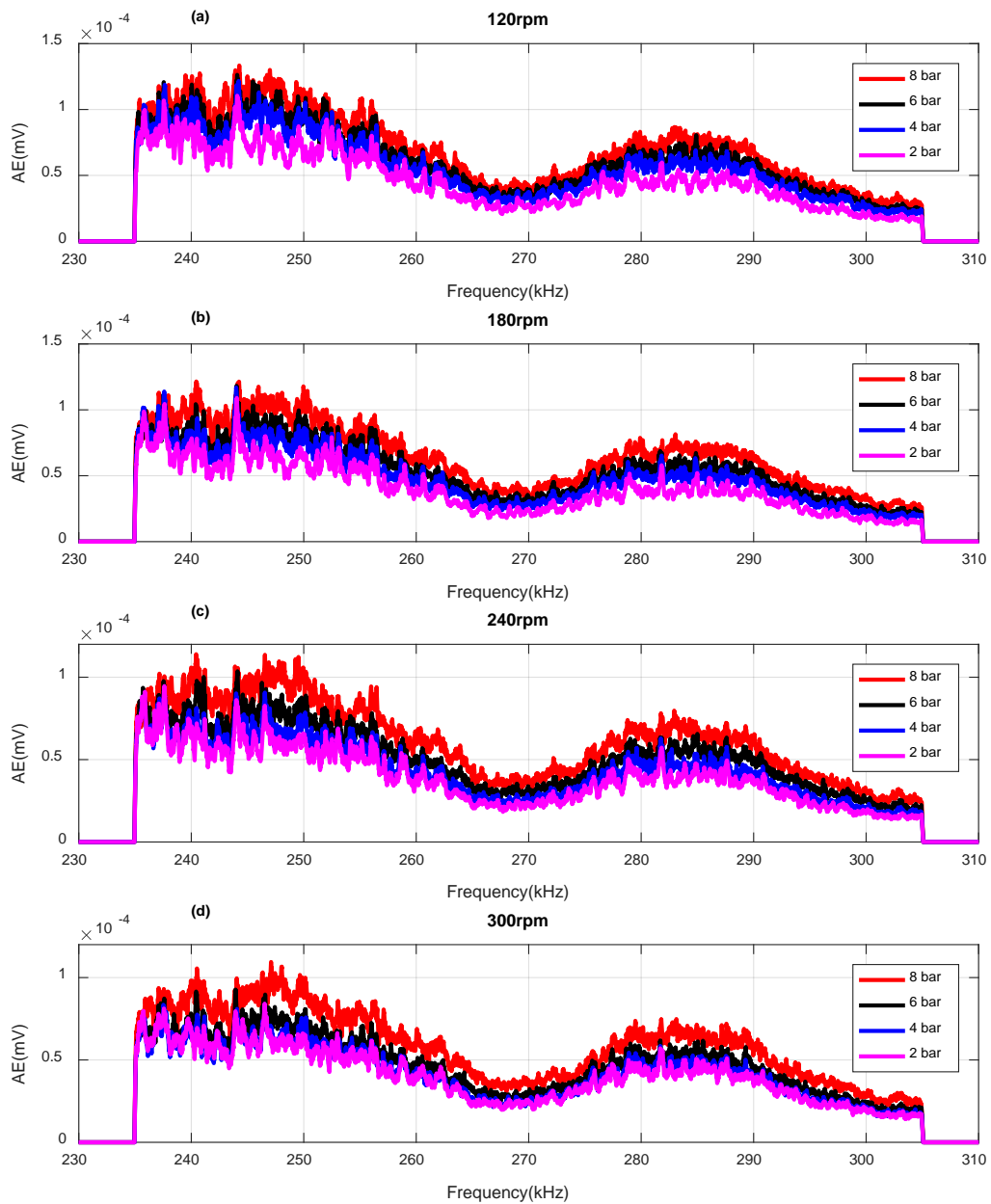


Figure 7.12 AE spectra for lower speeds and different sealed pressures

Based on Figure 7.12 , by increasing the speed in the mixed lubrication regime the amplitude of AE spectra decreases due to better lubrication conditions. In the most cases a clear separation between different sealed pressures are observed. As it is observed under the mixed lubrication condition the amplitude of AE spectra increases by increasing the load due to more asperity contact as discussed in Equation (5.32).

Figure 7.13 shows the AE spectra when the seals are working in the hydrodynamic lubrication regime. As it is observed, the amplitude of AE spectra increases with the speed increase however the spectrums in Figure 7.13 (a) to (d) are approximately similar to each other. This gives a good evidence that in the hydrodynamic lubrication regime the effect of sealed pressure is less significant as has been detailed in Equation (5.47).

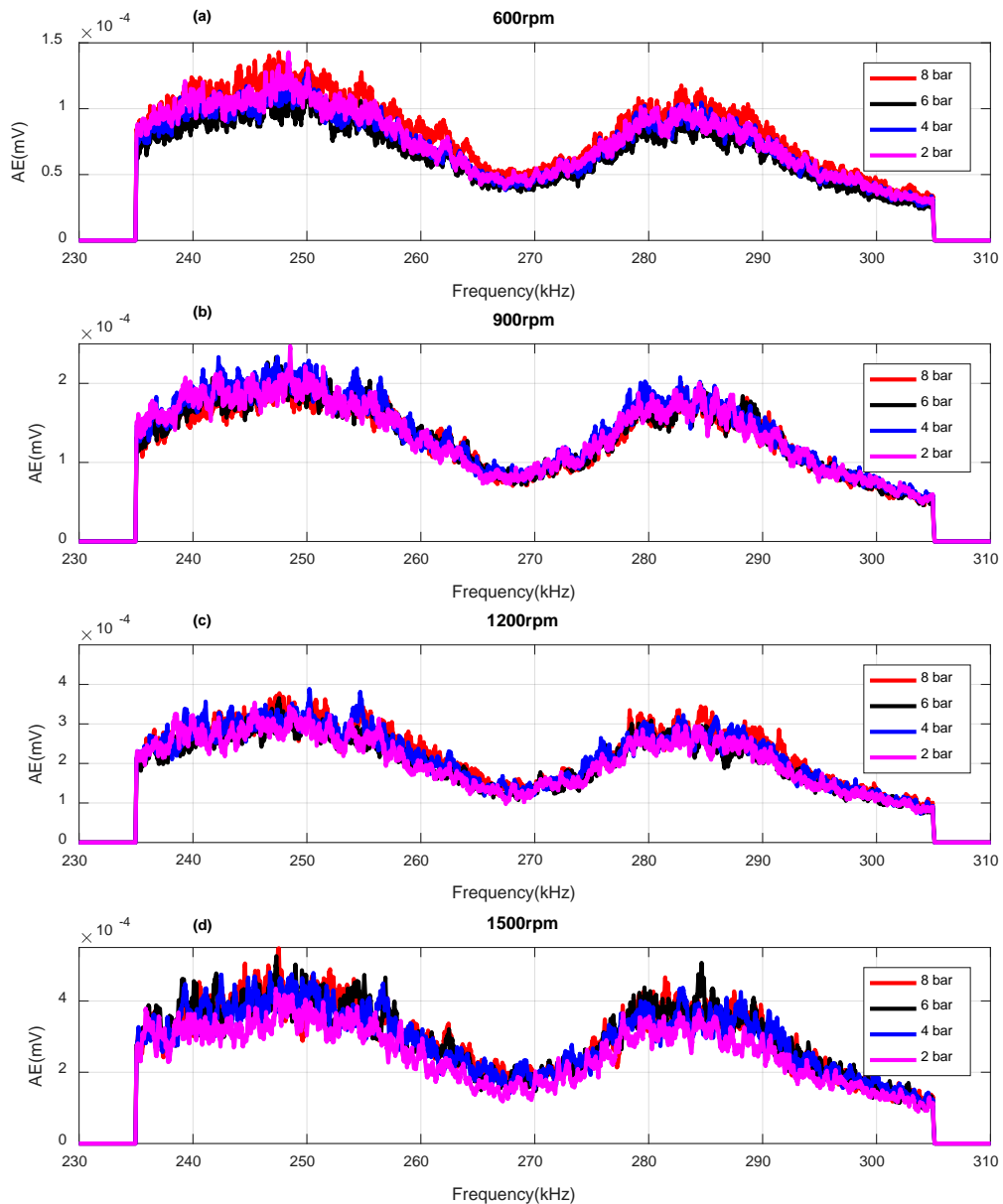


Figure 7.13 AE spectra for higher speeds and different sealed pressures

7.4 Model Verification

As discussed in Chapter 5, three different AE sources are dominant in the operation of mechanical seals i.e. asperity collision, viscous friction and flow induced asperity deformation. However, these AE sources interact each other during the operation of mechanical seals. Hence it is necessary to combine them properly and propose a comprehensive AE model that can predict the tribological behaviour of mechanical seals under different operating conditions. Since asperity collision is dominant AE source in the BL regime, the developed asperity contact model is reliable enough to be applied directly. However, for the ML and HL conditions, where the interaction between different AE sources happens, a combination of proposed models is needed. This section aims to demonstrate the changes in AE RMS value under ML and HL regimes.

7.4.1 The Influence of Sliding Speed on AE RMS

As indicated by the Equation (5.32), the AE RMS value in direct asperity contact determined by the total number of asperity contacts and the load they support if sealed pressure is constant and the statistical properties of surface topography do not change. Hence the AE model can be simplified and expressed as:

$$V_{rms} = K_1 \sqrt{N_{tot}} V \quad (7.1)$$

In the mixed lubrication regime, it is logical to assume that the number of asperity contact decreases by increasing the sliding speed due to improvement in lubrication condition. In this regime, direct asperity contact is confined by shearing in those lubricant layers that trapped between asperities. Hence final model for the mixed lubrication regime is extracted by considering the interaction of viscous friction and direct asperity contact. Based on the model developed for viscous friction, the RMS value of AE signals generated by viscous friction increases linearly with the sliding speed, Equation (5.62). Therefore, in the mixed lubrication regime the relationship between total contact number of asperities and sliding speed is given by:

$$N_{tot} = \frac{K_2}{V} \quad (7.2)$$

Substituting Equation (7.2) into Equation (7.1) the relationship between AE RMS value and sliding speed transforms to:

$$V_{rms} = K_3 V^{-\frac{1}{2}} \quad (7.3)$$

It should be noted that the predicted trend in Equation (7.3) is not achieved experimentally unless same portion of viscous friction and direct asperity contact happen simultaneously. However, in practice by increasing the sliding speed in the ML regime toward the transition point, the portion of asperity collisions decreases while the percentage of viscous friction increases. Hence the Equation (7.3) transforms to:

$$V_{rms} = K_v V^{-\frac{x}{2}} \quad (7.4)$$

where x depends on lubricant-asperity interactions and is equal to unit value if pure direct asperity contact accompanied by pure viscous friction in the mixed lubrication region. For the tests have been carried out in this research the variable x varies between 0.26 to 0.807 as illustrated in Figure 7.14.

In the hydrodynamic lubrication regime two AE sources are superimpose each other: viscous friction and flow induced asperity deformation. Based on Equation (5.47), the AE RMS value in flow induced asperity deformation determined by the total number of asperity deformations and sliding speed if other parameters are constant. Hence the AE model can be simplified as:

$$V_{rms} = K_3 \sqrt{N_{tot}} V \quad (7.5)$$

Under this conditions by increasing the speed more shearing occurs in the lubricant layers, Equation (5.62), and therefore more asperity deformation is generated due to interaction between stress field of fluid and surface asperities. Hence the relationship between the total number of asperity deformations and sliding speed is given by:

$$N_{tot} = K_4 V^x \quad (7.6)$$

where x depends on gap variation with the speed, as stated in waviness model developed by Lebeck [1]. Substituting Equation (7.6) into Equation (7.5) the relationship between AE RMS value and sliding speed transforms to:

$$V_{rms} = K_v V^{1+\frac{x}{2}} \quad (7.7)$$

For this study the positive variable x varies up to 0.636 as illustrated in Figure 7.14. Figure 7.14 (a)-(g) show the relationship between RMS value and the sliding speed when the rig operated under different sealed pressure from 2 bar to 8 bar with the step size of 1 bar. The beset curves are fitted on the test results using statistical analysis carried out in MATLAB. The coefficient of determination or (R^2) refers to the covering rate of default function in changes of dependent variables. The more this value is closer to the unity, the more the accuracy of fitness is achieved

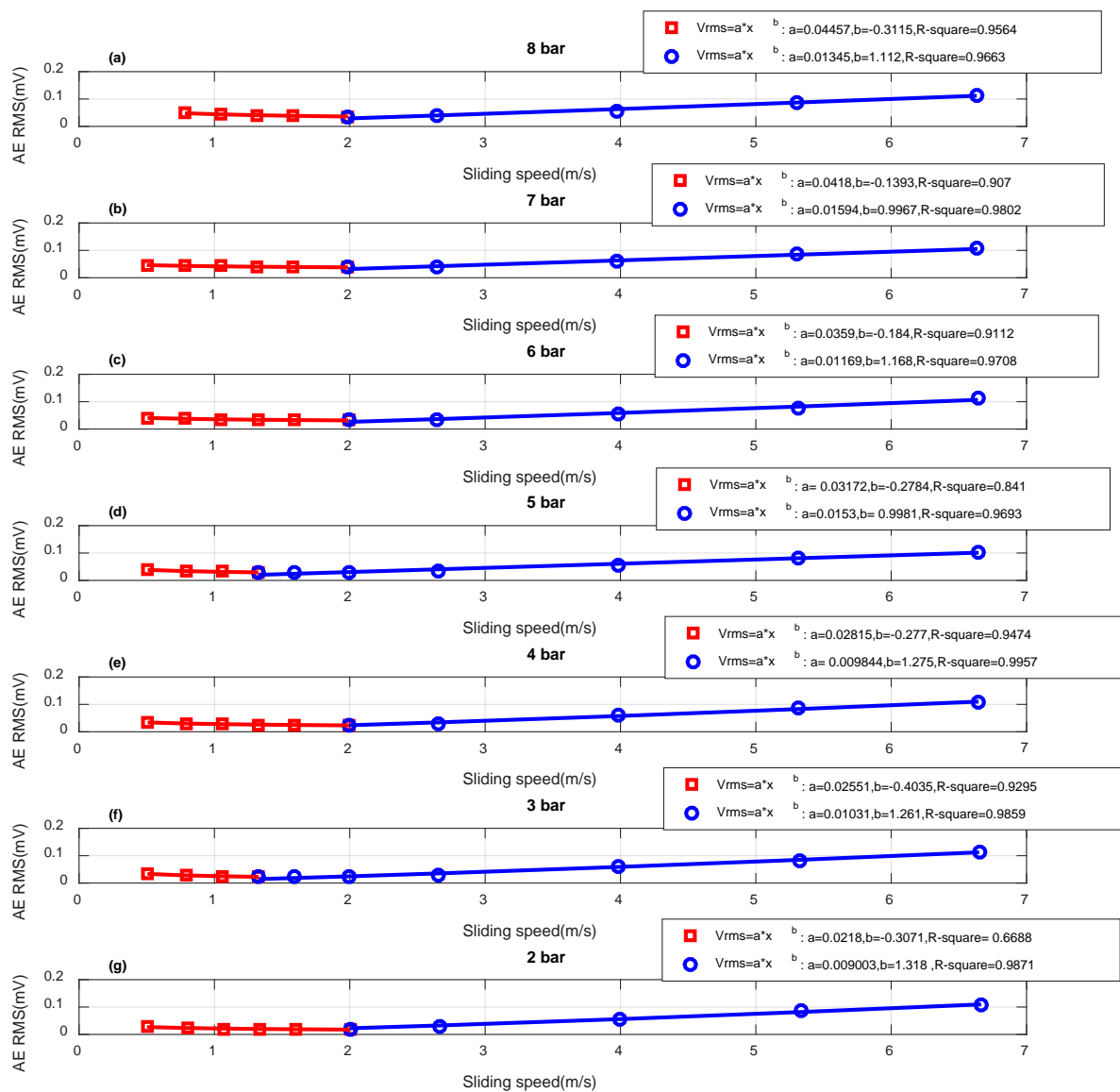


Figure 7.14 The relationship between AE RMS value and sliding speed

Since mechanical seals are ideally work around the transition point: the mixed to the hydrodynamic lubrication condition (see Section 2.2.2), the developed model may help for the purpose of fault detection in mechanical seals. On this basis any deviation from the

predicted trends can be considered as a developing fault whether it is in the mixed or hydrodynamic lubrication regimes.

7.4.2 The Influence of Sealed Pressure on AE RMS

As indicated by Equation (5.32), AE RMS value is influenced by the load that is supported by asperities. However, it is immediately noticed that this model cannot be applied to explain the recorded data since the load measured was the sealed fluid pressure rather than that supported by asperity contacts. Hence it is necessary to develop the AE model to correlate it to the sealed pressure.

Using Equation (2.3) for closing force and Equation (2.7) for opening force, the force equilibrium of mechanical seal can be expressed as

$$F_s + F_h = \int_{A_f} P_{hys} dA + \int_{A_f} P_{hyd} dA + \int_{A_f} P_{Contact} dA \quad (7.8)$$

Substituting Equation (2.4) into Equation (7.8) gives:

$$F_s + A_f \times (B \times \Delta P + P_a) = \int_{A_f} P_{hys} dA + \int_{A_f} P_{hyd} dA + \int_{A_f} P_{Contact} dA \quad (7.9)$$

Dividing both sides of Equation by A_f , the contact pressure can be expressed as:

$$P_{contact} = B P_f - P_a (B - 1) - \frac{\int_{A_f} P_{hys} dA + \int_{A_f} P_{hyd} dA - F_s}{A_f} \quad (7.10)$$

Define

$$P_c = -P_a (B - 1) - \frac{\int_{A_f} P_{hys} dA + \int_{A_f} P_{hyd} dA - F_s}{A_f} \quad (7.11)$$

Equation (7.10) is rewritten as:

$$P_{contact} = B P_f + P_c \quad (7.12)$$

With the help of Equation (7.12) it might be possible to estimate the contact pressure supported by asperities, which is a critical parameter to evaluate lubrication conditions in engineering applications. If contact pressure is positive there is some indirect rubbing between the rotating and stationary faces; this is a condition of low leakage. For contact pressure exactly zero the faces would not be rubbing but the resulting hydrodynamic lubrication conditions would allow increased leakage. For contact pressure to be negative the opening forces have overcome the closing forces and the seal has failed [88].

Substituting Equation (7.12) for contact pressure into Equation (5.32), and define all constant parameters as K_p then Equation (5.32) can be expressed as:

$$V_{rms} = K_p P_f + P_c \tag{7.13}$$

Therefore the AE RMS value varies linearly with the sealed pressure in mechanical seals, Figure 7.15.

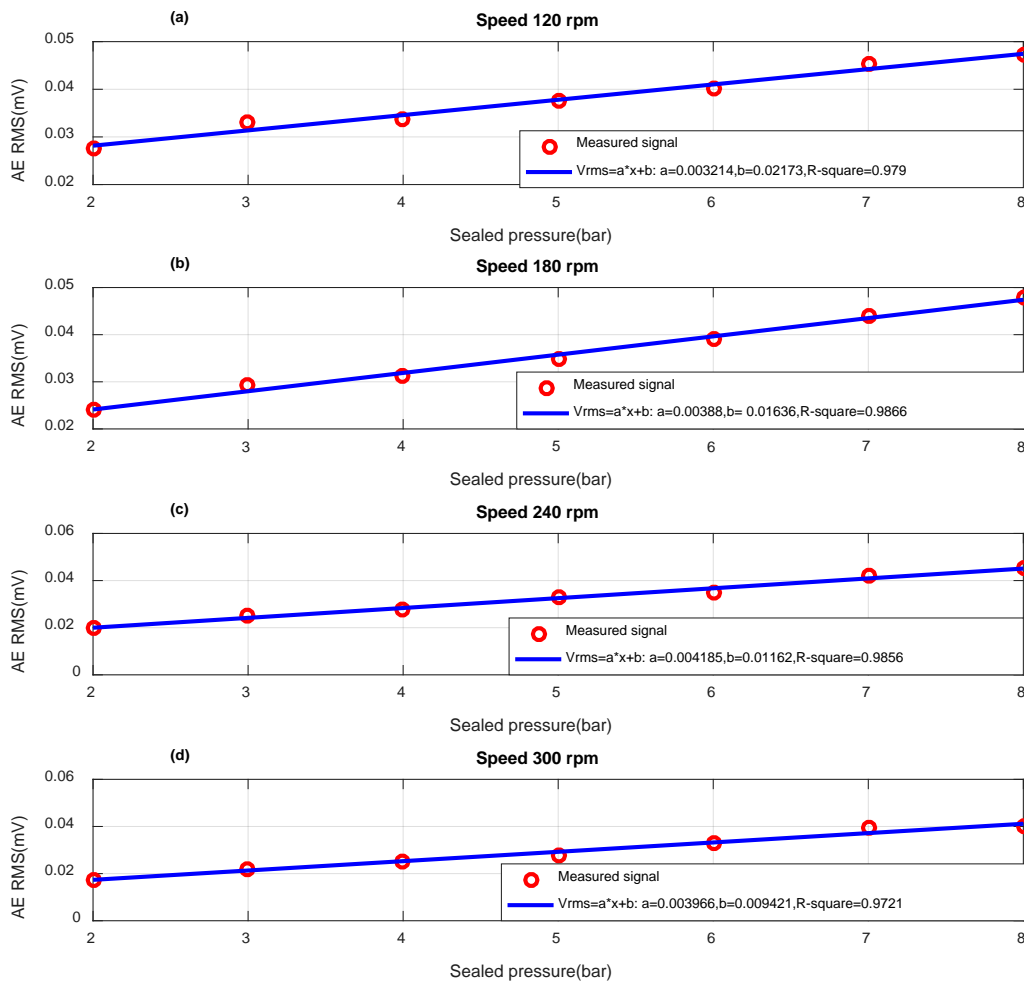


Figure 7.15 The relationship between AE RMS value and sealed pressure in ML region

Figure 7.15 presents the test results to investigate the effect of sealed pressure on AE RMS value when the seal operated at four different low speeds to simulate the mixed lubrication regime. As it is illustrated in Figure 7.15 (a)-(d), the liner polynomial trend predicted for sealed pressure by Equation (7.13) is achieved with good accuracy.

It is immediately noticed that the low speeds have been selected to simulate the more possibility of asperity contact. If high speeds were selected, for instance 1500 rpm where mechanical seals are operate in the hydrodynamic lubrication regime, then the experimental data would not follow the predicted trend, Figure 7.16.

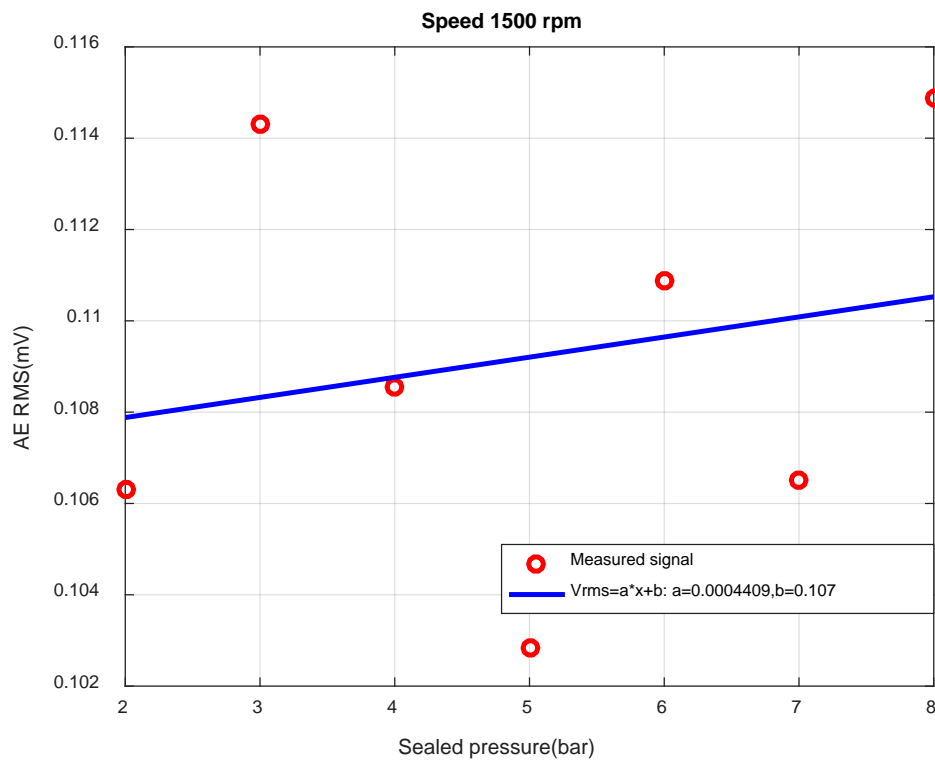


Figure 7.16 The relationship between AE RMS value and sealed pressure for higher speeds

7.5 Main Findings

The results of baseline analysis carried out in this research shows the effectiveness of the AE measurement system and signal processing method developed in this thesis for monitoring the tribological behaviour of mechanical seals. On the basis of the analysis of recorded AE signal, it was found that the main AE frequency range related to tribological behaviour of mechanical seals was between of 235-325 kHz and it has little shift across different tribological regimes.

Based on the analysis of time domain signal, the amplitude and number of burst type AE responses can be effectively used to characterize the tribological behaviour of mechanical seals.

Among the statistical features of AE waveform, the RMS values agree significantly with the mathematical model developed in Chapter 5 in terms of the sealed pressure and sliding speed. The good trend of AE RMS with the change of sealed pressure and sliding speed implies its potential to monitor the tribological behaviour of mechanical seals in a simple and effective way. It was shown that different lubrication regimes in mechanical seals can be detected based on the changes in the RMS value of AE signal. For the purpose of on-line condition monitoring and fault diagnosis, the AE RMS value could be used as a parameter triggering different levels of alarm in operation.

Kurtosis was found to be a useful statistical parameter to indicate the tribological behaviour of the sealing gap. The results of analysis show that kurtosis values of AE signals can be interpreted based on the theory model developed in Chapter 5 to distinguish different tribological regimes of mechanical seals. In addition, kurtosis analysis also reveals whether the deformation occurs only at some peak asperities or involved massive ones. This provides a real insight in the behaviour of operating mechanical seals and gives a good evidence of that kurtosis is an effective tool for the purpose of condition monitoring.

Chapter Eight;

Application of AE Measurements to the Fault Detection of Mechanical Seals

This chapter intended to carry out a fundamental investigation on the potential of the AE technology for the purpose of condition monitoring and fault detection in mechanical seals. The study conducted three groups of common faults: the partial dry running, the spring out test and the defective seal test. The main objective of this chapter is the comparison and discussion of the results of the faulty seal against the base line test in the time domain and frequency domain. The discussion is also made by comparing the results with the AE model developed in Chapters 5 and 7 so as to evaluate the model responses to the simulated faults. At the end of the chapter, conclusions are drawn on the basis of the information obtained in this experimental study.

8.1 Introduction

AE has been studied for fault detection in mechanical seals by some researchers [16, 29, 31], however typical fault cases have not been investigated successfully yet. For instance, Yamashina et al. reported that in 1977 the Exxon chemical company, USA, made an attempt to predict mechanical seal failures by acoustic emission monitoring. A similar attempt was made from 1982 through 1984 in Japan [29] with a different degree of positive outcome. In 1987 Yamashina et al. carried out a time domain analysis on the data obtained by experiments conducted on equipment in petroleum refinery plants and laboratories in Japan [29]. They reported that leakage in sealing gap results in a reduction of the AE amplitudes or an increase of the fluctuation of AE levels that will permit the prediction or detection of mechanical seal failures. In their research, the effect of different operating conditions on the performance of a faulty mechanical seal has not been considered. Therefore, it is unlikely practical to make a solid conclusion for the purpose of fault detection in industrial mechanical seals based on previous works as has been summarised in Table 1.2.

In this chapter, tribological AEs are investigated to estimate the state of mechanical seals and acquisition of some information by which common seal failures are predicted or detected. All experiments were conducted using the mechanical seal test rig presented in Chapter 6. The recorded data are processed using time domain and frequency domain analysis methods.

8.2 Partial Dry Running Test

Since mechanical seals are hydrostatically lubricated, running the test rig with the low values of sealed pressure will simulate the condition under which partial dry running occurs. This concept can be understood mathematically by Equation (7.10). For low sealed pressures the hydrostatic pressure in the sealing gap, P_{hys} , is too small and hence the closing pressure has to be supported by the asperity contact pressure, $P_{Contact}$, at lower speeds as well as hydrodynamic pressure, P_{hyd} , that is established at higher speeds. Therefore, the lower sealed pressures are used, the bigger is the positive asperity contact pressure. Too much contact pressure may cause significant dry rubbing, overheat and eventually failure of the mating rings. To avoid damaging the mating faces the sealed pressure was kept around 0.4 bar in this test, Figure 8.1.

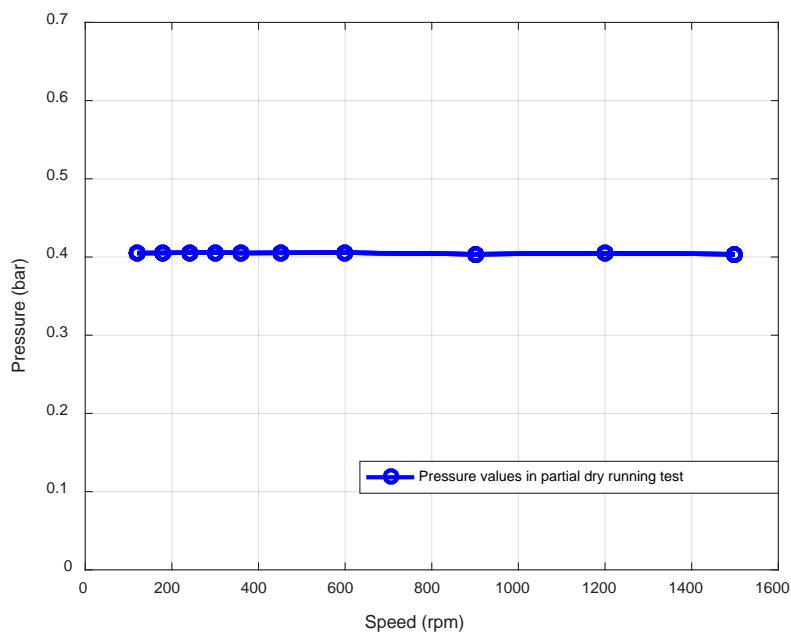


Figure 8.1 Sealed pressure values during the partial dry running test

8.2.1 Time Domain Analysis

To compare the AE responses of the partial dry running test with the baseline test, Figure 8.2 presents typical time domain signals under different speed and pressure settings. In each row sealed pressure is constant and speed increases gradually, and vice versa for each column. It is immediately noticed that partial dry running test has been carried out at constant sealed pressure (0.4 bar), and hence in each column the same signal is observed against the changes of the baseline due to the sealed pressure increase.

Since in the partial dry running test the sealing chamber is not pressurized, dry contact occurs between the mating faces. Moreover, the severity of asperity collisions is not confined by the lubricant film. Consequently, at low rotational speeds of shaft the peak asperity contact occurs under a poor lubrication condition. Hence as it is observed in Figure 8. 2, the number of burst responses is more in partial dry running test due to peak asperity contact increase. However, the amplitude of the baseline test is relatively higher due to the more asperity deformations (massive asperity contact) in the pressurized case.

By increasing the speed gradually, the seal faces become separated. Therefore, the severity of elastic asperity deformations increases significantly in the partial dry running test due to the slightly smaller sealing gap that is achieved in the absence of a strong hydrodynamic pressure lift up rather than the normal sealing gap in the baseline test. This can be better

understood to be the effect of total closing force decrease in partial dry running test, Equations (7.9), due to the lack of sealed pressure. To compensate the lower closing force, the smaller sealing gap is formed in partial dry running test that provides stronger flow of lubricant film, see Equations (5.8) to (5.11).

Consequently, at lower speeds the AE amplitude of the baseline is higher due to the fact that the severity of dry contact is not enough to generate higher rate of elastic energy release in the partial dry running test. However, in the hydrodynamic lubrication regime the amplitude of AE responses from the partial dry running test is higher due to sever flow induced bending of asperities. Therefore, the AE amplitude as well as the number of burst type responses in the partial dry running test go up significantly with speed increase in the hydrodynamic lubrication regime.

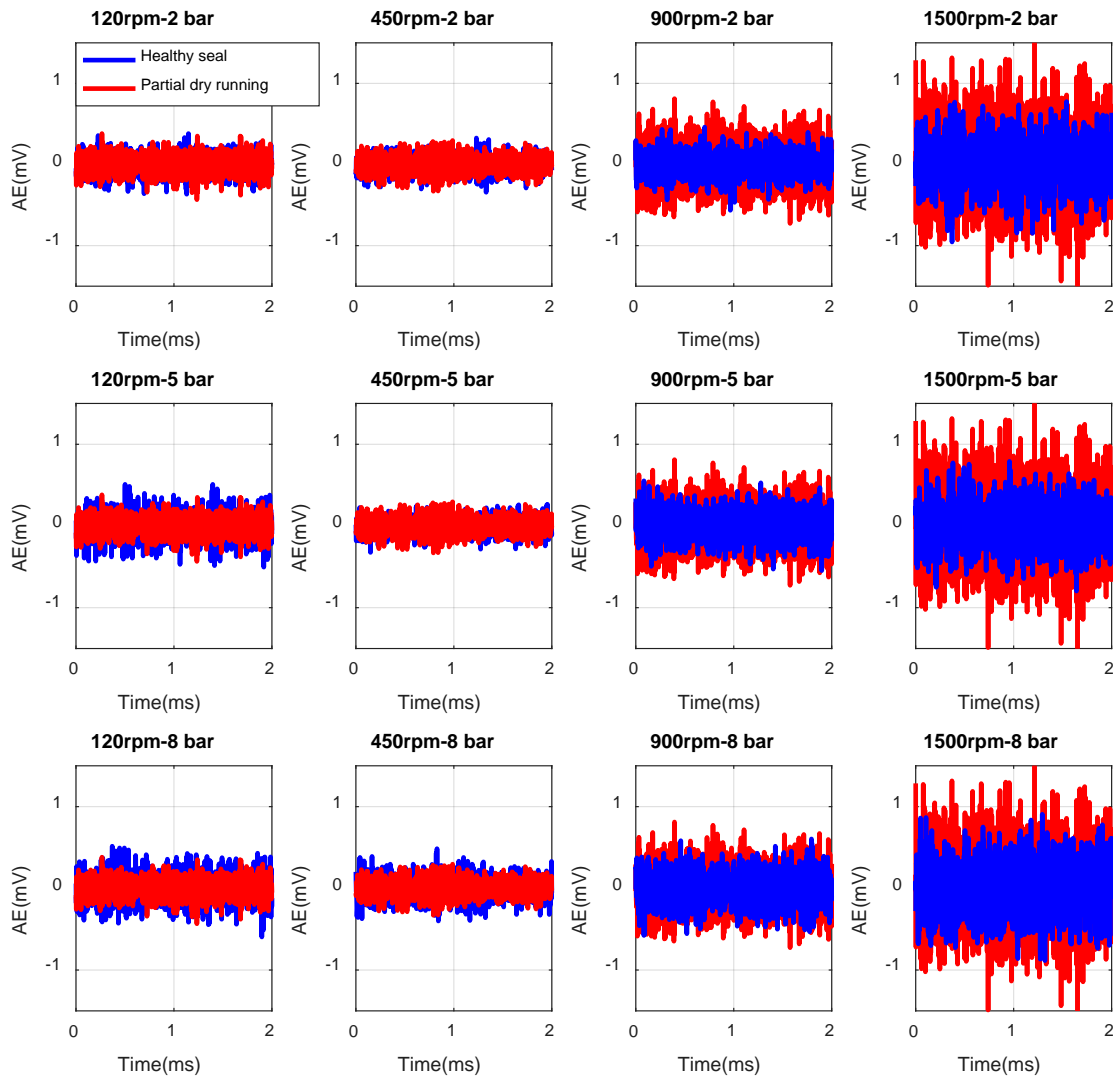


Figure 8.2 AE signal for healthy seal and partial dry running test

8.2.2 The Variation of AE RMS Value under Partial Dry Running Test

To compare the energy released due to AE activity in the sealing gap, the average RMS value of AE signals recorded during three different tests are calculated and presented for both baseline and partial dry running tests versus the actual speed of shaft, Figure 8.3.

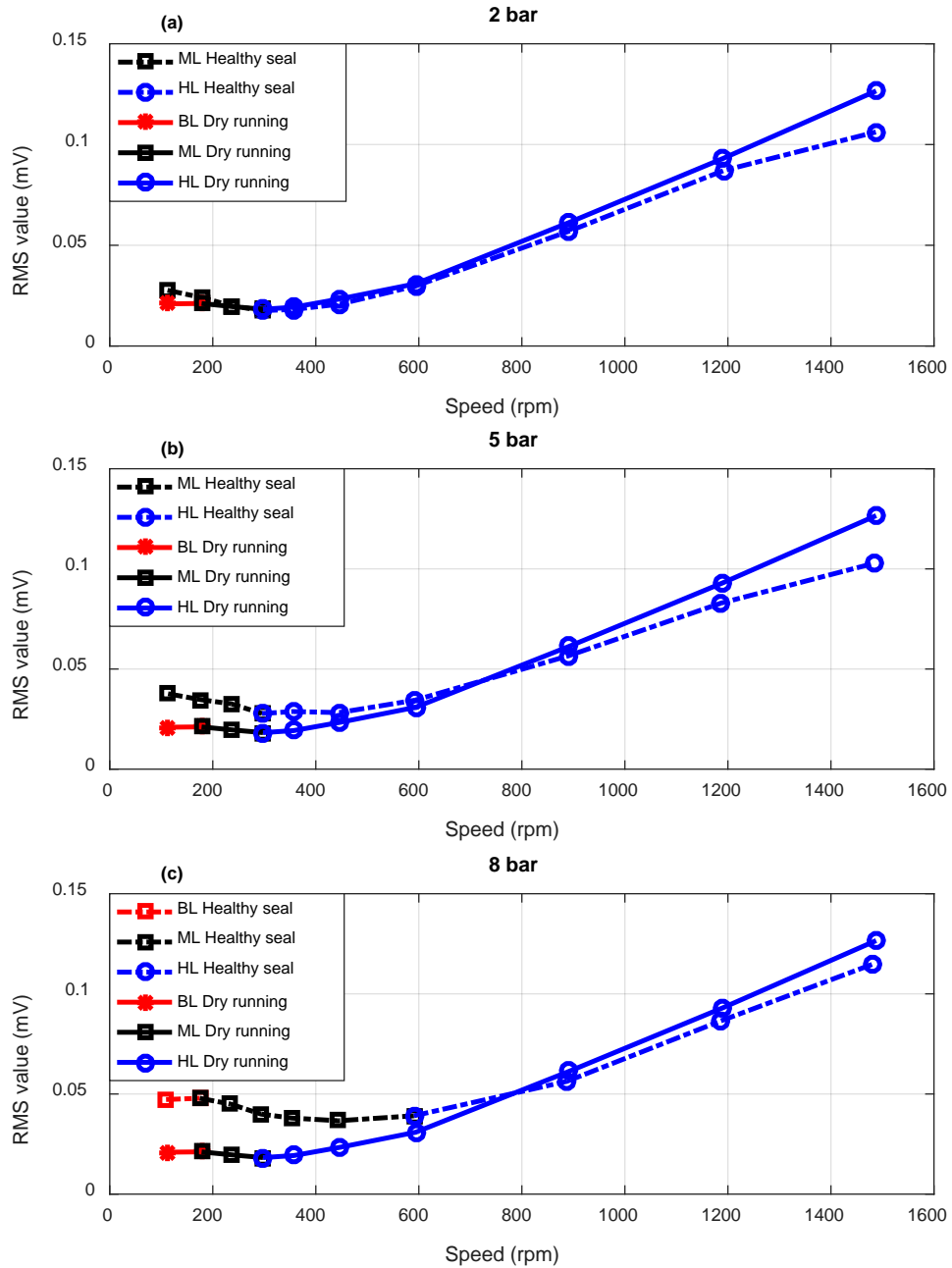


Figure 8.3 The AE RMS values for healthy seal and dry running test under different operating conditions

Based on Figure 8.3 in the partial dry running test the RMS value first increases by the speed increase from 120 rpm to 180 rpm indicating that the boundary lubrication regime is dominant. This confirms that dry rubbing between the mating faces happens at lower speeds that causes the RMS value goes up by the speed increase.

By increasing the speed gradually to the minimum point of the curve, RMS value goes down due to better lubrication condition in the mixed lubrication regime. As the speed increases gradually, transition from the mixed into the hydrodynamic lubrication regime occurs and RMS value increases again by the speed increase.

Compared with the base line test, the level of AE RMS value in the partial dry running test is lower at lower speeds due to the fact that the seals are pressurized in the baseline test. Therefore, massive asperity deformation occurs in the healthy case that generates higher level of AE energy. This could be better understood by considering Figures 8.3 (b) and (c), where the AE RMS level increases in the healthy case by the sealed pressure increase.

By increasing the speed into the hydrodynamic lubrication region, the AE RMS value of partial dry running test sees higher values rather than the baseline test due to more AE energy released from the flow induced asperity deformations. Under this condition the slightly smaller sealing gap is achieved for the partial dry running test that generates more elastic asperity deformations (e.g. flow induced asperity deformation and viscous friction in fluid layers) in the hydrodynamic lubrication region, Equations (7.9). The smaller sealing gap provides stronger flow of lubricant that causes more elastic asperity deformations.

Furthermore, the transition from the mixed to the hydrodynamic lubrication regime happens at lower speeds for partial dry running test compared with the baseline. This is mainly caused by the fact that seal faces are not pressurized in partial dry running test and hence the sealing gap increases easily (up to a threshold) by increasing the speed due to the establishment of hydrodynamic pressure lift up. In other words, the hydrodynamic lubrication is established at lower speeds in the absence of strong hydrostatic lubrication in partial dry running test.

8.2.3 The Variation of AE Kurtosis Value under Different Operating Conditions

In Figure 8.4 a comparison of AE kurtosis values is made between the baseline test and dry running test when sealed pressure is constant and speed increases gradually. As it is observed, at lower speeds in the partial dry running test the contact is confined to the asperity

tips that leads to more peaked probability density function due to lower values of RMS (or standard deviation). Therefore, kurtosis sees higher values compared with baseline. This gives a good evidence for the purpose of fault detection at lower speeds.

By increasing the speed into the hydrodynamic lubrication regime, the kurtosis values get closer to zero in both cases indicating that the distribution of AE signals is very close to the normal distribution. Therefore, this speed dependency of kurtosis value allows dry running to be indicated at lower speeds, where other time domain features do not make such a big difference with the baseline.

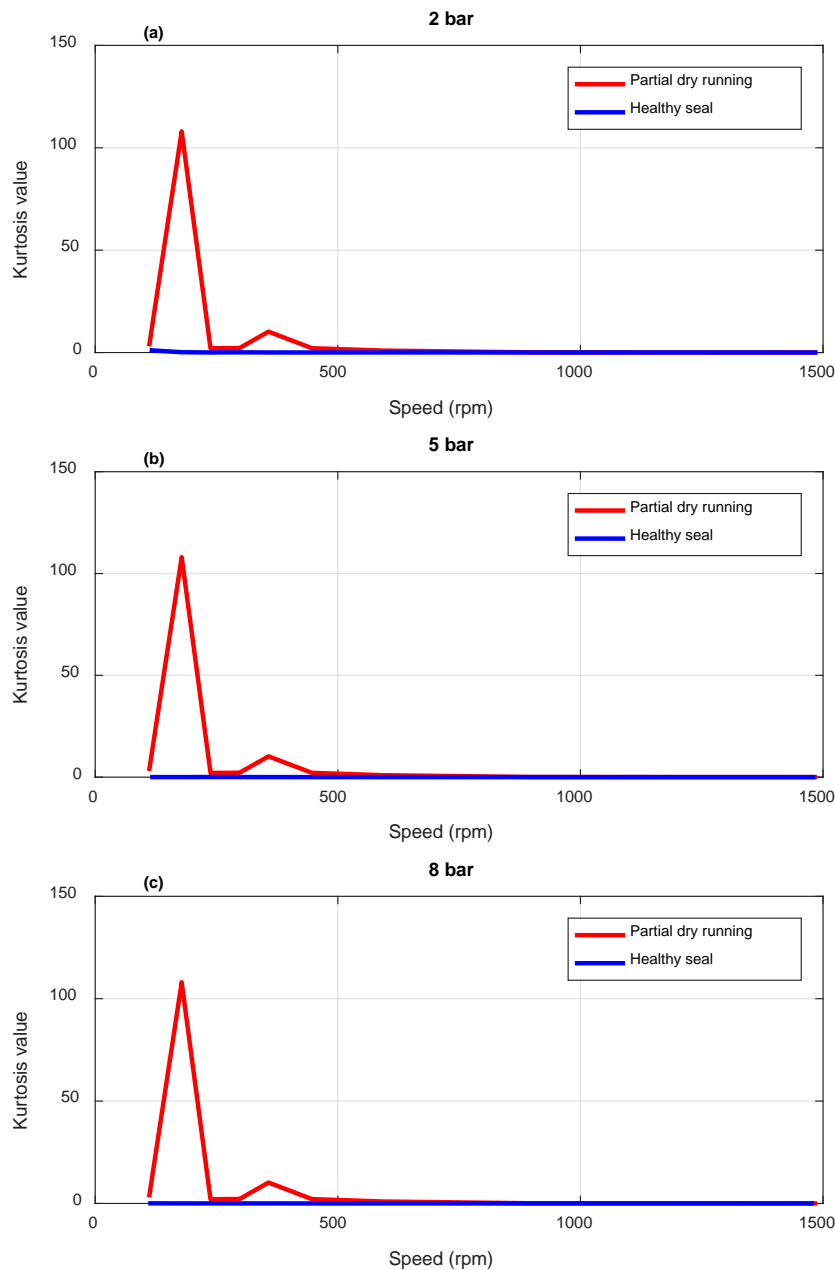


Figure 8.4 The AE kurtosis values for healthy seal and dry running test under different operating conditions

8.2.4 Frequency Domain Analysis

Figure 8.5 compares the spectra of AE signals for the baseline and partial dry running tests when the seal operates under different speed and pressure settings.

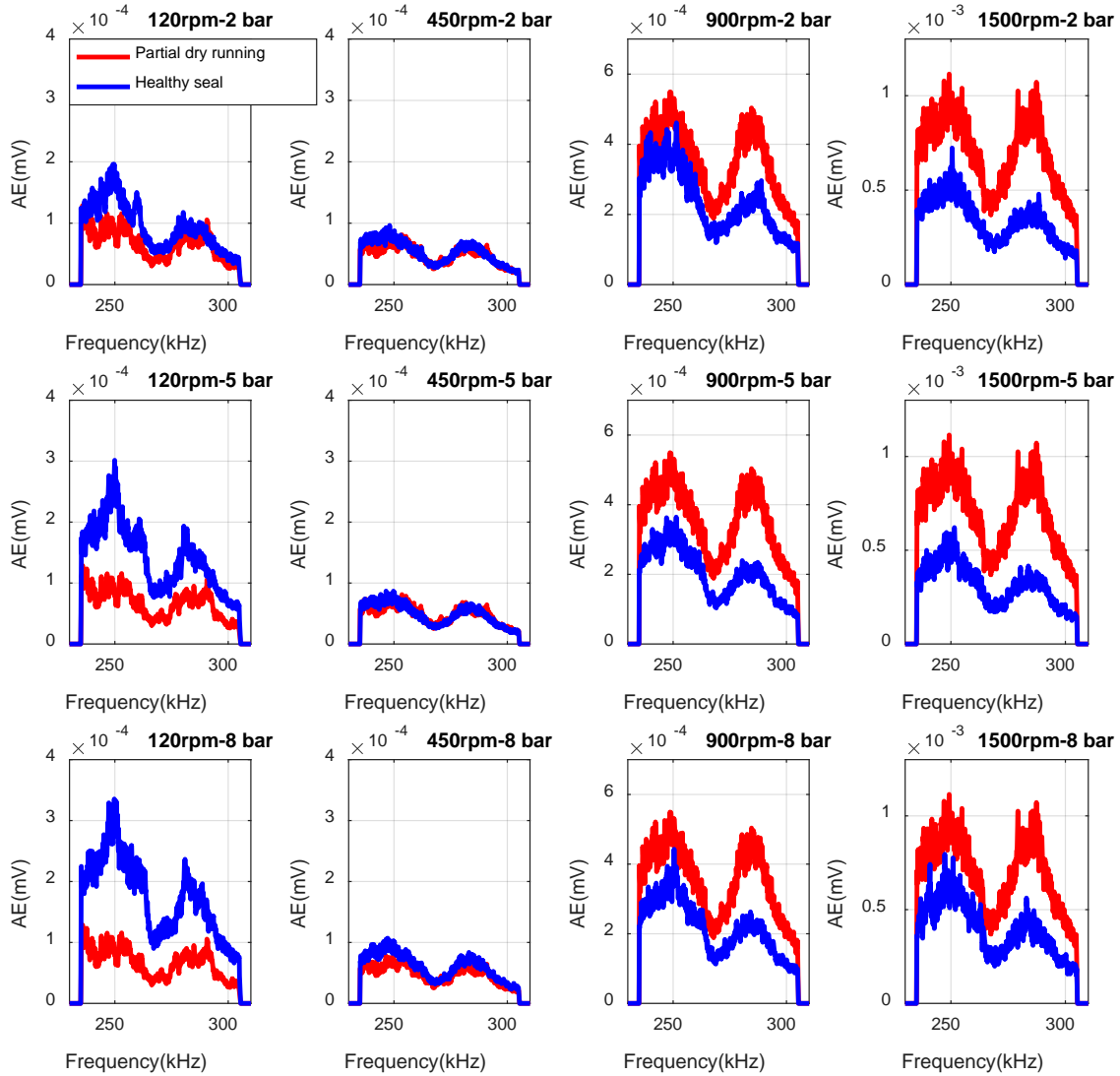


Figure 8.5 AE spectra for healthy seal and dry running test under different operating conditions

Based on Figure 8.5 at low speeds e.g. 120 rpm, by increasing the sealed pressure the amplitude of the baseline goes up due to more asperity contact happens in the healthy case, Equation (7.12). Although in partial dry running test dry asperity contact happens, the amplitude of the related spectra is slightly lower due to the fact that massive asperity contact does not occur. As speed increases gradually to the hydrodynamic lubrication regime, the severity of asperity deformations goes up due to speed increase, Equation (7.7). Here, the amplitude of AE spectra is higher for the faulty case due to slightly smaller sealing gap that

provides higher rate of AE energy release as depicted by Equations (7.9). In addition, better separation between two cases is observed rather than AE signal in time domain especially at lower speeds.

8.2.5 Model Response to Partial Dry Running Test

Now that the effectiveness of the mathematical models developed in Chapters 5 and 7 is well established to monitor the tribological behaviour of the sealing gap (see Section 7.4), it would be worthy to examine the response of model to the partial dry running test.

Figure 8.6 shows the relationship between AE RMS value and the sliding speed when the rig operates under partial dry running test. The beset curve is fitted on the test results using statistical analysis carried out in MATLAB.

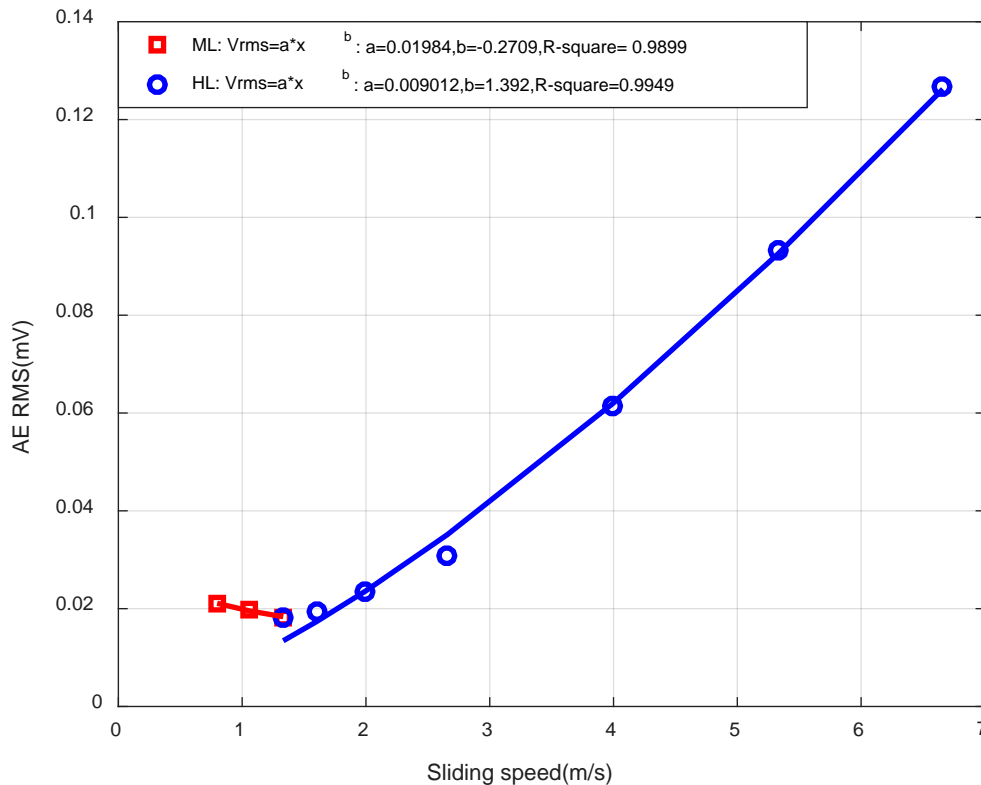


Figure 8.6 The relationship between AE RMS value and sliding speed in dry running test

Based on Figure 8.9 the power value obtained for rotational speed in the mixed lubrication regime is very close to the values that have been achieved for the healthy case (see section 7.4.1). Hence it is unlikely possible to detect partial dry running using the developed equations. In other words, the deviations from baseline is not enough to be detected by the model in the mixed lubrication condition.

The power trend achieved here for the sliding speed in the hydrodynamic lubrication regime, 1.329, is slightly bigger than the power trend achieved for healthy case in Section 7.4.1. A plausible explanation for this difference is that the rate of AE generated due to viscous friction and fluid induced asperity deformations in the hydrodynamic lubrication regime is higher for the partial dry running test than the base line as presented in previous discussions. However, this difference is not big enough that can be used for reliable model based condition monitoring of mechanical seals. In fact, the mechanism of AE sources in partial dry running test is similar to the healthy case and hence the developed equations cannot generate a remarkable difference.

8.3 Spring Fault Test

Based on the discussion made in Section 2.1.3 the spring force has an important role to insure positive closing force at low pressures as well as during assembly. The springs in seal head assembly may subject to fatigue and corrosion and hence fail to meet the expected functions. Examination of hundreds of seal failures by different researchers has revealed that most failures are not caused by seal wear out. For many failures the amount of wear is on the order of thousandths of a millimetre whereas the seal is designed for about 3-mm wear before failure [4, 88]. Buck reported that as the seal face wears away, the spring load decreases. For linear spring rates Buck proposed that [88]:

$$F_s = F_{si} \left(1 - \frac{\Delta L_w}{\Delta L_t}\right) \quad (8.1)$$

Where F_s is the spring force [N], F_{si} is the initial or as installed spring load [N], ΔL_w is the height worn away from the seal face during operation [m] and ΔL_t is the total spring compression (including preload) [m].

Therefore, it is necessary to study the changes in AE features with the spring force change. For the research purposes different experimental programs can be carried out to investigate the effect of spring fault on tribological behaviour of the sealing gap. For instance, it is possible to change the stiffness or make a fault in the spring itself. Since this thesis aims to provide some fundamental results on the effectiveness of the AE measurements for the purpose of fault detection in seals, as discussed in Section 6.5.5, the spring fault test were

carried out by taking off 2 springs out of 12 available springs in the seal head assembly. In theory the total stiffness of parallel springs is calculated based on Equation (8.2)

$$K_{ST} = K_{S1} + K_{S2} + \dots \quad (8.2)$$

where K_T is total stiffness and K_i is the stiffness of each spring

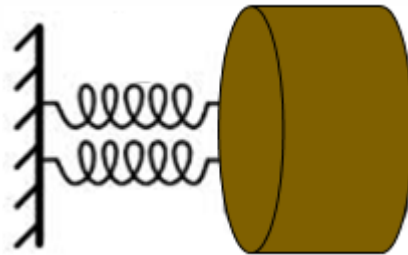


Figure 8.7 The concept of parallel springs

Based on Equation (2.3) by taking some springs off the spring force goes down however the net hydraulic loaded face area, A_h , remains unchanged with springs as shown with red circles in Figure 8.8. This causes the closing force decrease that is expected to lead to friction decrease in the sealing gap.



Figure 8.8 The concept of increase in the net hydraulic loaded area

8.3.1 Time Domain Analysis

Figure 8.9 compares the typical AE signals from the spring out test with the baseline under different speed and pressures settings. As it is observed in the most cases (except for hydrodynamic lubrication regime at 2 bar sealed pressure), the amplitude of AE signals and the number of burst type responses increase in the spring out test that does not support the conclusion made in previous section (decreasing in friction force). The most likely reason for increasing the friction force (and consequently AE activity) is that the sealing gap is

uneven with two springs out and that there are face regions which see higher contact pressure, hence higher AE level. Consequently, the amplitude of AE signals and the number of burst type responses increase due to higher elastic energy released from the mating asperities. The burst type AE responses are generated due to deformation of peak asperities, while massive asperity deformation generates continuous type AE signal. In either cases, it could be generated due to direct asperity contact or flow induced asperity deformations.

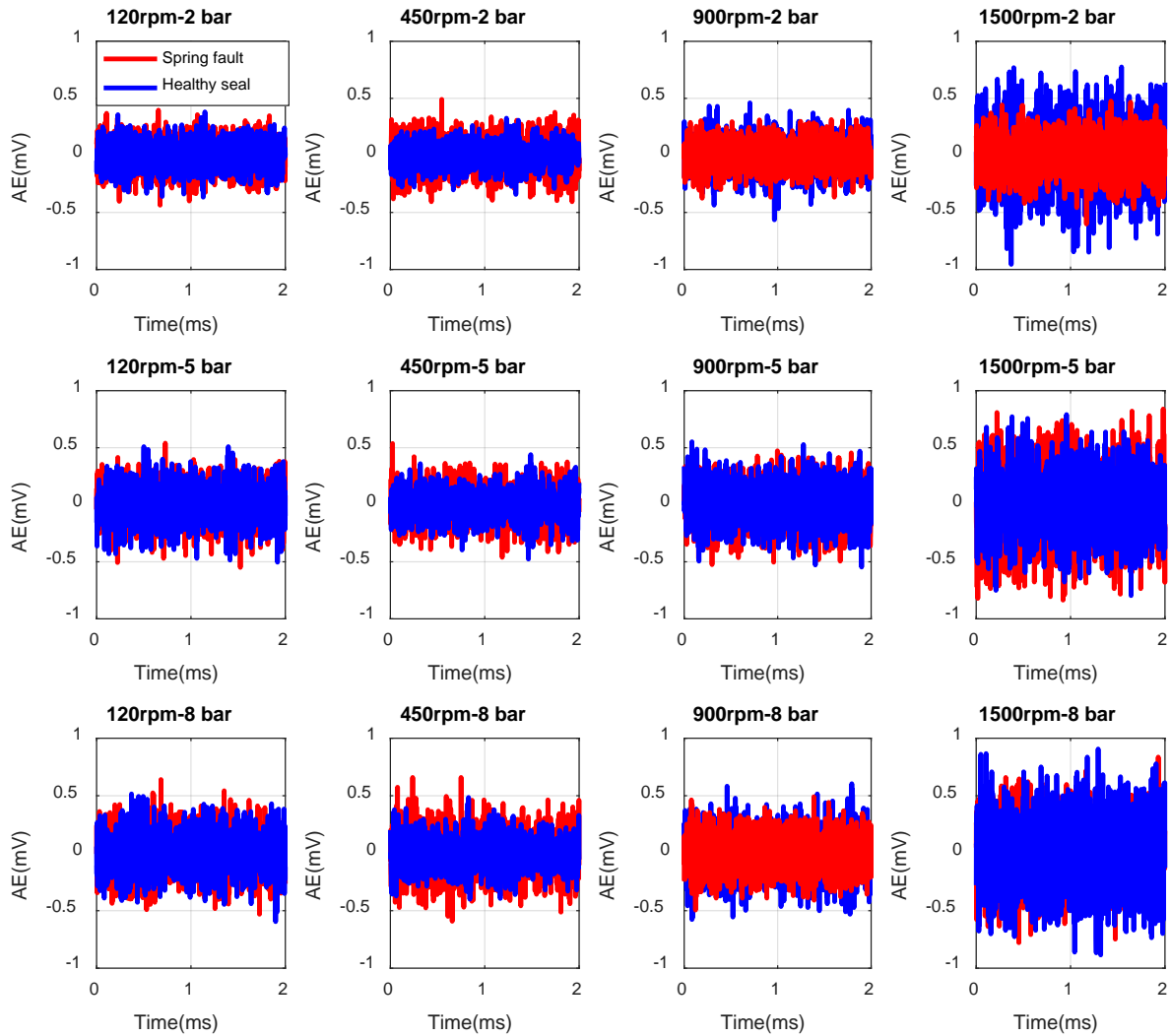


Figure 8.9 AE signal for healthy seal and spring out test

8.3.2 The Variation of AE RMS Value under Different Operating Conditions

To investigate the effect of taking two spring out on the level of AE activity, the average RMS value of AE signals recorded during three different tests are calculated and presented in Figure 8.10. As illustrated in Figure 8.10 for the experiments have been carried out at speeds less than 600 rpm, the base line test has a concave curve while for the spring out test

the AE RMS value sees a convex trend. This is due to the fact that the micro geometry of contact in the sealing gap is changed by taking two springs out, therefore uneven deformation occurs that affects the trend of AE RMS value curve. In addition, for the experiments have been conducted at lower speeds, the boundary lubrication regime is observed for the spring out test due to uneven sealing gap. Therefore, the RMS value is higher for the faulty seal at lower speeds indicating the more interaction between asperities and hence more AE activity.

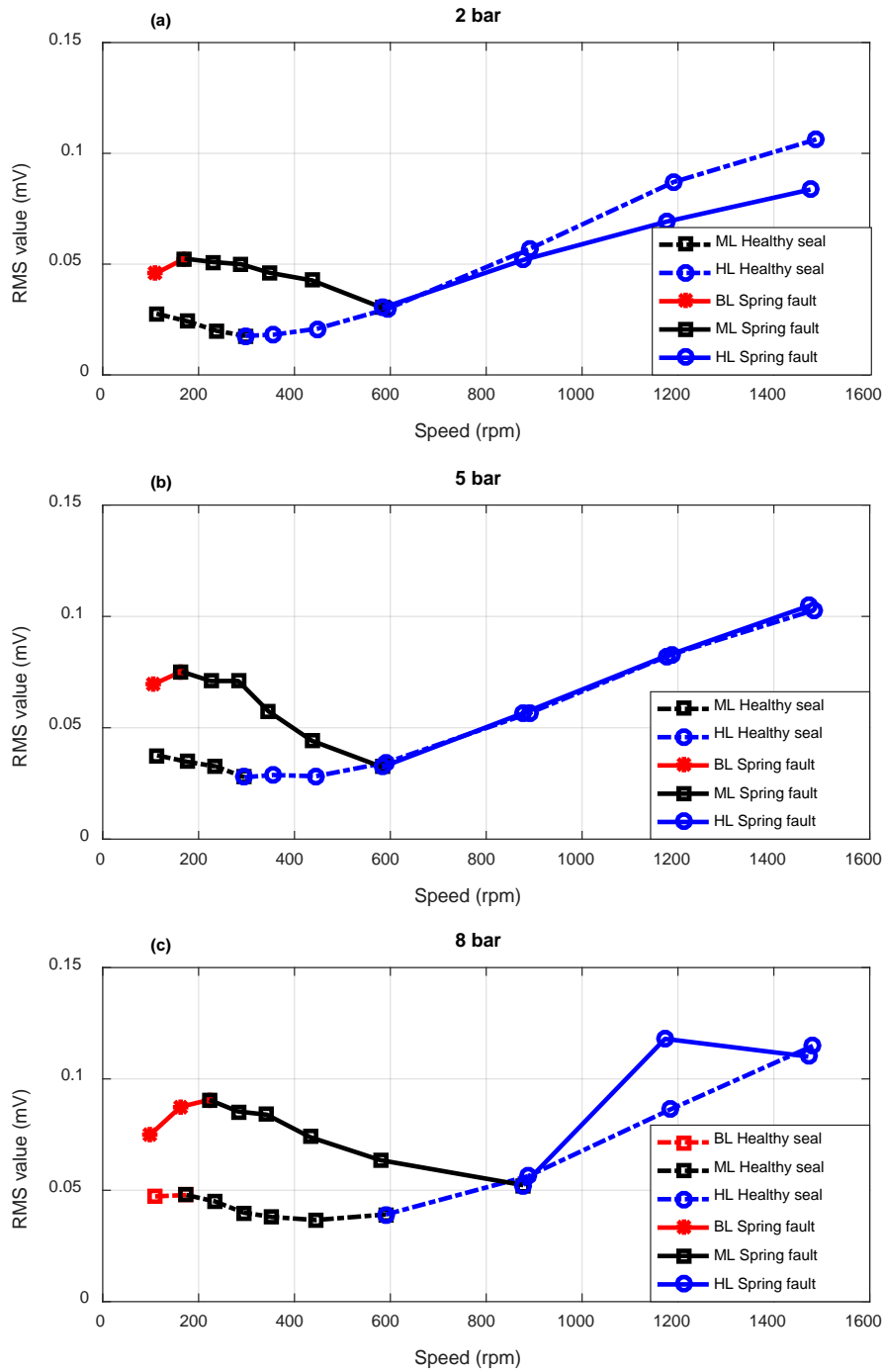


Figure 8.10 The AE RMS values for healthy seal and spring out test under different operating conditions

By increasing the speed into the hydrodynamic lubrication regime, AE RMS curves related to the faulty seal become more stable due to the separation of mating faces. However, the position of the curves shifts up and down by increasing the sealed pressures compared with the baseline. The uneven sealing gap also causes that the transition from the mixed to the hydrodynamic lubrication occurs at higher speeds.

8.3.3 The Variation of AE Kurtosis Value under Different Operating Conditions

Figure 8.11 compares the kurtosis of AE signals from the spring out test with the baseline under different speed and pressures settings.

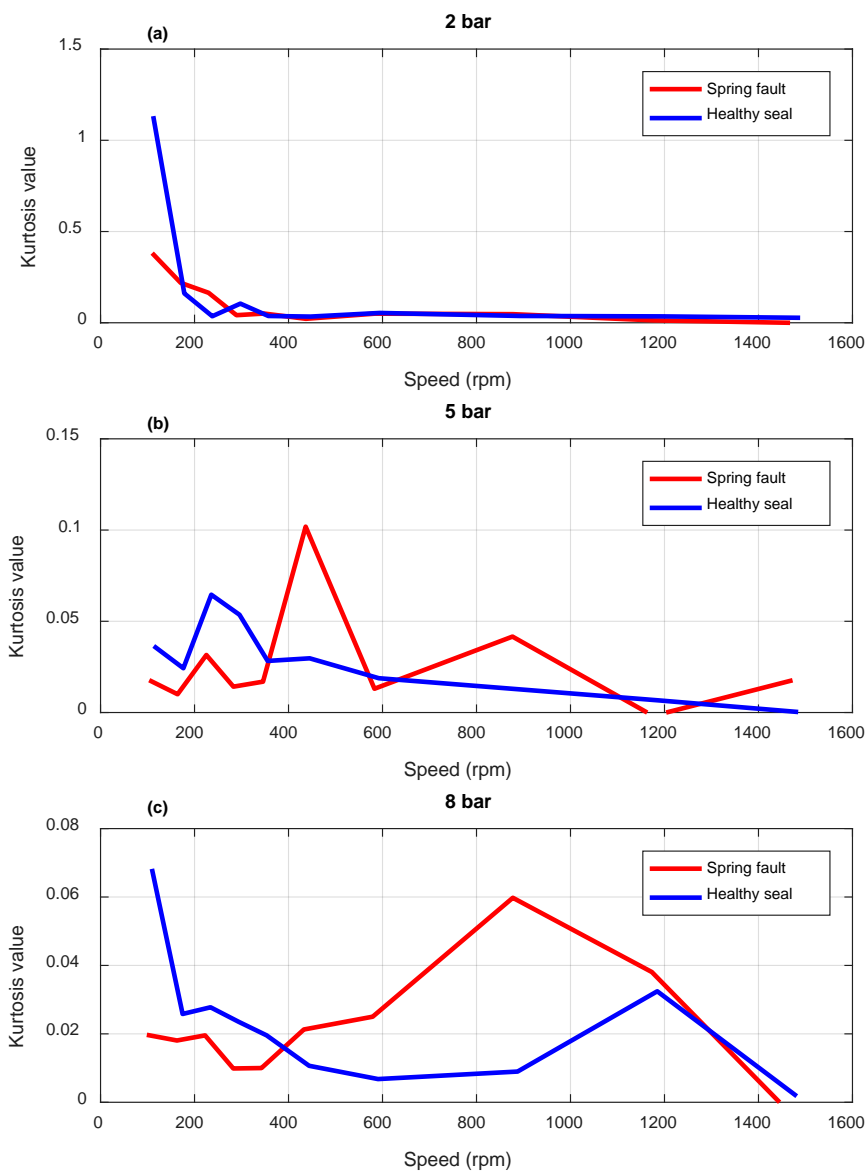


Figure 8.11 The AE RMS values for healthy seal and spring out test under different operating conditions

Since in the spring out test uneven sealing gap is achieved, uneven asperity deformations (whether in direct contact or fluid induced one) occurs. Consequently, at low sealed pressures (e.g. 2 bar, Figure 8.11 (a)) the kurtosis value of spring out test gets closer to the kurtosis value of Gaussian distribution. By increasing the sealed pressure, Figures 8.11 (a) - (c), more uneven deformations occur in the sealing gap that causes some fluctuations in the kurtosis trend especially in the mixed and hydrodynamic lubrication regimes. Therefore, this speed and load dependency of kurtosis allows that spring fault to be identified.

8.3.3 Frequency Domain Analysis

Figure 8.12 compares the spectra of AE signals from the spring out test with the baseline under different speed and pressures settings.

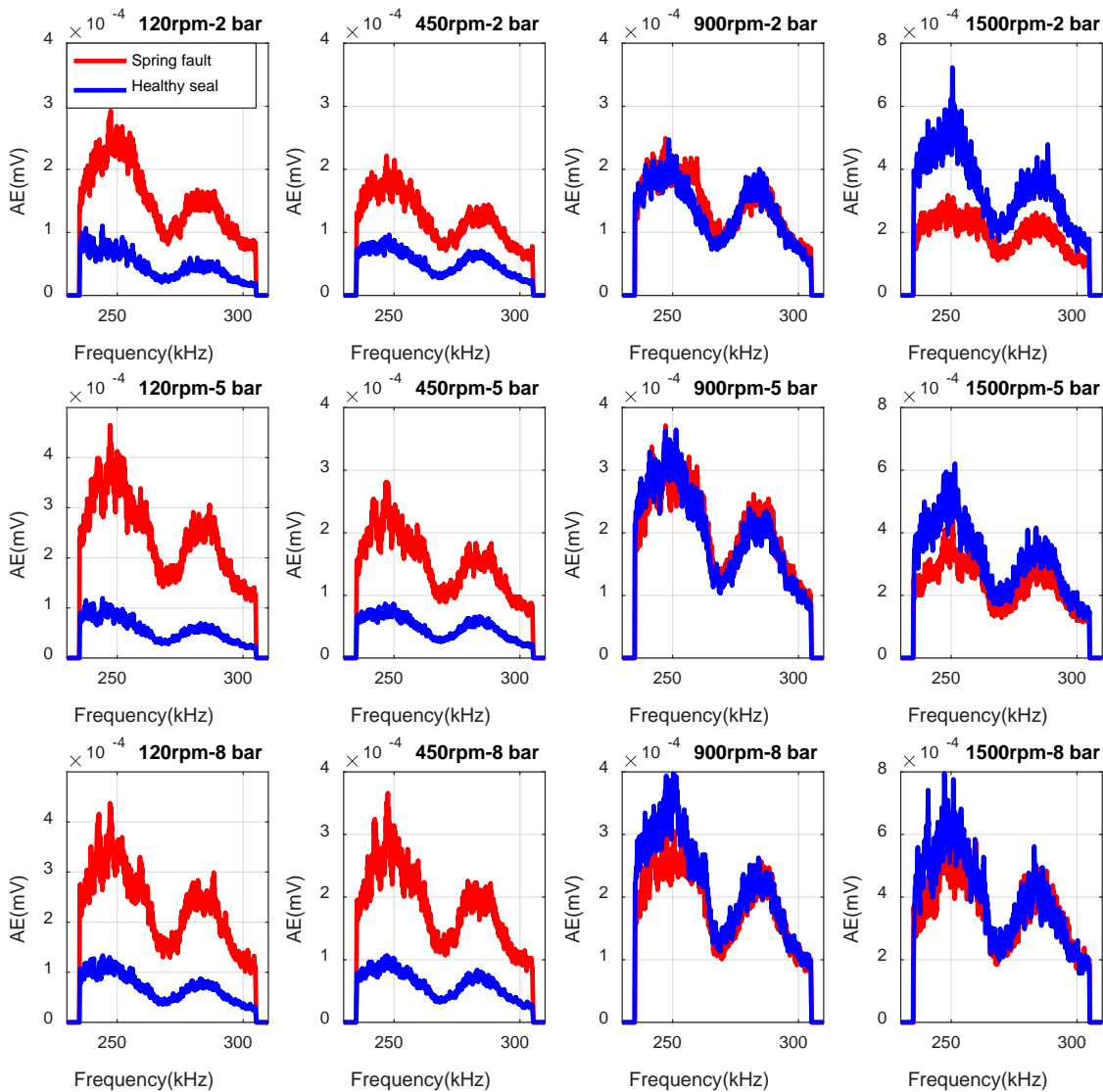


Figure 8.12 AE spectra for healthy seal and spring out test under different operating conditions

At lower speeds, i.e. 120 rpm or 450 rpm, the amplitude of spring out test is higher than the baseline due to more uneven deformation that generates higher rates of strain energy released in the sealing gap. By increasing the rotational speed of shaft, the amplitude of the faulty case becomes closer to the baseline gradually, indicating that the effect of uneven sealing gap on the AE spectra becomes less significant. Therefore, this dependency of AE spectra to the spring fault test has a promising potential to be used for the purpose of fault detection, especially at lower speeds where a remarkable difference is observed with the baseline.

8.3.4 Model Response to Spring Fault Test

To compare the results of AE RMS analysis related to spring out test with the proposed mathematical models, a statistical analysis was carried out in MATLAB, Figure 8.13 to Figure 8.15. It is noted that due to fluctuations in the AE RMS value related to 8 bar sealed pressure in the hydrodynamic lubrication region, the curve fitting was carried out for 7 bar sealed pressure as illustrated in Figure 8.15.

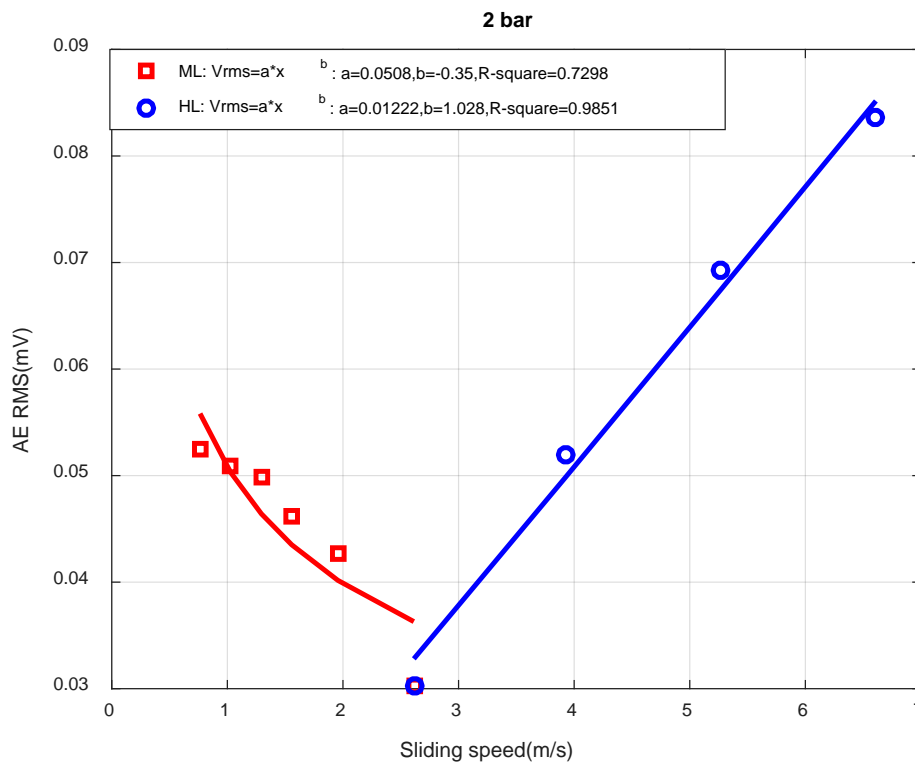


Figure 8.13 The relationship between AE RMS value and sliding speed in spring out test under 2 bar

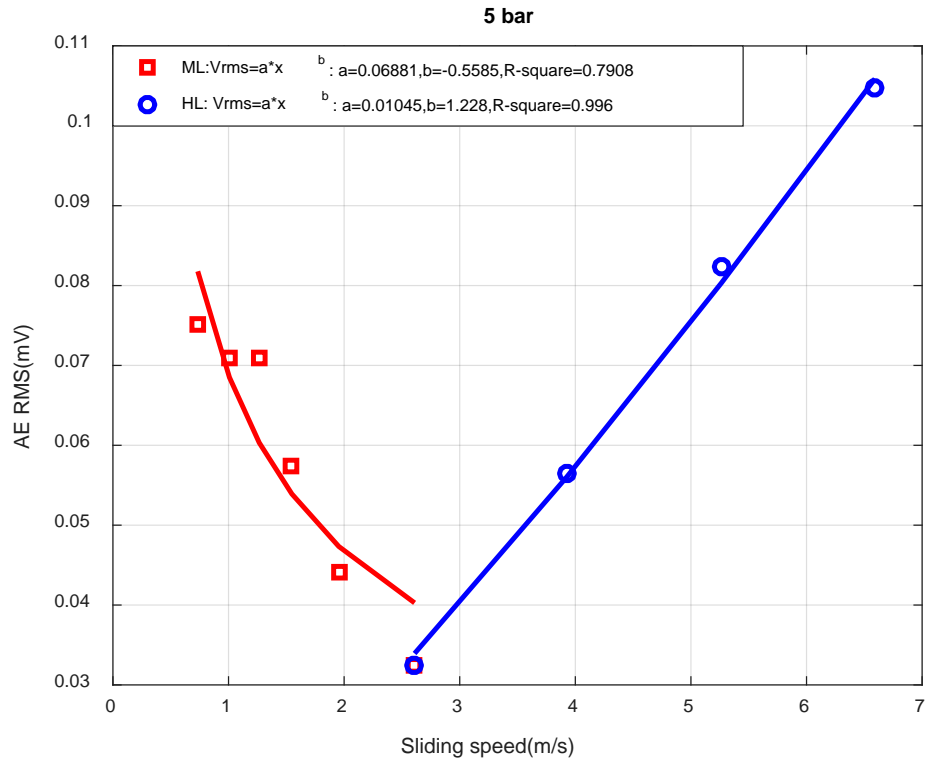


Figure 8.14 The relationship between AE RMS and sliding speed in spring out test under 5 bar

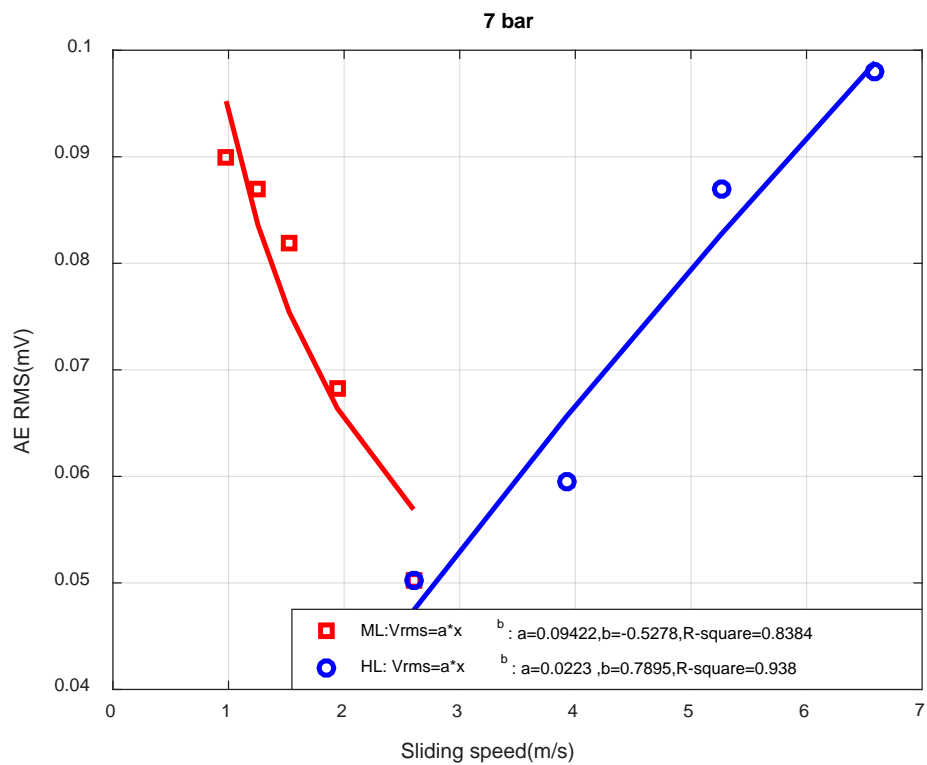


Figure 8.15 The relationship between AE RMS and sliding speed in spring out test under 7 bar

Based on Figures 8.13 to 8.15, the achieved values of coefficient of determination in the mixed lubrication region is significantly lower than the values achieve for baseline analysis (see Section 7.4). Hence this deviation from the baseline analysis which arises due to the concave nature of AE RMS value curves is useful for the purpose of fault detection. However, In the hydrodynamic lubrication regime the results are same as the baseline test indicating that the deviations from the baseline are not big enough to generate significant responses in model.

Figure 8.16 presents the test results to investigate the effect of sealed pressure on AE RMS value when the spring fault seal is operated at low speeds.

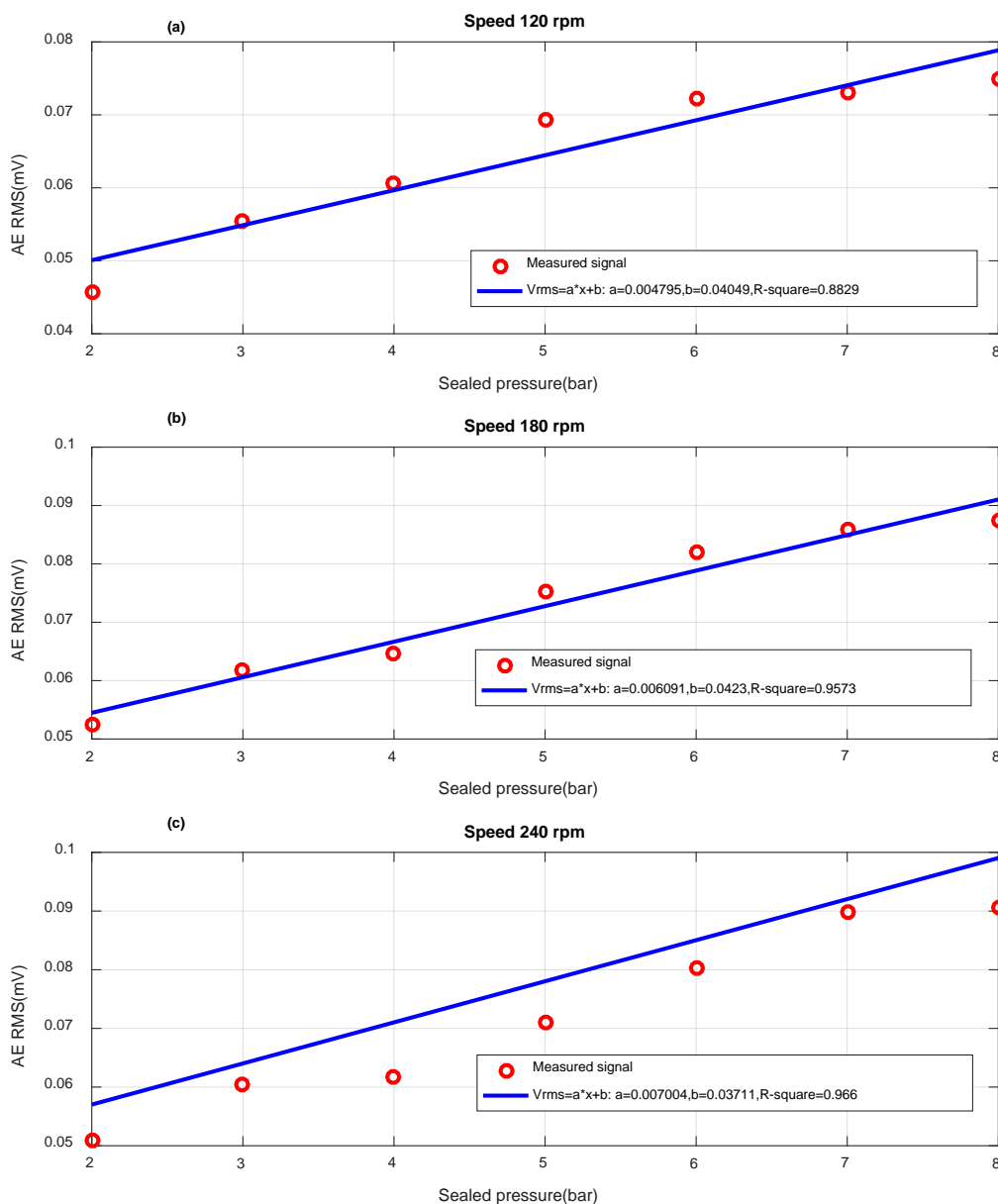


Figure 8.16 The relationship between AE RMS value and sealed pressure in defective seal test

As it is illustrated in Figure 8.16 (a)-(e), the liner polynomial trend predicted for contact load by Equation (7.13) is achieved with a good accuracy. The best coefficient of determination is achieved for speed 180 rpm, Figure 8. 21 (b). This gives a good evidence that developed model is effective to study the effect of sealed pressure on AE level especially when more elastic deformation occurs in the sealing gap.

8.4 Defective Seal Test

In addition to dry running and spring fault, other mechanisms may contribute to damage the mating faces. For instance heat checking is observed on the mating faces that radiates from the centre of the seal ring, Figure 8.17 (a). They may be caused by localized expansion resulting from sever temperature changes due to dry running or excessive pressures or rotational speeds. Moreover corrosion of a seal ring as a result of chemical attack may occur specially for seals that are used in corrosive atmospheres, Figure 8.17 (b). Sometimes the situation get worse and mating ring is cracked due to thermal or mechanical shock that is more observed in case of ceramic faces Figure 8.17 (c).

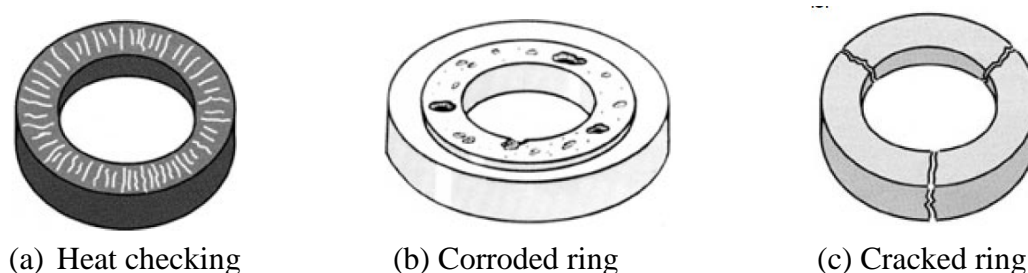


Figure 8.17 Common seal face defects

The defective seal faces reduce the sealing performance of a mechanical seal and may lead to higher values of leakage rate. Based on the Equation (7.10) if the sealed pressure goes down to a minimum possible level and spring force is not powerful enough, then the negative contact pressure is achieved. This means that opening forces overcome the closing forces and the mechanical seal is failed. It is immediately noted that when leakage occurs in mechanical seals, it may be due to an excessive liquid film which might be formed in the sealing gap or it may be due to excessive damage which might happen to the mating faces. The former is not the subject of this study and to investigate the latter, as discussed in Section 6.5.7, some damages were made on the mating ring to simulate the condition under that excessive wear and leakage occurs in mechanical seals.

8.4.1 Time Domain Analysis

To compare the AE responses related to the defective seal with the baseline, Figure 8.18 presents typical time domain signals under different speed and pressure settings. Since in the defective seal test the seal faces are scratched, hence at the low rotational speeds of shaft severe asperity contact happens especially on defective regions. As a consequence, the amplitude of the AE signals and number of burst type responses increase due to higher elastic energy that is released from the contact asperities, Equation (5.31).

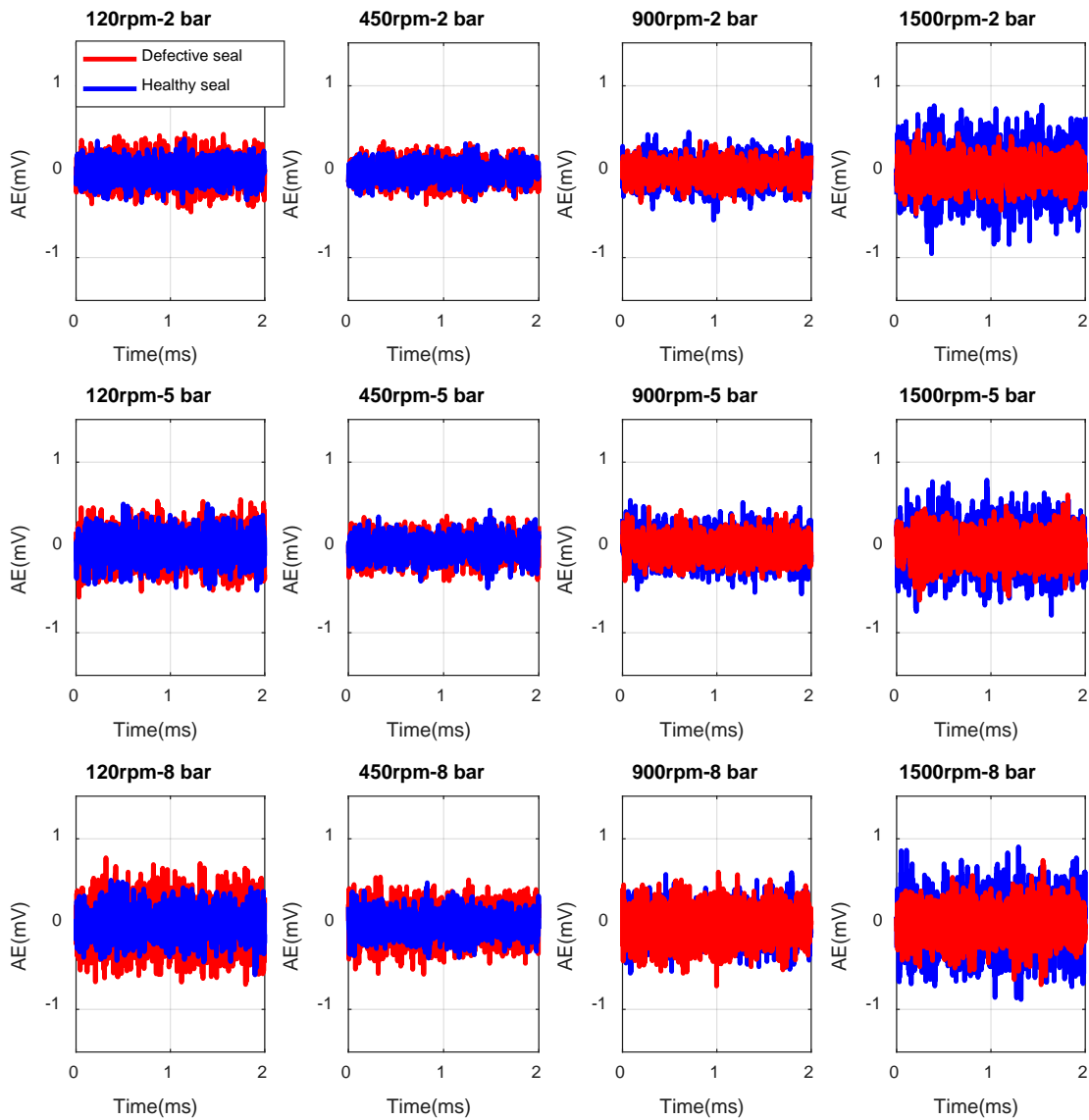


Figure 8.18 AE signal for healthy seal and defective seal test

By increasing the speed to the hydrodynamic lubrication regime the seals become fully separated and leakage occurs due to the fact that sealing is not performed properly. Under this condition a bigger sealing gap is achieved and therefore the stress field of lubricant film

is not strong enough to generate elastic deformation in the mating asperities, Equations (5.8) to (5.11). In addition, the shear rate in fluid lubricant decreases due to increase in the sealing gap, Equation (5.62). The most likely reason for the gap increase is thermally induced waviness caused by the cooler areas around the scratches versus region in between the scratches that generates higher hydrodynamic pressure lift up. Consequently, the AE amplitude and the number of burst type responses decrease.

8.4.2 The Variation of AE RMS Value under Different Operating Conditions

In Figure 8.19 a comparison of the average AE RMS values recorded during three different tests is made between the baseline test and defective seal test when sealed pressure is constant and speed increases gradually.

Based on Figure 8.19, for or the experiments have been conducted at lower rotational speeds of shaft (less than 200 rpm) an increase in the AE RMS value is observed due to sever asperity contact and excessive wear for the defective seal test. This indicates that for defective seal test the boundary lubrication regime is dominant at lower speeds. However, at same rotational speeds, boundary lubrication regime is not observed for the baseline at low or medium sealed pressures.

By increasing the speed gradually, the RMS value goes down due to improvement in the lubrication condition that occurs in the mixed lubrication regime. By increasing the speed into the hydrodynamic lubrication region the RMS value of AE signals related to the defective seal becomes passive and does not show significant change due to higher rates of leakage in the sealing gap.

Hence for the lower speeds the AE RMS value related to defective seal sees higher values compared with the baseline test. At higher rotational speeds of shaft, when transition to the hydrodynamic lubrication occurs and the mating faces become fully separated, AE RMS value does not change significantly by the speed increase. Under this condition, higher values of leakage rate occur at the sealing gap and the seal is failed.

Therefore, the variations in the AE RMS value is useful to detect wear at lower speeds and leakage at higher speeds. This is of high importance in engineering applications as the excessive loss of fluid from the sealing system indicates the failure of mechanical seals.

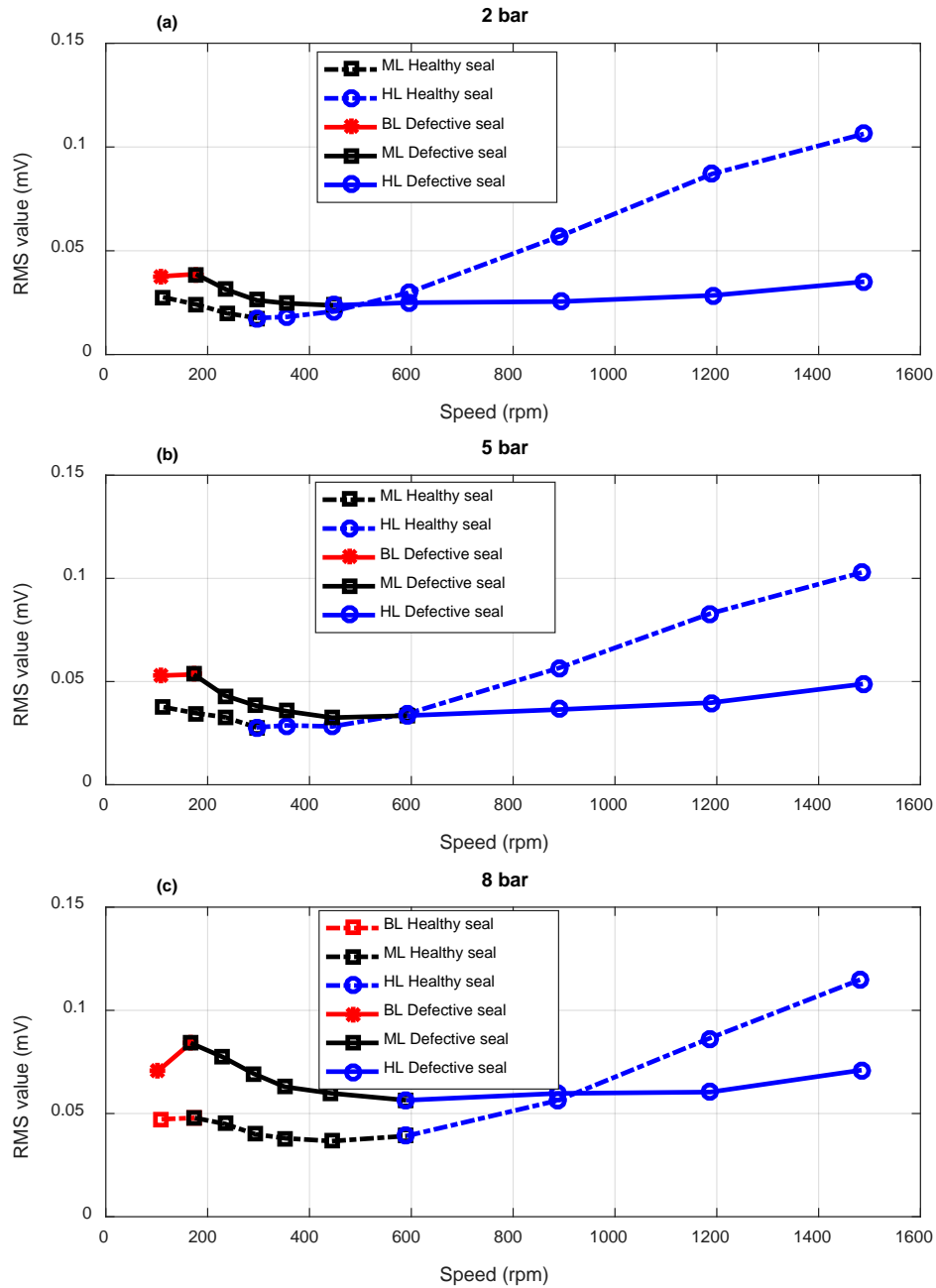


Figure 8.19 The AE RMS values for healthy seal and defective seal test under different operating conditions.

8.4.3 The Variation of AE Kurtosis Value under Different Operating Conditions

Figure 8.20 compares the kurtosis of AE signals from the defective seal test with the baseline under different speed and pressures settings. As illustrated in in previous section, at low rotational speeds the RMS value of AE signals sees higher values compared with the baseline. Higher RMS values refers to the higher standard deviation in AE signals as discussed in Section 7.3.3. The standard deviation increase in defective seal test can be understood to be the effect of changes in the surface topography. The surface texture of damaged seal includes

two components: standard seal surface finish and some sharp asperity peaks generated on scratched regions. The latter component causes higher standard deviation in AE signals recorded from the damaged seal compared with the healthy one. Therefore, kurtosis value of AE signals related to the defective seal test sees lower values at low speeds as illustrated in Figures 8.20 (a) to (c).

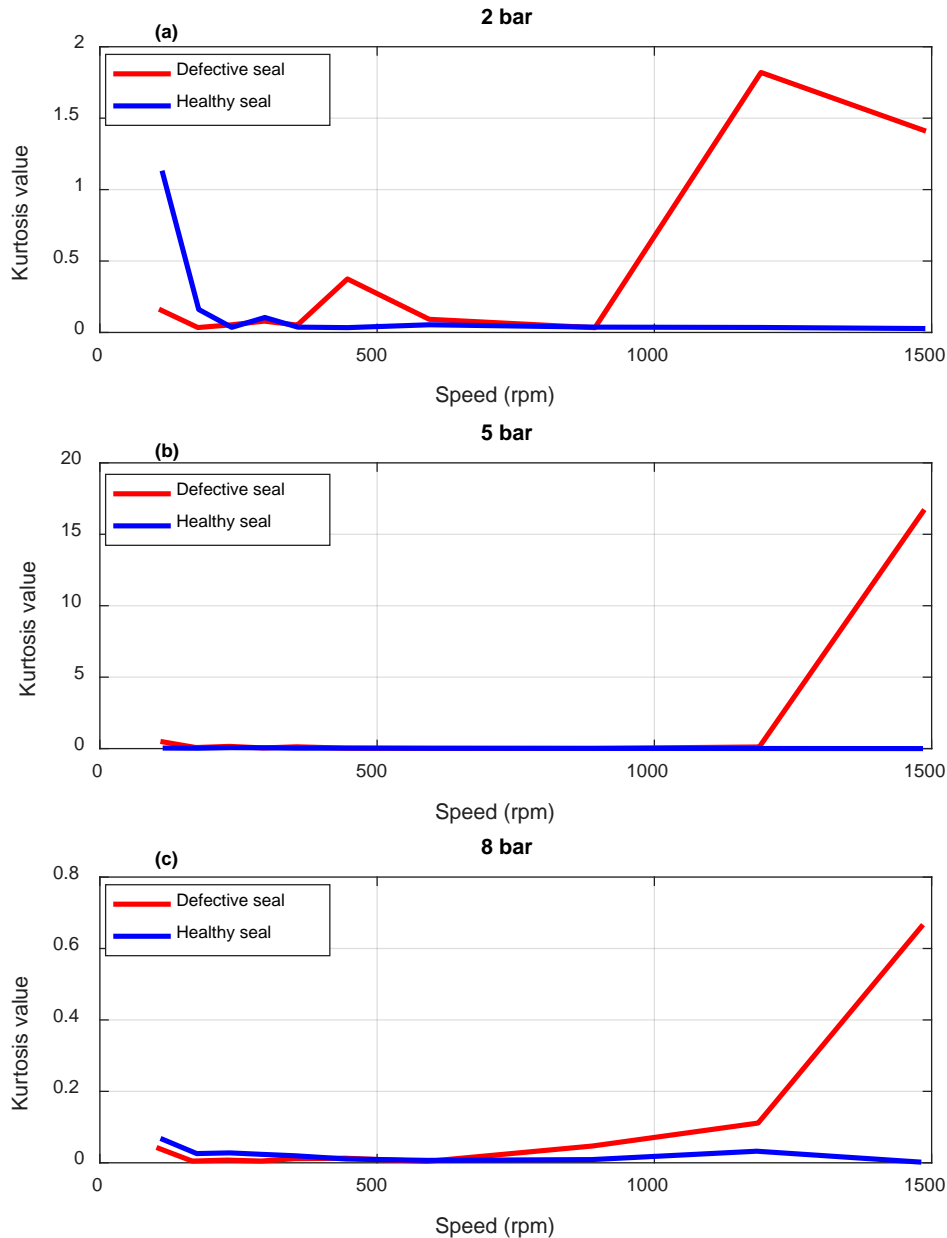


Figure 8.20 The AE kurtosis values for healthy and defective seal

By increasing the speed, the distribution of AE signals related to the base line test gets closer to the Gaussian distribution, whereas the kurtosis increases for defective seal because of standard deviation decrease. This could be understood to be the effect of leakage condition when the increase in the rotational speed of shaft does not lead to significant increase in AE

level up to a threshold (1200 rpm), see Figure 8.19. For the experiments have been carried out after this threshold, kurtosis starts going up again for the faulty case which is not consistent with the expected decreasing trend (as the RMS goes up in Figure 8.19), although it generates big deviation from the baseline that is useful for fault detection.

It is immediately noticed that the kurtosis of AE signals related to the defective seal test sees unexpected fluctuations especially at higher speeds. A plausible explanation is that kurtosis is more affected by the volume of asperity deformation (e.g. sealed pressure) rather than the severity of elastic deformations (e.g. sliding speed). For instance, by increasing the sealed pressure, Figure 8.20 (b)-(c), more asperities are deformed due to direct contact or fluid induced deformations. Therefore, the standard deviation of AE data increases that means kurtosis decrease.

8.4.4 Frequency Domain Analysis

In Figure 8.21 a comparison of AE spectra is made between the baseline test and defective seal test. As it is observed better separation between healthy and faulty case is achieved in spectra rather than the time domain signal.

At lower speeds of shaft, i.e. 120 rpm or 450 rpm, by increasing the sealed pressure the amplitude of AE signals related to the defective seal goes up significantly compared with the baseline due to sever asperity contact and exercise wear compared to the base line, Equation (5.31)

By increasing the speed to the mixed lubrication regime, the improvement in lubrication condition causes less direct asperity collisions and hence the amplitude of AE spectra goes down for both cases. This decreasing trend is more significant for defective seal rather than baseline.

In the hydrodynamic lubrication regime, the sealing gap becomes bigger and opening forces overcome the closing forces. Therefore, leakage occurs and mechanical seal is failed. As a result, the amplitude of AE spectra goes down significantly for defective seal compared to the baseline. Under this conditions the amplitude of AE spectra does not change significantly by increasing the load. This trend has been predicted by Equation (5.46), where it has been claimed that AE level has less connection with sealed pressure.

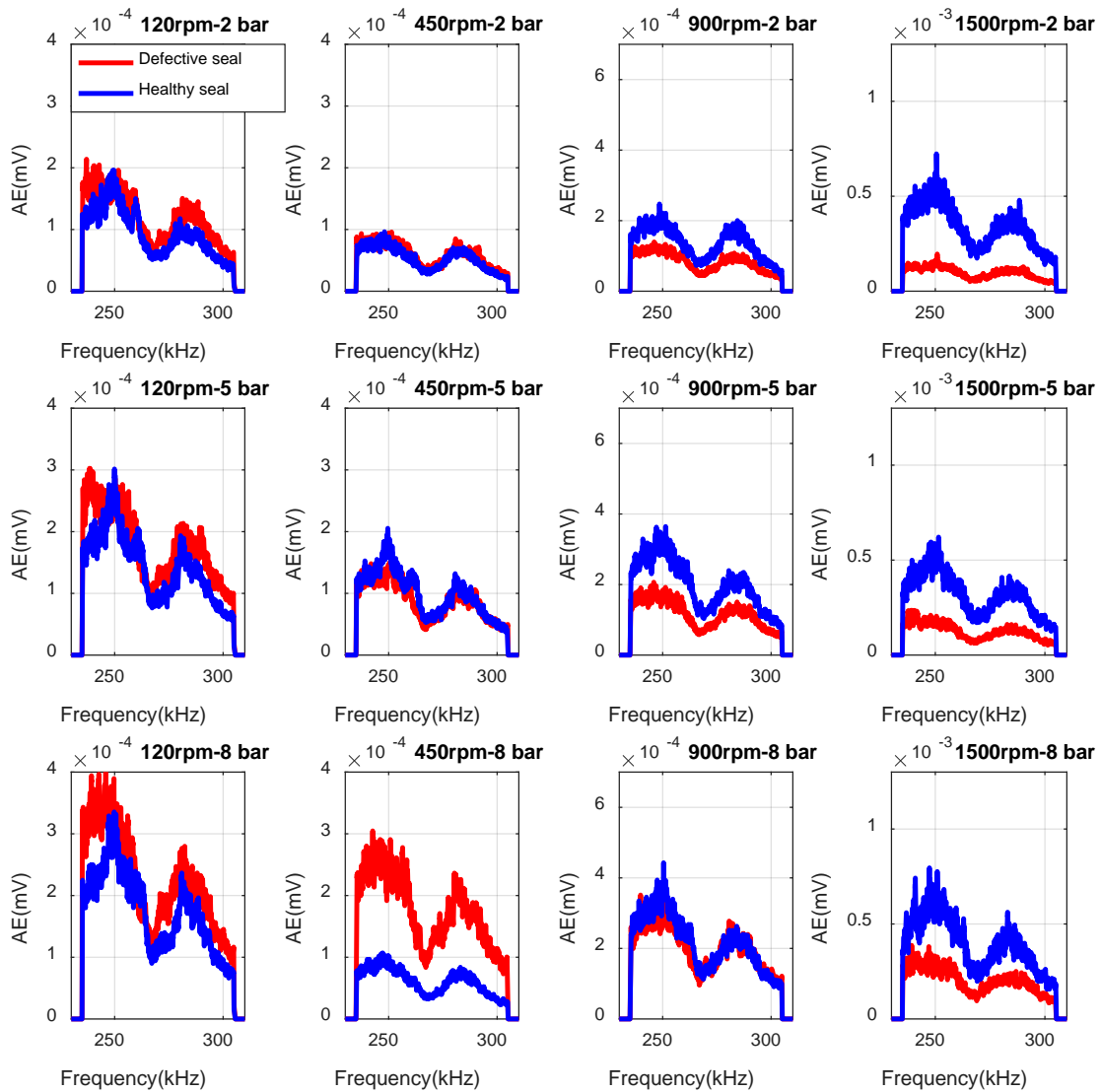


Figure 8.21 AE spectra for baseline and defective seal test

8.4.5 Model Response to Defective Seal Test

To investigate the dependency of AE RMS value on the sliding speed and sealed pressure during the defective seal test and to connect the results with the proposed mathematical models, a statistical analysis was carried out in MATLAB.

Based on Figure 8.22 the power trend achieved for sliding speed in the mixed lubrication regime (-0.5892) under 2 bar sealed pressure is very close to the value predicted by Equation (7.3) in direct asperity contact. This shows that sever asperity contact happens due to artificial scratches made on the mating ring. In spite of the fact that by increasing the sealed pressure to 5 bar and 8 bar more asperities come to contact but the power value of sliding speed decreases due to better lubrication that established, Figures 8.23 and 8.24. Under this

condition the power value achieved in the defective seal test lays into the range achieved for healthy seal (see Section 7.4.1) and hence generates the same responses as healthy seal for lower speeds. This may confirm the effectiveness of Equation (7.3) to predict the AE excitations due to asperity collisions.

Since the sealing performance of defective seal is not good enough, leakage happens in the hydrodynamic lubrication regime. As a result, a big difference is seen between the power trend predicted by Equation (7.7) for the sliding speed and what achieved in the defective seal test, see Figures 8.23 and 8.24. Based on Equation (7.7), the power value predicted by model is greater than unit value, however that trend is not achieved here. This gives good evidence that the Equation (7.7) can be effectively applied to detect the leakage condition which is the main situation that shows the failure of a mechanical seal. Moreover, the value of coefficient of determination is significantly lower than the achieved value in healthy case.

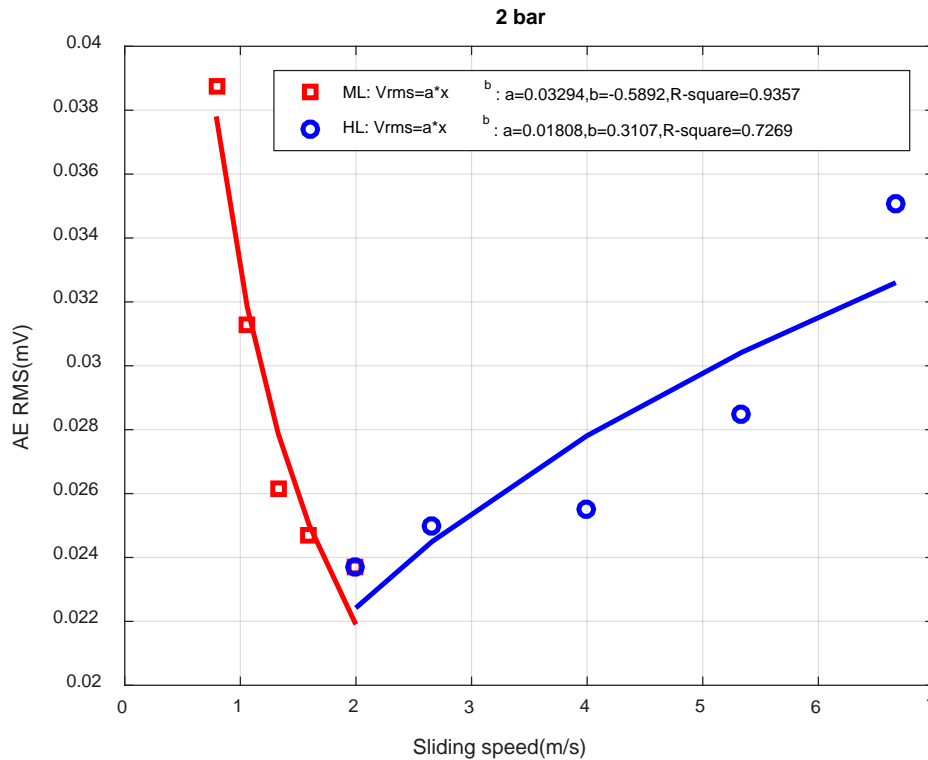


Figure 8.22 The relationship between AE RMS value and sliding speed in defective seal test under 8 bar

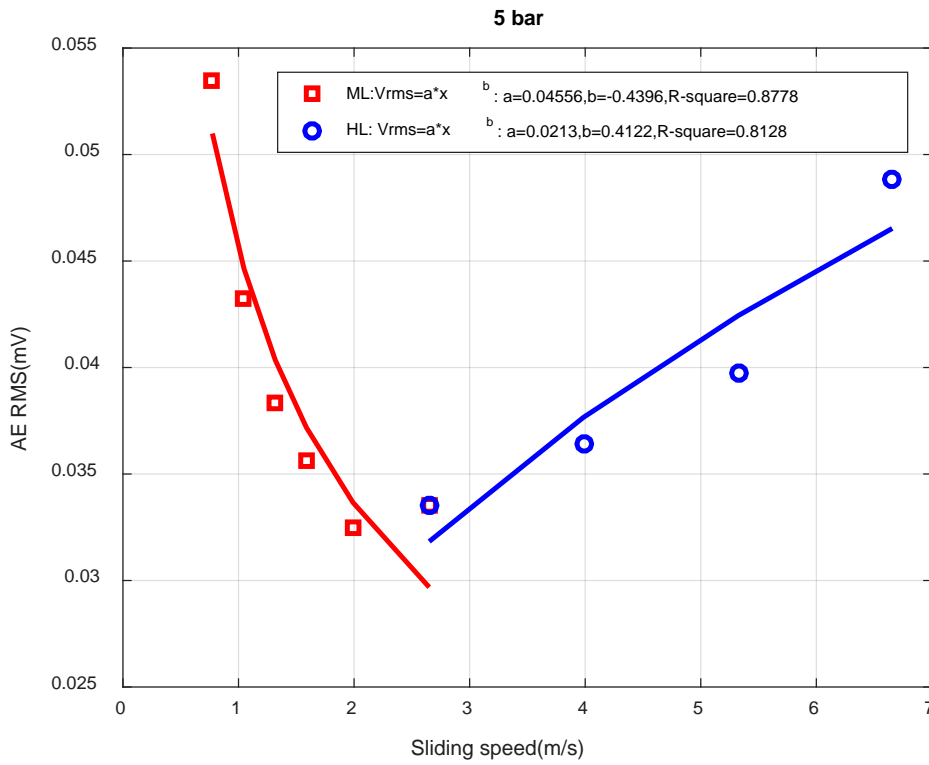


Figure 8.23 The relationship between AE RMS value and sliding speed in defective seal test under 5 bar

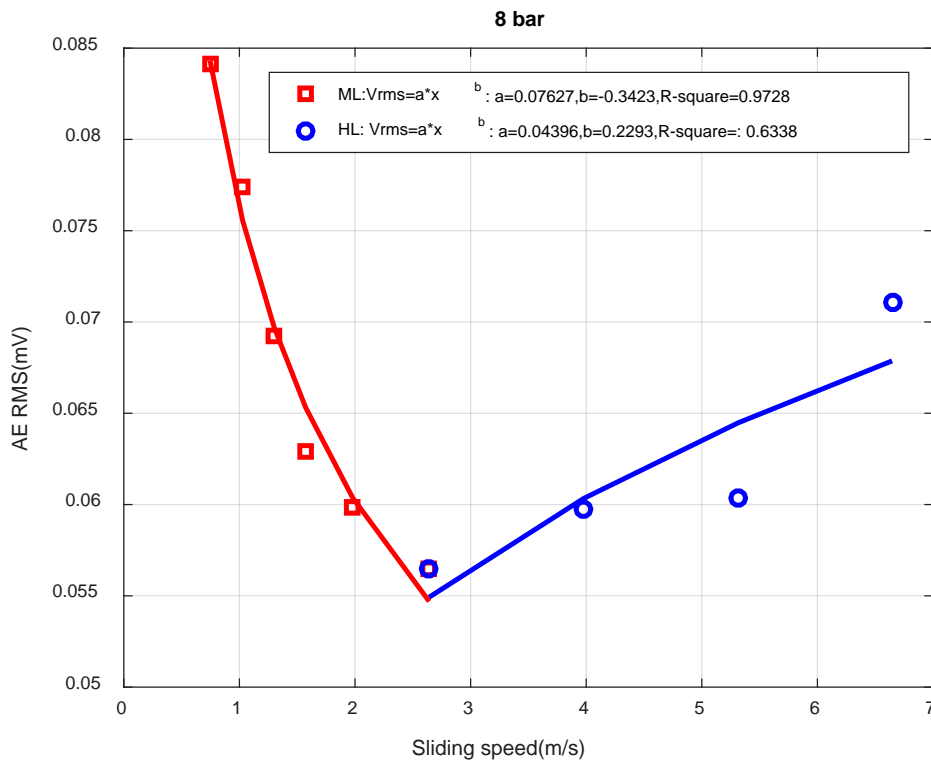


Figure 8.24 The relationship between AE RMS value and sliding speed in defective seal test under 8 bar

Figure 8.25 presents the test results to investigate the effect of sealed pressure on AE RMS value when the defective seal is operated at low speeds. As it is illustrated in Figure 8.25 (a)-(e), the liner polynomial trend predicted for contact load by Equation (7.13) is achieved with acceptable accuracy. The best coefficient of determination is achieved for speed 120 rpm, Figure 8.25 (a). In general, by increasing the speed the coefficient of determination goes down due to better lubrication condition and less asperity interactions.

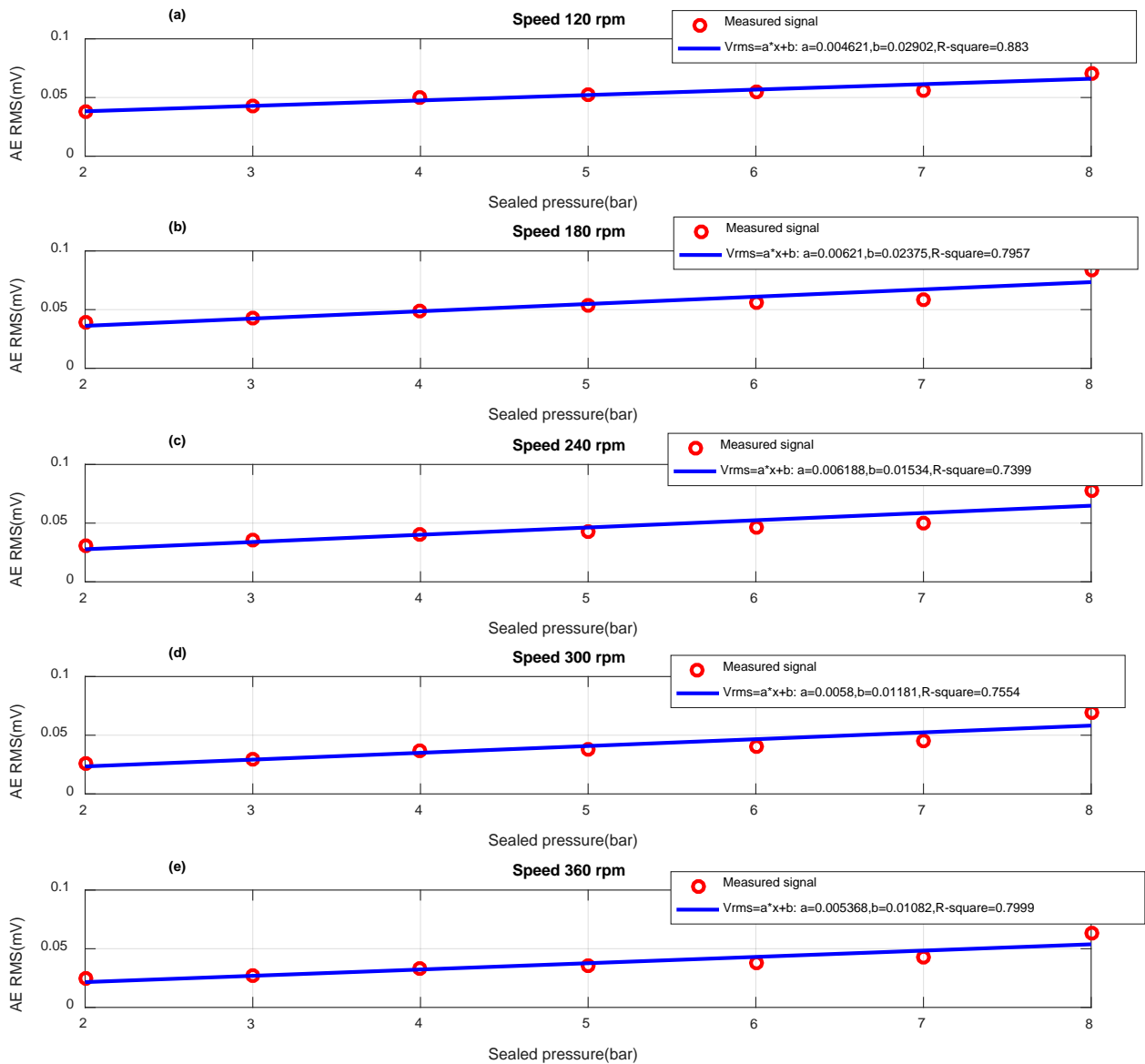


Figure 8.25 The relationship between AE RMS value and sealed pressure in defective seal test

8.5 Main Findings

In this chapter, AE responses were discussed to estimate the state of mechanical seals and acquisition of some information by which common seal failures i.e. dry running, spring fault, and damaged seal are detected. The AE features were used in this chapter are row time domain signal, RMS value of AE signal, Kurtosis and the amplitude in frequency domain

In partial dry running test as well as spring out test the amplitude of AE signal is higher for the faulty case and it includes more burst type AE responses. For defective seal test, the amplitude of AE signal as well as the number of burst type responses increases in low speed. By increasing the speed to the hydrodynamic lubrication regime, the seals become fully separated and leakage occurs due to the fact that sealing is not performed properly. Consequently, the AE amplitude and the number of burst type responses decrease.

Analysis the results of AE RMS value in terms of rotational speed of shaft shows a good sensitivity of this feature to the change in the frictional state of sealing gap. Whether more or less asperity deformation happen (depend on the type of fault and lubrication state) AE RMS value gives good response to the frictional state of sealing gap. The effectiveness of AE models developed in this work has been confirmed again. The developed equations are effectively able to detect the leakage which is the main failure symptom of mechanical seals.

To explain the results of kurtosis analysis, the main strategy developed in Chapter 7 was used. On the basis of this strategy, the kurtosis of AE data was shown to be an effective tool to separate healthy and faulty cases especially at lower speeds.

Analysis the results in frequency domain is in good agreement with analysis the amplitude of time domain signal. However, in some cases which the amplitude of AE signal is very close for both healthy and faulty case (such as in spring out test), the frequency domain analysis gives better separation between healthy and faulty case.

Chapter Nine;

Conclusions and Future Work

This chapter summarises the achievements and key conclusions arising from this thesis on the basis of the objectives defined in Chapter 1. This is started with a summary of the objectives, an explanation of how objectives were achieved and the key findings drawn from this research. This is followed by a summary of the author's key contributions to knowledge and the novel aspects of the research undertaken. Finally, suggestions are made for future research avenues in condition monitoring of mechanical seals that would advance the investigations presented in this research work.

9.1 Review of the Thesis Objectives and Achievements

The achievements and contributions of this work are presented in this chapter. This research has focused on the study of the tribological behaviour of mechanical seals for the purpose of on-line condition monitoring and fault detection

Theoretical analysis and experimental studies were carried out on the tribological AEs from a purposely built test rig, and a selection of signal processing methods were implemented to investigate the effect of tribological behaviour of sealing gap on the AE signal characteristics. The key challenge and focus of this research is to identify effective AE signatures and feature parameters for diagnosing mechanical seals under wide operating conditions. Focus is paid to explain the tribological behaviour of the mechanical seals based on a mathematical model that has been developed to describe the elastic energy released from dominant AE sources in the sealing gap. These are essential for condition monitoring and fault detection purposes in mechanical seals.

The key achievement of this study is that a novel AE based condition monitoring technique has been developed for monitoring the tribological behaviour of mechanical seals. This provides a fundamental basis for the purpose of fault detection in mechanical seals.

Following the key achievement, a number of main achievements are realised in this research, which are depicted as:

Objective 1: To perform a literature review and establish the theory, evidence and knowledge gaps in relation to nonlinear tribological behaviour and condition monitoring of mechanical seals.

Achievement 1: The concept of tribological behaviour of mechanical seals as well as the key parameters in operation of mechanical seals have been discussed in Chapter 2. Then different condition monitoring techniques were briefly reviewed to assist in understanding of their advantages and disadvantages to monitor the condition of mechanical seals, Section 4.1 includes a critical discussion of key studies in this area. On this basis, AE was selected to monitor the tribological behaviour of mechanical seals. By reviewing previous literature, it was also identified that direct asperity contact between the mating faces is considered as the main parameter for the failure of mechanical seals. However, it was understood from Chapter 2 that mechanical seals ideally work around the transition point from the mixed to the hydrodynamic lubrication regime, where the minimum level of rubbing (asperity contact)

occurs between mating faces. From here it was achieved that other mechanisms such as viscous friction in lubricant layers as well as flow induced asperity deformations are contributing in nonlinear tribological behaviour of mechanical seals. These novel concepts were discussed in Section 5.6 and 5.7.

Objective 2: To carry out a comprehensive literature review and provide a theoretical basis for monitoring the tribological behaviour of rotating machines based on AE measurements.

Achievement 2: The concept of AE condition monitoring as well as the effectiveness of technique for monitoring the condition of rotating machines were discussed in Chapter 4. A general discussion was made on the propagation modes of stress waves under different boundary conditions that mathematically shows the complexity of the AE phenomenon. It was found that to establish a successful condition monitoring system, the characteristics of AE waves in real measurement such as attenuation and distortion of wave form are needed to be fully understood.

Objective 3: To improve the performance of and design and construct new parts for available mechanical seal test rig to simulate wide range of operating parameters and desired faults.

Achievement 3: Based on the literature review has been carried out in this research it was found that little research on condition monitoring of mechanical seals using industrial test rigs are available. Hence as one of the objectives of this thesis, a novel test rig for research on the condition monitoring of mechanical seals was designed and constructed in Chapter 6. To ensure the test rig replicates the usual seal arrangement in practical applications such as pumps, real industrial mechanical seals rather than just pairs of face seal materials were employed. To get stronger AE signals, larger mechanical seals for larger pumps were selected. Since in the studies related to tribological behaviour of mechanical seals remarkable values of temperature rise have been reported, keeping the temperature near the isothermal condition was another objective itself. Hence a novel auxiliary circulating system was designed and added to the test rig. Using this system, the changes in temperature was so small (the temperature of working fluid was kept around $26 \pm 2^\circ\text{C}$ during tests) that it can be considered logically as a near isothermal conditions.

Objective 4: To model the acoustic emission level caused by different AE sources at the sealing gap in terms of operating speed, load and other working parameters.

Achievement 4: The development of an effective mathematical model that can predict the level of AE excitations from different source mechanism at the sealing gap was one of the main objectives of this research. Chapter 5 successfully proved an approach to mathematical modelling of strain energy released during the elastic deformation of asperities as well as shearing of the sealed fluid in the sealing gap, these are considered as the dominant AE sources in this research.

However due to importance of monitoring the tribological behaviour of mechanical seals it is worthy to develop a strong theoretical basis that can explain the level of AE signals from different lubrication conditions of mechanical seals. To achieve this the developed models for different AE source mechanisms were mixed together based on the tribological behaviour of mechanical seals in Sections 7.4.1 and 7.4.2. According to these models it is possible to describe AE level under different lubrication regimes of mechanical seals that has not been reported in previous works.

Objective 5: To develop MATLAB codes for processing the data outputs from the sensors.

Achievement 5: This thesis adopted the data-streaming technology and developed a novel AE measurement in Section 6.3. This novel system allowed sufficient original AE signal to be saved on a hard disk without any interruption. Processing and analysis was performed using MATLAB programming including time domain, frequency domain, time -frequency domain as well as useful statistical parameter analysis.

Objective 6. To design a comparative experimental program to find the proper frequency band that can present the tribological behaviour of sealing gap.

Achievement 6: One of the main objectives of this research was to identify the proper frequency range that can present the tribological behaviour of AE sources. As long as this objective is not achieved further processing of data may lead to wrong results. In general, the difficulty of the AE condition monitoring lies in the highly interacting influence of different AE sources as well as background noises on the generation of AE signals during the operation of mechanical seals. Hence a comparative experimental program was designed including three different tests: sealed free test, static test, transient speed test, Section 6.5. The recorded data were fed into an advance computing method in time-frequency domain so that reliable and effective results could be gained. Based on the results the main AE frequency band was found to be in the range of 270 ± 35 kHz and it did not shift under different operational conditions.

Objective 7. To design and carry out an experimental program that simulates different lubrication regimes in the operation of mechanical seals.

Achievement 7: To investigate the tribological behaviour of mechanical seals and provide a baseline for the research, a comprehensive experimental program has been designed and carried out. The aim of this experimental study was to demonstrate a correlation between AE signal parameters in time domain and frequency domain with different lubrication regimes of mechanical seals. To achieve this the experiment program has been designed with a matrix configuration including 7 different loads and 10 different speeds to simulate different lubrication conditions, as discussed in Section 6.5.4.

Objective 8. To extract of the effective AE features to monitor the tribological behaviour of mechanical seals.

Achievement 8: In spite of the fact that the analysis in the time-frequency domain has been carried out to distinguish signal from noise, it was not effective to indicate the mechanism of the frictional AE sources as well as severity of asperity deformations in the sealing gap. Hence to investigate the frictional behaviour of sealing gap under different lubrication regimes, the raw AE signals have been analysed in time domain and frequency domain that can provide much more details. Some simple statistical features including RMS and kurtosis are found to be useful to monitor the tribological behaviour of the sealing gap. The interconnections between these AE features and developed model have been demonstrated.

Objective 9. To implement experiments to replicate common faults in the mechanical seals.

Achievement 9: To prove the potential of the tribological AEs to detect the seal faults at early stages, three different common failure modes of mechanical seals were tested: partial dry running test, spring fault test and defective seal test. The main achievement of this original experimental program was to prove the significant change of the AE features from the faulty seal that makes it possible to perform a robust comparison against the baseline. The analysis of the experiment data verified the AE features extracted to study the baseline are also effective to detect faults in mechanical seals.

Objective 10: Study and verification of developed mathematical models to investigate tribological behaviour of mechanical seals and for detecting faults.

Achievement 10: The design of baseline experiment as well as fault simulation program were carried out to examine the change of AE signatures in terms of sealed pressure and sliding speed for both healthy and faulty conditions. It was found that there was underlying relationship between the AE RMS and the change of the operational conditions in mechanical seals (see Section 5.2). The results of the conducted experimental study also had a good agreement with the model developed in Chapter 6. This original work now is able to predict the AE level under different lubrication regimes of mechanical seals, especially in mixed and hydrodynamic lubrication regime where no previous model is available. In addition, a significant deviation from the model was observed when leakage occurred in mechanical seals. This gives a good evidence that the proposed equations are effective for the purpose of fault detection at early stages.

Objective 11: To provide future researches in condition monitoring of mechanical seals with a new and different idea for further work.

Achievement 11: A number of recommendations are given for future work (see Section 9.4) on the condition monitoring of mechanical seals using AE measurements. Furthermore, the mathematical model developed in this research is now ready to be used for more advanced examination in wider range of operating conditions.

9.2 Conclusions of the Research

The main objective of this research was to investigate the tribological behaviour of mechanical seals for on-line condition monitoring and fault diagnosis based on AE measurement. The following key conclusions can be drawn based on the theoretical and experimental studies which have been presented in the previous chapters.

9.2.1 Conclusions on the AE Measurement and Signal Processing

1. The barrier for a successful AE condition monitoring is the difficulty in distinguishing AE signals generated by the seal itself from those by other sources and from the background noise. Studies in Chapter 7 also shown that the resonate frequency of the AE sensor as well as natural frequency of mating ring may cause some difficulties in interpreting the results. This requires an appropriate experimental procedure and signal processing method.
2. Advanced data analysis can be conducted in the time domain, frequency domain and time-frequency domains by using the novel data streaming technology developed in

this work. The studies in Chapters 3 and 7 has proved that the analysis in the time-frequency domain can be used to distinguish the tribological AEs from the background noises. However, it is not effective to indicate the mechanism of the AE source mechanisms. The main reason of such a lack of efficiency is due to the complexity of frictional process that generates AE waves in the sealing gap. Therefore, to study the tribological behaviour of mechanical seals at different lubrication regimes, the raw AE signals have been analysed in time domain and frequency domain that can provide much more details.

9.2.2 Conclusions on Monitoring the Tribological Behaviour of Mechanical Seals using AE Measurements

1. The main AE frequency band during the operation of mechanical seals was in the range of 235 ± 35 kHz and it did not shift under different operational conditions.
2. Based on the results of transient speed test, the amplitude of AE signal increases by rotational speed increase at higher speeds. Since mechanical seals are designed to work in the hydrodynamic lubrication regime at higher speeds, it can be concluded that in addition to direct asperity contact other AE sources exist in the sealing gap.
3. Three main mechanisms are contributing to generate tribological AEs in the sealing gap i.e. direct asperity contact, fluid induced asperity deformation and viscous friction in the lubricant layers. The former is significant in the boundary lubrication regime and the latter is dominant in the hydrodynamic lubrication regime. In the mixed lubrication regime, the interaction between direct asperity contact and viscous friction generates high frequency AE signals.
4. Based on the mathematical models have been developed in this work, in direct asperity contact the root mean square value of AE signals is linearly proportional to the coefficient of friction and contact load. Also it is proportional to the square root of sliding speed. In viscous friction and fluid induced deformations the effect of sliding speed is dominant as the sealing gap changes by the speed change. In both models the root mean square of AE signals increases linearly with the sliding speed increase, also it is proportional with the square root of viscosity. In all models topography of the contact zone plays an important role.
5. Based on the understandings from modelling of AE source mechanisms (Section 7.4), the rate of AE energy release in the hydrodynamic lubrication regime can be

expressed as $\dot{U}_{AE} \propto \tau A V^\alpha \phi(z)$, while in the mixed lubrication regime the rate of AE energy release is given by $\dot{U}_{AE} \propto W^\beta V^\gamma \phi(z)$. Where τ is the shear strength of the lubricant layers, A is the sealing interface area, V is the sliding speed, α is a positive constant determined by the size of sealing gap and $\phi(z)$ is a dimensionless parameter refers to standard height distribution of asperities, W is the contact load, β is a positive constant determined by the number of contact asperities and γ is a positive constant determined by sliding distance between contact asperities.

6. When mating faces come to contact (e.g. by increasing the load) two types of asperity interaction occurs. First those asperities that their heights are larger than the average value of all asperity heights (it is called peak asperities) come to contact. Based on Equations (5.22) and (5.36), these asperities produce higher rates of AE excitations as they are subjected to more bending deformation. Therefore, the peak asperity deformation is responsible to generate burst type AE signals. By reducing the sealing gap those asperities that their heights are close to the average value of all asperity heights come to contact (massive contact) and hence more continuous type AE signal is generated.
7. When mating faces become separated (e.g. by increasing the speed) two types of asperity deformations occur in the hydrodynamic lubrication regime. First those asperities that their heights are close to the average value of all asperity heights become separated and continuous compression and release in them due to flow of lubricant fluid produces more continuous type AE signals. In the meantime, direct asperity collisions occur in the peak asperities that is responsible for the burst type AE signals. By increasing the speed gradually, the mating surfaces become fully separated and flow induced deformation in peak asperities generates burst type AE responses.
8. Based on the analysis of the time domain signal, burst type AE responses exist in different sealed pressure and speed settings. This confirms that in the boundary and mixed lubrication regimes directed peak asperity contact generates burst type AE responses while in the hydrodynamic lubrication regime, the flow induced deformation that occurs in the peak asperities is dominant and hence produces this type of AE signals.

9. The average value of AE RMS could be used as a parameter triggering different levels of alarm in a long term on-line condition monitoring of mechanical seals. The mathematical models and the results of experimental studies have been conducted in this thesis (Section 7.4) revealed that there was a strong relationship between the AE RMS value and the change of lubrication regimes in mechanical seals. A very good agreement was achieved between the predicted and measured signals, Chapters 7 and 8. The effectiveness of AE RMS together with the simplicity of its calculation made it an attractive AE feature for the condition monitoring of rotating machines.
5. Kurtosis was a useful AE feature to indicate the severity of asperity contact between mechanical seal faces during operation. It was found that the value of kurtosis could reveal whether the contact only involved some peak asperities or massive ones (Section 7.3.3). When peak asperity deformation happen the kurtosis sees higher values. The more massive asperity deformation happens; the more kurtosis is close to the one related to normal distribution. Hence it provided the feature to insight into the operational behaviour of mechanical seals under different tribological regimes.

9.2.3 Conclusions on Fault Detection in Mechanical Seals using AE Measurements

1. In the partial dry running test as well as spring out test the amplitude of AE signal is higher for the faulty case and it includes more burst type AE responses. This is mainly due to more energy release from elastic deformation of asperities due to dry contact and uneven deformation of the sealing gap. The former is more dominant in partial dry running test and the latter plays more important role in the spring out test. |
2. For the defective seal test, the amplitude of the AE signals as well as the number of burst type responses increase at low speed by the speed increase. By increasing the speed to the hydrodynamic lubrication regime, the seals become fully separated and leakage occurs due to the fact that sealing is not performed properly. Consequently, the AE amplitude and the number of burst type responses decrease.
3. Analysis the results of AE RMS value shows a good sensitivity of this feature to the change in the frictional state of the sealing gap. Whether more or less asperity deformation happen (depend on the type of fault and lubrication state) AE RMS value gives good response to the frictional state of sealing gap. Since the mathematical models developed in Chapter 5 are based on AE RMS value, this gives a good

evidence that using those equations it is possible to understand the complex tribological behaviour of the sealing gap even under faulty conditions.

4. When asperity deformations (whether direct contact or fluid induced) take place in peak asperities (such as in lower speeds for partial dry running test), the kurtosis sees higher values due to decrease in standard deviation of data. The more asperities which those heights are close to average value of asperity heights come in contact, the standard deviation sees higher values and hence the kurtosis goes down and gets closer to Gaussian distribution (such as in higher speeds for spring out test). In partial dry running test, the kurtosis sees higher values compared with baseline at low speeds. This gives a good evidence for the purpose of fault detection at lower speeds. However, it is immediately noticed that the kurtosis of AE signals related to the faulty case sees unexpected fluctuations especially at higher speeds. A plausible explanation is that kurtosis is more affected by the volume of asperity deformation (e.g. sealed pressure) rather than the severity of elastic deformations (e.g. sliding speed).
5. Analysis the results in frequency domain is in good agreement with analysis the amplitude of time domain signal. However, in some cases that the amplitude of AE signal related to faulty case is very close to baseline (such as spring out test), the frequency domain analysis gives better separation between healthy and faulty cases.

9.3 Novel Feature Summary and Contribution to the Knowledge

This section summarises main aspects of novelty in developing on-line condition monitoring for mechanical seals, which have been incorporated a number of important advancements that are novel and not previously implemented by other researchers and practitioners. The following are the highlighted novel points.

Novelty One:

The thesis has identified that the key factor for the condition monitoring of mechanical seals was the deformation of asperities as well as viscous friction in the sealing gap (Section 5.3). No previous research investigated the relationship between AE signals and novel AE sources introduced in this work to investigate the tribological behaviour of mechanical seals. It is novel to have proved that the AE signals from operation of mechanical seals are caused by the asperity deformations in different tribological regimes (Section 7.3).

Novelty Two:

It is believed that dynamic modelling of the AE signatures generated by the asperity deformations in the sealing gap is a novel and reliable approach. Using this model, it is possible to give a clear and comprehensive explanation to the change of AE features under both healthy and faulty conditions. Also modelling the AE generated by the viscous friction in fluid layer is part of the new knowledge produced in this thesis.

Novelty Three:

The author of this thesis believes that the combination of mathematical models developed for different AE sources in Chapter 7 produced general equations that can explain the tribological behaviour of mechanical seals under both healthy and faulty conditions. This is the first time that such a comprehensive model is proposed.

Novelty Four:

It is believed that the improvements in the primary design of test rig is novel due to the fact that it was not possible to run the primary rig under the speeds less than 600 rpm to simulate boundary and mixed lubrication regimes. Also author of this thesis believes that simulating defective seal and spring fault seal on previous configuration was not possible. Mechanical seals are fragile; every single component in the seal head assembly is designed to do a specific function. They are not designed to work even under very small degrees of faulty conditions. Author believes that running the test rig with the faulty seals so that it can simulate different lubrication regimes is novel. No previous work is available in this area.

Novelty Five:

The author of this thesis believes that the application of AE RMS value to identify different lubrication regimes under healthy and faulty conditions is part of the new knowledge produced in this thesis. Moreover, kurtosis of AE signal acquired from operational mechanical seals was given a physical meaning based on the mathematical models developed in this research. It is novel to relate the kurtosis to the tribological behaviour of mechanical seals.

9.4 Recommendations for Future Work

Recommendation 1: During this research three different faults have been simulated and the severity of fault was not investigated. The study of different degrees of damaged faces is

recommended. To simulate the condition under which leakage occurs in the mechanical seals, it is suggested to reduce the total stiffness by changing the springs rather than taking them off. Moreover, instead of partial dry running test, it is recommended to drain the sealing chamber slowly and investigate the changes in AE features. It is immediately noted that this may cause failure of the seals.

Recommendation 2: As discussed in Chapter 2 tribology has two aspects, friction and wear. Study the change of AE features under different degree of wear is recommended. To do this a pair of approximately unbalance mating faces can be used to provide more closing force in the sealing gap. It is expected that gradual wear happens until the failure of the seals. As discussed in Section 2.6, different wear mechanisms may contribute in the failure of the seals. Hence it is necessary to investigate which one is dominant under different lubrication regimes. Also mathematical models are needed to explain the RMS value of AE signals based on operating parameters of the rig under the wear condition.

Recommendation 3: Primary studies in this research shown that the temperature rise in the sealing gap is significant even if a good circulation for lubricant fluid is provided. The author believes that a strong correlation exists between AE RMS value and the temperature rise in the sealing gap. This is needed to be investigated in both theory and experiment. From the point of view of experiments, it is possible to locate two thermocouples in the back of the stationary ring to monitor the temperature change. A CFD analysis may help to extend the results to those operating conditions which are not possible to be simulated on the rig.

Recommendation 4: Useful AE features have been extracted in this research to identify the tribological behaviour of mechanical seals under healthy and faulty conditions. On the basis of these features, it is possible to develop an intelligent AE fault detector using metaheuristic algorithms or artificial neural networks. Since this thesis has developed an AE model to describe the tribological behaviour of the sealing gap under healthy and faulty conditions, it is possible to extend the data to those operating conditions which are not possible to be simulated on the rig.

Recommendation 5: Developing more advanced signal processing methods in the time, frequency and time-frequency domains is suggested. The advanced signal processing tool boxes developed in future research can be used to identify different lubrication regimes as well as different failure modes of mechanical seals. With the aid of this information it is possible to increase the reliability of mechanical seals both in design and manufacture.

Recommendation 6: Since it has been proven in Chapter 5 that a clear relationship exist between coefficient of friction and RMS value of AE signal in direct asperity contact, the dependency of AE level on the coefficient of friction needs to be investigated. It can be done by installing a torque meter on the shaft. To make more sensible results, application of lubricants with different viscosity (i.e. different oils) is recommended.

Recommendation 7: Based on the literature review has been done in Chapter 2, it was found that surface texture of mating faces has a significant effect on the hydrodynamic pressure build up. Also based on the models developed in Chapters 5 and 7, the AE level is influenced by surface roughness. Hence the effect of surface texture on the tribological behaviour of mechanical seals needs to be investigated. To do this it is possible to create different surface textures by rubbing the mating faces when abrasive diamond particle is spayed between them. Alternatively, a polishing plane can be used and seal faces can be slightly polished.

Recommendation 8: It has been illustrated in Chapter 6 the shaft of the test rig was supported by two deep grove ball bearings. Hence it is suggested to investigate the effect of bearing faults on the seal performance. Different test procedures such as single fault in a bearing, single fault in both bearings and combined faults can be considered. To interpret the results, proper signal processing algorithms should be applied.

Recommendation 9: In this research the effects of churning fluid in the seal chamber, as a significant AE source at higher speeds, has not been considered. Therefore, it is recommended to study the effects of AE excitations from the viscous friction in the sealing chamber on the signals generated by the AE source mechanisms (see Section 5.3) in the sealing gap. To investigate AE signal from churning fluid, it is suggested to take the mating ring of (while the primary ring is attached to the shaft) and run the rig at higher speeds. It is immediately noted that it is not possible to pressurize the seal chamber during this test.

Recommendation 10: In this research some AE features extracted from AE wave form in time domain (e.g. RMS and kurtosis) have been highlighted. Other potential useful features are needed to be more investigated. It is important to clarify the physical concept behind the such features.

Bibliography

1. Lebeck, A.O., *Principles and design of mechanical face seals*. 1991: John Wiley & Sons.
2. Lubbinge, H., *On the lubrication of mechanical face seals*. 1999: Universiteit Twente.
3. Payne, J.W., *Feasibility study of a controllable mechanical seal for reactor coolant pumps*. 2013.
4. Flitney, R.K., *Seals and sealing handbook*. 2011: Elsevier.
5. Summers-Smith, J.D., *Mechanical seal practice for improved performance*. 2005: Wiley.
6. Plumridge, J. and R. Page, *The development of more tolerant mechanical seals*, in *Proceedings of Shaft Sealing in Centrifugal Pumps*. 1992.
7. Flitney, B., *Review of features in Sealing Technology during the last year*. *Sealing Technology*, 2005. **2005**(5): p. 6-11.
8. Jianjun, S., W. Long, and G. Boqing, *The development course and the research trend of mechanical seal*. *Lubrication Engineering*, 2004(4): p. 128-134.
9. Wei, L., et al., *Research on friction characteristic of end faces of mechanical seals*, in *Advanced Tribology*. 2009, Springer. p. 304-308.
10. Ponce, D.C., *Condition monitoring of o-rings and Lip seals*. 2014, University of Sheffield.
11. Semple, A.J. and J. Carchpole, *Improving the reliability of seal systems for pipeline and high-pressure pumps*, in *Proceedings of Reliability of Sealing System for Rotating Machinery*. 1999: London.
12. de Azevedo, H.D.M., A.M. Araújo, and N. Bouchonneau, *A review of wind turbine bearing condition monitoring: State of the art and challenges*. *Renewable and Sustainable Energy Reviews*, 2016. 56: p. 368-379.
13. Zhu, G., *Computer prediction of mechanical seal performance and experimental validation*. *Proceedings of the Institution of Mechanical Engineers, Part J: Journal of Engineering Tribology*, 1999. 213(6): p. 433-449.
14. Davies, A., *Handbook of condition monitoring: techniques and methodology*. 2012: Springer Science & Business Media.
15. Sharma, D.M., *Condition monitoring of wind turbines: a review*. *Global Journal of Researches In Engineering*, 2013. 13(6).
16. Fan, Y.E., *Condition monitoring of mechanical seals using acoustic emissions*. 2007, University of Manchester.
17. Constantinescu, I. and I. Etsion, *Experimental of the Dynamic Behavior of Non-contacting Coned-faces Mechanical Seal*. *ASLE Transactions*, 1984. **27**(3): p. 263-270.
18. Green, I., *Real-time monitoring and control of mechanical face-seal dynamic behaviour*. *Sealing Technology*, 2001. 2001(96): p. 6-11.
19. Anderson, W., J. Jarzynski, and R. Salant, *Monitoring the condition of liquid-lubricated mechanical seals*. *Sealing Technology*, 2002. 2002(2): p. 6-11.
20. Reddyhoff, T., R. Dwyer-Joyce, and P. Harper, *Ultrasonic measurement of film thickness in mechanical seals*. *Sealing Technology*, 2006. 2006(7): p. 7-11.
21. AlShammari, F. and A. Addali, *Bearing Condition Monitoring with Acoustic Emission Techniques*. *World Academy of Science, Engineering and Technology, International Journal of Mechanical, Aerospace, Industrial, Mechatronic and Manufacturing Engineering*, 2015. **9**(12): p. 1828-1832.

22. Hawman, M. and W. Galinaitis. *Acoustic emission monitoring of rolling element bearings*. in *Ultrasonics Symposium, 1988. Proceedings., IEEE 1988*. 1988. IEEE.
23. Márquez, F.P.G., et al., *Condition monitoring of wind turbines: Techniques and methods*. *Renewable Energy*, 2012. 46: p. 169-178.
24. Toutountzakis, T., C.K. Tan, and D. Mba, *Application of acoustic emission to seeded gear fault detection*. *NDT & E International*, 2005. 38(1): p. 27-36.
25. Orcutt, F., *An investigation of the operation and failure of mechanical face seals*. *Journal of Lubrication Technology*, 1969. 91(4): p. 713-725.
26. Anderson, D., J. Jarzynski, and R. Salant, *Condition monitoring of mechanical seals: detection of film collapse using reflected ultrasonic waves*. *Proceedings of the Institution of Mechanical Engineers, Part C: Journal of Mechanical Engineering Science*, 2000. 214(9): p. 1187-1194.
27. Fan, Y.B., F.S. Gu, and A. Ball. *Acoustic emission monitoring of mechanical seals using MUSIC algorithm based on higher order statistics*. in *Key Engineering Materials*. 2009. Trans Tech Publ.
28. Li, X., et al., *The contact state monitoring for seal end faces based on acoustic emission detection*. *Shock and Vibration*, 2015. 2016.
29. Kataoka, T., C. Yamashina, and M. Komatsu. *Development of an incipient failure detection technique for mechanical seals*. in *Proceedings of 4th International Pump Symposium, Houston, Texas*. 1987.
30. Miettinen, J. and V. Siekkinen, *Acoustic emission in monitoring sliding contact behaviour*. *Wear*, 1995. 181: p. 897-900.
31. Mba, D., et al., *Application of acoustic emission technology for detecting the onset and duration of contact in liquid lubricated mechanical seals*. *Insight-Non-Destructive Testing and Condition Monitoring*, 2006. 48(8): p. 486-487.
32. Holenstein, A.P., *Diagnosis of mechanical seals in large pumps*. *Sealing Technology*, 1996. 1996(33): p. 9-12.
33. Hisakado, T., H. Suda, and M. Sekine, *Relation between lubricated wear of ceramics and acoustic emission characteristics*. *Tribology transactions*, 1998. 41(2): p. 209-216.
34. Boness, R. and S. McBride, *Adhesive and abrasive wear studies using acoustic emission techniques*. *Wear*, 1991. 149(1): p. 41-53.
35. Benabdallah, H. and D. Aguilar, *Acoustic emission and its relationship with friction and wear for sliding contact*. *Tribology Transactions*, 2008. 51(6): p. 738-747.
36. Sikorska, J. and D. Mba, *Challenges and obstacles in the application of acoustic emission to process machinery*. *Proceedings of the Institution of Mechanical Engineers, Part E: Journal of Process Mechanical Engineering*, 2008. 222(1): p. 1-19.
37. Tandon, N., K. Ramakrishna, and G. Yadava, *Condition monitoring of electric motor ball bearings for the detection of grease contaminants*. *Tribology international*, 2007. 40(1): p. 29-36.
38. Sadegh, H., A.N. Mehdi, and A. Mehdi, *Classification of acoustic emission signals generated from journal bearing at different lubrication conditions based on wavelet analysis in combination with artificial neural network and genetic algorithm*. *Tribology International*, 2016. 95: p. 426-434.
39. Morton, J.L. and J.G. Evans. *Developments in High Performance Seal Designs for Critical High Pressure Offshore and Pipeline Applications*. in *Proceedings of the Twentieth International Pump Users Symposium*. 2003.
40. Benedict, J.K., *Macro/micro-feature development for improved hydrodynamic performance at the mechanical seal interface via laser surface texturing*. 2011.

41. Etsion, I. and I. Front, *A model for static sealing performance of end face seals*. Tribology Transactions, 1994. 37(1): p. 111-119.
42. Tournerie, B. and J. Frene, *Principal research areas on mechanical face-seals*. Tribology international, 1984. 17(4): p. 179-184.
43. Lebeck, A., *Mixed lubrication in mechanical face seals with plain faces*. Proceedings of the Institution of Mechanical Engineers, Part J: Journal of Engineering Tribology, 1999. 213(3): p. 163-175.
44. Kajdas, C., E. Wilusz, and S. Harvey, *Encyclopedia of tribology*. Vol. 15. 1990: Elsevier.
45. Tichy, J.A. and D.M. Meyer, *Review of solid mechanics in tribology*. International Journal of Solids and Structures, 2000. 37(1): p. 391-400.
46. Jamari, J., *Running-in of rolling contacts*. 2006: University of Twente.
47. Vezjak, A. and J. Vizintin, *Experimental study on the relationship between lubrication regime and the performance of mechanical seals*. Tribology & Lubrication Technology, 2001. 57(1): p. 17.
48. Winer, W.O. and M.B. Peterson, *Wear Control Handbook*. 1980: American society of mechanical engineers.
49. Qiu, Y., *Hard Surface Coating Experimental Evaluation and Thermomechanical Analysis of a Seal with Micro Heat Exchanger*. 2002, Faculty of the Louisiana State University and Agricultural and Mechanical College In partial fulfillment of the Requirements for the degree of Master of Science in Mechanical Engineering In The Department of Mechanical Engineering by Yifan Qiu B. Engr., University of Science and Technology, Beijing.
50. Jiang, X., et al. *Paradigm shifts in surface metrology. Part I. Historical philosophy*. in *Proceedings of the Royal Society of London A: Mathematical, Physical and Engineering Sciences*. 2007. The Royal Society.
51. Whitehouse, D.J., *Handbook of surface and nanometrology*. 2010: CRC press.
52. Lebeck, A. *Face seal waviness—prediction, causes, and effects*. in *Proc. 10th Intl. Conf. on Fluid Sealing*. 1984.
53. Chengwei, W. and Z. Linqing, *Effect of waviness and roughness on lubricated wear related to running-in*. Wear, 1991. 147(2): p. 323-334.
54. Mayer, E. and B.S. Nau, *Mechanical seals*, ed. M.I.R. Association. 1992.
55. Standard, I. and B. ISO, *4287/1997. Geometrical product specifications (GPS)—Surface texture: Profile method—Terms, definitions and surface texture parameters*, 1997.
56. Nau, B., *Mechanical seal face materials*. Proceedings of the Institution of Mechanical Engineers, Part J: Journal of Engineering Tribology, 1997. 211(3): p. 165-183.
57. Minet, C., N. Brunetière, and B. Tournerie, *On the lubrication of mechanical seals with rough surfaces: A parametric study*. Proceedings of the Institution of Mechanical Engineers, Part J: Journal of Engineering Tribology, 2012: p. 1350650112461581.
58. Nyemeck, A.P., N. Brunetière, and B. Tournerie, *A multiscale approach to the mixed lubrication regime: application to mechanical seals*. Tribology Letters, 2012. 47(3): p. 417-429.
59. Minet, C., N. Brunetière, and B. Tournerie, *A deterministic mixed lubrication model for mechanical seals*. Journal of Tribology, 2011. 133(4): p. 042203.
60. Saha, A., et al., *Investigation of two different friction models from the perspective of friction-induced vibrations*. Tribology International, 2015. 90: p. 185-197.

61. Adams, G.G., S. Müftü, and N.M. Azhar. *A Nano-Scale Multi-Asperity Contact and Friction Model*. in *ASME 2002 International Mechanical Engineering Congress and Exposition*. 2002. American Society of Mechanical Engineers.
62. Simon, A. and R. Belles, *Estimated state-level energy flows in 2008*. 2011.
63. Dowson, D., *History of tribology*. 1979: Addison-Wesley Longman Limited.
64. Popova, E. and V.L. Popov, *The research works of Coulomb and Amontons and generalized laws of friction*. *Friction*, 2015. 3(2): p. 183-190.
65. Braun, O. and M. Peyrard, *Dependence of kinetic friction on velocity: Master equation approach*. *Physical Review E*, 2011. 83(4): p. 046129.
66. Faraon, I.C., *Mixed lubricated line contacts*. 2005: University of Twente.
67. Akay, A., *Acoustics of friction*. *The Journal of the Acoustical Society of America*, 2002. 111(4): p. 1525-1548.
68. Pasaribu, H.R., *Friction and wear of zirconia and alumina ceramics doped with CuO*. 2005: University of Twente.
69. Fang, G., J. Zhou, and J. Duszczuk, *Effect of pocket design on metal flow through single-bearing extrusion dies to produce a thin-walled aluminium profile*. *Journal of materials processing technology*, 2008. 199(1): p. 91-101.
70. Liu, G., J. Zhou, and J. Duszczuk, *FE analysis of metal flow and weld seam formation in a porthole die during the extrusion of a magnesium alloy into a square tube and the effect of ram speed on weld strength*. *Journal of materials processing technology*, 2008. 200(1): p. 185-198.
71. Li, L.-x., J. Zhou, and J. Duszczuk, *Prediction of temperature evolution during the extrusion of 7075 aluminium alloy at various ram speeds by means of 3D FEM simulation*. *Journal of Materials Processing Technology*, 2004. 145(3): p. 360-370.
72. Duan, X., X. Velay, and T. Sheppard, *Application of finite element method in the hot extrusion of aluminium alloys*. *Materials Science and Engineering: A*, 2004. 369(1): p. 66-75.
73. Wei, L., P.G. Zhang, and G.F. Fang. *Simulation Calculation of Friction Factor of the End Face for Mechanical Seals Based on Fractal Theory*. in *Applied Mechanics and Materials*. 2014. Trans Tech Publ.
74. Massaro, A., *The «mating pairs» concept for mechanical face seals*. *Lubrication engineering*, 1988. 44(5): p. 436-446.
75. Wassink, D.B., et al., *Physically based modeling of reciprocating lip seal friction*. *Journal of tribology*, 2001. 123(2): p. 404-412.
76. Buck, G., *Estimating heat generation, face temperature and flush rate for mechanical seals*. *PumpUsers Expo'99*, 1999: p. 167-172.
77. Somanchi, A.K., *A novel mechanical seal design with superior thermal characteristics*. 2004, Faculty of the Louisiana State University and Agricultural and Mechanical College In partial fulfillment of the Requirements for the degree of Master of Science in Mechanical Engineering In The Department of Mechanical Engineering By Anoop Kumar Somanchi B. Engr., RVR & JC College of Engineering.
78. Yu, X., S. He, and R. Cai, *Frictional characteristics of mechanical seals with a laser-textured seal face*. *Journal of Materials Processing Technology*, 2002. 129(1): p. 463-466.
79. Mayer, E., *Mechanical Seal*. 1981, Beijing.: Chemical Industry Press
80. Tabor, D., *Friction—the present state of our understanding*. *Journal of lubrication technology*, 1981. 103(2): p. 169-179.

81. Kato, K., *Classification of wear mechanisms/models*. Proceedings of the Institution of Mechanical Engineers, Part J: Journal of Engineering Tribology, 2002. 216(6): p. 349-355.
82. Williams, J., *Wear modelling: analytical, computational and mapping: a continuum mechanics approach*. Wear, 1999. 225: p. 1-17.
83. Sethuramiah, A., *Lubricated wear: science and technology*. Vol. 42. 2003: Elsevier Science Limited.
84. Meng, H. and K. Ludema, *Wear models and predictive equations: their form and content*. Wear, 1995. 181: p. 443-457.
85. Ludema, K., *Mechanism-based modeling of friction and wear*. Wear, 1996. **200**(1): p. 1-7.
86. Hsu, S. and M. Shen, *Wear prediction of ceramics*. Wear, 2004. **256**(9): p. 867-878.
87. Zmitrowicz, A., *Wear patterns and laws of wear—a review*. Journal of theoretical and applied mechanics, 2006. 44(2): p. 219-253.
88. Buck, G.S. *The Role of Hydraulic Balance in Mechanical Pump Seals*. in *Proceedings of the Seventh Turbomachinery Symposium*. 1978.
89. Cracaoanu, I., *Effect of macroscopic wear on friction in lubricated concentrated contacts*. 2010: University of Twente.
90. Karassik, I.J., et al., *Pump handbook*. Vol. 3. 1986: McGraw-Hill New York.
91. Warring, R.H., *Seals and sealing handbook*. 1981: Gulf Pub Co.
92. Tao, Z., *Analysis of Influence Factors of Friction Performance on Mechanical Seals*. Lubrication Engineering, 2000. **3**: p. 029.
93. Buck, G.S., *Pressure ratings of mechanical seals*. Sealing Technology, 1997. 1997(42): p. 8-12.
94. Brunetière, N. and B. Modolo, *Heat transfer in a mechanical face seal*. International Journal of Thermal Sciences, 2009. 48(4): p. 781-794.
95. Zhou, X., et al. *The Simulation Analysis of Spherical Mechanical Seal of Stern Shaft*. in *2015 International Industrial Informatics and Computer Engineering Conference*. 2015. Atlantis Press.
96. Pustan, M., O. Belcin, and C. Birleanu, *Mechanical seals with oscillating stator*. Meccanica, 2013. 48(5): p. 1191-1200.
97. Popa, N. and C. Onescu, *About the Tribological Behaviour of Ceramic Materials*. 2008, Tribology in Industry.
98. Wakely, K., *Mechanical seals: some developments in face materials*. Tribology international, 1986. 19(4): p. 198-203.
99. Miettinen, J., *Condition monitoring of grease lubricated rolling bearings by acoustic emission measurements*. 2000: Tampere University of Technology.
100. Drouillard, T., *A history of acoustic emission*. Journal of acoustic emission, 1996. 14(1): p. 1-34.
101. Purarjomandlangrudi, A. and G. Nourbakhsh, *Acoustic emission condition monitoring: an application for wind turbine fault detection*. International Journal of Research in Engineering Technology, 2013. 2(5): p. 907-918.
102. Förster, F. and E. Scheil, *Akustische untersuchung der bildung von martensitnadeln*. Zeitschrift für Metallkunde, 1936. 29: p. 245-247.
103. Kaiser, J., *An investigation into the occurrence of noises in tensile tests, or a study of acoustic phenomena in tensile tests*. Technische Hochschule, 1950.
104. Schofield, B., *Acoustic emission under applied stress*. 1963, DTIC Document.
105. Ohtsu, M., *The history and development of acoustic emission in concrete engineering*. Magazine of concrete research, 1996. 48(177): p. 321-330.

106. Gorman, M.R. and W.H. Prosser, *AE source orientation by plate wave analysis*. 1991.
107. Drouillard, T.F., *Anecdotal history of acoustic emission from wood*. 1990, EG and G Rocky Flats, Inc., Golden, CO (USA). Rocky Flats Plant.
108. Holroyd, T., *Acoustic emission & ultrasonics*. Machine and systems condition monitoring series, 2000.
109. Tan, C.K., P. Irving, and D. Mba, *A comparative experimental study on the diagnostic and prognostic capabilities of acoustics emission, vibration and spectrometric oil analysis for spur gears*. Mechanical Systems and Signal Processing, 2007. 21(1): p. 208-233.
110. Tandon, N. and A. Choudhury, *A review of vibration and acoustic measurement methods for the detection of defects in rolling element bearings*. Tribology international, 1999. 32(8): p. 469-480.
111. Rogers, L., *The application of vibration signature analysis and acoustic emission source location to on-line condition monitoring of anti-friction bearings*. Tribology international, 1979. 12(2): p. 51-58.
112. Al-Ghamd, A.M. and D. Mba, *A comparative experimental study on the use of acoustic emission and vibration analysis for bearing defect identification and estimation of defect size*. Mechanical systems and signal processing, 2006. 20(7): p. 1537-1571.
113. YOON, D.-J., et al., *Early detection of damages in journal bearings by acoustic emission monitoring*. Journal of acoustic emission, 1995. 13(1-2): p. 1-10.
114. Raharjo, P., et al., *An Investigation of Acoustic Emission Responses of a Self Aligning Spherical Journal Bearing*. 2011.
115. Towsyfyhan, H., et al., *Characterization of Acoustic Emissions from Journal Bearings for Fault Detection*. NDT 2013, 2013.
116. Loutas, T., et al., *Condition monitoring of a single-stage gearbox with artificially induced gear cracks utilizing on-line vibration and acoustic emission measurements*. Applied Acoustics, 2009. 70(9): p. 1148-1159.
117. Siores, E. and A. Negro, *Condition monitoring of a gear box using acoustic emission testing*. Materials evaluation, 1997. 55(2).
118. Eftekharijad, B. and D. Mba, *Seeded fault detection on helical gears with acoustic emission*. Applied Acoustics, 2009. 70(4): p. 547-555.
119. Tan, C.K. and D. Mba, *Limitation of acoustic emission for identifying seeded defects in gearboxes*. Journal of Nondestructive Evaluation, 2005. 24(1): p. 11-28.
120. Singh, A., D. Houser, and S. Vijayakar, *Detecting gear tooth breakage using acoustic emission: a feasibility and sensor placement study*. Journal of Mechanical Design, 1999. 121(4): p. 587-593.
121. MacIntire, P., *Nondestructive testing handbook: Acoustic emission testing*. 1987: American Society for Nondestructive Testing.
122. Miller, R., et al., *A reference standard for the development of acoustic emission pipeline leak detection techniques*. NDT & E International, 1999. 32(1): p. 1-8.
123. Ahadi, M. and M.S. Bakhtiar, *Leak detection in water-filled plastic pipes through the application of tuned wavelet transforms to acoustic emission signals*. Applied Acoustics, 2010. 71(7): p. 634-639.
124. El-Ghamry, M., R. Reuben, and J. Steel, *The development of automated pattern recognition and statistical feature isolation techniques for the diagnosis of reciprocating machinery faults using acoustic emission*. Mechanical Systems and Signal Processing, 2003. 17(4): p. 805-823.

125. Neill, G., et al., *Detection of incipient cavitation in pumps using acoustic emission*. Proceedings of the Institution of Mechanical Engineers, Part E: Journal of process mechanical engineering, 1997. 211(4): p. 267-277.
126. Alfayez, L., D. Mba, and G. Dyson, *The application of acoustic emission for detecting incipient cavitation and the best efficiency point of a 60kW centrifugal pump: case study*. Ndt & E International, 2005. 38(5): p. 354-358.
127. Wilkinson, P., et al., *Tool wear prediction from acoustic emission and surface characteristics via an artificial neural network*. Mechanical systems and signal processing, 1999. 13(6): p. 955-966.
128. Li, X., *A brief review: acoustic emission method for tool wear monitoring during turning*. International Journal of Machine Tools and Manufacture, 2002. 42(2): p. 157-165.
129. Nair, A., *Acoustic emission monitoring and quantitative evaluation of damage in reinforced concrete members and bridges*. 2006, Citeseer.
130. Hadzor, T.J., et al., *Development of acoustic emission evaluation method for repaired prestressed concrete bridge girders*, in *Report No. FHWA/ALDOT 930-601-1*. 2011. p. 162.
131. Grosse, C.U. and M. Ohtsu, *Acoustic emission testing*. 2008: Springer Science & Business Media.
132. Scruby, C., *An introduction to acoustic emission*. Journal of Physics E: Scientific Instruments, 1987. 20(8): p. 946.
133. Hase, A., H. Mishina, and M. Wada, *Correlation between features of acoustic emission signals and mechanical wear mechanisms*. Wear, 2012. 292: p. 144-150.
134. Lingard, S., C. Yu, and C. Yau, *Sliding wear studies using acoustic emission*. Wear, 1993. 162: p. 597-604.
135. Hase, A., M. Wada, and H. Mishina, *The relationship between acoustic emissions and wear particles for repeated dry rubbing*. Wear, 2008. 265(5): p. 831-839.
136. BSI, *Calibration and testing laboratory accreditation systems. General requirements for operation and recognition*, in *BS EN 45003:1995*. 1995: UK.
137. Graff, K.F., *Wave motion in elastic solids*. 1975: Courier Corporation.
138. Achenbach, J., *Wave propagation in elastic solids*. Vol. 16. 2012: Elsevier.
139. El-Shaib, M.N., *Predicting acoustic emission attenuation in solids using ray-tracing within a 3D solid model*. 2013, Heriot-Watt University.
140. Masserey, B., *Ultrasonic surface crack characterization using Rayleigh waves*. 2006, Diss., Technische Wissenschaften, Eidgenössische Technische Hochschule ETH Zürich, Nr. 16646, 2006.
141. Nashed, M.S., *Acoustic emission monitoring of propulsion systems: a laboratory study on a small gas turbine*. 2010, Heriot-Watt University.
142. Su, Z., L. Ye, and Y. Lu, *Guided Lamb waves for identification of damage in composite structures: A review*. Journal of sound and vibration, 2006. 295(3): p. 753-780.
143. Choi, S.-W., et al. *Ultrasonic plate wave properties in thin steel plates*. in *Control, Automation and Systems, 2008. ICCAS 2008. International Conference on*. 2008. IEEE.
144. Finlayson, R.D., et al. *Continuous health monitoring of graphite epoxy motorcases (GEM)*. in *NDE for Health Monitoring and Diagnostics*. 2003. International Society for Optics and Photonics.
145. Moore, P.O., R. Miller, and R. Hill, *Nondestructive Testing Handbook, Volume 6, Acoustic Emission Testing*, American Society for Nondestructive Testing. 2005, Inc.
146. Matthews, J.R., *Acoustic emission*. Vol. 2. 1983: CRC Press.

147. Scott, I.G., *Basic acoustic emission*. Vol. 6. 1991: CRC Press.
148. Pollock, A.A., *Classical wave theory in practical Acoustic Emission testing*. Japanese society of NDI, 1986: p. 708-720.
149. Mba, D. and L. Hall, *The transmission of acoustic emission across large-scale turbine rotors*. NDT & E International, 2002. 35(8): p. 529-539.
150. Nivesrangsan, P., J. Steel, and R. Reuben, *Acoustic emission mapping of diesel engines for spatially located time series—Part II: Spatial reconstitution*. Mechanical Systems and Signal Processing, 2007. 21(2): p. 1084-1102.
151. Theobald, P., B. Zeqiri, and J. Avison, *Couplants and their influence on AE sensor sensitivity*. Journal of Acoustic Emission, 2008. 26: p. 91-97.
152. BSI, *Condition monitoring and diagnostics of machines - Vocabulary*, in *BS ISO 13372:2004*. 2004.
153. Higgs, P.A., et al. *A survey on condition monitoring systems in industry*. in *Proceedings of the ASME 7th Biennial Conference on Engineering Systems Design and Analysis, Manchester, UK*. 2004.
154. Wowk, V., *Machinery Vibration, Measurement and Analysis, 1991*. McGraw Hill.
155. Wowk, V., *Machinery vibration: measurement and analysis*. 1991: McGraw Hill Professional.
156. Hassin, O., et al., *Journal bearing lubrication monitoring based on spectrum cluster analysis of vibration signals*. 2015.
157. Hamomd, O., et al., *A new method of vibration analysis for the diagnosis of impeller in a centrifugal pump*. 2014.
158. Elbarghathi, F., et al. *Two stage helical gearbox fault detection and diagnosis based on continuous wavelet transformation of time synchronous averaged vibration signals*. in *Journal of Physics: Conference Series*. 2012. IOP Publishing.
159. Zhang, Z. and X. Li. *Acoustic Emission Monitoring for Film Thickness of Mechanical Seals Based on Feature Dimension Reduction and Cascaded Decision*. in *Measuring Technology and Mechatronics Automation (ICMTMA), 2014 Sixth International Conference on*. 2014. IEEE.
160. Anderson, W.B., J. Jarzynski, and R.F. Salant, *A condition monitor for liquid lubricated mechanical seals*. Tribology transactions, 2001. 44(3): p. 479-483.
161. Mba, D., et al., *Detection of shaft-seal rubbing in large-scale power generation turbines with acoustic emissions. Case study*. Proceedings of the Institution of Mechanical Engineers, Part A: Journal of Power and Energy, 2004. 218(2): p. 71-81.
162. Miettinen, J. and P. Andersson, *Acoustic emission of rolling bearings lubricated with contaminated grease*. Tribology International, 2000. 33(11): p. 777-787.
163. Asamene, K. and M. Sundaresan, *Analysis of experimentally generated friction related acoustic emission signals*. Wear, 2012. 296(1): p. 607-618.
164. Benabdallah, H. and R. Boness, *Tribological behaviour and acoustic emissions of alumina, silicon nitride and SAE52100 under dry sliding*. Journal of materials science, 1999. 34(20): p. 4995-5004.
165. Matsuoka, K., D. Forrest, and T. Ming-Kai, *On-line wear monitoring using acoustic emission*. Wear, 1993. 162: p. 605-610.
166. Benabdallah, H., *Friction wear and acoustic emissions of some plastics sliding against Si 3 N 4*. Wear, 2008. 264(1): p. 152-156.
167. Bechhoefer, E., et al. *Signal processing techniques to improve an acoustic emissions sensor*. in *Annual Conference of the Prognostics and Health Management Society*. 2013.

168. Jardine, A.K., D. Lin, and D. Banjevic, *A review on machinery diagnostics and prognostics implementing condition-based maintenance*. Mechanical systems and signal processing, 2006. 20(7): p. 1483-1510.
169. Yang, H., J. Mathew, and L. Ma, *Vibration feature extraction techniques for fault diagnosis of rotating machinery: a literature survey*. 2003.
170. Sato, I., *Rotating machinery diagnosis with acoustic emission techniques*. Electrical engineering in Japan, 1990. 110(2): p. 115-127.
171. Wang, Q. and F. Chu, *Experimental determination of the rubbing location by means of acoustic emission and wavelet transform*. Journal of Sound and Vibration, 2001. 248(1): p. 91-103.
172. McCormick, A.C., *Cyclostationary and higher-order statistical signal processing algorithms for machine condition monitoring*. 1998, Citeseer.
173. Baydar, N. and A. Ball, *Detection of gear deterioration under varying load conditions by using the instantaneous power spectrum*. Mechanical Systems and Signal Processing, 2000. 14(6): p. 907-921.
174. Yang, D.-M., et al., *Third-order spectral techniques for the diagnosis of motor bearing condition using artificial neural networks*. Mechanical systems and signal processing, 2002. 16(2): p. 391-411.
175. Rehab, I., et al., *The fault detection and severity diagnosis of rolling element bearings using modulation signal bispectrum*. 2014.
176. Gu, F., et al., *A Novel Method for the Fault Diagnosis of a Planetary Gearbox based on Residual Sidebands from Modulation Signal Bispectrum Analysis*. 2014.
177. Towsyfy, H., et al. *Identification of lubrication Regimes in Mechanical Seals using Acoustic Emission for Condition Monitoring*. 2015.
178. Pan, M.-C., P. Sas, and H. Van Brussel. *Nonstationary time-frequency analysis for machine condition monitoring*. in *Time-Frequency and Time-Scale Analysis, 1996., Proceedings of the IEEE-SP International Symposium on*. 1996. IEEE.
179. Klein, R., D. Ingman, and S. Braun, *Non-stationary signals: phase-energy approach—theory and simulations*. Mechanical Systems and Signal Processing, 2001. 15(6): p. 1061-1089.
180. Kim, Y.Y. and E.-H. Kim, *Effectiveness of the continuous wavelet transform in the analysis of some dispersive elastic waves*. The Journal of the Acoustical Society of America, 2001. 110(1): p. 86-94.
181. Hora, P. and O. Červená, *Acoustic emission source modeling*. 2010.
182. Ihlenburg, F., *Finite element analysis of acoustic scattering*. Vol. 132. 2006: Springer Science & Business Media.
183. Jiaa, C. and D. Dornfeld, *Experimental studies of sliding friction and wear via acoustic emission signal analysis*. Wear, 1990. 139(2): p. 403-424.
184. Mullins, W., et al., *Examination on the use of acoustic emission for monitoring metal forging process: A study using simulation technique*. Scripta materialia, 1997. 36(9): p. 967-974.
185. Towsyfy, H., et al., *Characterization of Acoustic Emissions from Mechanical Seals for Fault Detection*. 2014.
186. Archard, J., *Contact and rubbing of flat surfaces*. Journal of applied physics, 1953. 24(8): p. 981-988.
187. Fan, Y., F. Gu, and A. Ball, *Modelling acoustic emissions generated by sliding friction*. Wear, 2010. 268(5): p. 811-815.
188. Sharma, R.B. and A. Parey, *Modelling of acoustic emission generated in rolling element bearing*. Applied Acoustics, 2017.

189. Boness, R., S. McBride, and M. Sobczyk, *Wear studies using acoustic emission techniques*. Tribology International, 1990. 23(5): p. 291-295.
190. Wang, L. and R. Wood, *Acoustic emissions from lubricated hybrid contacts*. Tribology International, 2009. 42(11): p. 1629-1637.
191. Huang, W., et al., *An acoustic emission study on the starting and stopping processes of a dry gas seal for pumps*. Tribology Letters, 2013. 49(2): p. 379-384.
192. Raharjo, P., *An Investigation of Surface Vibration, Airbourne Sound and Acoustic Emission Characteristics of a Journal Bearing for Early Fault Detection and Diagnosis*. 2013, University of Huddersfield.
193. Fadin, Y.A., et al., *Acoustic emission and surface roughness of brittle materials*. Technical Physics Letters, 2014. 40(12): p. 1089-1091.
194. Assi, G.R., *Mechanisms for flow-induced vibration of interfering bluff bodies*. 2009, Imperial College London.
195. Bearman, P.W., *Vortex shedding from oscillating bluff bodies*. Annual review of fluid mechanics, 1984. 16(1): p. 195-222.
196. Blevins, R.D., *Flow-induced vibration*. 1990.
197. Grant, I., *Flow Induced Vibrations in Pipes: a Finite Element Approach*. 2010.
198. Alber, T., B. Gibbs, and H. Fischer, *Characterisation of valves as sound sources: Fluid-borne sound*. Applied Acoustics, 2011. 72(7): p. 428-436.
199. Gao, J., W. Luedtke, and U. Landman, *Layering transitions and dynamics of confined liquid films*. Physical review letters, 1997. 79(4): p. 705.
200. Demirel, A.L. and S. Granick, *Glasslike transition of a confined simple fluid*. Physical review letters, 1996. 77(11): p. 2261.
201. Drummond, C. and J. Israelachvili, *Dynamic phase transitions in confined lubricant fluids under shear*. Physical Review E, 2001. 63(4): p. 041506.
202. Mazuyer, D., et al., *Friction dynamics of confined weakly adhering boundary layers*. Langmuir, 2008. 24(8): p. 3857-3866.
203. Sinou, J.-J., J. Cayer-Barrioz, and H. Berro, *Friction-induced vibration of a lubricated mechanical system*. Tribology International, 2013. 61: p. 156-168.
204. Wangenheim, M. and M. Kröger, *Avoidance of friction induced vibrations on seals*. PAMM, 2008. 8(1): p. 10389-10390.
205. Greenwood, J. and J. Williamson. *Contact of nominally flat surfaces*. in *Proceedings of the Royal Society of London A: Mathematical, Physical and Engineering Sciences*. 1966. The Royal Society.
206. Abdo, J. and K. Farhang, *Elastic-plastic contact model for rough surfaces based on plastic asperity concept*. International Journal of Non-Linear Mechanics, 2005. 40(4): p. 495-506.
207. Persson, B.N., *Contact mechanics for randomly rough surfaces*. Surface Science Reports, 2006. 61(4): p. 201-227.
208. Hurtado, J.A. and K.S. Kim. *Scale effects in friction of single-asperity contacts. I. From concurrent slip to single-dislocation-assisted slip*. in *Proceedings of the Royal Society of London A: Mathematical, Physical and Engineering Sciences*. 1999. The Royal Society.
209. Beer, F.P., et al., *Mechanics of Materials*, McGraw-Hill. 2006, Boston.
210. Vyas, P., *Effects of stochastic (random) surface roughness on hydrodynamic lubrication of deterministic asperity*. 2005.

Appendix A

Elastic Strain Energy Released in Deformation of a Single Asperity

The energy stored in an asperity due to elastic deformation is called elastic strain energy per unit volume which is equal to the area under the stress-strain curve, Figure A.1:

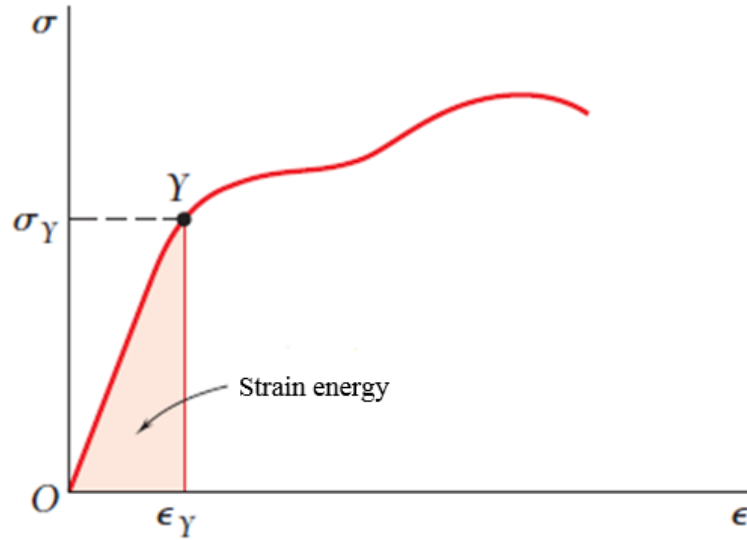


Figure A.1 The concept of strain energy [209]

where

σ is normal stress on an asperity

σ_y is the yield stress of asperity material

E is modulus of elasticity

ϵ is normal strains in an asperity due to applied stress

ϵ_y is the yield strain of asperity material

For any arbitrary value of strain in the elastic region the strain energy per unit volume, u , is calculated as:

$$u = \int_0^{\epsilon} \sigma d\epsilon = \int_0^{\epsilon} E \epsilon d\epsilon = E \frac{\epsilon^2}{2} = \frac{\sigma^2}{2E} \quad (\text{A.1})$$

In an asperity with a non-uniform stress distribution, the elastic strain energy can be expressed by integrating elastic strain energy per unit volume over the volume V of the asperity:

$$u = \lim_{\Delta V \rightarrow 0} \frac{\Delta U}{\Delta V} = \frac{dU}{dV} \quad (\text{A.2})$$

$$\rightarrow U = \int u dV$$

Using Equation (A.1) for values of u in the elastic region the strain energy can be expressed as:

$$U = \int_0^\varepsilon \frac{\sigma^2}{2E} dV \quad (\text{A.3})$$

The normal stress in bending of a single asperity is given by:

$$\sigma = \frac{M r}{I} \quad (\text{A.4})$$

where:

M is bending moment

r is asperity radius

I is area moment of inertia

Setting:

$$dV = dA dx \quad (\text{A.5})$$

Then the elastic strain energy can be expressed as:

$$U = \int_0^l \int \frac{M^2 r^2}{2EI^2} dA dx \quad (\text{A.6})$$

$$= \int_0^l \frac{M^2}{2EI^2} dx \int_A r^2 dA$$

Define:

$$I = \int_A r^2 dA \quad (A.7)$$

Thus Equation (A.6) can be rearranged as:

$$U = \int_0^l \frac{M^2}{2EI} dx \quad (A.8)$$

In the deformation of asperities (either due to direct contact or fluid flow), the bending moment M can be expressed as (see Figure A.2):

$$M = (F_f) \delta \quad (A.9)$$

Where F_f is tangential friction force in the direct asperity contact and δ is maximum deflection in the contact area

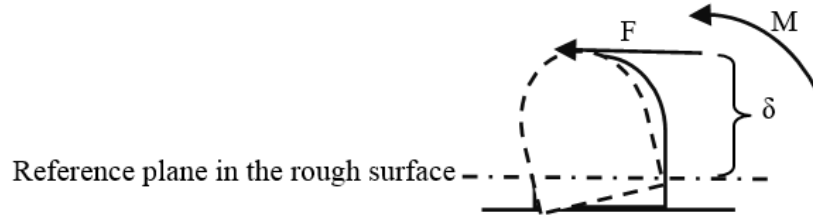


Figure A.2 Bending moment on a single asperity due to collision

Substituting Equation (A.9) into Equation (A.8) and set $l = \delta$ lead to:

$$U = \frac{F_f^2 \delta^3}{6EI} \quad (A.10)$$

Appendix B

PAC AE Sensor Calibration Curve

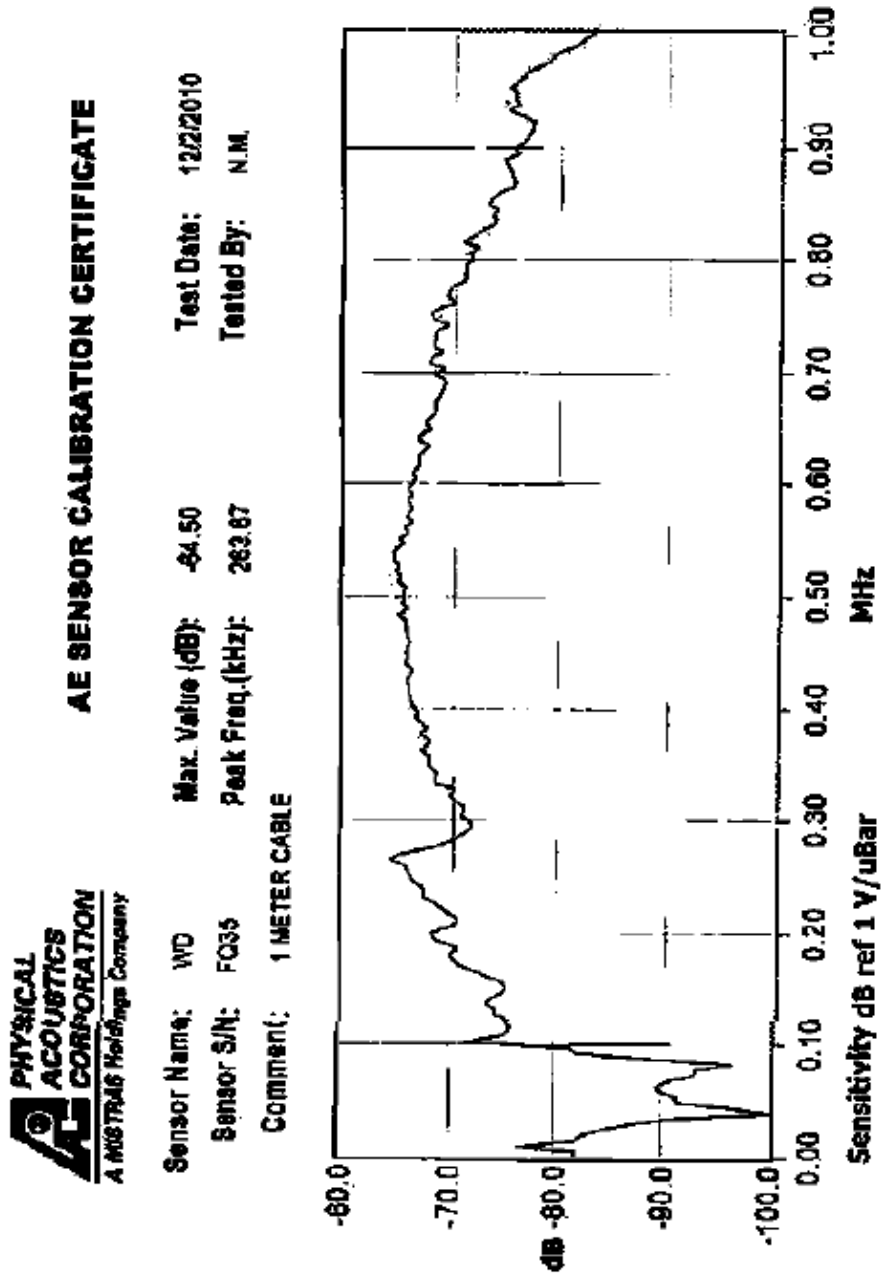


Figure B.1 AE sensor calibration certificate

Appendix C

The Main Dimensions of the Rig

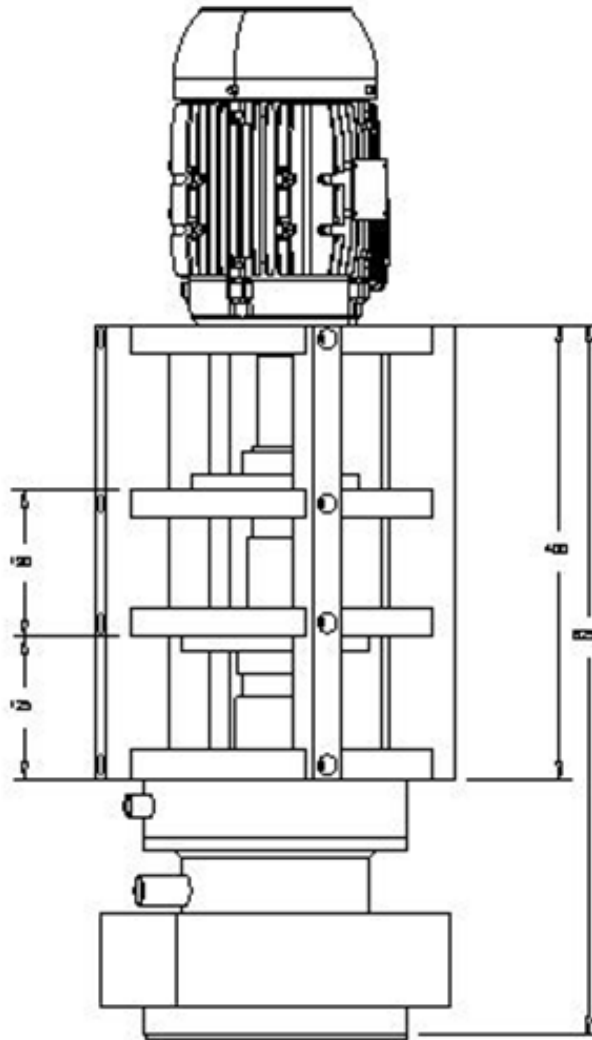


Figure C.1 The dimensions of the new rig (in millimetre)

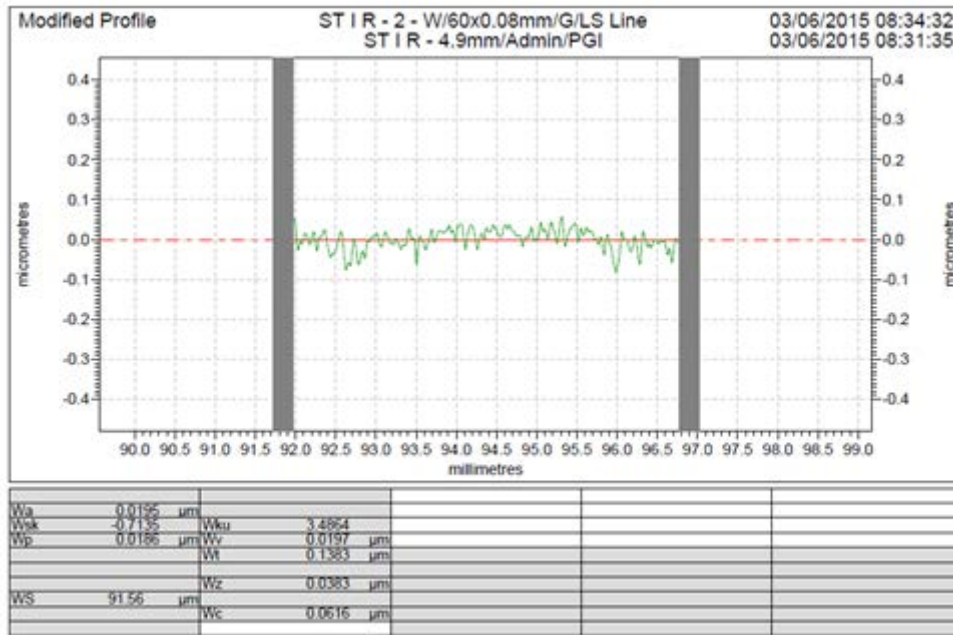


Figure D.3 Waviness profile for sample 1 before the tests

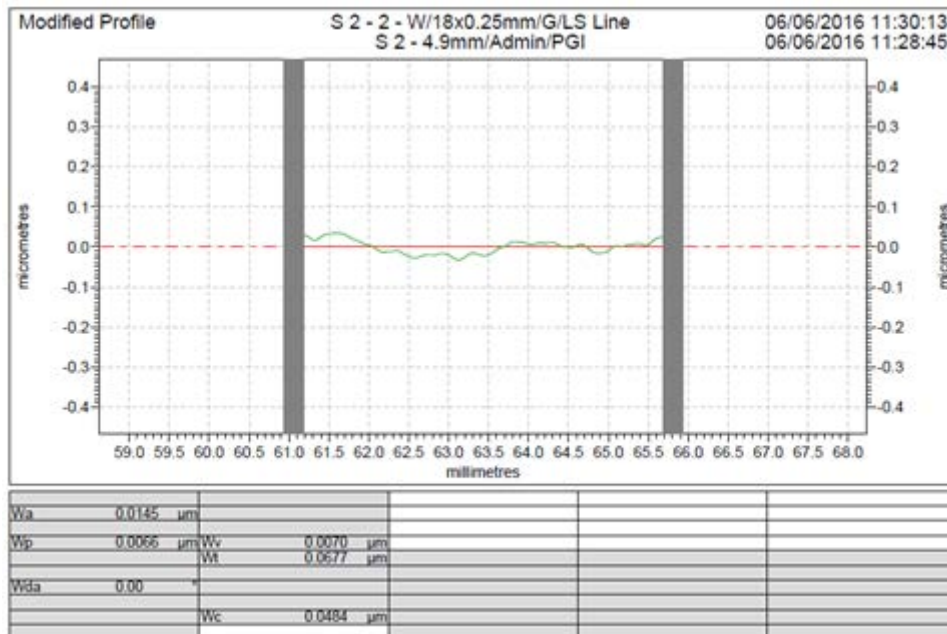


Figure D.4 Waviness profile for sample 1 after the tests

Appendix E

Results of Surface Roughness Measurements

Results of surface roughness measurements are presented in Tables E.1 and E.2. Based on the obtained results, it is found that the seal surfaces were well polished and meet the requirements due to running in and previous service work in the lab. Also no wear evidence was observed after the tests.

Table E. 1 The results of roughness measurements

Sample number	Ra of stationary ring (μm)		Ra of rotating ring (μm)	
	Before tests	After Tests	Before tests	After Tests
1	0.0246	0.0104	0.0545	0.0309
2	0.0222	0.0082	0.0225	0.0193
3	0.0219	0.0107	0.0229	0.0346
4	0.0205	0.0104	0.0280	0.0308
5	0.0229	0.0095	0.0166	0.0342
6	0.0213	0.0096	0.0251	0.0474
7	0.0223	0.0097	0.0206	0.0518
8	0.0239	0.0104	0.0252	0.0104

Table E. 2 The results of waviness measurements

Sample number	W_t of stationary ring (μm)		W_t of rotating ring (μm)	
	Before tests	After Tests	Before tests	After Tests
1	0.1383	0.0677	0.2999	0.3227
2	0.1280	0.0660	0.8765	0.1227
3	0.1286	0.0724	0.2684	0.1793
4	0.1011	0.0732	0.3095	0.6303
5	0.1263	0.0749	0.1650	0.2706
6	0.1212	0.0828	0.2958	0.4211
7	0.1401	0.0726	0.2873	0.5113
8	0.1373	0.0646	0.6399	0.2504

Appendix F: Calculation of the Resonant Frequency of the Stationary Ring

In general, the natural frequency of a vibrating system is given by (see Figure F.1):

$$\omega = \sqrt{\frac{K}{m}} \tag{F.1}$$

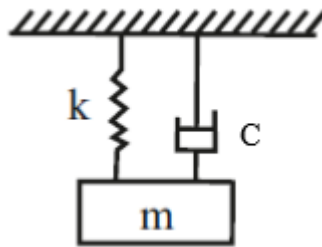


Figure F.1 The structure of spring and weight

where

- C is damping coefficient
- ω is natural frequency
- m is mass of the vibrating system
- K is stiffness of the vibrating system

The materials of the rotating and stationary ring are antimony carbon and silicon carbide respectively. Table F.1 lists all of the relative parameters used in this calculation.

Table F.1 The parameters of the rotating ring for the calculation of natural frequency

Description	Notation	Unit	Value
Inside diameter of sealing interface	Di	mm	80.42
Outside diameter of sealing interface	Do	mm	90.58
Balance diameter	Db	mm	82.55
Young's modulus of silicon carbide	E1	GPa	393
Shear modulus of silicon carbide	G1	GPa	162
Length of the stationary component	Lr	mm	16
Weight of stationary ring	m	gr	130
Density	D	gr/cc ³	3.21

F.1 Calculation of Longitudinal Vibration Frequency of the Ring

When an axial load is exerted the free end of a cantilever beam (see Figure F.2), the displacement of free end is given by:

$$\Delta = \frac{FL}{AE} \tag{F.2}$$

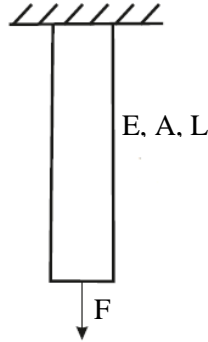


Figure F.2 Axial load on a vibrating system

where

- L is length of the beam
- A is area of the beam perpendicular to the load direction
- F is axial load
- E is elastic modulus of the beam
- Δ is displacement of free end

Considering the Equation (F.2), the stiffness of such a system can be expressed as:

$$K = \frac{AE}{L} \tag{F.3}$$

Substituting Equation (F.3) into Equation (F.1) the natural frequency related to axial load of a vibrating system can be calculated using Equation (F.4)

$$\omega_n = \sqrt{\frac{AE}{mL}} \tag{F.4}$$

In case of applied mechanical seal the sealing interface area is:

$$A = \frac{1}{4}(D_o^2 - D_i^2) = \frac{\pi}{4}(90.58 - 80.12)^2 = 1364.54 \text{ mm}^2 \quad (\text{F.5})$$

Thus using Table F.1 the longitudinal natural frequency of the system is:

$$\omega_n = \sqrt{\frac{1364.54 \times 393000}{0.130 \times 16}} = 16.05 \text{ kHz} \quad (\text{F.6})$$

Based on the above calculations the frequency band of 150-200 kHz is more affected by the resonant frequency of the stationary ring rather than the frictional state of the sealing gap.

F.2 Calculation of Torsional Vibration Frequency of the Ring

Based on the theory of vibration, the stiffness of such a vibrating system under torsional load equal to T can be expressed as:

$$K = \frac{GJ}{L} \quad (\text{F.7})$$

where

J is polar moment of inertia

G is shearing modulus of the beam

L is length of the beam (here is length of shaft, see Table 6.3)

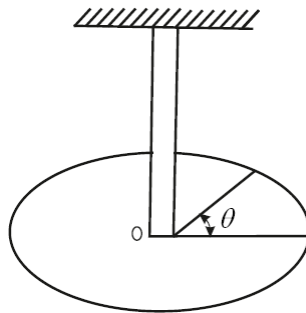


Figure F.3 Torsional load on a vibrating system

Based on the equations of motion, for the above system:

$$\begin{cases} I\ddot{\theta} + \frac{GJ}{L}\theta = 0 \\ \ddot{\theta} + \omega^2\theta = 0 \end{cases} \quad (\text{F.8})$$

Hence the natural frequency can be calculated using Equations (F.8):

$$\omega_n = \sqrt{\frac{GJ}{LI}} \quad (F.9)$$

Where I is moment of inertia of the vibrating system .In case of applied mechanical seal:

$$J = \frac{\pi}{32}(D_o^4 - D_i^4) = 2501279 \text{ mm}^4 \quad (F.10)$$

$$I = \frac{1}{2}m\left(\left(\frac{D_o}{2}\right)^2 + \left(\frac{D_i}{2}\right)^2\right) = 238.42 \text{ Kg.mm}^2 \quad (F.11)$$

where D_o and D_i are outside and inside diameter of stationary ring respectively. Hence substituting Equations (7.10) and (7.11) into on Equations (F.9) and considering Table F.1 the natural frequency related to torsional load on the stationary ring is:

$$\omega_n = \sqrt{\frac{162000 \times 2501279}{340 \times 238.42}} = 2.235 \text{ kHz} \quad (F.12)$$